The role of the Hippo pathway in etiology and progression of pancreato-biliary tumors and clear cell renal cell carcinoma

DISSERTATION
zur Erlangung des
Doktorgrades
(Dr. rer. nat.)

der
Mathematisch-Naturwissenschaftlichen Fakultät
der
Rheinischen Friedrich-Wilhelms-Universität Bonn

vorgelegt von

UTE THEODORA GESINA SCHÜTTE
aus Hannover

Bonn 2015

Angefertigt mit Genehmigung der Mathematisch-Naturwissenschaftlichen Fakultät
der Rheinischen Friedrich Wilhelms-Universität Bonn

Erstgutachter	Univ.-Prof. Dr. P. Brossart
Zweitgutachter	Univ.-Prof. Dr. G. Bendas

Tag der Promotion:	31.08.2015
Erscheinungsjahr:	2016

Die Untersuchungen zur vorliegenden Arbeit wurden auf Anregung von Herrn PD Dr. med. Georg Feldmann an der Medizinischen Klinik III des Universitätsklinikums der Rheinischen Friedrich-Wilhelms Universität Bonn in der Zeit von August 2009 bis Dezember 2013 durchgeführt. Die vorliegende Arbeit wurde im Sinne des § 6 der Promotionsordnung der Mathematisch-Naturwissenschaftlichen Fakultät der Rheinischen Friedrich-Wilhelms-Universität in der Fassung vom 03.06.2011 (korrigiert am 17.06.2011) durch Herrn Prof. Dr. med. Peter Brossart und Herrn Prof. Gerd Bendas betreut.

Meinen Großmüttern Theodora Rauen und Gesina Schütte gewidmet

Veröffentlichungen

Aus der vorliegenden Arbeit sind folgende Tagungsbeiträge und Publikationen hervorgegangen:

Originalarbeiten

Schütte, U., Bisht, S., Heukamp, L.C., Kebschull, M., Florin, A. Haarmann, J., Hoffmann, P., Bendas, G., Büttner, R., Brossart, P., Feldmann, G Hippo signaling mediates proliferation, invasiveness and metastatic potential of clear cell renal cell carcinoma, Translational Oncology, 7 (2), 309-21

Eine Genehmigung des Verlegers Elsevier für die Verwendung der publizierten Daten in dieser Dissertationsschrift liegt vor.

Poster

Schütte, U., Bisht, S., Haarmann, J., Kebschull, M., Heukamp, L.C., Büttner, R., Brossart, P., Feldmann, G. Yes-associated protein (YAP) erhöht Tumorigenität von ccRCC Zelllinien und vermittelt einen invasiven Phänotyp durch Interaktion mit der Endothelin-Achse und Kooperation mit c-Myc, Jahrestagung der Deutschen Gesellschaft für Hämatologie und Onkologie, 18.-22. Oktober 2013, Wien, Österreich

Dieser Beitrag wurde mit einem Posterpreis ausgezeichnet.

Schütte, U., Bisht, S., Haarmann, J., Kebschull, M., Heukamp, L.C., Büttner, R., Brossart, P., Feldmann, G. Yes-associated protein (YAP) and c-Myc: Partners in Crime in clear cell Renal Cell Carcinoma?, Keystone Symposium, 19.-23. Mai 2013, Monterey, Kalifornien, USA

Vorträge

Schütte, U., Bisht, S., Beckers, A., Esch, C., Heukamp, L.C., Zhou, H., Büttner, R., Brossart, P., Feldmann, G. Expression of Yes-associated protein (YAP) in clear-cell renal cell carcinoma, Vortrag auf der Jahrestagung der Deutschen Gesellschaft für Hämatologie und Onkologie, 1.-5. Oktober 2010, Berlin

Abstract

The role of the Hippo pathway in etiology and progression of pancreato-biliary tumors and clear cell renal cell carcinoma

Schütte, Ute Theodora Gesina

In the quest for the discovery of novel targets for cancer therapy, aberrantly reactivated embryonic signaling pathways have proven to be a rich mine and recent years have seen the introduction of the hedgehog-inhibitor cyclopamine into clinical practice. Dysfunctional signaling via the growth inhibitory embryonic signaling pathway clustered around the Hippo kinase and aberrant expression of its main target Yes-associated protein (YAP) is likewise emerging to be involved in maintenance and progression of various human cancers.

The purpose of this dissertation is to identify the incidence, functional relevance and mechanistic significance of aberrant Hippo signaling in etiology and progression of different solid tumor entities that vary in their biology as well as tissue of origin, but share an unfavorable clinical prognosis and the dire need for novel therapeutic approaches. Specifically cancers of the pancreato-biliary tract, more precisely pancreatic ductal adenocarcinoma (PDAC) and cholangiocarcinoma (CCC), as well as clear cell renal cell carcinoma (ccRCC) have been analyzed in the course of this dissertation. For these tumor entities initial evidence of aberrant Hippo signaling has been published.

In a first step, aberrant expression of the transcriptional co-activator YAP, which constitutes the principal target of the growth-inhibitory Hippo-pathway, was confirmed in human tumor tissue samples by immunohistochemistry. Nuclear YAP expression correlated with nodal stadium in PDAC and was also more frequent in ccRCC patients with tumor-positive lymph nodes. A common feature in all three tumor entities were solitary, fibroblast-like cells residing inside

the tumor adjacent stroma that were highlighted by robust nuclear YAP-staining, suggesting that YAP might be a mediator of tumor-stroma crosstalk.

In a second step, the role of aberrant YAP activity in tumor cell lines was examined by shRNA-mediated knockdown of the protein in selected, highly YAP-expressing cell lines. Phenotypic consequences of the knockdown included inhibition of cell proliferation as measured by the MTS-assay as well as impairment of colony formation *in vitro* for PDAC, CCC and ccRCC cell lines and decreased tumorigenicity *in vivo* for ccRCC cells in tumor xenograft experiments. However, shRNA-mediated YAP knockdown impaired *in vitro* cancer cell migration only in ccRCC cell lines.

In a third and final step, the transcriptomic output of YAP in the three different tumor entities was compared by gene expression analysis of YAP-knockdown vs. mock transfected cancer cell lines. Although the phenotype of YAP-knockdown cells was functionally similar in PDAC, CCC and ccRCC cell lines, the transcriptional output of the Hippo-YAP axis as determined by transcriptomic profiling appeared to be fundamentally different and seemed to be highly tissue context-dependent. In fact, certain pathways were activated by YAP-knockdown in one cell line while they were inhibited in another (e.g. MAPK in PK9 v. MZ1774 cells). As no single, clearcut mechanism of YAP-mediated tumorigenicity could be observed, mechanistic considerations were made for each of the three tumor entities individually and feature CTGF and Wnt-signaling for pancreatic cancer as well as c-Myc and endothelins in ccRCC. The observation of solitary cells that exhibit robust nuclear YAP-expression was common in all three tumor entities analyzed, suggesting a role of Hippo-YAP signaling in tumor-stroma crosstalk which is certainly a highly interesting starting point for future research.

Contents

List of Figures

List of Tables

List of Abbreviations

Listed are abbreviations and acronyms used in this dissertation with the exception of common scientific symbols and units as well as official gene and protein symbols for the sake of conciseness. Gene and protein symbols are expanded to the official gene or protein name when first mentioned.

ABCP	Apicobasal cell polarity proteins
APS	Ammonium persulfate
BilIN	Biliary intraepithelial neoplasia
BSA	Bovine serum albumine
CCC	Cholangiocarcinoma
ChIP-qPCR	Chromatin immunoprecipitation coupled with quantitative PCR
ChIP	Chromatin immunoprecipitation
DMEM	Dulbecco's modified Eagle's medium
DPBS	Dulbecco's phosphate-buffered saline
e.g.	*exempli gratia*, for example
EMT	Epithelial-mesenchymal transition
et al.	*et alii*, and others
FAMMMS	Familial atypical multiple mole melanoma syndrome
FCS	Fetal calf serum
FDR	False discovery rate

GPCR	G-protein-coupled receptor
HCC	Hepatocellular carcinoma
HRP	Horseradish peroxidase
IHC	Immunohistochemistry
IPMN	Intraductal papillary mucinous neoplasm
IPNB	Intraductal papillary neoplasms of the bile duct
LPA	Lysophosphatic acid
MCN	Mucinous cystic neoplasm
MEM	Minimal essential medium
miRNA	microRNA
NFDM	Nonfat dry milk
PanIN	Pancreatic intraepithelial neoplasia
PCR	Polymerase chain reaction
PDAC	Pancreatic ductal adenocarcinoma
PJS	Peutz-Jeghers Syndrome
PMSF	Phenylmethanesulfonyl fluoride
qPCR	Quantative polymerase chain reaction
rH	Relative humidity
RCC	Renal cell carcinoma
ccRCC	clear cell Renal cell carcinoma
RPMI	Roswell Park Memorial Institute medium
RT-qPCR	Reverse transcription quantative polymerase chain reaction
RT	Room temperature

S1P	Sphingosine 1-phosphate
SDS	Sodium dodecyl sulfate
SEM	Standard error of the mean
shRNA	Short hairpin RNA
siRNA	Small interfering RNA
TBS	Tris-buffered saline
TMA	Tissue microarray
UV	Ultra violet
v.	Version

1. Introduction

1.1. The Hippo pathway in development and disease

1.1.1. Evolutionary and physiological significance of the Hippo pathway

The Hippo pathway was named after the Drosophila hippo kinase that was initially discovered using genetic mosaic screening [63]. These techniques were developed to identify genes involved in regulating cell fate and cell proliferation in the fruit fly and provide useful tools to study the effects of genetic mutations that are otherwise embryonically lethal and can function as guiding experiments in the search for novel oncogenic pathways [12]. Drosophila clones expressing a mutated hippo protein displayed severely overgrown heads and eyes that were folded and darker than their wild type counterparts. This distinct phenotype inspired the name of the protein and, eventually the pathway around it [58].

The Hippo pathway is now considered to be a highly evolutionary conserved regulator of tissue growth and cell fate. Since it was first discovered, it has emerged as an integrator of signals from a vast network of proteins and is now considered an important regulator of key cellular processes, including organ size regulation, cell proliferation and survival as well as stem cell regulation [64].

The pathway is composed of a core kinase cascade that results in phosphorylation of the transcriptional co-activator yorkie (i.e. YAP and its paralogue TAZ in mammals). This phosphorylation promotes the cytoplasmic retention of this growth-promoting co-transcription factor by 14-3-3 proteins. Multiple upstream signals feed into the core signaling cascade and also the transcriptional output of yorkie/YAP/TAZ is dependent on tissue context and cell type and can vary greatly. In the following part, the members of the mammalian core signaling pathway, important upstream signals as well as transcriptional programs controlled by YAP and TAZ are reviewed and current understanding about the role of the Hippo pathway in neoplasia is recapitulated.

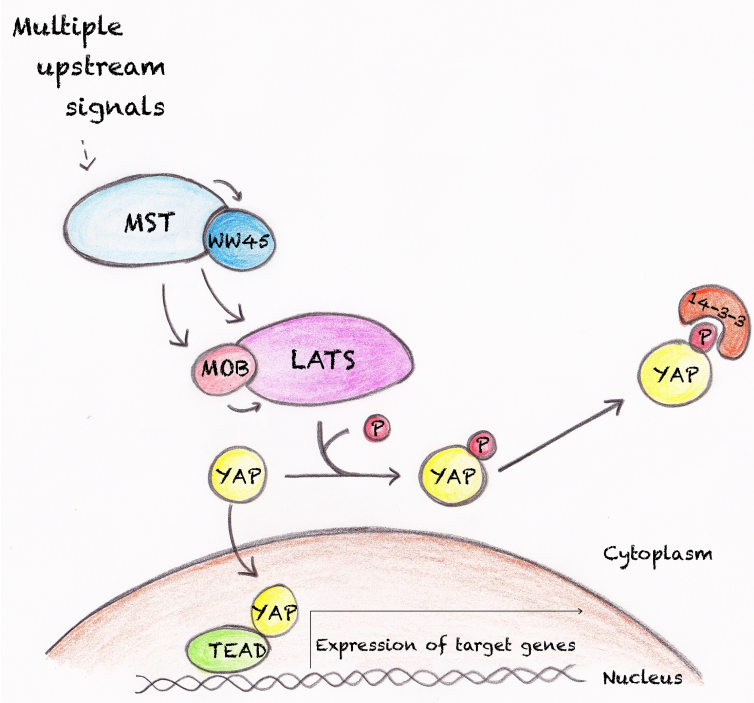

Figure 1.1.: Schematic overview of the core signaling cascade in mammals. Phosphorylation of YAP by the core signaling cassette leads to cytoplasmic retention of the transcriptional co-activator by 14-3-3 proteins. This marks YAP for ubiquitin-mediated proteolysis.

1.1.2. The core signaling cassette

The core signaling cassette of the Hippo signaling pathway is comprised of a set of highly evolutionary conserved kinases (see table 1.1 on page 3). In mammals two related serine/threonine kinases, *mammalian STE20-like protein kinase 1* (MST1, also known as STK4) and MST2 (also known as STK3) as well as *large tumor suppressor 1* (LATS1) and LATS2, form the main part of the core cassette, together with their adaptor proteins *Salvador homologue 1* (SAV1), *MOB kinase activator 1A* (MOB1A) and MOB1B. LATS1/2 in association with MOB1A/MOB1B phosphorylates the homologous oncoproteins *Yes-associated protein* (YAP) and *transcriptional co-activator with PDZ-binding motif* (TAZ), creating binding sites for 14-3-3 proteins and promoting their cytoplasmic retention and ubiquitin-mediated proteolysis [64]. Both YAP and TAZ are transcriptional co-activators that promote tissue growth and cell viability by regulating transcriptional activity in association with TEAD or SMAD transcription factors. Figure 1.1 provides a graphic overview of the interaction of the core pathway members.

Table 1.1.: Members of the Drosophila Hippo pathway and their mammalian counterparts

Drosophila gene	Mammalian orthologue	Reference
hippo	*MST1/MST2*	[63]
salvador	*SAV1*	[158]
warts	*LATS1/2*	[76, 158]
mats	*MOB1A/MOB1B*	
yorkie	*YAP1*, *TAZ*	[70]
scalloped	*TEAD1-4*	[93]

1.1.3. Multiple inputs into the Hippo Pathway

Multiple upstream branches feed into the Hippo pathway to control YAP/TAZ activity although not all upstream signals control YAP/TAZ by activation of the core signaling pathway. Some proteins form physical complexes with the transcriptional co-activators and sequester them at cell-cell junctions far away from the transcriptional machinery in the nucleus.

There is evidence of an evolutionary shift between Drosophila and mammalian systems regarding upstream input into Hippo signaling. While giant atypical cadherins like Fat and Dachsous are well-characterized upstream members of the Hippo network in Drosophila, they lack crucial domains in mammals and therefore do not interact with pathway members in the mammalian system [14].

Several tissue level processes have been linked to Hippo pathway activation in development and disease and will be briefly discussed below. Although the upstream Hippo signaling network comprises many proteins, the last molecular link between the cell surface and pathway activation or inhibition is in many cases still missing and conclusions rely on empirical evidence. Figure 1.2 on page 6 provides an overview over the current knowledge about the Hippo signaling network in mammalian cells.

Apicobasal cell polarity proteins

Apicobasal cell polarity proteins (ABCP) are responsible for the definition and maintenance of functionally distinct membrane surfaces in epithelial tissues. In mice, the ABCP protein Scribble can bind members of the Hippo core cassette and might thus promote LATS-dependent YAP phosphorylation [26]. Mislocalization and aberrant expression of

ABCP proteins has been observed in some cancers and could explain YAP/TAZ hyper-activity in human neoplasia [64, 71].

Mechanotransduction

Hippo pathway activation is dependent on the mechanical properties of the cellular microenvironment and has been shown to be sensitive to signals from the actin cytoskeleton in drosophila and mammals (reviewed in [64]). While stretching of cultured mammalian cancer cells leads to decreased Hippo pathway activity and nuclear YAP localization, compression of cells results in Hippo activation and YAP exclusion from the nucleus [37]. Although the detailed molecular mechanism is not yet fully understood, this finding has important consequences for the role of Hippo signaling in neoplasia: due to alterations of tissue architecture like changes in the extracellular matrix and infiltration of stromal and immune cells, tumor tissue has altered mechanical properties that increase tissue rigidity and might lead to YAP hyper-activation [37]. Recent studies have found that not only neoplastic cells but also cancer associated fibroblasts in breast cancer depend on YAP-signaling to promote malignant features of a tumor such as matrix-stiffening, cancer cell invasion and angiogenesis [21].

Cell-cell adhesion molecules

There is experimental evidence that compromised function of cell-cell adhesion molecules can lead to YAP/TAZ hyper-activation. Epithelial cells are connected to each other via protein complexes anchored in adherens junctions (intercellular junctions) and tight junctions (intercellular junctions in the apical regions of epithelial cells). Many proteins involved in the formation of these junctions have been shown to "handcuff" YAP and TAZ and to sequester them at cell junctions [64]. Notably Crumbs, angiomotins (AMOT), α-catenin and E-cadherin bind YAP/TAZ and physiologically suppress their activity [139].

Contact inhibition

The phenomenon that adherent cells cease to proliferate when they come into physical contact with their neighbors is defined as "contact inhibition". Loss of this characteristic is one trait of oncogenically transformed cells *in vitro* [68]. Overexpression of YAP and loss of upstream members of Hippo signaling, such as *neurofibromin 2* (NF2), can induce non-transformed cells to overcome contact inhibition [182]. Although the molecular mechanisms remain to be elucidated and the *in vivo* relevance of this finding is unclear, it has

been shown many times that the sub-cellular localization of YAP and TAZ is influenced by contact inhibition *in vitro* [63, 182].

Interaction with other signaling pathways

Pro-apoptotic stimuli, e.g. staurosporine treatment, have been shown to up-regulate MST1 activity [160] and the same is true for DNA damage [61]. Oncogenic stress signals, for example constitutively active Ras-signaling, physiologically also increase MST activity and Hippo-mediated apoptosis [81]. Furthermore, the Hippo pathway has been shown to integrate signals from several pathways that are known to carry oncogenic mutations, for example the Wnt-, TGF-β-BMP-, Hedgehog-, Notch-, insulin- and mTOR-signaling pathways [72].

G-protein coupled receptors

Recent work identified G-protein-coupled receptor (GPCR) signaling as one upstream regulator of the Hippo pathway [178]. Serum-borne Lysophosphatic acid (LPA) and Sphingosine 1-phosphate (S1P) activate $G_{12/13}$-coupled receptors which leads to the inhibition of LATS1/2 and consecutive derepression of YAP and TAZ. G_s-coupled receptors have the opposite effect and ultimately lead to YAP inhibition [178]. This is very interesting in light of recent results from a cell-based screening of small molecules in search of Hippo pathway stimulators that found dobutamine, an agonist for G_s-coupled β_1-adrenoceptors, as an effective inhibitor of YAP-dependent gene transcription [6]. GPCR signaling is frequently disturbed in cancer and accessible to small molecular therapies, which makes this a promising field for YAP directed cancer therapies [64].

1.2. Transcriptional Output of the Hippo pathway

The transcriptional output of the Hippo-regulated transcriptional co-activators YAP and TAZ are about as diverse as the upstream input feeding into the core signaling cassette. The transcriptional program is highly context and cell-type dependent and may result in growth suppression, mediation of stress-induced apoptosis, or the regulation of cell-fate decisions [58]. This is of course partly due to the fact that the transcriptional co-activators YAP and TAZ can partner with multiple different transcription factors.

The oncogenically relevant transcriptional responses of YAP seem to be regulated in coalition with the TEAD-family of transcription factors, which have been shown to control

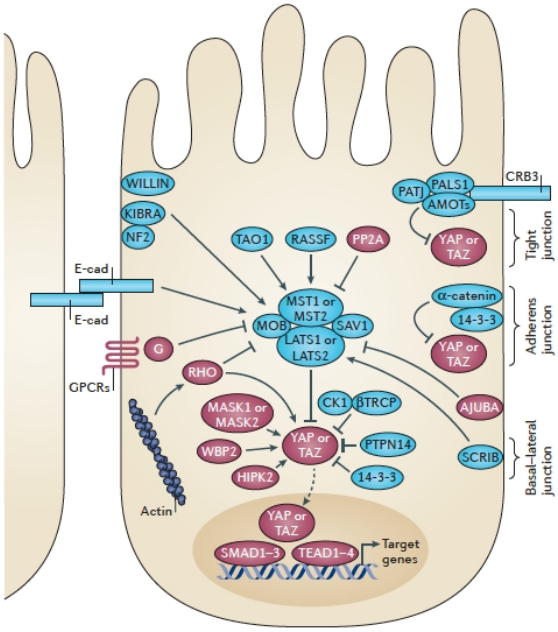

Figure 1.2.: Schematic overview of the Hippo signaling network in humans. Figure reprinted from [64] with permission from Macmillan Publishers Ltd.

transcriptional programs in Epithelial-mesenchymal transition (EMT), oncogenic transformation, inhibition of apoptosis as well as contact inhibition [58]. Curiously, YAP can also pair with p73 to elicit pro-apoptotic effects, a process that is equally dependent on core pathway members as the anti-apoptotic response initiated by the YAP-TEAD complex [156]. This can only be explained by cell-type and tissue context dependent input into the Hippo pathway, which underlines again how little is known about the precise mechanisms underlying its regulation. Another partner of YAP is the SMAD-family of transcription factors, and YAP can drive transcription downstream of the BMP pathway [1].

Recent findings excitingly revealed YAP as an important regulator of cell-density dependent microRNA (miRNA) biogenesis [111]. At low cell density, nuclear YAP binds and sequesters p72, which functions as a regulatory component of the miRNA processing machinery. At high cell density, Hippo-mediated cytoplasmic retention of YAP facilitates miRNA processing. Hence, YAP hyperactivity can result in widespread miRNA downregulation which is commonly found in a majority of human cancers [111, 177].

1.3. The Hippo pathway and cancer

Although YAP is frequently overexpressed in various human cancer tissues and promotes tumor cell properties, such as proliferation and resistance to apoptosis in epithelial cells, the explanation for Hippo pathway perturbation remains elusive. In the following part, influence of YAP on cancer cell properties as well as examples for Hippo pathway deregulation in cancer will be reviewed.

1.3.1. Influence on cancer cell properties

Proliferation

One of the most important features of cancer cells is their limitless replicative potential [62]. Dysfunctional Hippo signaling and resulting unrestrained YAP/TAZ activity have been linked to excess proliferation in murine models and human cancer tissues, as strikingly demonstrated in the murine liver [34]. This is at least partly due to evasion of p53- and Retinoblastoma (RB)-mediated senescence which constitute major tumor suppressor checkpoints [64].

Survival

The Hippo-YAP axis is further involved in another area of malignant transformation: evasion of apoptosis. YAP overexpression leads to inhibition of TNF- and Fas-induced apoptosis in the murine liver [34]. In cancer cell lines, resistance against chemotherapy-induced apoptosis as well as programmed cell death resulting from loss of cellular contact to the extracellular matrix (i.e. anoikis) have been observed by several groups [122, 184], providing a potential YAP-overexpressing subpopulation of tumor cells with the necessary features to relapse early after chemotherapy.

Maintenance of a stem cell-like phenotype

The cancer stem-cell hypothesis proposes subpopulations of tumor cells that assume cellular properties normally only associated with the regenerative cell compartment, for example a marked resistance towards chemotherapeutic drugs and the loss of mature differentiation markers. Both YAP and TAZ are enriched in multiple types of stem cells [69, 99] and YAP is physiologically expressed in the stem- and progenitor-cell compartments of various tissues and overexpression promotes expansion of this cell pool that can

culminate in tumorigenesis (e.g. hepatic oval cells, [95]). YAP overexpression therefore might contribute to neoplastic transformation by the establishment or maintenance of stem cell like properties.

Invasion and metastasis

Metastasis is defined as a multistep process that requires cancer cells to undergo EMT, to dissociate from the primary tumor and cross over into the blood or lymph stream, to resist anoikis during dissemination, and finally to establish a filial tumor colony at the distant site [64]. There are numerous papers that link dysfunctional Hippo signaling and YAP hyperactivity to tumor progression and metastasis. In one of the first papers that examined the role of the Hippo-YAP axis in cancer, Overholtzer *et al.* showed that YAP overexpression promotes EMT and suppresses anoikis in non-transformed mammary epithelial cells [122]. Loss of members of the growth-inhibitory Hippo pathway as well as YAP/TAZ overexpression was found to be more frequently associated with high-grade, metastatic malignancy in animal models (development of highly metastatic osteosarcomas in $Nf2^{+/-}$-mice, [106]) as well as human breast [24, 26] and prostate cancer [184].

1.3.2. Direct and indirect disruption of Hippo signaling in human cancer

Hippo pathway deregulation and consequent nuclear accumulation of its target YAP have been observed in many human tumor tissues. Nuclear YAP expression is detectable in about 62% of hepatocellular carcinomas [175], 36% of all lung adenocarcinomas [154] and even more frequent in non small cell lung cancer with 66.3% [172]. In those cancers, nuclear YAP expression is prognostically relevant and associated with shorter overall survival. In ovarian cancer, high nuclear YAP staining coupled with low cytoplasmic YAP immunoreactivity was found to be an independent prognostic marker for survival (hazard ratio of 7.8) and associated with a 50% decrease in 5-year overall survival rates as compared to patients with high nuclear/ high cytoplasmic, low nuclear/ high cytoplasmic, or low nuclear/ low cytoplasmic YAP staining patterns [60].

Despite overwhelming evidence of prognostically relevant Hippo pathway perturbation in multiple cancer tissues, the current understanding about the underlying cause is incomplete. Members of the Hippo signaling axis, especially of the core signaling cassette are infrequently mutated in human cancers. In contrast to other oncogenic signaling pathways and with the exception of neurofibromin 2 (*NF2*), no germline mutations of

Hippo pathway members have so far been linked to hereditary cancer syndromes and also somatic mutations appear to be relatively rare [64]. Amplification of the *YAP* gene and consecutive overexpression of YAP has been reported in various tumors [122, 180]. Deletions of *SAV1* as an example of upstream members of the Hippo pathway have been reported in clear cell renal cell carcinoma [105] but a more common scenario seems to be epigenetic silencing of Hippo core pathway members.

Due to this multitude of possible inputs into the Hippo signaling pathway and its interaction with various other signaling pathways, it is very likely that Hippo signaling is indirectly disrupted. Cross-talk has been reported between the Hippo pathway and Wnt-, TGF-β-BMP-, Hedgehog-, Notch-, insulin- or mTOR-signaling [72], all of which represent signaling pathways frequently found to be aberrantly activated by oncogenic mutations in cancer [75, 167].

1.4. Pathogenesis and molecular biology of tumor entities analyzed

1.4.1. Pancreatic ductal adenocarcinoma

Epidemiology

Cancers of the pancreas in the vast majority of cases (>95%) arise from the exocrine compartment of the organ [3], and typically present as solid ductal adenocarcinomas with a dense stroma. Less than 5% of all pancreatic neoplasms are cystic lesions [92]. Pancreatic ductal adenocarcinoma (PDAC) accounts for over 90% of all pancreatic cancers and is one of the most fatal malignant tumor as of to date. It is usually diagnosed at advanced, already metastatic stages and almost invariably leads to death within few months after diagnosis. This dire prognosis is reflected in the current cancer statistics published by the American Cancer Society for 2013 [3]. In the United States, PDAC represents the 10th most common cancer diagnosis in men and the 9th most common cancer diagnosis in women with an estimated 45,220 new cases per year. Of these, an estimated 38,460 patients will succumb to their disease within the same year. PDAC is accountable for 7% of all cancer deaths, thus representing the 4th most common cause of cancer-related mortality in men and women alike. It is about 30% more common in men than in women and incidence and death rates increase with age, showing a steep increase after the age of fifty. The incidence rates have increased slightly but steadily over the last 10 years (2000-2009) in the United States [3], while the overall prognosis remained poor, despite recent advances in understanding the molecular pathology of the disease and the availability of novel treatment options.

Pancreatic cancer is now generally recognized as a genetic disease not arising de novo but originating from histologically well-defined non-invasive precursor lesions (e.g. Pancreatic Intraepithelial Neoplasia, PanIN). Progression of PanINs to invasive carcinoma is believed to be a multistep process resulting in accumulation of inherited and acquired mutations in cancer-related genes. Histopathologic progression towards pancreatic cancer is closely mirrored by genetic progression [104]. This paradigm correlates well with the increase of incidence and mortality rates with age as well as with attributed risk factors of PDAC. Two major modifiable risk factors have been identified in smoking and obesity, each increasing the lifetime risk of developing PDAC by about 20% [3].

Table 1.2.: Syndromes associated with the formation of PDAC

Syndrome	Affected gene	Comments
Hereditary breast/ovarian cancer	*BRCA2*	ca. 5%-17% of inherited pancreatic cancers harbor BRCA2 mutations
Familial atypical multiple mole melanoma syndrome (FAMMMS)	*CDKN2A/p16*	mutation increases the lifetime risk about 13-22-fold
Peutz-Jeghers Syndrome (PJS)	*STK11/LKB1*	11%-36% chance of developing PDAC during lifetime
Hereditary pancreatitis	*PRSS1*	mutation increases the lifetime risk about 70-fold, about 40%-55% will develop PDAC during lifetime

BRCA2: breast cancer 2, early onset, *CDKN2A/p16*: cyclin-dependent kinase inhibitor 2A, *STK11/LKB1*: serine/threonine kinase 11, *PRSS1*: protease, serine, 1 (trypsin 1)

Since the pathomechanistic basis of PDAC is genetic, there are not surprisingly inherited genetic features that considerably increase the lifetime risk of PDAC. A family history of pancreatic cancer increases the general risk of PDAC by twofold, seven- nine-fold if one 1st degree relative is afflicted, 17-32-fold if three or more 1st degree relatives have been diagnosed [3]. It is estimated that 5%-10% of all PDAC cases are inherited and arise either on the background of a known cancer syndrome or in association with hereditary pancreatitis or cystic fibrosis, or are referred to as familial pancreatic cancers without association with a known syndrome [134]. Table 1.2 provides an overview of genetic syndromes that predispose to development of pancreatic cancer and lists their respective underlying genetic mutations [3, 134].

It is now known that most of the above-mentioned syndromes do not predominantly result in pancreatic but rather in other forms of cancer. The majority of inherited pancreatic cancer cases is not associated with a known clinical syndrome, and familial pancreatic cancer kindreds have been reported to harbor clearly defined mutations in other genes, for example palladin [130]. These points illustrate that there is a wide spectrum of genetic alterations in a given pancreatic cancer lesion and a study of 99 human pancreatic tumors identified well over 3,000 genomic aberrations in total [11]. There are, however, methods that provide a way to spot order among the chaos. In a study published by Jones and

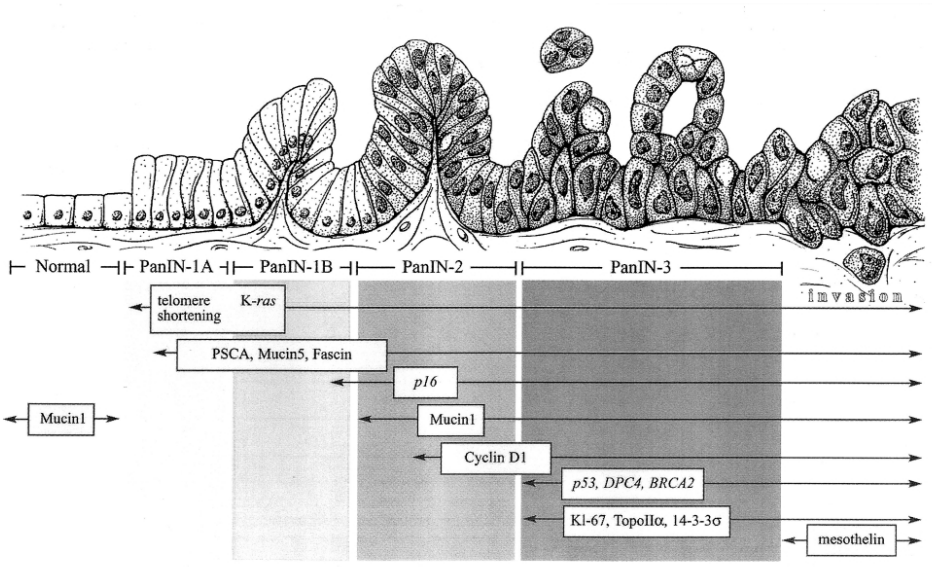

Figure 1.3.: Pancreatic carcinogenesis is a multistep process. Figure reprinted from [103] with permission from Macmillan Publishers Ltd.

colleagues in 2008, 24 pancreatic cancers were analyzed by next generation sequencing methods and although the individual mutations observed were manifold and marked by considerable inter-individual variations, the group identified twelve core signaling pathways that were almost uniformly affected across all PDAC samples analyzed [75]. Some of the most common genetic alterations affecting these pathways are discussed in more detail in the following section.

Molecular pathology

The pathogenesis of cancer is based on a variety of genetic changes culminating in invasive disease [167]. In line with this view, pancreatic cancer is today regarded as a genetic disease, which arises from morphologically and genetically clearly defined precursor lesions through stepwise accumulation of genetic alterations [44]. These precursor lesions comprise Pancreatic intraepithelial neoplasia (PanIN), which can be subclassified into PanIN-1, PanIN-2, and PanIN-3 lesions depending on the degree of cytologic and architectural atypia, intraductal papillary mucinous neoplasms (IPMN) and mucinous cystic neoplasms (MCN). PDAC may develop from any type of these precursor lesions with PanIN being the most common origin.

Mutations of genomic DNA within oncogenes and tumor suppressor genes are involved as well as epigenetic changes and aberrations of transcriptional patterns. Genetic changes may also affect caretaker genes like genes of the Fanconi's anemia DNA repair pathway that normally function to minimize genetic alterations during DNA replication thus leading to accumulation of additional genetic mutations and facilitating progression towards invasive carcinoma. Mutations of mitochondrial DNA are also very frequently observed in PDAC and non-malignant precursor lesions [43]. The hallmark-mutations of oncogenes and tumor-suppressor genes that are acquired along the pathogenic cascade of pancreatic cancer development follow here.

KRAS Activating point mutations of the oncogene *KRAS* occur in almost 90% of all PDAC cases. Most commonly they affect codon 12, 13 or 61 and result in abrogation of the intrinsic GTPase activity of the RAS-protein, which leads to constitutive activation of the intracellular signaling cascade [43]. Acquisition of constitutively active KRAS is among the first genetic changes in PDAC and is already present in nonmalignant precursor lesions. About 30% of PanIN-1 lesions harbor an activating point mutation of the *KRAS* gene [114].

CMYC, AKT2, EGFR Other oncogenes involved in the molecular pathogenesis of pancreatic cancer are *CMYC*, *AKT2*, and *EGFR*. Although mutations of those oncogenes are less frequent, they represent potential therapeutic targets and experimental evaluation is currently underway [43]. *CMYC* is amplified and subsequently overexpressed in 50-60% of pancreatic cancers while amplifications of *AKT2* are detected in less than 5% of cases [43]. Nevertheless, the Akt signaling pathway is activated in 30 to 40% of pancreatic cancers indicating additional activating mechanisms and underscoring the potential therapeutical relevance of Akt-targeting [133]. Constitutive EGFR pathway activation by amplification of the *EGFR* gene or by other mechanisms have likewise been described in pancreatic cancer [43].

CDKN2A/p16 The *CDKN2A/p16* gene is located on the short arm of chromosome 9 (9p) and encodes the cell-cycle regulator protein p16INK4A, which exerts function via the p16/Rb pathway and inhibits cell cycle progression through the G_1-S checkpoint. In over 90% of PDAC it is inactivated by either homozygous deletion (approx. 40% of cases), intragenic mutation (40%) or epigenetically by hypermethylation of its promoter (10-15%) [5]. The loss of function mutation of the *CDKN2A* gene is thought to be an early event

during the multistep process towards invasive carcinoma and can already be observed in 30% of PanIN-1, 55% of PanIN-2, and 71% of PanIN-3 lesions, respectively [140].

DPC4/SMAD4/MADH4 Deleted in pancreatic carcinoma 4 (DPC4/SMAD4/MADH4) is located on chromosome 18q21 and loss of function mutations can be observed in approx. 55% of all PDAC cases while they occur only very rarely in other malignancies [43]. Inactivation is mediated by mutation of one allele with concomitant loss of the second allele (25% of cases) or homozygous mutation (30% of cases) resulting in reduced growth inhibition and increased proliferation via impaired TGF-β signaling. Loss of *DPC4* constitutes a rather late event in pancreatic cancer development and is usually only observed in a minority of PanIN-3 lesions [174].

TP53 The oncogene *TP53* on chromosome 17p usually induces cell cycle arrest and apoptosis in response to DNA damage and is inactivated due to intragenic mutation with loss of the second allele in 50-75% of pancreatic cancers. Loss of function of TP53 facilitates the acquisition of additional genetic mutations and is considered to be a late event in pancreatic cancer development as nuclear accumulation of mutated TP53 can only be observed in advanced PanIN-3 lesions [174].

1.4.2. Biliary tract carcinoma

Epidemiology of biliary tract cancers

The structure of the biliary tract can be compared to a tree: the trunk is formed by the common bile duct with the ampulla of Vater opening into the duodenum at its bottom. The trunk then branches out into the cystic duct with the attached gallbladder, and further up turns into the common hepatic duct which then parts into the large hepatic bile ducts. Those large intrahepatic bile ducts split twig-like into a network of small intrahepatic bile ducts that form the canopy of the biliary tree. Invasive carcinomas can arise in all parts of the biliary tree and include cancers of the gallbladder as well as cancers of the intrahepatic and extrahepatic bile ducts. Although they are often grouped together, differences in epidemiology and pathobiology warrant their classification into two separate entities.

Gallbladder carcinoma Carcinoma of the gallbladder develops from the epithelial lining of the organ and represents the most frequent malignant tumor of the biliary tract.

It arises more frequently in women and displays a heterogeneous geographic distribution with higher incidence rates in Mexico and South America as compared to Western countries [92]. Very often (60% to 90% of cases), gallbladder carcinoma develops on the basis of cholelithiasis and it is suspected that recurring trauma and chronic inflammation inflicted by gallstones contribute to the development of gallbladder carcinoma. Carcinoma of the gallbladder is often discovered incidentally during surgery for removal of gallstones and the presenting symptoms are often indistinguishable from those of cholelithiasis. Consequentially, diagnosis is generally very late and tumors are often not resectable, leading to a very low 5-year overall survival rate of 5% [92].

Cholangiocarcinoma Cholangiocarcinoma (CCC) is the second most common hepatic malignancy after hepatocellular carcinoma (HCC). Cancers of the hepatobiliary tract account for 13% of cancer-related deaths worldwide and about 10-20% of these are attributable to cholangiocarcinoma [13]. While HCC is thought to arise from hepatocytes, cholangiocarcinomas are defined as hepatobiliary cancers with features of cholangiocyte differentiation, although the cell of origin is a matter of some debate, as will become apparent below [132]. Based on their anatomic location, CCC are classified into three subtypes that are distinct in epidemiology, etiology and pathogenesis. They are: firstly intrahepatic cholangiocarcinoma, secondly perihilar cholangiocarcinoma, also referred to as "Klatskin-Tumor", and finally distal cholangiocarcinoma. The second-order bile ducts serve as a demarcation between intrahepatic and perihilar cholangiocarcinoma while the cystic duct separates perihilar from distal cholangiocarcinomas [132]. The latter two have been grouped together as extrahepatic cholangiocarcinomas but differences in frequency, pathobiology and management have led to the understanding that they are two separate entities [78]. Perihilar CCC is the most common subtype (50%-60%), followed by distal CCC (about 20%) and intrahepatic CCC (up to 20%). A small subset of 5% consists of tumors with multiple foci [78].

Not unlike PDAC, CCC is diagnosed usually at late, unresectable stages and the prognosis is generally grim with 5-year-survival rates ranging at around 10% which is slightly improved after attempted curative resection to 20%-40% [107]. Mean survival times post-surgery range from 6 to 18 months, regardless whether aggressive resection or palliative surgery is performed [92]. CCC has a slight male predominance and develops later in life, with the median age at diagnosis in Western countries being >65 years [13]. For reasons yet unknown, incidence and mortality rates of intrahepatic CCC have been increasing worldwide, while those of extrahepatic CCC have remained stable [132].

Although most cases of CCC are sporadic, some risk factors have been established. The geographic occurrence of these factors varies greatly and explains the geographic variability of incidence rates of CCC, which are the highest in Southeast Asia (113 per 100,000 in Thailand in contrast to 0.1 per 100,000 in Australia for intrahepatic CCC) [132]. The main risk factor for the development of CCC seems to be chronic biliary inflammation, although the underlying cause varies geographically as well. In Asian countries infections with the hepatobiliary flukes *Opisthorchis viverrini* and *Clonorchis sinensis* and hepatholithiasis are more prevalent and predispose for the development of CCC, while in Western countries primary sclerosing cholangitis, a chronic disease of suspected autoimmune genesis, is the primary predisposing condition and is associated with a 5%-10% lifetime prevalence of CCC [132]. Further risk factors include infection with hepatitis B or hepatitis C virus and liver cirrhosis.

Pathobiology

Cell of origin Distal and perihilar CCC are thought to arise from cholangiocytes that line the larger intrahepatic as well as the extrahepatic bile ducts and form the biliary epithelium. Cholangiocytes are mucin-producing cuboidal cells that contribute to bile secretion – a task mainly performed by hepatocytes – via net release of bicarbonate and water. Intrahepatic CCC on the other hand may not have a single lineage and there is evidence that they develop from either biliary epithelial cells or hepatic progenitor cells (oval cells) [132]. It has also been proposed that CCC could arise from transdifferentiated hepatocytes that have reverse-developed into liver cancer stem cells which in turn can give rise to hepatocellular or cholangiocellular carcinoma [67]. The multiple-lineage hypothesis is supported by the fact that the histologic presentation of CCC and particularly intrahepatic CCC is diverse and rare subtypes include combined hepatocellular/cholangiocellular carcinomas [132].

Role of biliary inflammation Although the majority of biliary carcinomas are sporadic, the known risk factors and predisposing conditions all involve chronic biliary inflammation, making inflammatory processes a likely contributing factor to biliary carcinogenesis. Inflammation produces a wide array of mediators like cytokines, growth factors and kinases that can influence cellular processes crucial in carcinogenesis including regulation of the cell-cycle and cell proliferation, senescence and apoptosis. Key mediators involved in biliary carcinogenesis have been identified and characterized. *Inducible nitric oxide syn-*

thase (iNOS) is activated by inflammatory mediators leading to oxidative DNA damage while DNA repair enzymes are inhibited [73]. The cytokine *interleukin-6* (IL-6) is secreted by CCC cells as well as tumor-associated immune cells and increases the expression of the antiapoptotic protein *myeloid cell leukemia sequence 1* (MCL1) via constitutive activation of the *signal transducer and activator of transcription* (STAT) pathway and activates STAT3 in a *janus kinase* (JAK)-dependent manner [132].

Cholestasis and bile acids contribute to the inflammatory environment by activating growth factor signaling like *epidermal growth factor receptor* (EGFR) and increasing the expression of *cyclooxygenase-2* (COX2). Bile contains a high concentration of oxysterols which are products of the oxidative degradation of cholesterol and function as endogenous ligands for the hedgehog signaling pathway. Oxysterols have likewise been implicated to foster biliary carcinogenesis [132].

Development via precursor lesions As seen for a lot of epithelial tumor entities such as colon carcinoma, prostate cancer or PDAC (as discussed above), there has been increasing evidence in recent years that the development of cancers of the biliary tract is equally most accurately described by a multistage progression model that includes the formation of precursor lesions in healthy biliary epithelium which will eventually give rise to invasive carcinoma. Precancerous changes in the gallbladder and the biliary tract are likewise characterized by increasing degrees of atypia of the tissue architecture that are accompanied by molecular changes affecting tumor suppressor and oncogenes although the knowledge about the molecular signature of precursor lesions of the biliary system is merely fragmentary to date. In line with their classification as two separate entities, there are histologically and molecularly distinct precursor lesions of invasive gallbladder and cholangiocarcinoma [65].

There are two major types of precancerous lesions that may develop into invasive cholangiocarcinoma: *biliary intraepithelial neoplasia* (BilIN) and *intraductal papillary neoplasms of the bile duct* (IPNB). **BilINs** are only microscopically detectable, flat and do not form masses which is why they are usually asymptomatic. The lesions are characterized histologically by columnar epithelial cells that exhibit multilayering of abnormal nuclei as well as the formation of desmoplastic stroma. The degree of cellular atypia increase from low-grade BilINs (BilIN1-2) towards high-grade BilIN3 and *carcinoma in situ*. **IPNBs** are papillary lesions that form masses inside the bile ducts, eventually becoming macroscopically visible and causing biliary obstruction which makes them clinically detectable.

IPNBs are thought to give rise to about 10%-15% of bile duct tumors and occur in predominantly in extrahepatic, sometimes in large intrahepatic bile ducts [82].

Similarly, there are **BilINs of the gallbladder** that share microscopic characteristics with their counterparts in the bile ducts and arise in the cholecystic mucosa. They are often found next to invasive carcinomas and are mostly detected at cholecystectomies. The presence of BilIN3 lesions is a strong indicator of invasive carcinoma of the gallbladder. *Intracholecystic papillary-tubular neoplasms of the gallbladder* are preinvasive dysplastic epithelial lesions that form exophytic mucosal tumors. They typically form solitary masses larger than 1 cm in diameter and can likewise produce clinical symptoms that may lead to an early detection with more favorable outcome for the patient [82].

Molecular pathology The evaluation of the molecular pathology is ongoing and the molecular cascade of biliary carcinogenesis is considerably less well defined than in PDAC. Nevertheless the association of morphological changes with a mutational spectrum of oncogenes and tumor suppressor genes has been demonstrated in several studies. The most important genes are discussed here. It will become apparent that there is considerable overlap between the mutational spectrum of PDAC and CCC. Activation of **KRAS** is found in subsets of both CCC and gallbladder carcinoma. While activation of the oncogene is observed in 40%-50% of intrahepatic CCCs and occurs in about 30% of gallbladder carcinomas, it is less frequent in extrahepatic CCCs (10%-15%). Mutations in *v-raf murine sarcoma viral oncogene homolog B1* (BRAF), an important downstream mediator of oncogenic KRAS signaling were observed in an additional 30% (gallbladder carcinomas) or 20% (intrahepatic CCC), respectively. Of note, those mutations occurred mutually exclusive, suggesting the activation of the Ras/Raf/MAPK signaling axis as a key event in biliary carcinogenesis [65].

The spectrum of tumor suppressor gene mutations seen in biliary tract carcinomas largely mirrors that of other GI malignancies like PDAC and includes loss of function of CDKN2A, TP53 (tumor protein p53), and SMAD4. The cell-cycle regulator protein **CDKN2A/p16** is frequently mutated in biliary tract cancers by mechanisms such as promotor hypermethylation, homozygous deletion, and inactivating point mutations. Frequencies as high as 88% have been reported for intrahepatic CCC and range around 50% for both extrahepatic CCC and gallbladder carcinoma [65]. Inactivation of **TP53** has been reported to occur in cancers of the biliary tree with frequencies of 30%-40%, regardless of the site of origin. A mouse model of CCC combining the expression of constitutively active Kras with the inactivation of p53 in hepatic precursor cells has recently

been published. These animals develop precancerous lesions that mimic human BilINs which progress into invasive carcinoma of CCC or mixed (HCC/CCC) histology [119]. Inactivation of **SMAD4** has been reported for CCC, although frequencies vary greatly with 15%-50% for extrahepatic and 10%-15% for intrahepatic CCC [65].

Desmoplastic reaction and cancer associated fibroblasts Like PDAC, intrahepatic and perihilar CCCs are characterized by an intense desmoplastic reaction which surrounds the relatively sparse tumor cells with a dense, fibroblast-rich stroma. The stroma in fact comprises most of the tumor mass and it is suspected that it promotes tumor progression by cross-talk between cancer cells and stromal components, such as cancer-associated fibroblasts, which have been studied in the setting of biliary tract carcinoma. Although the cellular origin of cancer-associated fibroblasts remains to be elucidated – hypotheses include hepatic stellate cells, portal fibroblasts or bone marrow-derived precursor cells as candidates – they have been shown to stimulate production of the extracellular matrix by secretion of growth factors like *connective tissue growth factor* (CTGF), *transforming growth factor-β* (TGF-β), *platelet derived growth factor* (PDGF) and *insulin-like growth factor binding proteins* (IGFBPs) [132].

1.4.3. Renal cell carcinoma

Epidemiology of renal cell carcinoma

Renal cell carcinoma (RCC) represents the majority (80%-85%) of all primary malignant tumors of the kidney and is thought to arise from the renal tubular epithelium. RCC accounts for about 2-3% of all malignant diseases in adults with ccRCC being the most common histological subtype that represents 70-80% of all cases [131]. Worldwide, incidence registers at 209,000 cases *per annum* while the annual mortality rate is around 102,000. A steady increase in incidence and mortality rates for all stages of RCC has been reported for the last 20 years [131]. RCC is a cancer of the elderly and most patients are diagnosed in the sixth or seventh decade of their lives. There is a noticeable male predominance with men being affected about twice as often as women [92]. While patients with organ-confined disease profit greatly from curative partial or radical nephrectomy with 5-year survival rates as high as 85%, the prognosis of metastatic renal cancer remains poor with 5-year survival rates of less than 10% despite the emergence of novel targeted therapies such as antiangiogenic drugs and mTOR inhibitors during the past decade [2]. About 20%-30% of patients present with metastatic disease and an additional 20%-30%

relapse after attempted curative surgery, illustrating the need for a better understanding of the pathobiology of RCC for the development of novel therapeutic options [2].

The vast majority of renal cell carcinomas are sporadic, nevertheless certain factors increasing the lifetime risk have been identified. Modifiable risk factors include active and passive cigarette smoking, which increases the risk of developing RCC about 2-3 fold, obesity, exposure to cadmium and hypertension [92, 131]. RCC seems to be more common in patients with chronic renal conditions such as end-stage renal disease, acquired renal cystic disease or tuberous sclerosis [131]. In fact, the risk of developing RCC is increased by approximately 30-fold in patients who develop acquired polycystic disease as a complication of chronic dialysis [92].

About 2%-3% of RCC cases present in the context of an inherited cancer syndrome (see Table 1.3 on page 21). Of these, the study of *von Hippel-Lindau syndrome* has provided valuable insight into the pathogenesis of ccRCC. The function of the protein encoded by the affected *VHL* gene is similarly lost in a large number of sporadic ccRCC cases and *VHL* mutation seems to be one of the major underlying events driving ccRCC pathogenesis.

Pathobiology

Subtypes Today, RCC is not considered to be one homogeneous entity, but rather a collection of different tumor types that are derived from distinct parts of the nephron. About 70%-80% of cases present as **ccRCC** which are usually solitary, unilateral, highly vascularized masses, and are histologically characterized by cells with clear cytoplasm that resemble plant cells due to storage of high amounts of lipids and glycogen, embedded in scarce surrounding stroma [92]. The tumor margins tend to be clearly defined but projections into the surrounding parenchyma as well as formation of filial nodules occur, which illustrates the aggressive nature of this invasive carcinoma. Vascular invasion via the renal vein is very frequent, at late stages reaching as far as the inferior vena cava [92]. Papillary RCC comprises 10%-15% of all RCC cases and is characterized by a papillary growth pattern and tumors with multiple foci that often affect both kidneys at the same time. Both clear cell and papillary RCC are thought to arise from the cells of the proximal tubule of the nephron [20]. A third subtype is comprised of chromophobe RCCs which account for 3%-5% of all RCC cases and are derived from the intercalated cells of the collecting duct [92].

Table 1.3.: Cancer syndromes predisposing for RCC, modified from [2] with permission from S. Karger AG.

Syndrome	Affected gene & chromosomal location	Clinical manifestations
von Hippel-Lindau syndrome	*VHL* 3p25-26	**ccRCC**, CNS haemangioblastoma, phaeochromocytoma
Hereditary papillary renal carcinoma	*cMET* 7q31	**papillary RCC**
Hereditary leiomyomatosis and RCC	*FH* 1q42	**papillary RCC**, leiomyomas of skin or uterus, uterine leiomyosarcomas
Birt-Hogg-Dubé	*FLCN* 17p11	Oncocytoma, **chromophobe RCC**, hybrid oncocytic tumor (less frequently, clear cell or papillary RCC), cutaneous fibrofolliculomas
Familial RCC associated with constitutional chromosome 3 translocation	*FHIT* and others 3p and 3q	**Clear cell RCC**

VHL: von Hippel-Lindau, *cMET*: met proto-oncogene, *FH*: fumarate hydratase, *FLCN*: folliculin, *FHIT*: fragile histidine triad

The scope of the study presented in this dissertation is limited to ccRCC as the most frequent subtype of RCC, which is why I will focus on the molecular features of this entity in the following part.

***VHL* and hypoxia-related genes** The genetics and molecular pathology of ccRCC are unique and distinct from other solid cancers. While known cancer genes like the *RAS*-family, *BRAF*, *TP53*, *RB* and *CDKN2A* are largely not part of the mutational spectrum, the vast majority of ccRCCs harbor inactivating mutations in the *VHL* gene, which in turn does not play a large role in most other tumor entities [31]. *VHL* encodes the substrate region of an E3-ubiquitin ligase complex that marks the α-subunit of hypoxia-inducible factor (HIF) transcription factors for degradation. HIF1α or HIF2α associate with HIF1β to form a heterodimeric transcription factor. The heterodimer binds to hypoxia-responsive elements in the regulatory regions of genes and induces the transcription of hypoxia-inducible genes that regulate angiogenesis, metabolism and pH control, among others. The polyubiquitination mediated by the *VHL* gene product depends on the hydroxylation of conserved protein residues of the HIF1/2α proteins in the presence of oxygen. In conditions of hypoxia these residues remain unhydroxylated prohibiting the ligation of ubiquitin, thus permitting HIF to activate the hypoxia pathway [20]. *VHL* lies within a 43-Mb region on chromosome 3p that is monoallelically deleted in approximately 90% of ccRCC tumors. The remaining copy is lost by mutation in about 55% of sporadic ccRCC and the gene is inactivated by promotor hypermethylation in an additional 10% of cases [31]. Inactivation of VHL seems to be an important and early event in renal carcinogenesis as it can be observed even in the smallest renal tumor masses [20]. There seem to exist two distinct subtypes of ccRCC characterized by the expression of genes associated with cellular hypoxia: Dalgliesh and colleagues reported upregulation of hypoxia-associated genes in 75 out of 91 ccRCC cases, most of which also carried a VHL-inactivating mutation [31]. This group proposed a classification into hypoxic and non-hypoxic tumors and reported a distinct mutational and gene expression signature for the two classes [31].

One can further subdivide ccRCC tumors according to the expression profile of the HIF isoforms. Tumors either express HIF1α and HIF2α simultaneously or HIF2α alone. The associated molecular signature is distinct. Tumors expressing both isoforms reportedly exhibit activation of the Akt/mTOR and MAPK pathways and show higher response rates towards antiangiogenetic therapies [20]. Tumors expressing only HIF2α meanwhile are associated more frequently with amplification in the region chromosome 8q24 encompassing the *MYC* gene which is concomitantly overexpressed.

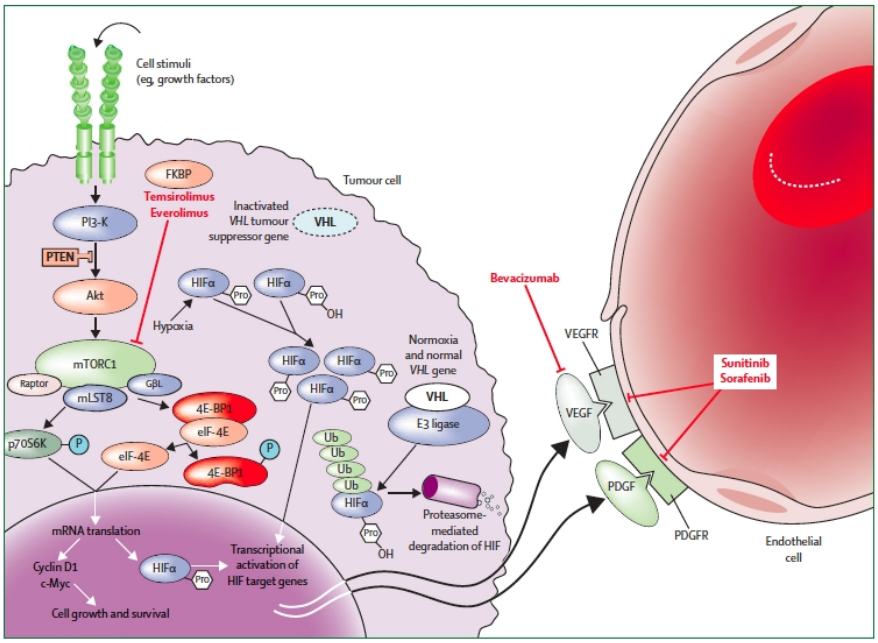

Figure 1.4.: VHL and HIF in the context of targeted therapy. Figure reprinted from [131] with permission from Elsevier.

Inactivation of histone modifying genes Although the loss of *VHL* gene function is undoubtedly an important and early event in renal carcinogenesis, there are certainly other factors involved as well: despite continued efforts, targeted deletion of *VHL* in the murine kidney has not led to an experimental animal model that faithfully recapitulates human carcinogenesis [125]. Interestingly, the region of LOH on chromosome 3p further comprises three other genes frequently mutated in ccRCC: polybromo-1 (*PBRM1*, mutated in 50%), BRCA1-associated protein-1 (*BAP1*, mutated in 15%) and SET domain containing 2 (*SETD2*, mutated in 15%). Of these, mutations in *PBRM1* and *BAP1* tend to be mutually exclusive [125]. Pena-Llopis and colleagues outlined a model for ccRCC development which proposes *VHL* mutation as an early event that is followed by a loss of 3p. The group proposes subsequent mutations in the remaining alleles of *PBRM1* or *BAP1*, respectively, as a divide between distinct molecular subtypes of ccRCC [125]. Intriguingly, the histone H3 lysine 36 methyltransferase *SETD2* was independently identified to harbor inactivating mutations in a subgroup of ccRCC in a large study sequencing 3,544 protein-coding genes of 101 ccRCC cases alongside two other histone modifying genes, *JARID1C* and *UTX* [31]. Mutations within the chromatin remodeling landscape might therefore represent another crucial part in the puzzle of ccRCC-carcinogenesis.

Hippo pathway deregulation in ccRCC The same large systematic sequencing study by Dalgliesh et al. revealed a subgroup of ccRCC tumors within the non-hypoxic class that display somatic truncating mutations in the *NF2* gene. In contrast to the histone-modifying genes *JARID1C* and *SETD2*, none of the *NF2*-mutant ccRCC samples harbored a *VHL* mutation [31]. *NF2* is a member of the Hippo pathway upstream of the core kinase cassette. To this date it is the only pathway member that is a recognized cancer gene in the catalogue of somatic mutations in cancer (COSMIC) and that can be considered a *bona fide* tumor suppressor gene homozygously mutated in about 2% ccRCC cases [64]. Germline-mutations of *NF2* predispose for neurofibromatosis II, a hereditary cancer syndrome associated with the development of acoustic neuromas, meningiomas and schwannomas [31]. Targeted knockout of *NF2* in the proximal convoluted epithelium of *Villin-Cre;NF2*$^{flox/flox}$-mice leads to the formation of intratubular neoplasia within 3 months which progresses to invasive carcinoma in 6-10 month old mice [112]. This model can therefore be considered the first to faithfully depict human renal carcinogenesis, albeit only for a subset of ccRCC tumors.

In addition to mutational events concerning Hippo pathway members, downregulation of the core pathway member SAV1 and consecutive nuclear accumulation of YAP has been reported for a significant subgroup of ccRCC tumors [105]. Of note, copynumber loss on chromosome 14q22, i.e. in the region of the *SAV1* gene, has been previously described in high-grade ccRCC by different groups [49, 105, 176].

1.5. Question addressed in this dissertation

Dysfunctional Hippo signaling and nuclear YAP hyperactivity can be observed in many human tumor tissues. The first question addressed in this dissertation is whether YAP is differentially expressed in human tumor tissue samples in the three entities PDAC, biliary cancer and ccRCC and whether nuclear YAP expression correlates with clinico-pathologic parameters in these tissues.

In a second step, the role of aberrant YAP activity in tumor cell lines is examined by shRNA-mediated knockdown of the protein in selected, highly YAP expressing cell lines. Phenotypic consequences of the knockdown are examined by a wide range of cell-based *in vitro* and *in vivo* assays and results among the three different tumor entities are compared. One of the lead questions, especially regarding the high tissue-context dependency, is whether there is a common phenotype across different types of cancer.

In a third and final step, the transcriptomic output of YAP in the three different tumor entities is compared by gene expression analysis of YAP-knockdown vs. mock transfected cancer cell lines. Hypothetically, the transformative transcriptional output of YAP should display some overlaps in different cancer cells but should also reflect differences in cell types. From the gene expression data, mechanistic considerations for the role of YAP activity in etiology and progression of PDAC, biliary cancers and ccRCC will be attempted.

2. Materials

2.1. Equipment

Table 2.1.: Equipment

Appliance/ tool	**Manufacturer**
Air displacement pipettes (0.1-2.5 µl; 0.5-10.0 µl; 2-20 µl; 10-100 µl; 20-200 µl; 100-1000 µl)	Eppendorf AG, Hamburg, Germany
Air displacement pipettes (0.5-10 µl; 20-200 µl; 100-1000 µl)	Biohit mLINE, Sartorius Biohit Liquid Handling Oy, Helsinki, Finland
Autoclave (tissue culture)	Systec GmbH, Wettenberg, Germany
Balance	Sartorius TE601, Sartorius AG, Göttingen, Germany
Blotting unit	Mini TransBlot Cell, BIO-RAD Laboratories, Hercules, California, USA
Casting unit	BIO-RAD Laboratories, Hercules, California, USA
Cell counter	Scepter 2.0 handheld automated cell counter, Merck Millipore, Billerica, Massachusetts, USA
Cell culture centrifuge	Centrifuge 5810R, Eppendorf AG, Hamburg, Germany
Cell culture incubator	Sanyo MCO18-AIC, Panasonic Healthcare, Osaka, Japan
Digital calipers	Milomex, Pulloxhill, United Kingdom

Table 2.1.: Equipment (continued)

Appliance/ tool	**Manufacturer**
Electrophoresis chamber (horizontal)	PEQLAB 40-1214 and 40-0708, PEQLAB Biotechnologie GmbH, Erlangen, Germany
Electrophoresis power supply	Consort EV 202, Sigma-Aldrich, St. Louis, Missouri, USA
Electrophoresis unit (vertical)	Mini PROTEAN Tetra Cell, BIO-RAD Laboratories, Hercules, California, USA
Freezer (-20 ^{o}C)	Siemens, München, Germany
Freezer (-80 ^{o}C)	Forma 905 -86C ULT Freezer, Thermo Fisher Scientific, Waltham, Massachusetts, USA
Gel documentation system	$ChemiDoc^{TM}$ BIO-RAD Laboratories, Hercules, California, USA
Ice machine	Scotsman AF 20, Scotsman Ice Systems, Vernon Hills, Illinois, USA
Illumina iScan	Applied Biosystems, Darmstadt, Germany
Inverted microscope	Nikon Eclipse TS100, Nikon Instruments Europe B.V., Düsseldorf, Germany
Laminar flow hood, biosafety level II	MSC Advantage (1,8m), Thermo Fisher Scientific, Waltham, Massachusetts, USA
Magnetic stirrer	ARE Heating Magnetic Stirrer, VELP Scientifica, Usmate, Italy
Microcentrifuge	Centrifuge 5430R, Eppendorf AG, Hamburg, Germany
Microscope with camera, upright	Nikon H 550S, Nikon Instruments Europe B.V., Düsseldorf, Germany
Microwave	Panasonic NN-E245WB, Panasonic, Osaka, Japan
Mini centrifuge	miniSpin plus, Eppendorf AG, Hamburg, Germany

Table 2.1.: Equipment (continued)

Appliance/ tool	**Manufacturer**
Mini centrifuge	MiniStar Silverline, VWR, Radnor, Pennsylvania, Germany
Mr. Frosty	Nalgene, Thermo Fisher Scientific, Waltham, Massachusetts, USA
Orbital shaker	Rotamax 120, Heidolph Instruments GmbH, Schwabach, Germany
pH Meter	S20 $SevenEasy^{TM}$ pH, Mettler-Toledo GmbH, Gießen, Germany
Pipette controller for serological pipettes	PIPETBOY acu, INTEGRA Biosciences AG, Zizers, Switzerland
Precision balance	Extend ED124S, Sartorius AG, Göttingen, Germany
Probe sonicator	Branson SLPe 4C15, Branson Ultrasonics, Danbury, Connecticut, USA
Realtime PCR machine	$Realplex^2$ Mastercycler epgradient S, Eppendorf AG, Hamburg, Germany
Refrigerator (+4°C)	Siemens, München, Germany
Rotating tube shaker (1.5 ml)	Intelli-Mixer RM-2M, ELMI Ltd., Riga, Latvia
Shaker incubator	Certomat IS, B. Braun Biotech International, Melsungen, Germany
Spectrophotometer	NanoDrop ND-1000 (PeqLab, Erlangen, Germany)
Suction pump	Membranpumpe MP060E, ilmvac GmbH, Ilmenau, Germany
Thermocycler	Mastercycler pro, Eppendorf AG, Hamburg, Germany
Thermomix	Thermomixer comfort, Eppendorf AG, Hamburg, Germany
Tube rotator	Roller mixer SRT9, Bibby Scientific Limited, Staffordshire, United Kingdom

Table 2.1.: Equipment (continued)

Appliance/ tool	Manufacturer
Ultra deep freezer (-150 ºC)	SANYO MDF-C2156VAN, Panasonic Healthcare, Osaka, Japan
Vortex	2_*X*3 VELP Scientifica, Usmate, Italy
Waterbath	WNB22, Memmert GmbH, Schwabach, Germany

2.2. Consumables

Table 2.2.: Consumables

Item	Manufacturer
6 well tissue culture plates	Sarstedt AG, Nümbrecht, Germany
24 well tissue culture plates	Sarstedt AG, Nümbrecht, Germany
96 well tissue culture plates, flat bottom	Corning Inc., Corning, New York, USA
transwell 24 well plates	BD Biosciences, San Jose, California, USA
Sterile pipettes (5 ml, 10 ml, 25 ml, 50 ml)	Greiner Bio-One GmbH, Frickenhausen, Germany
Sterile conical centrifuge tubes, PP (15 ml, 50 ml)	Greiner Bio-One GmbH, Frickenhausen
1,5 ml microcentrifuge tubes	Sarstedt AG, Nümbrecht
Sterile filtered pipette tips (10 µl, 20 µl, 200 µl, 1000 µl)	Nerbe plus GmbH, Winsen/Luhe, Germany
Pipette tips (1-10 µl, 2-200 µl, 100-1000 µl)	Nerbe plus GmbH, Winsen/Luhe, Germany
8,0 µm cell culture inserts	BD Biosciences, San Jose, California, USA
Tissue culture flasks, (25 cm^2, 75 cm^2, 175 cm^2)	Sarstedt AG, Nümbrecht, Germany
Tissue culture plates, 150 mm	Sarstedt AG, Nümbrecht, Germany
Cell scraper, 1.7 mm blade	Sarstedt AG, Nümbrecht, Germany
Cryo tubes, 2.0 mm, PP, sterile	Sarstedt AG, Nümbrecht, Germany

Table 2.2.: Consumables (continued)

Item	Manufacturer
Scepter Sensors, 60 µm	Merck Millipore, Billerica, Massachusetts, USA
Microscopic slides	Engelbrecht Medizin- und Labortechnik, Edermünde, Germany
Cover slips	Engelbrecht Medizin- und Labortechnik, Edermünde, Germany
Pasteur pipettes, glass	Brand GmbH, Wertheim, Germany
Nuclease-free microcentrifuge tubes (0.2 ml, 0.5 ml 1.5 ml)	Nerbe plus GmbH, Winsen/Luhe
Syringes (2 ml, 20 ml)	Becton, Dickinson and Company, Franklin Lakes, New Jersey, USA
Syringe filters, 0.45 µm pore size	Filtropur S 0.45, PES-Membran, Sarstedt AG, Nümbrecht, Germany
Syringe filters, 0.22 µm pore size	Filtropur S 0.2, PES-Membran, Sarstedt AG, Nümbrecht, Germany

2.3. Chemicals and reagents

2.3.1. Reagents

Table 2.3.: Chemicals and reagents

Product	Manufacturer
2-propanol	AppliChem, Darmstadt, Germany
4-iodophenylboronic acid (4-IPBA)	Sigma-Aldrich, St. Louis, Missouri, USA
Acetic acid, glacial	Merck, Darmstadt, Germany
Agarose, standard	Carl Roth, Karlsruhe, Germany
Agarose, 4%, sterile	Life Technologies, Carlsbad, California, USA
AKASOLV Aqua Care	Dr. Kilic AKADIA-CHEMIE, Mannheim, Germany
Ammonium persulfate (APS)	Carl Roth, Karlsruhe, Germany

Table 2.3.: Chemicals and reagents (continued)

Product	Manufacturer
β-mercaptoethanol	Sigma-Aldrich, St. Louis, Missouri, USA
Bovine serum albumin, fraction V, molecular biology grade	Carl Roth, Karlsruhe, Germany
Citric acid, anhydrous	AppliChem, Darmstadt, Germany
Crystal violet	Sigma-Aldrich, St. Louis, Missouri, USA
Cytoseal 60	Thermo Fisher Scientific, Waltham, Massachusetts, USA
Dimethyl sulfoxide (DMSO), cell culture grade	Sigma-Aldrich, St. Louis, Missouri, USA
Disodium ethylenediaminetetraacetate (Na_2(EDTA)) dihydrate	Sigma-Aldrich, St. Louis, Missouri, USA
Ethanol, 70%, denatured	Otto Fischar, Saarbrücken, Germany
Ethanol, anhydrous, molecular biology grade	AppliChem, Darmstadt, Germany
Ethidium bromide solution (10 mg/ml)	Sigma-Aldrich, St. Louis, Missouri, USA
Formaldehyde, 37%, analytical grade	Merck, Darmstadt, Germany
Formalin, 4%	Otto Fischar, Saarbrücken, Germany
Fugene 6	Roche Applied Science, Penzberg, Germany
Glycerol	Merck, Darmstadt, Germany
Glycine, synthetical quality	Carl Roth, Karlsruhe, Germany
Hematoxylin solution, Harris modified	Sigma-Aldrich, St. Louis, Missouri, USA
Hydrochloric acid	Carl Roth, Karlsruhe, Germany
Igepal CA 630	Sigma-Aldrich, St. Louis, Missouri, USA
Luminol	Sigma-Aldrich, St. Louis, Missouri, USA
Matrigel	BD Biosciences, Franklin Lakes, New Jersey, USA
Methanol, analytical grade	AppliChem, Darmstadt, Germany
Nonfat dry milk	Carl Roth, Karlsruhe, Germany
Nuclease-free water	Life Technologies, Carlsbad, California, USA
Phosphatase inhibitor cocktail 2	Sigma-Aldrich, St. Louis, Missouri, USA

Table 2.3.: Chemicals and reagents (continued)

Product	**Manufacturer**
Phosphatase inhibitor cocktail 3	Sigma-Aldrich, St. Louis, Missouri, USA
Ponceau S solution	Sigma-Aldrich, St. Louis, Missouri, USA
Protease inhibitor cocktail	Sigma-Aldrich, St. Louis, Missouri, USA
RotiLoad, 4 × loading dye	Carl Roth, Karlsruhe, Germany
Rotiphorese NF-Acrylamide/ bis solution, 30% (29:1)	Carl Roth, Karlsruhe, Germany
Sodium dodecyl sulfate (SDS), molecular biology grade	AppliChem, Darmstadt, Germany
Sodium acetate trihydrate	Merck, Darmstadt, Germany
Sodium chloride, analytical grade	AppliChem, Darmstadt, Germany
Sodium hydrogen carbonate ($NaHCO_3$)	Merck, Darmstadt, Germany
Sodium hydroxide, pellets	Sigma-Aldrich, St. Louis, Missouri, USA
Sodium hydroxide solution, 5 N	Carl Roth, Karlsruhe, Germany
Sodium deoxycholate	Sigma-Aldrich, St. Louis, Missouri, USA
TEMED (N,N,N',N'-Tetramethylene-ethylenediamine)	Carl Roth, Karlsruhe, Germany
TRITON X-100	Sigma-Aldrich, St. Louis, Missouri, USA
Trizma base	Sigma-Aldrich, St. Louis, Missouri, USA
Xylenes, histological grade	AppliChem, Darmstadt, Germany

2.3.2. Ready-made kits

Table 2.4.: Ready-made kits

Product	Manufacturer
BCA Assay	Thermo Fisher Scientific, Waltham, Massachusetts, USA
CellTiter 96 AQueous One Solution Cell Proliferation Assay	Promega, Fitchburg, Wisconsin, USA
HumanHT-12v4.0 Expression Bead Arrays	Illumina, San Diego, California, USA
Illumina Total Prep RNA Amplification Kit	Illumina, San Diego, California, USA
LB Amp Ready Mix	Fermentas by Thermo Fisher Scientific, Waltham, Massachusetts, USA
LB Liquid Amp Ready Media	Fermentas by Thermo Fisher Scientific, Waltham, Massachusetts, USA
PureYield Plasmid Midiprep	Promega, Fitchburg, Wisconsin, USA
QiaPrep Spin Miniprep	Qiagen, Hilden, Germany
Qiashredder	Qiagen, Hilden, Germany
RNase free DNase I Set	Qiagen, Hilden, Germany
RNeasy Mini Kit	Qiagen, Hilden, Germany

2.3.3. Biochemicals and enzymes

Table 2.5.: Biochemicals and enzymes

Product	Manufacturer
dNTP Set, 100 mM Solutions	Fermentas by Thermo Fisher Scientific, Waltham, Massachusetts, USA
DreamTaq Green DNA Polymerase	Fermentas by Thermo Fisher Scientific, Waltham, Massachusetts, USA
FastDigest BamHI	Fermentas by Thermo Fisher Scientific, Waltham, Massachusetts, USA
High Capacity cDNA Reverse Transcription Kit	Life Technologies, Carlsbad, California, USA

Table 2.5.: Biochemicals and enzymes (continued)

Product	**Manufacturer**
Protein A agarose	Sigma-Aldrich, St. Louis, Missouri, USA
Protein G plus agarose	Santa Cruz Biotechnology, Santa Cruz, California, USA
RiboLock RNase Inhibitor	Fermentas by Thermo Fisher Scientific, Waltham, Massachusetts, USA
Sonicated salmon sperm DNA	Applichem, Darmstadt, Germany
SYBR Premix Ex Taq™ (Tli RNase H Plus)	TaKaRa Bio Europe, Saint-Germain-en-Laye, France

2.4. Antibodies

Table 2.6.: Primary Antibodies

Primary antibodies for Immunohistochemistry		
Antigen	**Clone/ catalogue no.**	**Manufacturer**
Cytokeratin	mouse monoclonal, clones AE1/AE3/ M3515	Dako, Glostrup, Denmark
EDN2	rabbit polyclonal/ NBP1-87942	Novus Biologicals, Littleton, Colorado, USA
SAV1	mouse monoclonal, clone 3B2/ H00060485-M02	Abnova, Taipei City, Taiwan
YAP	rabbit polyclonal/ 4912	Cell Signaling Technology, Danvers, Massachusetts, USA
pYAP	rabbit polyclonal/ 4911	Cell Signaling Technology, Danvers, Massachusetts, USA
Primary antibodies for Western blot		
Antigen	**Clone/ catalogue no.**	**Manufacturer**
GAPDH	rabbit monoclonal, clone 14C10/ 2118	Cell Signaling Technology, Danvers, Massachusetts, USA
LKB1	mouse monoclonal, clone Ley 37/G6/ sc-32245	Santa Cruz Biotechnology, Santa Cruz, California, USA
SAV1	mouse monoclonal, clone 3B2/ H00060485-M02	Abnova, Taipei City, Taiwan
TEF-1/TEAD1	mouse monoclonal, clone H-4/ sc-376113	Santa Cruz Biotechnology, Santa Cruz, California, USA
TEF4/TEAD2	rabbit polyclonal/ sc-67115	Santa Cruz Biotechnology, Santa Cruz, California, USA
VGLL1	rabbit polyclonal/ ab48921	Abcam, Cambridge, United Kingdom
YAP	rabbit polyclonal/ sc-15407	Santa Cruz Biotechnology, Santa Cruz, California, USA
YAP	rabbit polyclonal/ 4912	Cell Signaling Technology, Danvers, Massachusetts, USA
pYAP	rabbit polyclonal/ 4911	Cell Signaling Technology, Danvers, Massachusetts, USA

Primary antibodies for Chromatin Immunoprecipitation		
Antigen	**Clone/ catalogue no.**	**Manufacturer**
Acetyl Histone H3	rabbit polyclonal/ 06-599B	Merck Millipore, Billerica, Massachusetts, USA
normal rabbit IgG	rabbit polyclonal/ PP64B	Merck Millipore, Billerica, Massachusetts, USA
normal mouse IgG	mouse monoclonal, clone 3B2/ sc-69786	Santa Cruz Biotechnology, Santa Cruz, California, USA
TEF-1/TEAD1	mouse monoclonal, clone H-4/ sc-376113X	Santa Cruz Biotechnology, Santa Cruz, California, USA
TEF4/TEAD2	rabbit polyclonal/ sc-67115X	Santa Cruz Biotechnology, Santa Cruz, California, USA
YAP	mouse monoclonal, clone G-6/ sc-376830X	Santa Cruz Biotechnology, Santa Cruz, California, USA

Table 2.7.: Secondary Antibodies

Secondary antibodies for Western blot		
Antigen	**Clone/ catalogue no.**	**Manufacturer**
Rabbit IgG	goat polyclonal, HRP-coupled/ 7074	Cell Signaling Technology, Danvers, Massachusetts, USA
Mouse IgG	horse polyclonal, HRP-coupled/ 7076	Cell Signaling Technology, Danvers, Massachusetts, USA

2.5. Plasmids

For the generation of stable knockdowns, clones expressing sequences for short hairpin RNAs directed against mRNA of YAP1 were ordered from The RNAi Consortium (TRC) Lentiviral shRNA Library, available at Open Biosystems, a branch of Thermo Scientific Inc.. Two clones showing the best knockdown efficiency in preliminary experiments were selected from a set of five and used in the experiments for this dissertation.

Table 2.8.: Plasmids

shRNA-plasmids		
Name	**Mature antisense shRNA-sequence**	**Source, Reference**
pLKO.1 Clone TRCN0000107268 "YAPshRNA#4"	AAA GGA TCT GAG CTA TTG GTC	Open Biosystems by Thermo Scientific, [161]
pLKO.1 Clone TRCN0000107269 "YAPshRNA#5"	AAG GAT CTG AGC TAT TGG TCG	Open Biosystems by Thermo Scientific, [161]
pLKO.1	empty vector	Open Biosystems by Thermo Scientific, [161]
Packaging plasmids		
Name	**Purpose**	**Source, Reference**
pCMV-VSV-G	carries sequence of the VSV-G protein for pseudotyping of lentiviral particles	Addgene plasmid no. 8454, [155]
pCMV-dR8.2	packaging plasmid for construction of replication-deficient lentiviral particles	Addgene plasmid no. 8455, [155]

2.6. Oligonucleotides

Sequences for oligonucleotides were retrieved from published literature where indicated. Primer sequences for RT-qPCR were retrieved from PrimerBank (http://pga.mgh.harvard.edu/primerbank/index.html) [152, 153, 170, 171]. Primers for ChIP-qPCR were designed using Primer3 [87, 164] and blasted against the reference assembly of the human genome provided by the *GeneBank* of the National Institute of Health, Bethesda, Maryland, USA (http://ncbi.nlm.nih.gov) to check for unintentional products on off-target sequences. Parameters on Primer3 were set to meet the requirements of primers for RT-qPCR experiments (length of oligonucleotides: 18-22 bp, product length: <150 bp, T_m: 58-62 ºC)

All primers were ordered at a synthesis scale of 25 nmoles from Life Technologies (Carlsbad, California, USA). Oligonucleotides were desalted and shipped freeze-dried at room temperature. They were reconstituted with nuclease-free water to obtain a 100 μM stock solution (stored at -20 ºC) which was further diluted 1:10 into working solutions kept at 4 ºC. Concentration in PCR reactions was 0.5 μM unless indicated otherwise.

Table 2.9.: Oligonucleotides

Primer	**Sequence 5' – 3'**	
	Primers for PCR	
Myco C	GGG AGC AAA CAG GAT TAG ATA CCC T	[165]
Myco D	TGC ACC ATC TGT CAC TCT GTT AAC CTC	[165]
	Primers for RT-qPCR	
CD74 sense	CCG GCT GGA CAA ACT GAC A	
CD74 antisense	GGT GCA TCA CAT GGT CCT CTG	
CDH6 sense	AGA ACT TAC CGC TAC TTC TTG C	
CDH6 antisense	TGC CCA CAT ACT GAT AAT CGG A	
CDK6 sense	CCA GAT GGC TCT AAC CTC AGT	
CDK6 antisense	AAC TTC CAC GAA AAA GAG GCT T	
CTGF sense	AAA AGT GCA TCC GTA CTC CCA	
CTGF antisense	CCG TCG GTA CAT ACT CCA CAG	
CYR61 sense	GGT CAA AGT TAC CGG GCA GT	
CYR61 antisense	GGA GGC ATC GAA TCC CAG C	

Table 2.9.: Oligonucleotides(continued)

Primer	**Sequence 5' – 3'**
DUSP10 sense	TGA AGC ACA CTC GGA TGA CC
DUSP10 antisense	CCT CGA ACT CTA GCA ACT GCC
EDN1 sense	AGA GTG TGT CTA CTT CTG CCA
EDN1 antisense	CTT CCA AGT CCA TAC GGA ACA A
EDN2 sense	CGT CCT CAT CTC ATG CCC AAG
EDN2 antisense	AGG CCG TAA GGA GCT GTC T
F3 sense	GGC GCT TCA GGC ACT ACA A
F3 antisense	TTG ATT GAC GGG TTT GGG TTC
FOLR1 sense	GCT CAG CGG ATG ACA ACA CA
FOLR1 antisense	CCT GGC CCA TGC AAT CCT T
GADD45 sense	TGC TGT GAC AAC GAC ATC AAC
GADD45 antisense	GTG AGG GTT CGT GAC CAG G
GAPDH sense	TGC ACC ACC AAC TGC TTA GC
GAPDH antisense	GGC ATG GAC TGT GGT CAT GAG
IGFBP3 sense	AGA GCA CAG ATA CCC AGA ACT
IGFBP3 antisense	GGT GAT TCA GTG TGT CTT CCA TT
IGFBP5 sense	TGA CCG CAA AGG ATT CTA CAA G
IGFBP5 antisense	CGT CAA CGT ACT CCA TGC CT
KLF6 sense	GGC AAC AGA CCT GCC TAG AG
KLF6 antisense	CTC CCG AGC CAG AAT GAT TTT
MYC sense	GTC AAG AGG CGA ACA CAC AAC
MYC antisense	TTG GAC GGA CAG GAT GTA TGC
NDRG1 sense	CTC CTG CAA GAG TTT GAT GTC C
NDRG1 antisense	AGA GCC ATG TAA AGT CTC GAT GT
PLAC8 sense	GTG TGA CTG TTT CAG CGA CTG
PLAC8 antisense	CTG CAA CTT GAC ACC CAA GG
S100P sense	AAG GAT GCC GTG GAT AAA TTG C
S100P antisense	ACA CGA TGA ACT CAC TGA AGT C
SNX4 sense	GAG TCA GAG CTA GAG TAG CAG AT
SNX4 antisense	ATG GCA CTC CAT TCA CTG AAA A
TAGLN sense	CCG TGG AGA TCC CAA CTG G
TAGLN antisense	CCA TCT GAA GGC CAA TGA CAT

Table 2.9.: Oligonucleotides(continued)

Primer	**Sequence 5' – 3'**	
THBS1 sense	AGA CTC CGC ATC GCA AAG G	
THBS1 antisense	TCA CCA CGT TGT TGT CAA GGG	
VGLL1 sense	TCA GAG TGA AGG TGT GAT GCT	
VGLL1 antisense	GCA CGG TTT GTG ACA GGT ACT	
YAP1 sense	TAG CCC TGC GTA GCC AGT TA	
YAP1 antisense	TCA TGC TTA GTC CAC TGT CTG T	
Primers for ChIP-qPCR		
GAPDH sense	TAC TAG CGG TTT TAC GGG CG	[108]
GAPDH antisense	TCG AAC AGG AGG AGC AGA GAG CGA	[108]

2.7. Cell culture supplies

2.7.1. Cell culture reagents

Table 2.10.: Cell culture reagents

Basic media	
DMEM, high glucose (4,5 g/l), stable glutamine	PAA Laboratories, Pasching, Austria
DMEM, low glucose (1 g/l), stable glutamine	Life Technologies, Carlsbad, California, USA
M3 BaseA medium, with antibiotics	Incell, San Antonio, Texas, USA
OptiMEM I	Life Technologies, Carlsbad, California, USA
RPMI 1640, stable glutamine	PAA Laboratories, Pasching, Austria
Supplements	
Reagent	**Manufacturer**
recombinant human Endothelial Growth Factor (EGF)	ReliaTech, Wolfenbüttel, Germany
Fetal calf serum (FCS), standard, heat inactivated	PAA Laboratories, Pasching, Austria
MEM vitamin solution, 100 ×	Sigma-Aldrich, St. Louis, Missouri, USA
MEM Non-essential amino acids, 100 ×	PAA Laboratories, Pasching, Austria
Sodium pyruvate, 100 mM	PAA Laboratories, Pasching, Austria
Antibiotics	
Gentamycin 50 mg/ml, CELLPURE	Carl Roth, Karlsruhe, Germany
Penicillin/Streptomycin, 10,000 I.U./ml and 10,000 µg/ml	PAA Laboratories, Pasching, Austria
Plasmocin, 25 mg/ml	Invivogen, San Diego, California, USA
Puromycin, 10 mg/ml	Life Technologies, Carlsbad, California, USA
Buffers and solutions	
DPBS without Ca^{2+} or Mg^{2+}	PAA Laboratories, Pasching, Austria
Trypsin-EDTA, 0.05 %/ 0.02 % in PBS	PAA Laboratories, Pasching, Austria

2.7.2. Cell culture media

Table 2.11.: Cell culture media

293FT medium	
DMEM, high glucose (4,5 g/l), stable glutamine	500 ml
FCS, heat inactivated	50 ml
MEM Non-essential amino acids	5.5 ml
Sodium pyruvate, 100 mM	5.5 ml
Penicillin/Streptomycin, 10,000 I.U./ml and 10,000 µg/ml	5.5 ml
Plasmocin 25 mg/ml	100 μl
DMEM full medium	
DMEM, high glucose (4,5 g/l), stable glutamine	500 ml
FCS, heat inactivated	50 ml
Penicillin/Streptomycin, 10,000 I.U./ml and 10,000 µg/ml	5.5 ml
Plasmocin 25 mg/ml	100 μl
HPNE medium	
DMEM, low glucose (1 g/l), stable glutamine	375 ml
M3 BaseA medium, with antibiotics	125 ml
FCS, heat inactivated	25 ml
Gentamycin 50 mg/ml	250 μl
rh EGF	10 μg/ml
Penicillin/Streptomycin, 10,000 I.U./ml and 10,000 µg/ml	5.5 ml
Plasmocin 25 mg/ml	100 μl
RPMI full medium	
RPMI 1640, stable glutamine	500 ml
FCS, heat inactivated	50 ml
Penicillin/Streptomycin, 10,000 I.U./ml and 10,000 µg/ml	5.5 ml
Plasmocin 25 mg/ml	100 μl

PL medium	
DMEM, high glucose (4,5 g/l), stable glutamine	500 ml
FCS, heat inactivated	50 ml
MEM vitamin solution	5.5 ml
MEM Non-essential amino acids	5.5 ml
Sodium pyruvate, 100 mM	5.5 ml
Penicillin/Streptomycin, 10,000 I.U./ml and 10,000 µg/ml	5.5 ml
Plasmocin 25 mg/ml	100 μl

Cell lines transduced with lentivirus were selected by adding the appropriate, predetermined concentration of puromycin to the regular full cell culture medium. Selected puromycin-resistant polyclonal cell lines were kept continuously in selection medium.

2.7.3. Cell lines

Pancreatic cancer cell lines

Table 2.12.: PDAC cell lines

Cell line	**Catalogue No./ Reference**	**Source**
AsPC-1	ATCC-CRL-1682	American Type Culture Collection, Manassas, Virginia, USA
Description:	AsPC-1 is an adherent cell line derived from malignant ascites of a 62-year-old Caucasian woman with pancreatic adenocarcinoma.	
BxPC-3	ATCC-CRL-1687	American Type Culture Collection, Manassas, Virginia, USA
Description:	BxPC-3 is an adherent cell line derived from a pancreatic tumor of a 61-year-old Caucasian woman with pancreatic adenocarcinoma.	
Capan-1	ATCC-HTB-79	American Type Culture Collection, Manassas, Virginia, USA
Description:	Capan-1 is an adherent cell line derived from the liver metastasis of a 40-year-old Caucasian man with pancreatic adenocarcinoma.	
CFPAC	ATCC-CRL-1918	American Type Culture Collection, Manassas, Virginia, USA
Description:	CFPAC is an adherent cell line derived from the liver metastasis of a 26-year-old Caucasian man with pancreatic ductal adenocarcinoma and cystic fibrosis.	
E3LZ10.07 (syn. A10.7)	[30], [39]	Kindly provided by Prof. Dr. Anirban Maitra, Johns Hopkins University, Baltimore, Maryland, USA
Description:	E3LZ10.07 is an adherent cell line derived from the liver metastasis of a 60-year-old man with pancreatic ductal adenocarcinoma.	

Table 2.12.: PDAC cell lines (continued)

Cell line	Catalogue No./ Reference	Source
L3.6pl	[18]	Kindly provided by Prof. Dr. Anirban Maitra, Johns Hopkins University, Baltimore, Maryland, USA
Description:	L3.6pl is a highly metastatic adherent cell line derived via several cycles of in vivo-selection of the human pancreatic adenocarcinoma cell line COLO357 in nude mice. COLO357 cells were derived from the lymph-node metastasis of a 77-year-old African-American woman with pancreatic ductal adenocarcinoma [110].	
MIAPaCa-2	ATCC-CRL-1420	American Type Culture Collection, Manassas, Virginia, USA
Description:	MIAPaCa-2 is an adherent cell line derived from the pancreatic tumor of a 65-year-old Caucasian man with pancreatic cancer.	
PANC-1	ATCC-CRL-1469	American Type Culture Collection, Manassas, Virginia, USA
Description:	PANC-1 is an adherent cell line derived from the pancreatic ductal tumor of a 56-year-old Caucasian man with pancreatic epithelioid carcinoma.	
Panc 1.98 (syn. Pa20C)	[30]	Kindly provided by Prof. Dr. Anirban Maitra, Johns Hopkins University, Baltimore, Maryland, USA
Description:	Panc 1.98 is an adherent cell line derived from the primary pancreatic tumor of a 69-year-old man with pancreatic ductal adenocarcinoma.	
Panc 10.05	ATCC-CRL-2547	American Type Culture Collection, Manassas, Virginia, USA
Description:	Panc 10.05 is an adherent cell line derived from the pancreatic tumor of an adult Caucasian man with pancreatic adenocarcinoma.	

Table 2.12.: PDAC cell lines (continued)

Cell line	Catalogue No./ Reference	Source
PK9	[83]	Kindly provided by Prof. Dr. Anirban Maitra, Johns Hopkins University, Baltimore, Maryland, USA
Description:	PK9 is an adherent cell line derived from a tumor of the head of the pancreas of a patient with moderately differentiated tubular adenocarcinoma of the pancreas.	
Su86.86	ATCC-CRL-1837	American Type Culture Collection, Manassas, Virginia, USA
Description:	Su86.86 is an adherent cell line derived from the liver metastasis of a 57-year-old Caucasian woman with pancreatic ductal adenocarcinoma.	
SW 1990	ATCC-CRL-2172	American Type Culture Collection, Manassas, Virginia, USA
Description:	SW 1990 is an adherent cell line derived from the splenic metastasis of a 56-year-old Caucasian man with pancreatic adenocarcinoma.	

All human pancreatic cancer cell lines were cultured in PL medium, see 2.11. Lentivirally transduced Panc 10.05 or PK9 cells were selected in PL medium containing 3.0 μg/ml puromycin and maintained continuously in selection medium.

Cholangiocellular carcinoma cell lines

Table 2.13.: CCC cell lines

Cell line	Catalogue No./ Reference	Source
G-415	[88]	Kindly provided by Prof. Dr. Anirban Maitra, Johns Hopkins University, Baltimore, Maryland, USA
Description:	G-415 is an adherent cell line derived from malignant ascites of a 68-year-old man with gallbladder adenocarcinoma.	

Table 2.13.: CCC cell lines (continued)

Cell line	Catalogue No./ Reference	Source
GBD-1	[147], [98]	Kindly provided by Prof. Dr. Anirban Maitra, Johns Hopkins University, Baltimore, Maryland, USA
Description:	GBD-1 is an adherent cell line derived from a lymph-node metastasis of a 58-year-old man with poorly differentiated adenocarcinoma of the gallbladder.	
HuCCT-1	[109]	Kindly provided by Prof. Dr. Anirban Maitra, Johns Hopkins University, Baltimore, Maryland, USA
Description:	HuCCT-1 is an adherent cell line derived from malignant ascites of a 56-year-old man with moderately differentiated intrahepatic cholangiocellular carcinoma.	
Nec	[40], [41]	Kindly provided by Prof. Dr. Ulrich Spengler, Rheinische Friedrich-Wilhelms-Universität, Bonn, Germany
Description:	Nec is an adherent cell line derived via in vivo-selection of the human cholangiocellular adenocarcinoma cell line ETK-1 by serial transplantation in nude mice. ETK-1 cells were derived from the malignant ascites of a 64-year-old Japanese patient with intrahepatic cholangiocellular carcinoma [40].	
RBE	[40], [41]	Kindly provided by Prof. Dr. Ulrich Spengler, Rheinische Friedrich-Wilhelms-Universität, Bonn, Germany
Description:	RBE is an adherent cell line derived from the malignant ascites of a 64-year-old Japanese woman with intrahepatic cholangiocellular carcinoma.	

Table 2.13.: CCC cell lines (continued)

Cell line	**Catalogue No./ Reference**	**Source**
SNU308	[91]	Korean Cell Line Bank, Seoul National University College of Medicine, Seoul, Korea
Description:	SNU308 is an adherent cell line derived from the primary tumor of a Korean patient with moderately differentiated adenocarcinoma of the gallbladder.	
SNU478	[91]	Korean Cell Line Bank, Seoul National University College of Medicine, Seoul, Korea
Description:	SNU478 is an adherent cell line derived from the primary tumor of a Korean patient with poorly differentiated adenocarcinoma of the ampulla of Vater.	
TFK-1	ACC-344 and [136]	Leibniz Institute-DSMZ German Collection of Microorganisms and Cell Cultures, Braunschweig, Germany
Description:	TFK-1 is an adherent cell line derived from the primary tumor of a 63-year-old male patient with extrahepatic cholangiocellular carcinoma.	

All human biliary cancer cell lines were cultured in RPMI full medium, see 2.11. Lentivirally transduced Nec or G-415 cells were selected in RPMI full medium containing 3.0 μg/ml puromycin and maintained continuously in selection medium.

Renal cell carcinoma cell lines

Table 2.14.: RCC cell lines

Cell line	Catalogue No./ Reference	Source
A498	ATCC-HTB-44	American Type Culture Collection, Manassas, Virginia, USA
Description:	A498 is an adherent cell line derived from the primary tumor of a 52-year-old female patient with renal cell carcinoma.	
ACHN	ATCC-CRL-1611	American Type Culture Collection, Manassas, Virginia, USA
Description:	ACHN is an adherent cell line derived from the malignant pleural effusion of a 22-year-old Caucasian male patient with widely metastatic renal adenocarcinoma.	
Caki-2	ATCC-HTB-47	American Type Culture Collection, Manassas, Virginia, USA
Description:	Caki-2 is an adherent cell line derived from the primary tumor of a 69-year-old Caucasian male patient with clear cell renal cell carcinoma.	
MZ1774	[143]	Kindly provided by Prof. Dr. Peter Brossart, Rheinische Friedrich-Wilhelms-Universität, Bonn, Germany
Description:	MZ1774 is an adherent cell line derived from the primary tumor of a patient with renal cell carcinoma.	
B1	[163]	Kindly provided by Prof. Dr. Ingo Schmidt-Wolf, Rheinische Friedrich-Wilhelms-Universität, Bonn, Germany
Description:	B1 is an adherent cell line derived from the primary tumor of a patient with renal cell carcinoma.	

Table 2.14.: RCC cell lines (continued)

Cell line	**Catalogue No./ Reference**	**Source**
B3	[163]	Kindly provided by Prof. Dr. Ingo Schmidt-Wolf, Rheinische Friedrich-Wilhelms-Universität, Bonn, Germany
Description:	B3 is an adherent cell line derived from the primary tumor of a patient with renal cell carcinoma.	
RCC177	[148]	Kindly provided by Prof. Dr. Ingo Schmidt-Wolf, Rheinische Friedrich-Wilhelms-Universität, Bonn, Germany
Description:	RCC177 is an adherent cell line derived from the primary tumor of a patient with renal cell carcinoma.	

Human RCC cell lines A498, Caki-2, MZ1774, B1, B3, and RCC177 were cultured in RPMI full medium (see 2.11) while ACHN was maintained in DMEM full medium (see 2.11) Lentivirally transduced A498, MZ1774 or ACHN cells were selected in RPMI or DMEM full medium containing 3.0 μg/ml puromycin and continuously maintained in selection medium.

Other cell lines

Table 2.15.: Other cell lines

Cell line	Catalogue No./ Reference	Source
293FT	R700-07	Life Technologies, Carlsbad, California, USA
Description:	The 293FT Cell Line is derived from the 293F Cell Line and stably expresses the SV40 large T antigen from the pCMVSPORT6TAg.neo plasmid. Expression of the SV40 large T antigen is controlled by the human cytomegalo-virus (CMV) promoter and is high-level and constitutive. Studies have demonstrated maximal virus production in human 293 cells expressing SV40 large T antigen [115], making the 293FT cell line a suitable host for generating lentiviral constructs. The parental 293 cell line is a permanent line established from primary embryonal human kidney transformed with sheared human adenovirus type 5 DNA [50]. 293FT cells were used in this study as a host cell line to generate lentiviral particles.	
hTERT-HPNE	ATCC-CRL-4023	American Type Culture Collection, Manassas, Virginia, USA
Description:	The hTERT-HPNE cell line was developed from normal human pancreatic ductal cells of a healthy 52-year-old male donor by transduction with a retroviral expression vector (pBABEpuro) containing the hTERT gene. The infected cells became positive for telomerase, failed to senesce, and continued to proliferate. HPNE cells were found to have properties of the intermediary cells formed during acinar-to-ductal metaplasia, which included their undifferentiated phenotype, expression of Nestin and, evidence of active Notch signaling. HPNE cells were used as a normal control cell line alongside malignant PDAC cell lines.	

293FT cells were maintained in 293FT medium (2.11) as per instructions provided by the distributor. Human pancreatic nestin-expressing (HPNE) cells were cultured as previously described by Lee et al. [94], see 2.11.

2.8. Experimental animals

2.8.1. CD1$^{nu/nu}$-mice

Nude mice were first discovered in 1962, when a spontaneous mutation in the *FOXN1* gene caused the hairless "nude" phenotype [46]. This mutation also causes the absence of a functional thymus, therefore the animals cannot generate mature T-cells and are unable to mount most immune responses adequately. This immune-defect makes them suitable hosts for tumor-xenograft studies because they fail to mount an adequate immune response against foreign tissue and therefore tolerate and maintain growing human cancer cells.

The CD1$^{nu/nu}$ strain was developed from the transfer of the nude gene from Crl:NU-Foxn1^{nu} to a CD-1 mouse through a series of crosses and backcrosses beginning in 1979 at Charles River, Wilmington, MA.

For xenograft experiments, six-week-old, male CD1$^{nu/nu}$ mice were ordered from Charles River, Wilmington, Massachusetts, USA and kept in the laboratory animal facility of the University of Bonn („Haus für Experimentelle Therapie“ HET) in specific pathogen free (SPF) conditions. The animals were provided with food and water *ad libitum*.

2.9. Solutions and buffers

Stock Solutions

Table 2.16.: 1 M Tris-HCl, pH 7.4

Component	Composition
Trizma base	121.14 g
ultrapure water	ad 1.0 l
Dissolve in approximately 800 ml ultrapure water, adjust pH to 7.4 with concentrated hydrochloric acid. Fill up to 1.0 l with ultrapure water.	

Table 2.17.: 1.0 M Tris-HCl, pH 8.0

Component	Composition
Trizma base	121.14 g
ultrapure water	ad 1.0 l
Dissolve in approximately 800 ml ultrapure water, adjust pH to 8.0 with concentrated hydrochloric acid. Fill up to 1.0 l with ultrapure water.	

Table 2.18.: 0.5 M Tris-HCl, pH 6.7

Component	Concentration
Trizma base	60.57 g
ultrapure water	ad 1.0 l
Dissolve in approximately 800 ml ultrapure water, adjust pH to 6.7 with concentrated hydrochloric acid. Fill up to 1.0 l with ultrapure water.	

Table 2.19.: 1.5 M Tris-HCl, pH 8.8

Component	Concentration
Trizma base	181.71 g
ultrapure water	ad 1.0 l
Dissolve in approximately 800 ml ultrapure water, adjust pH to 8.8 with concentrated hydrochloric acid. Fill up to 1.0 l with ultrapure water.	

Table 2.20.: 250 mM EDTA, pH 8

Component	Concentration
Na_2−EDTA × 2 H_2O	23.26 g
ultrapure water	ad 250.0 ml
Dissolve in approx. 200 ml ultrapure water, adjust pH to 8 with 5 N NaOH. Fill up to 250.0 ml with ultrapure water.	

Table 2.21.: 10% (w/v) SDS

Component	Concentration
SDS	10 g
ultrapure water	ad 100.0 ml
Dissolve in approx. 80 ml ultrapure water. Fill up to 100.0 ml with ultrapure water.	

Table 2.22.: 250 mM Luminol

Component	Amount
Luminol	443 mg
DMSO	ad 10.0 ml
Dissolve in DMSO and distribute into 260 μl aliquots. Store aliquots at -20 ºC	

Table 2.23.: 90 mM 4-IPBA

Component	Amount
4-IPBA	1115 mg
DMSO	ad 50.0 ml
Dissolve in DMSO and distribute into 1150 μl aliquots. Store aliquots at -20 ºC	

General Buffers and Solutions

Table 2.24.: 0.05% (w/v) Crystal violet solution

Component	Concentration
Crystal violet	250 mg
ultrpure water	ad 500.0 ml
Dissolve in approx. 400 ml ultrapure water. Fill up to 500.0 ml with ultrapure water.	

Table 2.25.: 10 × citrate buffer, pH 6.0 (IHC)

Component	Amount	Conc.
Citric acid	19.2 g	100 mM
ultrapure water	ad 1.0 l	
Dissolve in approx. 800 ml ultrapure water, adjust pH to 6.0 with 5 N NaOH fill up to 1.0 l with ultrapure water.		

Table 2.26.: 10 × TBS, pH 8.0

Component	Amount	Conc.
1 M Tris−HCl, pH 8.0	100.0 ml	100 mM
NaCl	48.15 g	825 mM
ultrapure water	ad 1.0 l	
Dissolve in approx. 800 ml ultrapure water, fill up to 1.0 l with ultrapure water.		

Table 2.27.: 10 × TBS, pH 7.4

Component	Amount	Conc.
1 M Tris−HCl, pH 7.4	100.0 ml	100 mM
NaCl	48.15 g	1.5 M
ultrapure water	ad 1.0 l	
Dissolve in approx. 800 ml ultrapure water, fill up to 1.0 l with ultrapure water.		

Table 2.28.: TBST 0.01%

Component	Composition
10 × TBS	100.0 ml
Tween 20	1 ml
ultrapure water	ad 1.0 l
Dilute 1:10 with ultrapure water and add Tween 20.	

Table 2.29.: 50 × TAE-buffer

Component	Amount	conc.
Trizma base	242.0 g	40 mM
Glacial acetic acid	57.1 ml	20 mM
500 mM EDTA, pH 8	100 ml	1 mM
ultrapure water	ad 1.0 l	
Dissolve in approx. 800 ml ultrapure water, fill up to 1.0 l with ultrapure water.		

Table 2.30.: 10% APS (w/v)

Component	Amount
APS	1.0 g
ultrapure water	ad 10.0 ml
Dissolve in ultrapure water to a final volume of 10.0 ml and distribute into 100 μl aliquots and store at -20 °C	

Table 2.31.: PMSF

Component	Amount	Conc.
PMSF	871 mg	100 mM
Ethanol, anhydrous	ad 50.0 ml	
Dissolve in anhydrous ethanol to a final volume of 50.0 ml and store at -20 °C		

Buffers for Western blot

Table 2.32.: Stacking gel buffer, pH 6.8

Component	Amount	Conc.
Trizma base	45.4 g	M
10 % SDS	13.39 ml	
ultrapure water	ad 500.0 ml	
Dissolve in approx. 400 ml ultrapure water, adjust pH to 6.8 with concentrated hydrochloric acid. Fill up to a final volume of 500.0 ml with ultrapure water.		

Table 2.33.: Separating gel buffer, pH 8.8

Component	Amount	Conc.
Trizma base	18.9 g	M
10 % SDS	13.39 ml	
ultrapure water	ad 500.0 ml	
Dissolve in approx. 400 ml ultrapure water, adjust pH to 6.8 with concentrated hydrochloric acid. Fill up to a final volume of 500.0 ml with ultrapure water.		

Table 2.34.: 10 × Running buffer

Component	Amount	Conc.
Trizma base	30 g	250 mM
Glycine	144 g	1.92 M
SDS	10 g	1 % (w/v)
ultrapure water	ad 1.0 l	
Dissolve in ultrapure water to a final volume of 1.0 l		

Table 2.35.: 10 × Transfer buffer

Component	Amount	Conc.
Trizma base	30 g	250 mM
Glycine	144 g	1.92 M
ultrapure water	ad 1.0 l	
Dissolve in ultrapure water to a final volume of 1.0 l		

Table 2.36.: RIPA lysis buffer

Component	Amount	conc.
Igepal CA 630	2.5 ml	1%
Sodium deoxycholate	1.25 g	0.5%
10 % SDS	2.5 ml	0.1 %
250 mM EDTA	2.0 ml	2 mM
DPBS	ad 250.0 ml	
Dissolve in DPBS to a final volume of 250.0 ml		

Table 2.37.: ECL solution

Component	Amount	Conc.
1.5 M Tris-HCl, pH 8.8	3.3 ml	100 mM
250 mM Luminol	250 μl	1.25 mM
90 mM $_4$−IPBA	1111 μl	2 mM
ultrapure water	ad 50.0 ml	
Dissolve in ultrapure water to a final volume of 50.0 ml and store at 4 °C protected from light. Add 0.5 μl of 30 % H_2O_2 freshly to each milliliter of solution before use.		

Table 2.38.: Western blot stripping buffer

Component	Concentration
β-Mercaptoethanol	1.74 ml
10% SDS	50 ml
0.5 M Tris−HCl, pH 6.7	31.3 ml
ultrapure water	ad 250.0 ml
Dissolve to a final volume of 250.0 ml in ultrapure water. Store protected from light.	

Solutions for Chromatin Immunoprecipitation (ChIP)

All solutions for ChIP were prepared with nuclease-free water.

Table 2.39.: 3M Sodium acetate, pH 5.5

Component	Concentration
Sodium acetate × 3 H_2O	3 M
Dissolve and adjust pH to 5.5 with acetic acid.	

Table 2.40.: 1.5M Tris-HCl, pH 8

Component	Concentration
Trizma base	1.5 M
Dissolve and adjust pH to 8.0 with concentrated hydrochloric acid.	

Table 2.41.: 0.5M EDTA, pH 8

Component	Concentration
Na_2−EDTA × 2 H_2O	0.5 M
Dissolve and adjust pH to approx. 8 with 5N NaOH.	

Table 2.42.: 10% SDS

Component	Concentration
SDS	10% (w/v)
Dissolve in water.	

Table 2.43.: 5 M NaCl

Component	Concentration
NaCl	5 M
Dissolve and adjust pH to approx. 8 with 5N NaOH.	

Table 2.44.: ChIP quencher

Component	Concentration
Glycine	2.5 M
Dissolve in water.	

Table 2.45.: ChIP lysis buffer

Component	Concentration
SDS	1% (w/v)
Tris-HCl, pH 8	50 mM
EDTA	20 mM
Dissolve and dilute in water.	

Table 2.46.: ChIP sonication buffer

Component	Concentration
SDS	0.25% (w/v)
NaCl	200 mM
sonicated salmon sperm DNA	0.1 mg/ml
Dissolve and dilute in water.	

Table 2.47.: ChIP dilution buffer

Component	Concentration
SDS	0.01% (w/v)
EDTA, pH 8	1.2 mM
Tris−HCl, pH 8	16.7 mM
TRITON X-100	1.1% (w/v)
NaCl	167 mM
Dissolve and dilute in water.	

Table 2.48.: ChIP wash buffer A

Component	Concentration
SDS	0.1%
EDTA, pH 8	2 mM
Tris−HCl, pH 8	20 mM
TRITON X-100	1%
NaCl	150 mM
Dissolve and dilute in water.	

Table 2.49.: ChIP wash buffer B

Component	Concentration
SDS	0.1%
EDTA, pH 8	2 mM
Tris−HCl, pH 8	20 mM
TRITON X-100	1%
NaCl	500 mM
Dissolve and dilute in water.	

Table 2.50.: ChIP TE buffer

Component	Concentration
EDTA, pH 8	1 mM
Tris−HCl, pH 8	10 mM
Dissolve and dilute in water.	

Table 2.51.: ChIP elution buffer

Component	Concentration
SDS	1%
$NaHCO_3$, pH 8	100 mM
Dissolve and dilute in water.	

2.10. Software

Table 2.52.: Software

Name	Purpose	Source
JabRef reference manager, v. 2.9.2	Reference management and bibliography	Open source, downloaded from http://jabref.sourceforge.net
GIMP - The GNU Image Manipulation Program, v. 2.6.6	Image editing	Open source, downloaded from http://www.gimp.org
Image Lab, v. 2.0 build 8	Image acquisition and editing	Bio-Rad Laboratories, Hercules, California, USA
Microsoft© Excel 2008 for Mac, v. 12.3.6	Data analysis	Microsoft Corporation, Redmond, Washington, USA
Optima Microplate Reader Software Package, v. 2.2OR2	Data acquisition	BMG Labtech, Ortenberg, Germany
Pannoramic Viewer, v. 1.15.2	Image analysis	3DHISTECH Kft., Budapest, Hungary
Prism4 for Macintosh, v. 4.0a	Statistical analysis, graphic processing	GraphPad Software Inc., La Jolla, California, USA
SPSS	Statistical analysis, data mining	IBM Deutschland GmbH, Ehningen, Germany
TextMate, v. 1.5.11	Text editing using LaTeX	MacroMates Ltd., Limassol, Cyprus
Realplex, v. 2.2	Data acquisition and analysis	Thomson Reuters, New York City, New York, USA

3. Methods

3.1. Cell culture methods

3.1.1. Culturing cell lines from cryoconserved freezebacks

Cryoconserved aliquots of cell lines were taken from storage in ultra-deep freezers and rapidly defrosted by incubation in a 37 ºC warm waterbath. The liquid cell suspension was mixed with 9 ml pre-warmed full growth medium and cells were pelleted at 300 × g and room temperature (RT) for 5 minutes. Cell pellets were resuspended in full growth medium and cells were seeded into T25 or T75 tissue culture flasks, depending on cell number and age of freezebacks and subsequently incubated at 37 ºC, 5% CO_2, and 90% relative humidity (rH).

3.1.2. Trypsinization and subculture of cell lines

Adherent cells were grown in a monolayer in T75 tissue culture flasks and cell culture medium was changed every 2-3 days. Once cells reached 80-90% confluency, the monolayer was washed twice with 10 ml DPBS without Ca^{2+} or Mg^{2+} and incubated with 2 ml of 0.05% Trypsin-EDTA solution for 3-5 minutes at 37 ºC, 5% CO_2, and 90% rH. Single cell suspensions were transferred into sterile 15 ml conical tubes after addition of 8 ml full growth medium per flask to stop the trypsin-reaction. Cells were pelleted at 300 × g and RT for 5 minutes and cell pellets were resuspended in 10 ml full growth medium. To subculture cell lines, 1-2 ml of the cell suspension were seeded into T75 tissue culture flasks containing 8 or 9 ml of full growth medium to achieve a ratio of 1:5 or 1:10, respectively and transferred back to the incubator.

3.1.3. Cryoconservation of cell lines

Cells were trypsinized and pelleted after addition of 8 ml full growth medium to stop the trypsin-reaction. Cells were pelleted at 300 × g and RT for 5 minutes. Cell pellets

were resuspended in cryomedium to achieve a cell concentration of roughly 2.5 $\times$ 10^6 cells per ml. Cell suspensions were distributed to cryotubes and transferred inside a freezing container to the -80 °C freezer to ensure gradual freezing (-1 °C/minute). Cryotubes were subsequently transferred to the -150 °C freezer for long-term storage.

3.1.4. Cell count using the Scepter automated cell counter

Cells were trypsinized and single cell suspensions were prepared as described above. Small aliquots of the suspensions were diluted 1:5 or 1:10 in microcentrifuge tubes with full growth medium or DPBS. Cells were counted using the Scepter 2.0 handheld automated cell counter with 60 μm sensors according to the manufacturer's instructions. Cell concentrations were adjusted for the dilution factor and cell suspensions were used in downstream experiments.

3.1.5. Monitoring of cultures for *Mycoplasma sp.* infection

Apart from employing appropriate aseptic techniques while working with mammalian cell cultures as well as prophylactic application of an antimycoplasma active agent to the cell culture media, cells in culture were routinely monitored for infection with *Mycoplasma sp.* by screening for contamination with Mycoplasma-DNA present in the cell culture supernatant via polymerase chain reaction (PCR). The method was developed by van Kuppeveld et al. [165] and the primers cover the most common strains. An aliquot of 200 μl cell culture medium was removed after incubation with the cells for at least 48 h and inactivated by incubation at 95 °C for 10 minutes. 2 μl of this preparation was used as template for the PCR reaction and both positive and negative controls were included.

Table 3.1.: PCR reaction mix:

Reagents	Concentration
PCR Buffer	10 $\times$
$MgCl_2$	50 mM
dNTP-Mix	10 mM
Primer Mix	1 μM
Template DNA	2 μl per reaction
Nuclease-free water	μl per reaction
DreamTaq Polymerase	0.5 U per reaction

Table 3.2.: PCR program (33 cycles)

Temperature [ºC]	Time [s]
94	180
94	30
55	30
72	45

PCR products were analyzed by electrophoresis on a 2 % agarose gel. Only proven non-contaminated cell lines were used in experiments.

3.2. Molecular biology methods

3.2.1. Generation of shRNA-mediated YAP-knockdowns

Purpose In order to characterize the role of the YAP protein, cell lines expressing high basal levels of YAP were selected and YAP was stably downregulated by RNA-interference techniques. The impact of the YAP-downregulation on the phenotype and the transcriptional program of the cell lines was then analyzed in *in vitro* and *in vivo* experiments.

Heat shock-transformation of ONEShot TOP10/P3 cells and propagation of plasmids in *E.coli*

ONEShot TOP10/P3 competent E.coli cells were thawed on ice and 1-10 μl plasmid DNA (overall amount < 10 μg) was added to the cells. After gentle mixing, cells were incubated on ice for 30 minutes. A heat shock was performed by immersing the tubes containing cells and DNA for 30 s in a water bath (42 ºC) and placing them on ice immediately after this. Cells were incubated in a shaker incubator for 60 minutes at 37 ºC, 225 rpm upon addition of 250 μl SOC medium per tube. A 100 μl aliquot of the culture was streaked on LB agar plates containing 50 μg/ml ampicillin and plates were incubated at 37 ºC overnight. Single colonies were picked and inoculated with 5 ml LB medium containing 50 μg/ml ampicillin overnight at 37 ºC, 225 rpm. Plasmids were extracted from these pre-cultures and the identity of the plasmids was confirmed by restriction digest and subsequent gel electrophoresis. An aliquot of the pre-culture was inoculated with 100 ml

LB medium containing μg/ml ampicillin at a 1:1000 ratio and was placed inside the shaker incubator at 37 °C, 225 rpm for overnight incubation. For long-term storage, aliquots of the pre-culture were mixed with 15% sterile glycerol and shock-frozen in liquid nitrogen.

Extraction of plasmids

Plasmid extraction from 5 ml pre-cultures was performed using the Qiaprep Spin Miniprep Kit according to the manufacturer's instructions. Plasmids from larger culture volumes were extracted using the PureYield Plasmid Midi-prep System and vacuum manifold as per the manufacturer's instructions. Concentration and purity of the extracts was determined spectrophotometrically using a NanoDrop UV-spectrophotometer.

Restriction digest of plasmid-DNA

To identify plasmids after colony picking and purification, restriction digest of the plasmid extracts was performed. The pLKO.1-, pCMV-dR8.74 and VSVg plasmids were digested using Fast Digest BamHI.

Table 3.3.: Restriction digest reaction mix:

Component	Volume [μl]
Nuclease-free water	15
10 × FastDigest Green buffer	2
Template DNA	2
FastDigest BamHI	1

The reaction mix was prepared at room temperature, mixed gently and briefly centrifuged to collect the liquid at the bottom of the tube. The reaction was incubated at 37 °C for 5 minutes and thermal inactivation was performed at 80 °C for 5 minutes. Fragment size was analyzed via gel electrophoresis on a 2% agarose gel.

Production of lentiviral particles

Lentiviral particles were produced by cotransfection of the pCMV-VSVg, pCMV-dR8.74 and the respective pLKO.1 plasmids into the human embryonic kidney cell line 293FT. 293FT cells were seeded into 24 well plates at a concentration of 50,000 cells/well. After overnight incubation to ensure adherence of cells, medium was exchanged and Fugene 6

mediated transfection was performed 4 hours later. First Fugene 6 was mixed with serum-free OptiMEM medium and incubated at room temperature for 5 minutes and incubation was continued for additional 20 minutes upon addition of plasmid DNA.

Table 3.4.: Fugene 6 transfection mix:

Component	Amounts per well
Fugene 6	6 μl
OptiMEM	15 μl
pCMV-dR8.74	125 ng
pCMV-VSVg	50 ng
pLKO.1	200 ng

Upon completion of incubation, the Fugene-DNA complex was added drop-wise to each well and plates were returned to the incubator for overnight incubation at 37 ^{o}C, 5% CO_2, and 90% rH. Medium was exchanged the next morning and replaced with 500 μl fresh medium and plates were returned to the incubator. On the third day, supernatants containing lentiviral particles were collected, supernatants from multiple wells containing the same parental plasmids were pooled, and filtered using a syringe filter with 0.45 μm pore size. Supernatants containing lentiviral particles were aliquoted and stored at -80 ^{o}C for future use. 500 μl fresh medium was added per well and plates were returned to the incubator. Harvest of lentiviral supernatants was repeated the following day after which cells were discarded. All steps were carried out following biosafety level 2 regulations and consumables waste was destroyed by autoclaving.

Determination of puromycin sensitivity of tumor cell lines Recipient human tumor cell lines were seeded at a density of 200,000 cells/well into 6 well tissue culture plates. After overnight incubation to ensure adherence of cells, puromycin containing medium was added at the following concentrations (2 wells per concentration): 0.0 μg/ml, 0.1 μg/ml, 0.2 μg/ml, 0.4 μg/ml, 0.6 μg/ml, 0.8 μg/ml, 1.0 μg/ml, 1.25 μg/ml, 1.5 μg/ml, 2.0 μg/ml, 2.5 μg/ml, 3.0 μg/ml. Cells were monitored for 10 days and the lowest puromycin concentration achieving 100% cytotoxicity was chosen for selection of resistant cells upon lentiviral transduction.

Lentiviral transduction of tumor cell lines Parental human tumor cell lines were seeded at a density of 200,000 cells/well and incubated overnight at 37 °C, 5% CO_2, and 90% rH to ensure adherence of cells. Following exchange of medium on the next morning, cells were transduced with 500 μl (high titer) or 50 μl (low titer) of lentiviral supernatant. Plates were returned to the incubator for another 48 hours and medium was exchanged to medium containing the predetermined concentration of puromycin. Puromycin selection of resistant tumor cells was performed and cells were cultured in the presence of puromycin throughout all experiments. Low passage, polyclonal, lentivirally transduced cell lines were frozen for future use. All steps were carried out following biosafety level 2 regulations and consumables waste was destroyed by autoclaving.

3.2.2. RNA isolation

RNA extraction from cultured cells

Cells were harvested as per general cell culture protocol and were washed once with DPBS. Cells were lysed in RLT buffer spiked 1:1000 with β-Mercaptoethanol and the lysate was homogenized using QiaShredder columns. RNA was extracted using the RNeasy Mini kit as per the manufacturer's specifications including an on-column DNA digest step using Qiagen's RNase-free DNase I Set. RNA was eluted using 30-50 μl of nuclease-free water and RNA concentration was measured using the NanoDrop instrument. RNA concentration was adjusted to 50 ng/μl with nuclease-free water and stored at -80 °C.

RNA extraction from tissues

Freshly harvested xenograft tumor tissue was snap-frozen in liquid nitrogen and finely ground using a pre-chilled mortar and pestle. Ground, frozen tissue was transferred into a chilled microcentrifuge tube and lysed in RLT buffer spiked 1:1000 with β-mercapto-ethanol and the lysate was homogenized using QiaShredder columns. RNA was extracted using the RNeasy Mini kit as per the manufacturer's specifications including an on-column DNA digest step using Qiagen's RNase-free DNase I Set. RNA was eluted using 30-50 μl of nuclease-free water and RNA concentration was measured using the NanoDrop instrument. RNA concentration was adjusted to 50 ng/μl with nuclease-free water and stored at -80 °C.

3.2.3. Transcriptomic profiling

Microarray experiments were carried out on Illumina Bead Arrays by Dr. Per Hoffmann of the core facility of the Institute of Human Genetics, University Hospital of Bonn. Raw data was generated and retrieved from the core facility and data analysis was performed by Dr. Moritz Kebschull of the Department of Periodontology, Operative and Preventive Dentistry of the University Hospital of Bonn.

Hybridization to Illumina Bead Arrays and data acquisition

An amount of 100 ng total RNA was subjected to a single round of in vitro transcription and biotin labeling using the Illumina TotalPrep RNA Amplification Kit. The resulting cRNA was hybridized on HumanHT-12 v4.0 Expression BeadArrays according to the manufacturers protocols using an automated liquid handling pipeline and scanned on an iScan System.

Data analysis

Expression data were exported as unnormalized sample and control probe profiles from the Illumina GenomeStudio software and analyzed using R/ Bioconductor [47] and limma [151]. Data were quality weighed, backgroundcorrected, quantilenormalized, logtransformed and explored for differentially expressed genes with a Benjamini-Hochberg false discovery rate (FDR) of 0.05 using Bayesian statistics. Differential regulation of signaling pathways was performed using the signaling pathway impact analysis algorithm as described by Tarca et al. [159].

Experimental details and results following the Minimum Information About a Microarray Experiment (MIAME) standards are available at the Gene Expression Omnibus (accession number GSE50053) [17].

3.2.4. Reverse transcription quantitative Polymerase Chain Reaction (RT-qPCR)

cDNA generation

RNA was reverse transcribed using random primers and the High Capacity cDNA Reverse Transcription Kit according to the manufacturer's specifications.

RT-qPCR

Reverse transcription quantitative PCR was performed using the SYBR© Premix Ex Taq™ (Tli RNase H Plus) kit on a Reaplex2 Mastercycler real-time PCR system. Relative fold levels were determined using the $2^{(-DeltaDeltaCt)}$ method [101], with GAPDH used as house-keeping control.

3.3. Cell biology methods

3.3.1. Cell viability assay (MTS-assay)

Principle Determination of cell viability was performed using the 3-(4,5-dimethyl-2-yl)-5-(3-carboxymethoxyphenyl)-2-(4-sulfophenyl)-2H-tetrazolium (MTS)-assay. This colorimetric method employs the tetrazolium derivative 3-(4,5-dimethyl-2-yl)-5-(3-carboxymethoxyphenyl)-2-(4-sulfophenyl)-2H-tetrazolium and phenazine ethosulfate as an electrocoupling reagent. The tetrazolium derivative is reduced by NADPH or NADH produced in metabolically active cells into a colored formazan product that is soluble in tissue culture medium [7]. The quantity of the formazan product is determined photometrically at 490 nm and is directly proportional to the number of living cells in culture [27].

Procedure Cells were trypsinized and the cell number was determined as described above. Cell suspensions were adjusted to c = 10,000 cells/ ml and 200 μl cell suspension was seeded per well into flat bottom 96 well plates. Following overnight incubation in full growth medium to ensure adherence of the cells to the surface of the vessel, medium was exchanged to 100 μl full growth or low serum medium as per experimental layout and plates were incubated for additional 0, 48 and 96 hours. All experiments were set up in quadruplicates and results were normalized to the mean cell viability at 0 hours. For experimental readout at specified time points, 20 μl CellTiter 96 Aqueous One solution was added to each well and absorbance at 492 nm was determined using a 96 well plate reader upon incubation of plates at 37 ^{o}C, 5% CO_2, and 90% rH for 2 hours.

3.3.2. Replating efficiency assay

Principle The ability to form colonies from single cells is considered a hallmark property of cancer cells *in vitro*. The replating efficiency assay assesses the extent of this property. Single cell suspensions are diluted to 500-1000 cells per milliliter and seeded into normal

culture vessels at very low densities to prevent cell-cell contact. Cultures are kept for a defined length of time and the number of colonies formed from single are counted.

Procedure Cells were trypsinized and the cell number was determined as described above. Cell suspensions were adjusted to c = 500 cells/ ml and 2 ml cell suspension was seeded per well in full growth medium into 6 well plates. Once colonies became visible, cells were fixed for with 70% ethanol for 2 minutes and stained with a 0,05% aqueous solution of crystal violet for 2 minutes. Plates were washed twice with 2 ml DPBS and stained colonies were air-dried. Images of colonies were acquired by trans-UV illumination using a gel documentation system and ImageLab software. Colonies were counted and colony counts were normalized to the mean colony count of mock-transduced cell lines.

3.3.3. Soft-Agar assay

Principle In the process of metastasis, single cancer cells detach from the parental tumor and the surrounding matrix, translocate into the bloodstream and establish a filial tumor from a single cell at a distant site. The ability of cells to survive in the absence of a stable surface to anchor with – extracellular matrix proteins *in vivo* or tissue culture treated plastic surfaces *in vitro* – is termed anchorage-independent growth. The loss of anchorage-dependency in epithelial cells correlates with the ability to form tumors in animal models and is considered a strong indicator of malignant transformation [142]. This assay measures the ability of cells to form colonies in a matrix of soft agar that doesn't provide a solid phase substrate to attach to.

Procedure Cells were trypsinized and the cell number was determined as described above. Cell suspensions were adjusted to c = 50,000 cells/ ml. Soft-Agar Assays were set up in six-well plates with a bottom layer of 1% agarose, an intermediate layer containing 0,6% agarose and 10,000 cells per well, as well as a final layer of medium only. Plates were incubated for 4 weeks at 37 ºC and medium was exchanged once per week. Upon termination of the experiment, medium was removed and plates were incubated for two hours with 2 ml of a 0,05% aqueous solution of crystal violet at 37 ºC, 5% CO_2, and 90% rH. Plates were washed twice with 2 ml DPBS per well and colonies were visualized by trans-UV illumination using the gel documentation system. Colonies were counted and colony counts were normalized to the mean colony count of mock-transduced cell lines.

3.3.4. Boyden chamber assays

Principle Cell migration is defined as the directed movement of cells on a 2D-substrate, such as basal membrane, extracellular matrix *in vivo* or the plastic surface of a culture vessel *in vitro* [90]. The assay used in this study was first developed by Boyden in 1962 to analyze the migratory capacity of leukocytes in response to chemotactic cues [16]. The principle relies on two medium-containing chambers separated by a porous membrane. Importantly, the pores have to be smaller than the migrating cells in order to rule out passive "drop"-effects and assess only active transmigration. Cells are seeded into the upper chamber, migrate horizontally towards the next available pore, and transmigrate vertically into the lower chamber. The assay used in this study relies on the principle established by Boyden but uses ready-made inserts containing membranes with 8 μm pores for an easy set-up.

Procedure Boyden Chamber assays were set up in 24-well transwell plates with 8 μm pore size cell culture inserts. Cells were trypsinized and the cell number was determined as described above. Cell suspensions were adjusted to c = 50,000 cells/ ml and 1 ml cell suspension per well was applied into the cell culture insert resting in one well of the plate on 1 ml of full growth medium. Transwell migration was assessed after 48 and 72 hours incubation at 37 ^{o}C, 5% CO_2, and 90% rH. Cells adherent at the bottom of the filter were fixed in 70% ethanol and stained with hematoxyllin. Cells were counted in three randomly selected microscopic fields and means and standard deviations were calculated.

3.3.5. Generation of s.c. xenografts

Principle Human to mouse tumor xenografts are an important means to study tumorigenicity of certain tumor cell lineages as well as the molecular genetics of human cancer because they accurately mirror the entire spectrum of genetic alterations of the neoplastic cell compartments of the human parental tumors. To generate human to mouse tumor xenografts, patient-derived tumor tissue or human cancer cells are either injected or surgically implanted into immunocompromised mouse strains, usually either athymic Nude mice, who lack a functional T cell system or Severe Combined Immunodeficient (SCID) mice, who present with highly impaired T and B cell immune responses. Because of their respective immune defects, those mice tolerate the xenotransplanted cells and allow the foreign cells to proliferate. While this model represents a unique platform to study genetic mutations and aberrations, the xenogenic system naturally fails to appropriately depict

features of the disease normally conveyed by the tumor microenvironment, especially effects conferred by the host immune system [141].

Procedure All animal experiments described were approved by the Government of the State of North Rhine-Westphalia. Mice were maintained according to the guidelines of the Federation of European Laboratory Animal Science Associations (FELASA). To generate subcutaneous xenografts, ACHN YAP-knockdown and ACHN mock-transfected cells in log growth phase were harvested by trypsinization, counted and subsequently injected into the flanks of five male athymic $CD1^{nu/nu}$ mice, each. 2.5×10^6 cells suspended in a total volume of 250 µL [full growth medium/ Matrigel (BD Biosciences), 1:1 (v/v), pre-chilled to 4^oC], were subcutaneously injected into the flanks of 6 to 8 weeks old mice. Starting ten days after the injection of tumor cells, tumor dimensions were determined twice a week by use of digital calipers, and tumor volumes (V) were determined as V = 1/2(ab2), with a being the longest and b the shortest orthogonal tumor diameter. Mice were sacrificed by incubation with CO_2 after six weeks and tumors were harvested and cryopreserved or formalin-fixed for later analysis.

3.4. Immunological methods

3.4.1. Immunohistochemistry

Tumor tissue samples

All tumor samples were collected from the archives of the Institutes of Pathology of the Universities of Bonn (PDAC and CCC cases) and Cologne (ccRCC cases). The samples were formalin fixed and paraffin embedded as part of routine diagnostic procedures. Clinicopathological data was obtained from case records provided by the Institutes of Pathology, Universities of Bonn and Cologne, respectively. All tumors were clinically and pathologically identified as being the primary and only neoplastic lesion and classified according to WHO guidelines.

Generation of Tissue Micro Arrays (TMA)

Tissue microarrays were constructed from paraffin-embedded tissue blocks of pancreatic ductal adenocarcinomas and their companion normal tissues as described initially by Sauter et al. [86]. Three 0.5 mm core needle samples of the preexisting paraffin-embedded

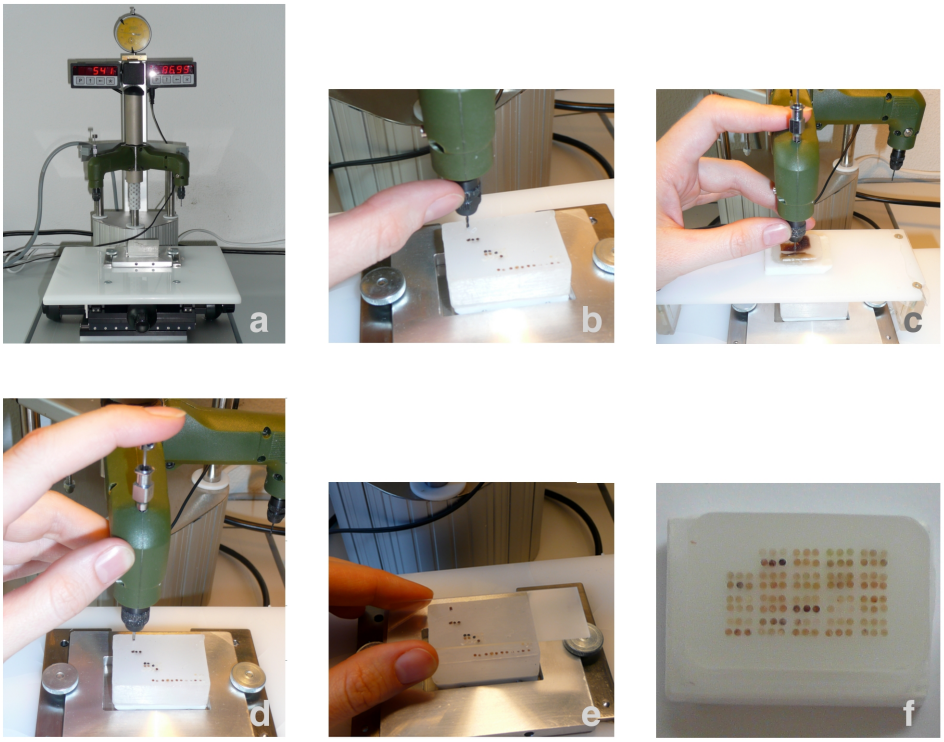

Figure 3.1.: Generation of Tissue Micro Arrays (TMA) Spots in the recipient block are targeted using the microdials of the tissue arrayer (a) and a hole is drilled into the recipient block with the drilling arm of the tissue arrayer (b). Tissue cores are punched using the punching arm (c) and transferred to the recipient block (d). Tissue cores are inserted seamlessly into the recipient block (e). Finished TMA (f).

tissues from each tumor and companion normal tissue specimen were obtained and then re-embedded in an arrayed master block using a manual tissue arrayer. For a description of the procedure see Figure 3.1.

Immunohistochemistry

Paraffin-embedding of formalin-fixed tissues as well as cutting the paraffin-embedded tissue into sections was performed by the diagnostic laboratories as part of routine diagnostic procedures by the Institutes of Pathology of the University of Bonn or Cologne. Immunohistochemistry was performed at the same place either on a Dako Techmate 500 using the Dako REAL Detection System, Peroxidase/AEC, Rabbit/Mouse-Kit (Bonn) or on a LabVision 480S using the Histofine Simple Stain Mouse MAX PO kit (Cologne).

Table 3.5.: Antibodies and conditions used for Immunohistochemistry

Antibody	Dilution	Antigen Retrieval
YAP	1:100	Citrate buffer, pH 6; pressure cooker
pYAP	1:500	Citrate buffer, pH 6; pressure cooker
SAV1	1:100	Citrate buffer, pH 6; pressure cooker
EDN2	1:100	Citrate buffer, pH 6; pressure cooker
Cytokeratin	1:200	Citrate buffer, pH 6; pressure cooker

Evaluation of staining intensity Stained slides of TMAs were scanned with a Pannoramic 250 slide scanner and staining was reviewed using the "Pannoramic Viewer"-software. Staining intensity was evaluated individually in a blinded fashion using a four-tiered scoring system.

Table 3.6.: Scoring system

Staining intensity	Score
absent immunoreactivity	0
weak immunoreactivity	1
intermediate immunoreactivity	2
strong immunoreactivity	3

Correlation with clinicopathologic parameters and statistical analysis was performed using IBM SPSS Statistics 21 for Windows.

3.4.2. Western blot

Protein extraction Cells were trypsinized, pelleted and the cell pellets were washed with DPBS. Cells were lysed in Radioimmunoprecipitation assay buffer supplemented with protease and phosphatase inhibitor cocktails (200 μl lysis buffer per T75 tissue culture flask). In case of cryopreserved tumor tissue, frozen tissue chunks were pulverized in liquid nitrogen using mortar and pestle and ground tissue was lysed in 200 μl lysis buffer. Lysates were incubated on ice for 30 minutes and vortexed every 10 minutes. Lysates were cleared by centrifugation at 20,000 $\times$ g, 4 ^{o}C for 30 minutes and supernatants were collected. Estimation of protein concentration was carried out using the bicinchoninic acid

(BCA) assay on aliquots that had been diluted with lysis buffer at a ratio of 1:5. Lysates were aliquoted to avoid multiple freeze-thaw cycles and stored at -80 °C for long-term storage.

Gelelectrophoresis and transfer 50 μg of total protein was mixed with loading dye, loaded on 10% SDS-polyacrylamide gels, and electrophoresed at 100 V until the front had migrated within the last centimeter of the gel. Separated proteins were transferred onto nitrocellulose membranes at 250 mA for 52 minutes. Successful transfer was controlled by performing Ponceau S staining of the membranes. Membranes were blocked in 5% BSA to prevent unspecific binding.

Probing, reprobing and detection The blots were probed with antibodies against YAP (Cell Signaling, Danvers, MA) and GAPDH (Cell Signaling) as well as secondary, HRP-coupled antibodies directed against rabbit or mouse IgG, respectively (Cell Signaling). Detection was performed using a solution of 4-iodophenylboronic acid (4IPBA) and luminol [53]. Concentration and medium of antibodies used are shown below.

Table 3.7.: Antibodies and conditions used for Western blot

Antibody	Dilution	Blocking reagent
YAP	1:200	5% BSA in TBS-T
pYAP	1:500	5% BSA in TBS-T
GAPDH	1:1000	5% BSA in TBS-T
goat anti-rabbit IgG-HRP	1:2000	5% BSA in TBS-T
SAV1	1:500	5% NFDM in TBS-T
LKB1	1:500	5% NFDM in TBS-T
MST2	1:5000	5% BSA in TBS-T

3.4.3. Chromatin Immunoprecipitation (ChIP)

Principle

Chromatin Immunoprecipitation (ChIP) was developed as a tool to investigate direct interactions between proteins and DNA, such as transcription factors, polymerases and DNA-modifying enzymes. Initially designed to explore interactions between RNA polymerase II and transcribed and poised genes in *Escherichia coli and* Drosophila [48, 121]

the technique was further developed and adapted for use in mammalian cells [123]. Today ChIP is a highly valuable method for the characterization of chromatin-interacting proteins.

Cells are grown in the desired experimental conditions and growing cells are reversibly crosslinked using formaldehyde, thus preserving a "snapshot" of protein-chromatin interactions at a given time-point. The chromatin is subsequently extracted and sheared by sonication to obtain fragments ranging between 200-1000 bp in size. The pre-cleared chromatin is immunoprecipitated with the antibody of choice and those chromatin fragments bound to the antibody are pulled down using protein A/G coupled agarose beads. Crosslinking is reversed thermically, bound protein is digested and DNA is purified to obtain the starting material for analysis of those regions of the genome that interact with the protein of interest. The analysis can be qualitative or quantitative, for example by comparing the level of enrichment for a putative transcription factor binding site in the promotor region of a candidate target gene of a given transcription factor in two experimental conditions by quantitative realtime PCR (qPCR). Using next-generation sequencing technologies, the eluate of immunoprecipitated DNA-fragments can be mapped onto the reference genome of a given species and the transcriptional landscape of a transcription factor at a given timepoint can be analyzed quite conclusively. Figure 3.2 on page 76 provides a stepwise overview of the technique while a detailed summery of the experimental procedure is given below.

In this study, ChIP was employed to determine whether the transcriptional coactivator YAP interacts with the promotor region of specific candidate target genes in clear cell renal cell carcinoma (ChIP-qPCR).

Cross-link and cell collection

Cells were seeded into 150 mm round tissue culture dishes and grown in a monolayer to approximately 70% confluency. Fresh 37% formaldehyde was added to a final concentration of 1% and cells were fixed at room temperature for 8 minutes with gentle agitation. Residual formaldehyde was quenched by addition of 2.5 M glycine to a final concentration of 125 mM into the medium and incubation for 5 minutes at room temperature. Upon completion of incubation, cells were placed on ice and washed twice with ice-cold DPBS.

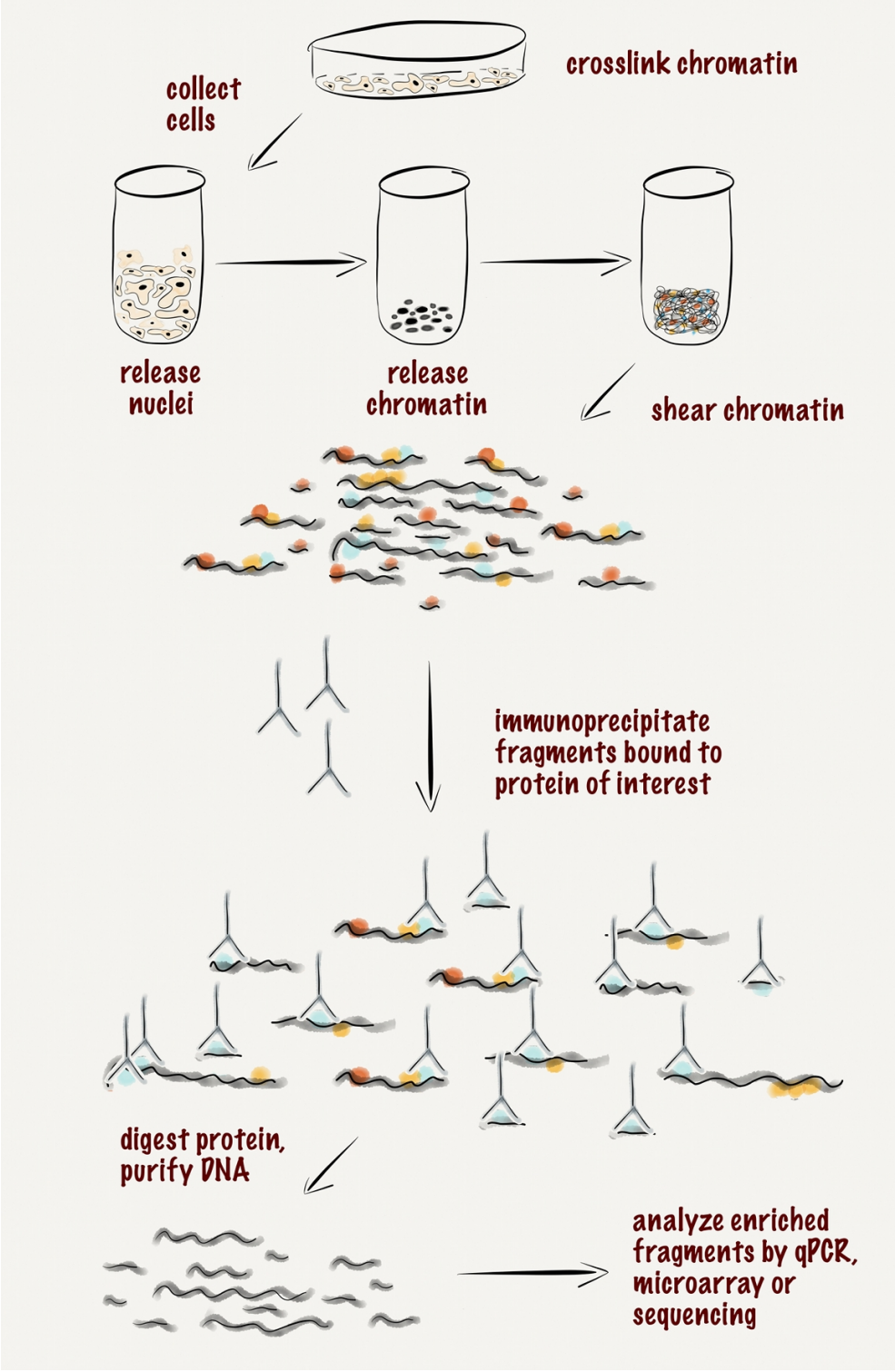

Figure 3.2.: Experimental workflow of ChIP, compiled according to [108]

Lysis and sonication

The monolayer of cells was covered with 1.5 ml of DPBS supplemented with protease- and phosphatase inhibitor cocktails and cells were removed from the wall of the culture vessel using a cell scraper. The cell suspension was collected in 15 ml conical tubes and cells were pelleted for 5 minutes at 3000 rpm and 4 ºC. The cell pellet was resuspended in 500 μl ChIP lysis buffer and incubated for 10 minutes on ice to break up the cell membrane and release the nuclei which were collected by centrifugation at 3000 rpm for 5 minutes at 15 ºC. The pellet containing the nuclei was resuspended in 500 μl ChIP sonication buffer and incubated for 15 minutes on ice. The 15 ml conical tube containing the cell lysates were fixed using clamps and submerged into iced water. The chromatin was sonicated using a Branson 450 SLPe probe sonicator to obtain fragments ranging from 200-1000 bp. Preliminary experiments were performed to determine optimal shearing conditions for the cell lines analyzed. The precise parameters are given below:

Table 3.8.: Sonication conditions for ChIP

Cell line	Concentration (cells/ml)	Amplitude	No. of cycles	Duration $'ON'$	Duration $'OFF'$
MZ1774	2×10^7	50%	5	15 s	60 s
PK9	1×10^7	1^{st}: 65% 2^{nd}: 50%	1^{st}: 2 2^{nd}: 3	10 s	55 s

The correct fragment size distribution of the sheared, cross-linked chromatin was verified by performing electrophoresis of an aliquot (10 μl) of reverse-cross-linked, sheared DNA in a 1% agarose gel.

Immunoprecipitation and elution

The sheared, cross-linked chromatin was incubated for two hours at 4 ºC with a mixture of 20 μl protein G PLUS-agarose and 40 μl protein A-agarose that were washed once with 400 μl ChIP dilution buffer in order to minimize unspecific binding to the agarose beads. The pre-cleared chromatin was removed from the beads and diluted 1:10 with ChIP dilution buffer. 800 μl diluted chromatin were incubated overnight with the indicated amount of primary antibody at 4 ºC under continuous rotation. One aliquot of 800 μl was marked "$Input$" and conserved at -20 ºC.

Table 3.9.: Antibody conditions for ChIP

Antibody	Isotype	Amount per IP
Acetyl-Histone H3	rabbit polyclonal	10 μg
normal rabbit IgG	rabbit polyclonal	10 μg
YAP	mouse monoclonal	10 μg
TEF-1 (TEAD1)	mouse monoclonal	10 μg
normal mouse IgG	mouse monoclonal	10 μg

For all immunoprecipitations using primary antibodies raised in rabbit (i.e. anti-Acetyl-Histone H3 and rabbit IgG), 40 μl protein A-agarose beads were blocked by incubating them with 400 μl ChIP dilution buffer supplemented with 0.5 mg/ml BSA and 0.1 mg/ml salmon sperm DNA overnight at 4 ^{o}C with continuous rotation. All other immunoprecipitations using primary antibodies raised in mouse were carried out using pre-blocked protein G PLUS-agarose. In these cases, 20 μl of protein G PLUS-agarose was put directly into the samples. In order to pull down those DNA-fragments bound to primary antibody, pre-blocked protein A- or protein G PLUS-agarose beads were added to the corresponding samples and incubated at 4 ^{o}C for two hours with continuous rotation. Upon completion of incubation the immune-precipitated complexes were washed five times with 400 μl of ChIP wash buffer A, four times with 400 μl of ChIP wash buffer B, and once with 400 μl of ChIP TE buffer. After washing, the immune-precipitated complexes as well as 1/10 of the Input-sample were incubated under continuous rotation with 200 μl ChIP elution buffer for 15 minutes at room temperature. This step was repeated once and the supernatants of both incubation steps were combined to obtain 400 μl of eluate.

Reversal of cross-links and DNA purification

In order to reverse the protein-DNA cross-links, NaCl was added to a final concentration of 200 mM and samples were incubated overnight with gentle agitation at 65 ^{o}C. 20 μg of each Proteinase K and RNase A were added to each sample the next morning and the mixtures were incubated at 45 ^{o}C for two hours.

Upon completion of incubation DNA was extracted using the phenol/chloroform-method. One volume of phenol/chloroform/isoamylic alcohol (25:24:1) was added to each sample and mixed by shaking vigorously for one minute. After centrifugation for 10 minutes at >20 000×g, the aqueous supernatants containing DNA were transferred to new micro-

centrifuge tubes and 1/10 volume of 3 M sodium acetate stock and 20 μg of glycogen as a carrier for the DNA was added to the aqueous phase which was then mixed with 2,5 volumes of absolute ethanol and placed overnight at -20 ºC for precipitation of DNA.

The next morning, the precipitated DNA was pelleted by centrifugation at >20 000×g, 4 ºC for 40 minutes and the pellets were rinsed with ice-cold 70% ethanol (prepared from absolute ethanol). DNA was again pelleted by centrifugation at >20 000×g, 4 ºC for 25 minutes and the pellets were air-dried upon careful decantation of the supernatant before they were resuspended in 20 μl of nuclease-free water.

DNA-analysis by ChIP-qPCR

Real Time quantitative PCR was performed using the SYBR® Premix Ex Taq™ (Tli RNase H Plus) kit on a Reaplex2 Mastercycler real-time PCR System. Relative fold levels were determined using the $2^{(-DeltaDeltaCt)}$ method [101], with results normalized to the normal IgG controls.

3.5. Statistical analysis

Fisher's exact test and two-tailed Student's t-tests were done using GraphPad Prism for Macintosh, version 4.0a. $P < 0.05$ was regarded to be statistically significant. Unless indicated otherwise, results are shown as mean ± standard error of the mean (SEM).

4. Results & Discussion

4.1. Nuclear YAP expression is frequent in patients with PDAC, biliary carcinoma and ccRCC

Deregulation of the Hippo pathway is frequently observed in a wide variety of human malignancies [64]. Although the effect of this perturbance becomes easily observable in the form of YAP derepression and consecutive nuclear overexpression by neoplastic cells, the underlying cause remains elusive and even enigmatic. For several tumor entities subgroups have been described where nuclear YAP overexpression can be attributed to the loss-of-function of specific members of the canonical Hippo pathway or other, non-canonical upstream interaction partners. In almost all of these cases, these loss-of-function mutations cannot provide a comprehensive explanation for every instance, where nuclear YAP overexpression is observed [64]. This points to a potentially widespread deregulation of the upstream signaling network reflecting the extensive array of upstream signals feeding into the core signaling cassette and the many direct interaction partners of YAP.

In the following chapter, the frequency of Hippo pathway perturbation as measured by nuclear YAP overexpression is determined using immunohistochemistry on collections of tumor tissue samples of patients with PDAC, biliary carcinoma and ccRCC. For those tumor entities there is only limited data on the status of the Hippo-target YAP available so far. In a second step, hypotheses concerning the potential mechanisms of Hippo pathway perturbation with regard to specific members of the upstream YAP-interaction partners (both canonical and non-canonical) are made and tested either by immunohistochemistry on patient samples or immunoblotting on cell line extracts.

4.1.1. Analysis of nuclear YAP expression and disruption of Hippo signaling in PDAC

YAP is frequently overexpressed in PDAC patients

YAP has been shown to be overexpressed in PDAC tissues, although studies have been limited in scope and only evaluated 20 or 64 patients, respectively [33, 34]. In order to evaluate the expression status of YAP in PDAC, tissue microarrays were constructed containing samples of tumor and matched adjacent normal tissue of 145 patients who underwent surgery at the University Hospital of Bonn between 1999 and 2009. Anonymized clinicopathological data was recovered from case records kept at the archives of the Institute of Pathology at the University Hospital Bonn. Staining was evaluable for the tumor samples of 143 patients and staining of the adjacent normal tissue was available of 128 patients. As shown in Figure 4.1 on page 82, YAP is frequently strongly expressed in the nuclei of PDAC patients whereas strong nuclear expression was only occasionally observed in normal pancreatic ducts. Intriguingly, the hierarchy of the pancreatic ductal architecture is highlighted by a gradient of YAP expression with centroacinar cells and neoductuli displaying the strongest nuclear and cytoplasmic YAP immunoreactivity, which then gradually decreases in smaller towards larger pancreatic ducts, where nuclear YAP expression is hardly detectable (see 4.1 A, C & E).

High nuclear YAP expression correlates with nodal stadium in PDAC patients

Next, correlation of nuclear YAP immunoreactivity with clinicopathological parameters was examined. Anonymized clinicopathological data concerning tumor grade, stage and nodal status as well as staining intensities were compiled for each case and fed into SPSS for statistical analysis. The relationship between nuclear YAP staining intensities and each parameter was calculated using three different statistical models, the Pearson product-moment correlation coefficient, Kendall's tau rank correlation coefficient as well as Spearman's rank correlation coefficient, in order to include both linear and non-parametric statistical models.

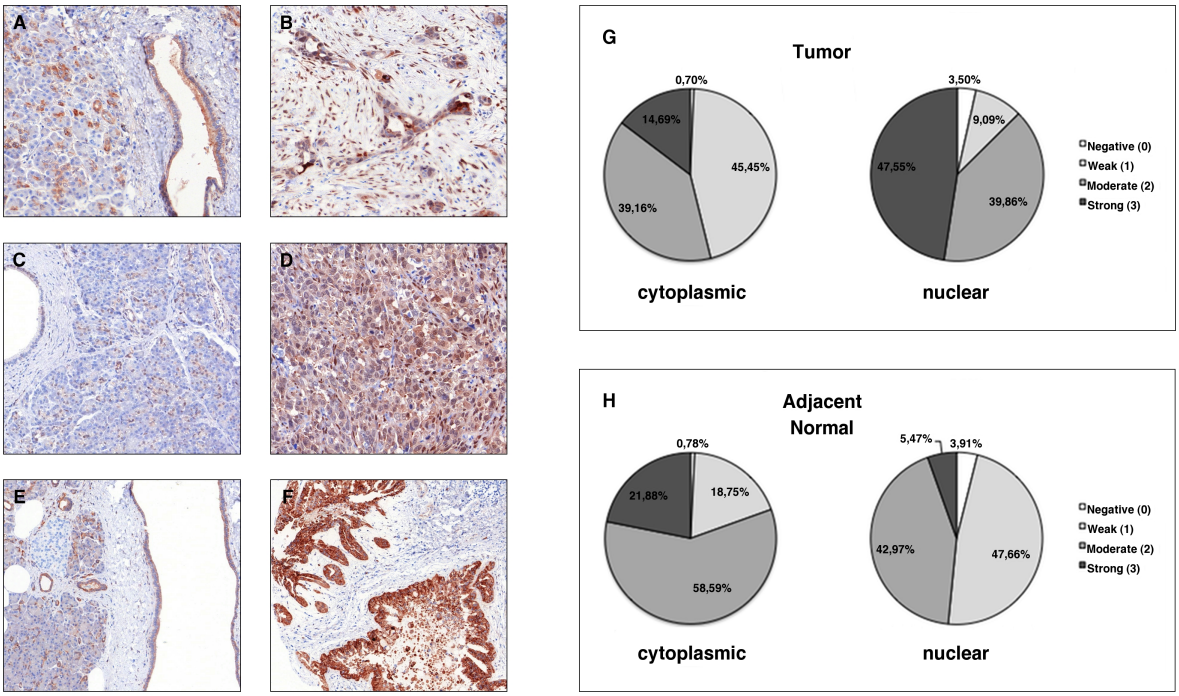

Figure 4.1.: Nuclear overexpression of YAP in PDAC patients. Shown are examples of YAP immunolabeling of normal ductal epithelium (A, C, E) and neoplastic tissue (B, D, F; images are shown in 100 × magnification) of three representative cases of PDAC. The first case exhibits weak to moderate staining (predominantly cytoplasmic) in normal pancreatic ductal epithelium of larger ducts in tumor-adjacent normal tissue (A) with strong, predominantly nuclear staining in corresponding samples of PDAC (B). Weak to negative nuclear or cytoplasmic YAP immunoreactivity in normal ductal epithelium (C) was associated with moderate to strong nuclear and cytoplasmic YAP expression in the corresponding tumor samples (D) in a second exemplary case of PDAC. Thirdly, weak cytoplasmic and negative nuclear staining in normal ductal epithelium (E) coupled with strong cytoplasmic and weak nuclear immunoreactivity in corresponding tumor samples (F) were likewise detected, as shown in this third case of PDAC. Although an inter-individual variation in staining patterns as illustrated by the examples above was observed, overall statistical analysis of staining intensity in all 143 cases revealed that YAP shows predominantly nuclear expression in PDAC with moderate to strong staining in approx. 85% of all cases examined (G, n=143) with only approx. 48% of adjacent normal tissue (epithelial cells of larger pancreatic ducts) exhibiting moderate to strong nuclear staining (H), that was mostly accompanied by equally strong cytoplasmic staining.

Table 4.1.: Correlation of nuclear YAP expression with clinicopathological parameters in PDAC patients

		Nuclear YAP score (tumor cells)				**Pearson**		**Kendall's**		**Spearman's**	
		0	**1**	**2**	**3**	**Corr. coeff.**	***p***	**tau**	***p***	**rho**	***p***
G	1	0	0	1	0	0,069	0,42	0,062	0,447	0,065	0,447
	2	1	9	24	30						
	3	2	4	32	37						
pT	I	0	0	1	1	0,089	0,295	0,087	0,277	0,092	0,277
	II	1	3	3	3						
	III	3	9	52	62						
	IV	0	1	1	1						
pN	0	4	5	15	14	0,205	0,024	0,162	0,062	0,171	0,061
	1	2	8	32	42						

While the nuclear immunoreactivity for YAP in PDAC tumor cells does not correlate with tumor grade or stage, moderate to high nuclear YAP expression is significantly more frequent in patients who display lymph node metastases at the time of surgery using the statistical model of Pearson's product-moment correlation coefficient (Pearson's r = 0,205, $p = 0{,}024$), while just failing to meet the criteria of statistical significance in both Kendall's tau rank correlation coefficient (Kendall's tau = 0,162, $p = 0{,}062$) and Spearman's rank correlation coefficient (Spearman's rho = 0,171, $p = 0{,}061$).

Analysis of protein expression in a panel of PDAC-cell lines

A panel of 13 pancreatic cancer cell lines as well as the immortalized normal pancreatic ductal cell line HPNE were subjected to Western blot analysis. Basal YAP-expression was observed in non-malignant hTERT-HPNE cells and almost all PDAC cell lines examined with the exception of Capan-1 (Figure 4.2).

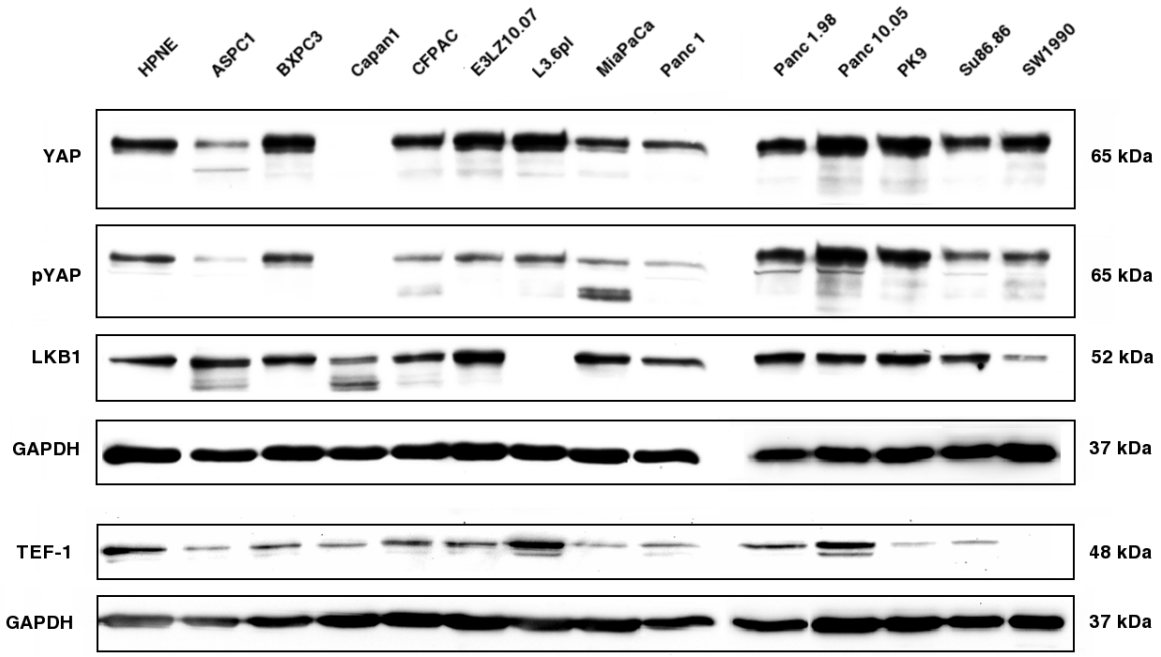

Figure 4.2.: Expression of YAP and interaction partners in a panel of PDAC-cell lines. Displayed are images of two Western blots analyzing two different aliquots of the same protein extracts of the indicated pancreatic cancer cell lines. GAPDH-expression was used to confirm loading of equal amounts of total protein.

Protein expression levels varied greatly, ranging from strong signals (PK9, Panc 10.05 and L3.6pl) to barely detectable bands (AsPC-1). Notably, the immortalized normal pancreatic ductal cell line HPNE displayed high basal levels of YAP, inconsistent with the histological findings. This might be due to the transformation process needed to create the immortalized cell line.

The liver kinase B1 (LKB1) is a tumor suppressor which has been implicated in the pathogenesis of familial pancreatic cancer and is the underlying mutation in Peutz-Jeghers Syndrome, a hereditary disease predisposing for the formation of pancreatic cancer (refer

to page 11). Recently, LKB1 has been shown to control phosphorylation and subsequent degradation of YAP in a mechanism that was independent of the canonical core cassette [118]. In order to evaluate a potential pathomechanistic relationship in PDAC, the membranes were subsequently probed with antibodies targeting pYAP and LKB1. While there is no correlation observable across the board, and most cell lines display robust LKB1-expression, LKB1 is lost in L3.6pl cells. While information on the mutational status of the LKB1-gene in L3.6pl cells was not available and the cause of the loss of this protein is speculative, the pYAP/YAP expression ratio appears to be low in L3.6pl cells, which is consistent with decreased YAP-phosphorylation. The TEAD family of transcription factors has been described as the principal partner of YAP to elicit its oncogenic, pro-proliferative and proinvasive properties and there is considerable overlap in promotors occupied by both YAP and TEAD1 in the breast cancer cell line MCF10A [93, 183]. The expression of the family member TEF-1 (TEAD1) could be detected in all cell lines examined with the exception of SW1990, although expression levels were variable.

4.1.2. Analysis of nuclear YAP expression and disruption of Hippo signaling in CCC patients

Analysis of YAP-protein expression in 14 CCC patients by immunohistochemistry

Formalin fixed and paraffin embedded tumor and adjacent normal tissue of fourteen patients with biliary carcinoma who had undergone surgery at the University Hospital of Bonn between 2004 and 2008 were analyzed with regard to YAP expression status by immunohistochemistry (see Table 4.2 on page 87). As observed in normal pancreatic tissue, the hierarchy of the branches of the biliary tree is represented by a gradient of YAP protein expression with small ducts exhibiting strong nuclear immunoreactivity and larger ducts displaying only weak nuclear staining. Oval cells, which form the precursor cell department within the liver and are able to differentiate into hepatocytic as well as cholangiocytic lineages, stain highly positive for YAP as previously described for murine tissue [95]. Kupffer cells, which form a specialized macrophage cell compartment within the space of Dissé are equally highlighted by strong YAP expression.

Within the premalignant and malignant cell compartment, cells that had undergone metaplasia stained positive, while neoplastic cells exhibited a more complex staining pattern. In general, YAP was expressed by the majority of CCC tumors analyzed and staining intensity seemed to increase with degree of differentiation with highly differentiated tumors exhibiting strong nuclear staining and poorly differentiated tumors exhibiting weaker nuclear YAP levels (see Figure 4.3 on page 88 and Table 4.2 on 87). Curiously, tumors with histological features close to those of hepatic precursor or stem cells (oval cells) stained highly positive for YAP, somewhat contradicting the previous observation. Cancer associated fibroblasts residing in the tumor adjacent stroma were often found to contain a marked amount of nuclear YAP (Figure 4.3, B). While it is speculative to report correlations with regard to the small number of tumors examined, YAP highlighted formations of invasive tumor cells in those cases where perineural invasion or lymph node metastases were present (patients 3, 4, 5 and 10, see Figure 4.3, E-H). In some cases, the YAP content of these cells was decidedly elevated as compared to the main tumor (e.g. patient 10).

Table 4.2.: Expression of YAP in tumor tissue of biliary cancer patients

Patient	Diagnosis	Score Tumor		Normal	
		cytoplasmic	nuclear	cytoplasmic	nuclear
1	perihilar CCC	1	0	1	1
2	extrahepatic CCC	0	2	0	1
3	perihilar CCC	1	1	1	0
4	extrahepatic CCC	1	1	1	2
5	extrahepatic CCC, highly differentiated	0	0	0	0
6	intrahepatic CCC	1	1	0	1
7	intrahepatic CCC, stem cell histology	0	2	0	0
8	extrahepatic CCC	1	0	0	2
9	extrahepatic CCC	0	1	0	2
10	intrahepatic CCC	1	2	0	0
11	CCC, stem cell histology	1	2	1	1
12	extrahepatic CCC	1	2	1	2
13	intrahepatic CCC, highly differentiated	0	1	0	2
14	CCC	2	0	2	0

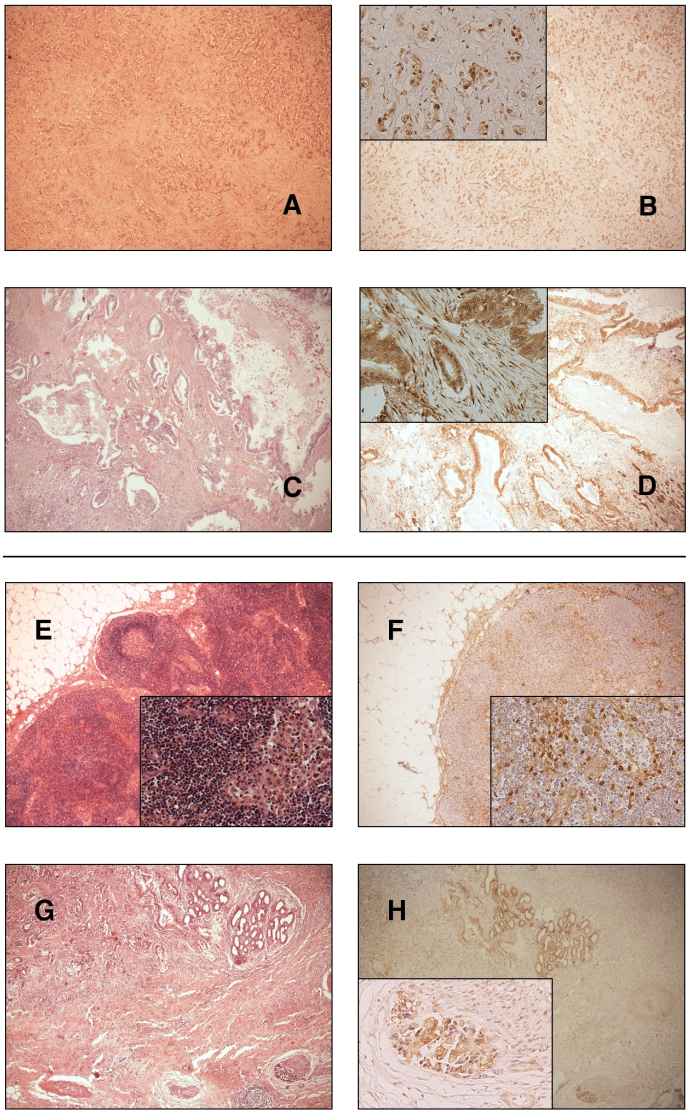

Figure 4.3.: YAP is highly expressed by tumors of the biliary tract and highlights invasive tumor cell formations. Nuclear YAP expression is observable in the majority of CCC tumors analyzed. Shown are HE stainings and YAP immunolabeling of two representative tumors. Patient 10 exhibited strong YAP-positivity that focused on the nuclei of cancer cells (A, B), while patient 3 displayed equivocal nuclear and cytoplasmic staining of tumor ducts. Often, cancer associated fibroblasts that showed very strong nuclear YAP content were found in the tumor surrounding stroma (B, inset). Formations of invasive tumor cells were highlighted by a particularly high nuclear YAP content, even if the main tumor displayed weaker staining. A lymph node metastasis found in the tissue of patient 5 exhibited single invasive, highly YAP positive cells (E, F) while perineural invasion in the case of patient 4 was marked by bands of tumor cells with elevated YAP expression levels (G, H). Images are shown in 40 × magnification with insets in 200 × magnification.

Analysis of protein expression in a panel of biliary carcinoma cell lines

A panel of eight biliary carcinoma cell lines was subjected to Western blot analysis. High levels of basal YAP expression was observed across the board and while expression of pYAP was considerably weaker, even minimal to absent in GBD-1, NEC, SNU478 and TFK-1, suggesting that YAP is highly active.

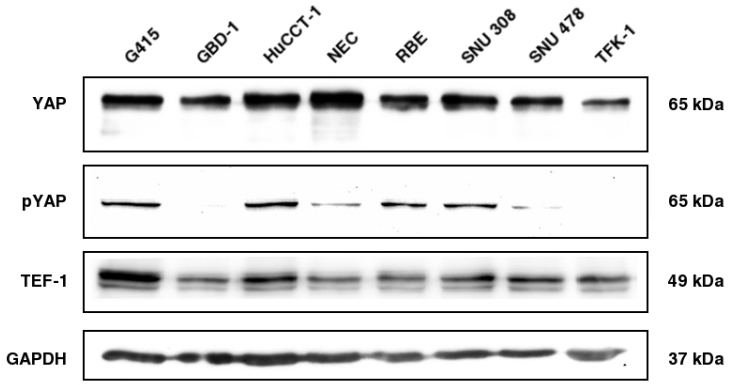

Figure 4.4.: Expression of YAP and pYAP in a panel of CCC-cell lines

The potential of high transcriptional YAP activity is corroborated by the expression of YAP's principal interaction partner TEF-1 by every single biliary carcinoma cell line examined. In contrast to the examined panel of PDAC cell-lines, expression levels of TEF-1 in CCC cell-lines were quite homogenous.

4.1.3. Analysis of nuclear YAP expression and disruption of Hippo signaling in RCC patients

Analysis of YAP-protein expression in 31 ccRCC patients by immunohistochemistry

In order to determine the extent of abnormal YAP activity in ccRCC patients, tissue samples (tumor and adjacent normal tissue) of 31 patients who had undergone surgery for renal tumors and were diagnosed with ccRCC at the University Hospital of Cologne were analyzed for YAP protein expression by immunohistochemistry. YAP expression was detected in normal as well as neoplastic renal tissue, but displayed marked differences with regard to the staining pattern.

In non-neoplastic renal parenchyma, strong nuclear YAP expression was observed in podocytes and differential expression was registered in the proximal and distal compartments of the renal tubules. While the distal segments of the renal tubule consistently exhibited strong cytoplasmic and nuclear immunolabeling, significantly weaker YAP expression was observed in the proximal tubules, the putative site of origin of ccRCC (Figure 4.5 A, B). In RCC tissue samples nuclear upregulation of YAP expression was found in 20 of 31 cases (65%, $p<0.0001$) as compared to the proximal tubules in the adjacent normal tissue.

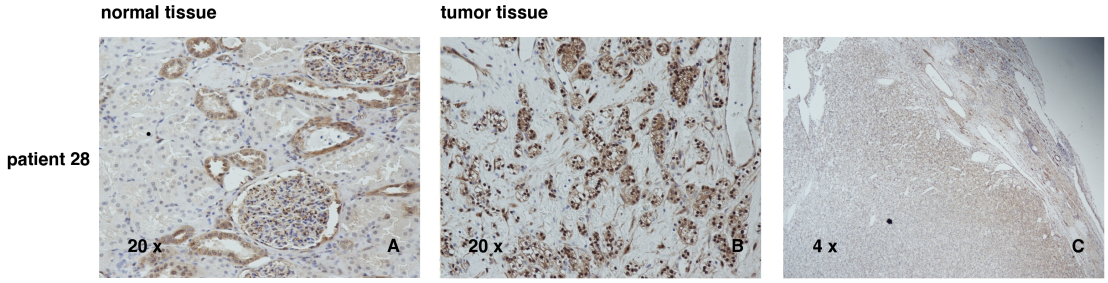

Figure 4.5.: Expression of YAP in ccRCC patients. Immunohistochemistry of tumor tissue of 31 ccRCC patients showed distinct staining of normal renal parenchyma with proximal tubule cells exhibiting only minimal to weak nuclear staining (A) whereas most tumors showed moderate to strong nuclear YAP immunoreactivity (B). YAP positivity was stronger at the tumor margins (C).

There was no apparent correlation of YAP positivity with tumor grade or other clinicopathologic parameters, which might be due to the small sample size, with 22 out of

31 cases being histopathologically classified as grade 2. However, vascular invasion or lymph node metastases were reported for 9/30 cases and of these, 7 exhibited marked YAP positivity.

Interestingly, YAP staining intensity was considerably more prominent at the tumor margins representing the invasive front of the tumor. Additionally, in several patients that showed high expression levels of YAP, solitary keratin and YAP double-positive tumor cells invading the surrounding lymphocyte rich stroma were observed, suggesting a possible role of Hippo signaling in ccRCC tumor cell invasion *in vivo* (Figure 4.5 (C) and Figure 4.6 (A-D)).

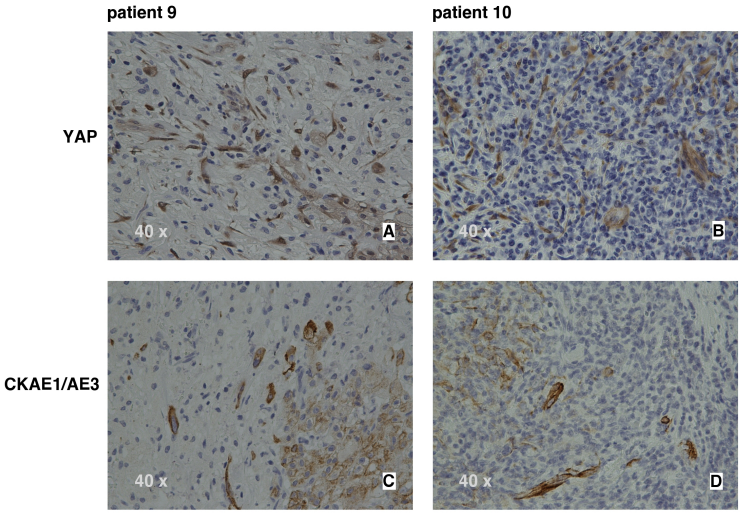

Figure 4.6.: YAP highlights invading tumor cells. Immunohistochemistry of YAP in ccRCC tissue highlights single cells invading tumor-adjacent stroma (A, B), that also exhibit positivity for cytokeratin (C, D).

Salvador/SAV1 is a member of the canonical Hippo pathway and has been reported to be lost in the ccRCC cell line ACHN in one of the first papers on the function of the Hippo pathway in drosophila and mammals [158]. Copy number loss of chromosome 14q22.1 where the *SAV1* gene is located as well as downregulation of the protein has been reported for a subset of ccRCC by various groups [105, 176], but it is interesting to determine to what extent loss of SAV1 correlates with YAP positivity and whether there are any cases that are double positive, suggesting additional mechanisms of Hippo pathway perturbation in ccRCC.

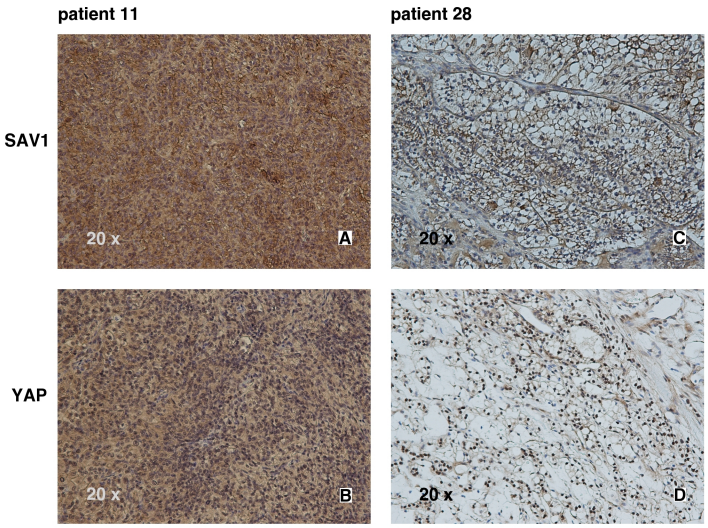

Figure 4.7.: Nuclear YAP localization correlates with loss of SAV1 in ccRCC tumors. Loss of SAV1 immunoreactivity was frequently associated with sequestration of YAP expression to the nucleus of tumor cells (C, D) whereas retained SAV1 expression results in mainly cytoplasmic YAP expression (A, B).

Immunohistochemistry revealed strong cytoplasmic SAV1 expression in normal tubular epithelial cells, but immunolabeling was lost in adjacent neoplastic cells in 16 of 31 cases. Weak or absent SAV1 expression was found to correlate with a predominantly nuclear staining pattern for YAP whereas sustained SAV1 expression was associated with a predominantly cytoplasmic or equivocal pattern (p=0.0091; see Table 4.3 and Figure 4.7).

Table 4.3.: Loss of SAV1 immunoreactivity correlates with nuclear localization of YAP.

		YAP expression		
		cytoplasmic	nuclear	total
SAV1	positive	13	2	15
	weak or negative	6	10	16
	total	19	12	31
Fisher's exact test P = 0,0091				

It has to be emphasized that this correlation was only observed between the two specific parameters of *SAV1 positivity* and *YAP staining pattern*, and there are cases, that can be classified as double positive for YAP and SAV1 (refer to Figure 4.7, D for an example) as well as a small subset that shows nuclear YAP localization with sustained SAV1 expression, suggesting additional mechanisms apart from loss of SAV1 that lead to Hippo pathway perturbation and pathological YAP signaling in ccRCC.

Expression of YAP and interaction partners in a panel of RCC-cell lines

In a panel of seven ccRCC cell lines, basal YAP expression was found in all cell lines examined, although expression levels varied greatly, with some cell lines expressing very high levels of YAP. The phosphorylated form of the transcriptional coactivator constitutes the inactive form of YAP. Cell lines with high basal levels of total YAP contained minimal (ACHN) to absent (MZ1774) levels of pYAP pointing towards high transcriptional activity of YAP. ccRCC cell lines further consistently expressed high levels of TEF-1, the major interaction partner of YAP, with one exception being MZ1774 where expression levels were lower.

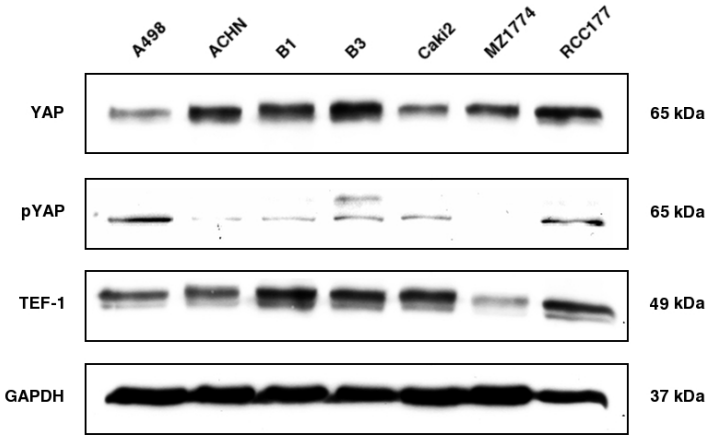

Figure 4.8.: Expression of YAP, pYAP and TEF-1 in a panel of RCC-cell lines. Basal expression of YAP was observed in all ccRCC cell lines examined, whereas expression of the inactive form pYAP was minimal to absent in cell lines expressing high basal levels of YAP. The transcription factor TEF-1, a major interaction partner of YAP, was found in all ccRCC cell lines analyzed.

In a second step, the extent of expression of the member of the canonical Hippo pathway SAV1 was examined in this panel of ccRCC cell lines. As previously described, SAV1 expression was completely lost in ACHN cells, due to a homozygous deletion on chromosome 14q13-14q22 [158]. In the examined panel, there was no second case of total loss of SAV1 expression, although A498, MZ1774, B3 and RCC177 displayed very low levels of the protein, to some degree consistent with their high levels of YAP expression.

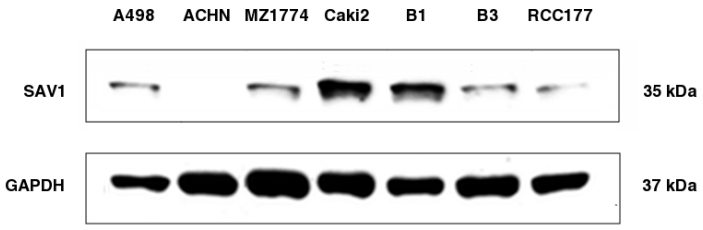

Figure 4.9.: Expression of the Hippo pathway member SAV1 in a panel of RCC-cell lines. With the exception of ACHN, all ccRCC cell lines express the member of the canonical Hippo pathway SAV1, although expression levels in A498, MZ1774, B3 and RCC177 are very low.

4.1.4. Summary and Conclusion

Upregulation of nuclear YAP expression is present in a considerable subset of all tumor entities examined, although frequencies are variable. Nuclear YAP expression correlates with nodal stadium in PDAC and is more frequent in patients with ccRCC that has spread to the regional lymph nodes. Contrary to previous studies, there was no correlation between tumor grade and YAP positivity in PDAC [33]. In CCC, the data on a relatively small series of 31 cases suggest that elevated YAP levels highlight formations of invading tumor cells when lymph node metastases or perineural invasion are present, even if the main tumor is not characterized by particularly high nuclear YAP levels.

In all three cancers, solitary, fibroblast-like cells inside the tumor adjacent stroma that were highlighted by robust nuclear YAP staining could be observed. In two cases of ccRCC, these stained likewise positive for cytokeratin and were thus identified as single tumor cells invading the surrounding fibrous tissue, suggesting that aberrant YAP-signaling might at least in a subset of cases be involved in mediating epithelial-to-mesenchymal transition as has previously been described for other aberrantly re-activated embryonic signaling pathways in malignant tumors. This will certainly not be true for all solitary, highly YAP positive cells residing in the tumor adjacent stroma and it has to be assumed that the majority are indeed cancer-associated fibroblasts. There is an ongoing debate about the crosstalk between neoplastic cells and the surrounding stromal compartment with regard to the extent of the contribution of the tumor microenvironment to tumor progression and invasion. Notably, both PDAC and cancers of the biliary tract can trigger an intense desmoplastic reaction and the specific types of tumor associated fibroblasts influencing tumor progression and tumor microenvironment have been described in both entities (see [4] for a review on the role of pancreatic stellate cells in PDAC and [65] for the role of hepatic stellate cells and activated fibroblasts in disease progression of biliary cancers). Importantly, YAP directly promotes the transcription and expression of connective-tissue growth factor (CTGF), a cytokine that has been shown to be crucial for the formation of the desmoplastic stroma in PDAC [4, 34].

In all cell lines with high YAP activity, a member of the TEAD-family of transcription factors was simultaneously present providing the prerequisite for YAP to exert its pro-tumorigenic and pro-invasive properties [93]. Lamar *et al.* reported enhanced metastatic potential of breast cancer as well as melanoma cells with increased YAP/TEAD activity; they concluded that YAP can promote metastasis through its TEAD-interaction domain [93]. This is significant with regard to the association of high nuclear YAP levels with

pro-invasive properties such as correlation with nodal status or upregulation in invading tumor cells, that was observed in all three tumor entities analyzed. However, in light of a recent paper by Shao *et al.* showing that YAP can functionally substitute RAS in cancer cells depending on continued RAS-signaling for survival, the solitary importance of pro-tumorigenic signaling via the YAP/TEAD complex has to be put in perspective. YAP rescues cell viability and tumorigenicity in RAS-dependent cancer cell-lines via up-regulation of immediate early genes such as *MYC* and *FOS* as well as EMT-genes that is independent of TEAD although the actual interaction partner remained elusive [144]. This in turn means that YAP could potentially exert its oncogenic properties in cell-lines with little to no TEAD expression – as observed in several PDAC cancer cell lines – via an alternative route.

Based on the experimental data discussed in this thesis, there is no single, universal, clearcut mechanism apparent that conclusively explains the derepression of YAP in the three tumor entities analyzed. All currently postulated hypotheses as discussed here can provide an explanation for a subgroup of cases, but point towards a more widespread deregulation of upstream members of the Hippo-signaling network. In line with these observations, conditional knockout of NF2, an upstream activator of the growth inhibitory Hippo pathway, in the proximal tubular epithelium of Villin-Cre;Nf2$^{(lox/lox)}$ mice leads to intratubular neoplasia and invasive carcinoma which resembles human RCC in a mouse model of renal cell carcinoma [112]. Recent reports also linked the renal cilia-associated proteins NPHP4 and NPHP9 to Hippo-signaling in both oncogenically transformed and normal kidney epithelial cells. These proteins were found to prevent LATS-dependent phosphorylation of YAP, thus controlling YAP activation and mediating cell proliferation [54, 55].

4.2. YAP-deficient cancer cell lines display overlapping but distinct phenotypes

Having established the ample occurrence of YAP overexpression in PDAC, CCC and ccRCC, the next step was to analyze the functional significance of YAP-induced transcription for cancer cell properties *in vitro* and *in vivo*. An approach using RNA-interference, more specifically: short hairpin RNAs, was chosen in order to downregulate the YAP protein and to characterize functional properties of YAP-deficient as compared to non-modified cell lines.

RNA-interference RNA-interference is a mechanism naturally occurring in all eukaryotic cells in order to regulate the expression of specific genes in a targeted manner. Double-stranded RNA inhibits gene expression by targeted destruction of specific mRNAs, a process that serves two purposes: firstly, the destruction of potentially harmful nucleotide sequences, such as viral RNA or transposons. Secondly, the targeted regulation of gene expression is mediated in part by microRNAs which are endogenously produced and mark certain mRNAs for degradation. RNA interference can lead to the downregulation of specific proteins, if mRNA of that protein is targeted and degraded, or similarly, to the upregulation of protein expression, when mRNA of regulatory structures is targeted and the production of said protein is disinhibited. This RNA-dependent gene silencing process is governed by the RNAi pathway in eukaryotic cells, first described by Andrew Fire and Craig C. Mello [45], who shared the 2006 Nobel Prize in Physiology or Medicine for their discovery.

Feeding into the RNAi pathway are long double-stranded RNA molecules, originating either from endogenous primary miRNAs, that are transcribed in the nucleus and then translocate into the cytoplasm, or from exogenous sources such as viral infections or laboratory manipulations. Long double-stranded RNA molecules are cleaved by the enzyme Dicer into shorter fragments of double-stranded RNA (about 20 bases long) termed "small interfering" or siRNA. Double-stranded siRNA splits into two strands, the passenger strand, which is swiftly degraded, and the guide or antisense strand, which is bound by the RNA induced silencing complex (RISC). When the guide strand bound to RISC pairs with its complementary mRNA, the newly assembled double-strand is cleaved and degraded by the protein Argonaute, a component of RISC.

Gene silencing by introduction of short hairpin RNAs The physiologic process of RNA interference has been developed into widely used tools for molecular biology and experimental therapeutics. Generally, two routes have been established to introduce RNA sequences targeting specific mRNAs into cells. siRNA is either directly introduced into the cytosol by transfection techniques, thus creating a temporary downregulation of the target mRNA. Alternatively, a sequence coding for short hairpin RNAs (shRNAs) is introduced into the genome of the cells, mostly by lentiviral transduction, creating a stable knockdown of the target mRNA and protein. shRNAs mimic miRNA function and are processed accordingly.

Two major *caveats* have to be taken into account when designing an shRNA-experiment. First, there is the possibility that the introduced mature antisense strand of the siRNA will pair with mRNA of multiple genes in addition to the intended target mRNA thus creating unspecific "off-target" effects.

Second, double-stranded RNA molecules have the capacity to alert the innate immune system and elicit the mammalian interferon response thus creating incalculable "off-topic" effects. It is generally believed that this potential confounding effect plays a major role particularly with longer double-stranded RNA molecules, but the interactions of siRNA with the immune system are manifold and "off-topic" effects require appropriate controls also in classic siRNA or shRNA experiments.

It is therefore indispensable to verify potential effects of shRNA-mediated knockdowns on *in vitro* or *in vivo* properties of cells using at least two different sequences of antisense-RNA and control against cells transduced with non-silencing controls. Substantial knock-down needs to be verified on mRNA as well as protein-level. These guidelines where observed while designing the RNAi experiments presented in this study.

Experimental road map For each of the tumor entities analyzed, two to three cell lines exhibiting high basal YAP expression levels were chosen and YAP activity was abrogated by shRNA-mediated knockdown. For each of the respective parental cell lines at least two different shRNA sequences directed against *YAP* (designated "YAPshRNA#4" and "YAPshRNA#5") were used and compared to untransduced as well as to mock-transduced mass clones in order to control for unspecific, off-target effects. After confirmation of sufficient YAP-knockdown on the protein level, the phenotype of YAP-deficient cell lines was characterized employing cell-based *in vitro* and, where available, *in vivo* models.

4.2.1. PDAC

Downregulation of YAP diminishes proliferation of PDAC cell lines

Two PDAC cell lines with high basal YAP expression levels – PK9, and Panc 10.05 – were selected and aberrant YAP activity was inhibited by shRNA-mediated knockdown. Consistent stable knockdown of endogenous YAP was confirmed by Western blot analysis (Figure 4.10).

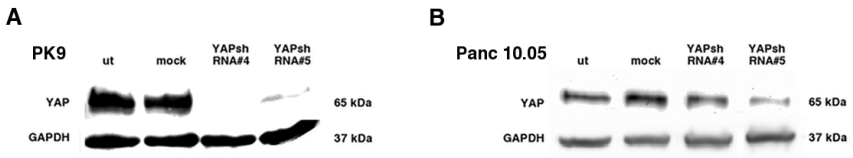

Figure 4.10.: Confirmation of consistent stable knockdown. Sufficient shRNA-mediated YAP-knockdown in PK9 (A) and Panc 10.05 (B) cells is stable and consistent on the protein level as determined by Western blot.

The first cellular property analyzed was the time-dependent increase of viable cell mass as determined by the MTS assay. This parameter is used as a reasonably reliable surrogate for cellular proliferation (see 3.3.1 on 68). In both cell lines, YAP-knockdown led to a significant time-dependent reduction of net cell growth as compared to mock-transduced cells (Figure 4.11).

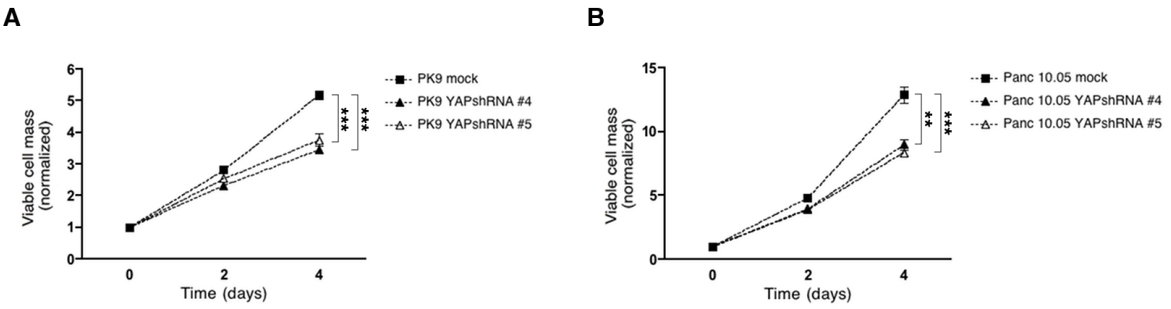

Figure 4.11.: YAP-knockdown decreases proliferation of PDAC cell lines. Knockdown of endogenous YAP led to a highly significant reduction in viable cell mass after 96 hours for PK9 (A) and Panc 10.05 cells (B). ** $p < 0.01$, *** $p < 0.001$

YAP-knockdown does not affect migration of PDAC-cell lines

Next, effects of YAP-knockdown on *in vitro* cell migration was assessed by Boyden Chamber assays. No difference in time-dependent cell migration was detected between mock-transduced and YAPshRNA-transduced Panc 10.05 and PK9 mass clones (see Figure 4.12 on page 102) All experiments were done in triplicates and repeated twice.

YAP-deficient PDAC cell lines display reduced colony-forming capacity

Anchorage-independent growth and colony formation in soft agar is a widely accepted *in vitro* surrogate phenotype of malignantly transformed cells. YAP-knockdown potently and reproducibly abrogated anchorage-independent growth of PK9 cells in soft agar (mean reduction of colony counts by 67.80% ± 1,25%, n=4, $p<0.0001$ for clone #4, and 71.00% ± 3.40%, n=4, $p<0.0001$ for clone #5, respectively; see Figure 4.13,A).

To determine potential effects of YAP-knockdown on the ability to form colonies from single PDAC cells, replating efficiency assays were performed using single cell suspensions. The ability of PK9 YAP-knockdown cells to form colonies from single cells in this setting was significantly reduced as compared to mock-transduced controls (mean reduction of colony counts by 70.20% ± 5.73%, n=8, $p<0.0001$ for clone #4, and 43.40% ± 6.46%, n=8, $p<0.0001$ for clone #5, respectively; see Figure 4.13, B). Of interest, the colonies formed by YAPshRNA knockdown cells were not only less numerous but also smaller in size as compared to their mock-transduced counterparts, reflecting the extend of YAP-knockdown as well as reduced *in vitro* net cell growth as already observed previously in MTS assays.

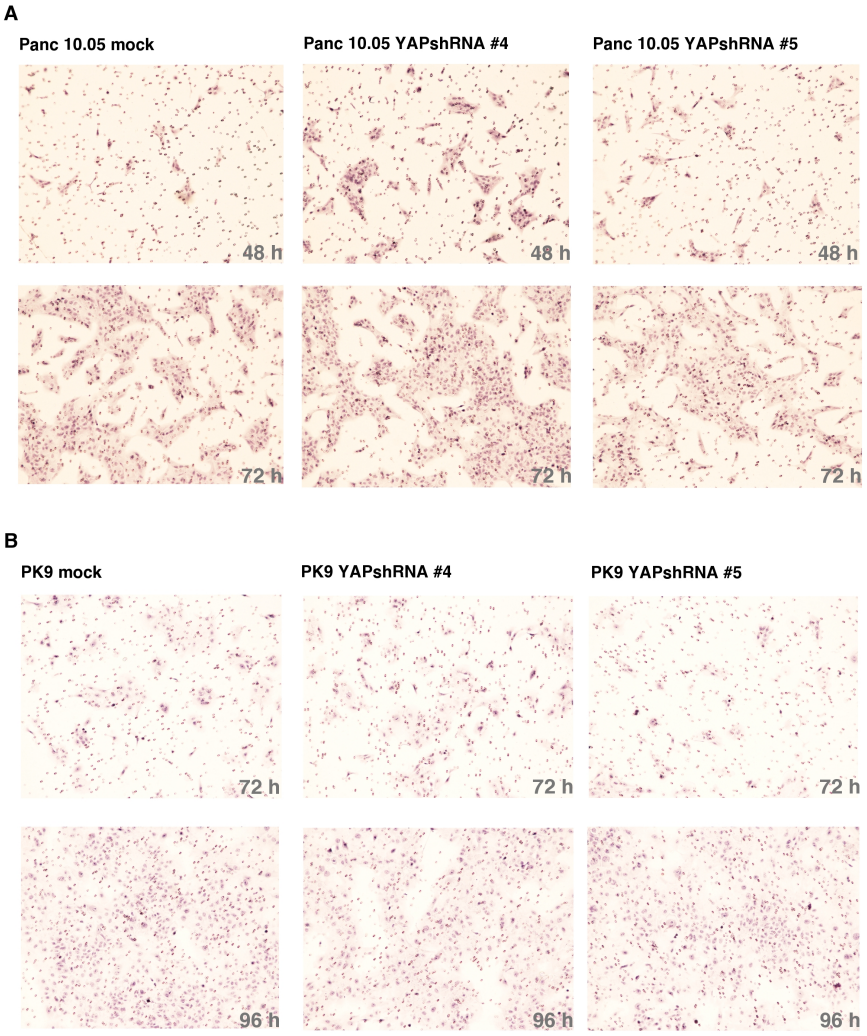

Figure 4.12.: YAP-knockdown does not affect migratory potential of PDAC cell lines. YAP downregulation did not affect PDAC migration in Boyden chamber assays. Transwell migration through 8 µm pore filters was assessed after 48 and 72 hours in the cell lines Panc 10.05 (A) and PK9 (B).

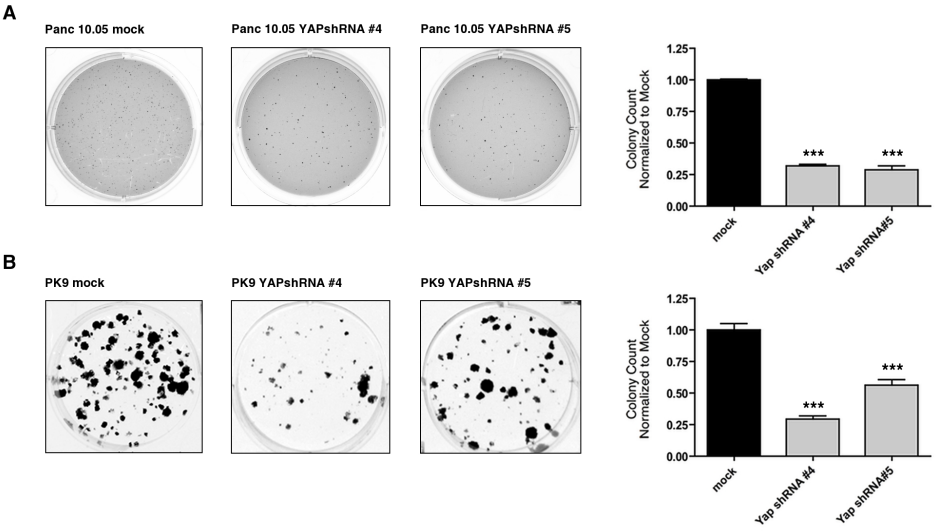

Figure 4.13.: YAP-knockdown decreases anchorage-independent colony formation of PDAC cell lines. Downregulation of YAP significantly reduced anchorage-independent growth in soft-agar of the PDAC cell line Panc 10.05 (A). Likewise, colony formation as measured by replating efficiency assays was reduced in YAP-knockdown cells (B). Representative images and combined colony counts of two (A) and four (B) independent experiments are shown.

4.2.2. Biliary cancers

Downregulation of YAP in diminishes proliferation of biliary cancer cell lines

Two biliary cancer cell lines with high basal YAP expression levels – G-415, and Nec – were picked and aberrant YAP activity was cut off by shRNA-mediated knockdown. Consistent stable knockdown of endogenous YAP was confirmed by Western blot analysis (Figure 4.14).

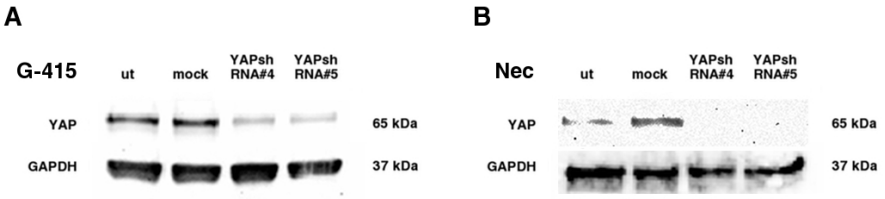

Figure 4.14.: Confirmation of consistent stable knockdown. Sufficient shRNA-mediated YAP-knockdown in G-415 (A) and Nec (B) cells is stable and consistent on the protein level as determined by Western blot.

The first cellular property analyzed was the time-dependent increase of viable cell mass as determined by the MTS assay. This parameter is used as a reasonably reliable surrogate for cellular proliferation (see 3.3.1 on page 68). In both cell lines, YAP-knockdown led to a significant time-dependent reduction of net cell growth as compared to mock-transduced cells (Figure 4.15).

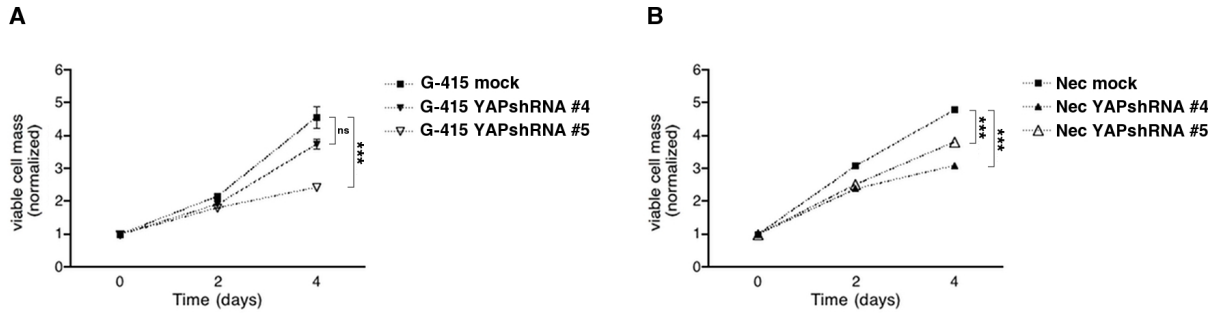

Figure 4.15.: YAP-knockdown decreases proliferation of biliary cancer cell lines. Knockdown of endogenous YAP led to a highly significant reduction in viable cell mass after 96 hours for G-415 (A) and Nec cells (B). ** $p < 0.01$, *** $p < 0.001$

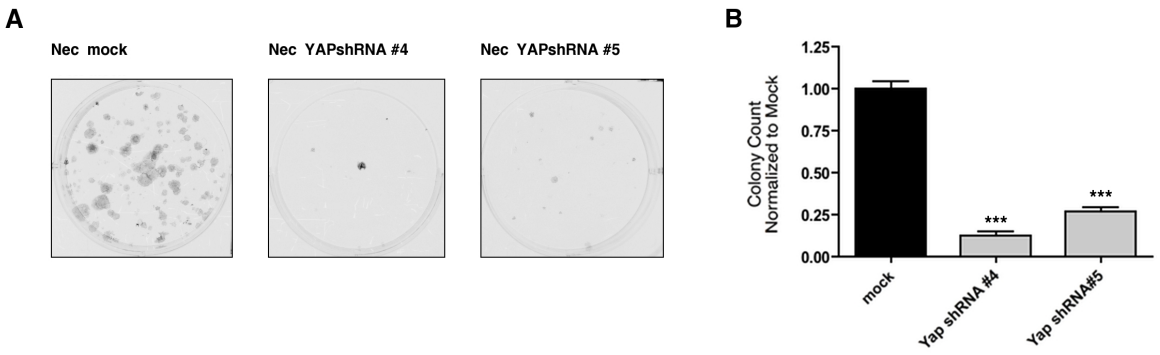

Figure 4.16.: YAP-knockdown decreases colony formation of biliary cancer cell lines. Downregulation of YAP significantly reduced colony formation as measured by replating efficiency assays in Nec YAP-knockdown cells. Representative images (A) and combined colony counts (B) of two independent experiments are shown.

An impact of YAP-knockdown on biliary cancer cell migration as determined by the Boyden chamber assay could not be determined, as non-transduced, mock-transduced and shRNA-transduced mass clones of both G415 and Nec cells failed to transmigrate into the lower chamber in this set-up.

YAP-deficient biliary cancer cell lines display reduced colony-forming potential

To determine potential effects of YAP-knockdown on the ability to form colonies from single biliary cancer cells, replating efficiency assays were performed using single cell suspensions. The ability of Nec YAP-knockdown cells to form colonies from single cells in this setting was significantly reduced as compared to mock-transduced controls (mean reduction of colony counts by 87.30% $\pm$ 5.27%, n=4, $p<0.0001$ for clone #4, and 73.30% $\pm$ 5.51%, n=4, $p<0.0001$ for clone #5, respectively; see Figure 4.16, B). Of interest, the colonies formed by YAPshRNA knockdown cells were not only less numerous but also smaller in size as compared to their mock-transduced counterparts, reflecting the extend of YAP-knockdown as well as reduced in vitro net cell growth as already observed previously in MTS assays.

4.2.3. Renal Cell Carcinoma

Downregulation of YAP diminishes growth of ccRCC-cell lines

Three ccRCC cell lines with high basal YAP expression levels - A498, ACHN and MZ1774 - were picked and dysfunctional Hippo-signaling and aberrant YAP activity was abrogated by shRNA-mediated knockdown. Consistent stable knockdown of endogenous YAP was confirmed by Western blot analysis (Figure 4.17).

Figure 4.17.: shRNA-mediated YAP-knockdown in ccRCC cells. Stable knockdown was confirmed by Western blot analysis in A498 (A), ACHN(B), and MZ1774(C) cells.

In all of the three cell lines examined, YAP-knockdown led to a significant time-dependent reduction of net cell growth as compared to mock-transduced cells ($p<0.001$, Figure 4.18). Cell viability as determined by the MTS-assay was used as a surrogate parameter for cell proliferation.

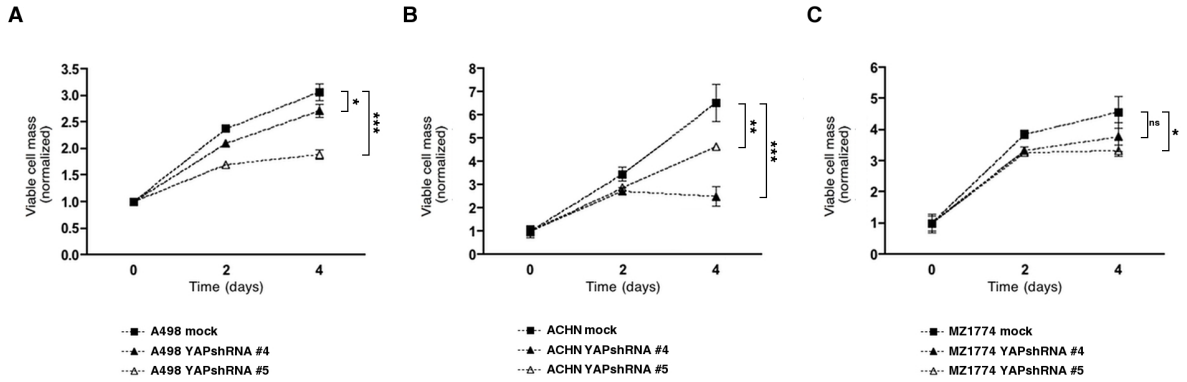

Figure 4.18.: YAP-knockdown decreases proliferation of ccRCC cell lines. Stable YAP-knockdown resulted in significantly reduced cell viability as determined by MTS-assay, a surrogate marker for cell proliferation, in A498 (A), ACHN (B), and MZ1774 cells (C). * $p < 0.05$, ** $p < 0.01$, *** $p < 0.001$

YAP-knockdown significantly impairs migration of ccRCC-cell lines

Next, effects of YAP-knockdown on *in vitro* cell migration was assessed by Boyden Chamber assays. A considerable reduction of ccRCC migration was observed in response to YAP-knockdown in all three cell lines examined ($p < 0.001$; Figure 4.19 on page 108), consistent with the observation that high YAP expression levels are associated with invasive properties *in vivo* (as observed in patient tumor tissue samples, see section 4.1.3, page 90). All experiments were done in triplicates and repeated twice.

YAP-knockdown decreases colony formation in ccRCC cell lines

To determine potential effects of YAP-knockdown on the ability to form colonies from single cells and expand clonally, replating efficiency assays were performed using dilute, single cell suspensions. The ability of ACHN-YAPshRNA#4 cells to form colonies from single cells in this setting was significantly reduced as compared to mock-transduced ACHN controls (mean reduction of colony counts by 66.3% ± 6.04%, n=6, $p<0.0001$, Figure 4.20, A). Interestingly, the colonies formed by YAP-knockdown cells were not only less numerous but also smaller in size, reflecting reduced in vitro net cell growth as already observed previously in MTS assays.

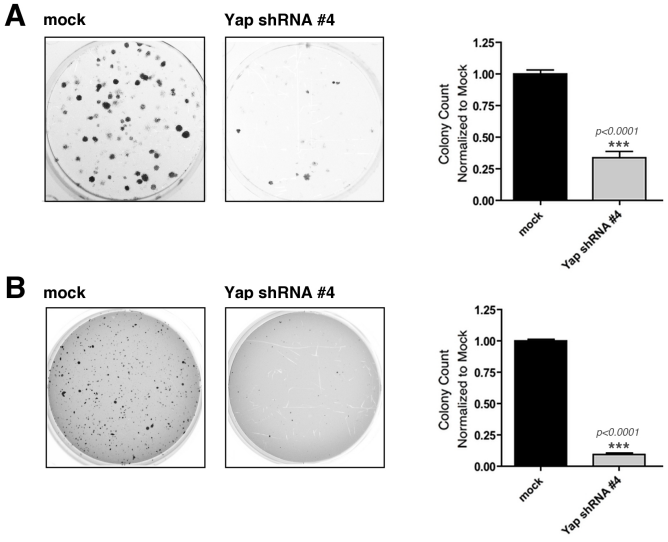

Figure 4.20.: shRNA-mediated YAP-knockdown reduces colony formation and abates anchorage-independent growth of ccRCC cells. Downregulation of YAP significantly reduced the number of colonies formed in replating efficiency assays (A) as well as anchorage-independent growth in soft agar of the ccRCC cell line ACHN (B). Representative images and combined colony counts of three independent experiments are shown.

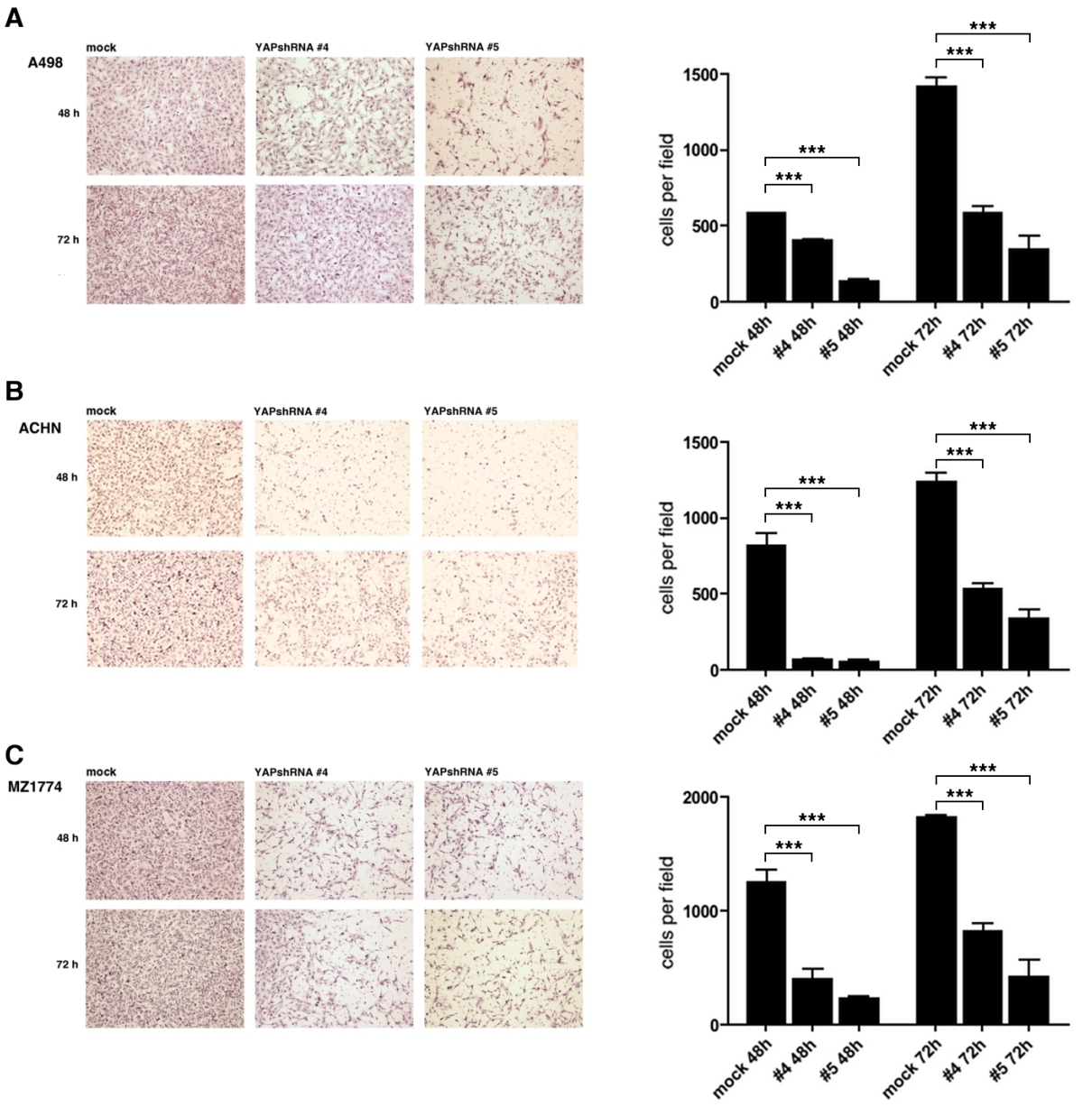

Figure 4.19.: YAP-knockdown impairs migratory potential of ccRCC cell lines. YAP downregulation resulted in marked inhibition of ccRCC migration in Boyden chamber assays. Transwell migration through 8 µm pore filters was assessed after 48 and 72 hours in the cell lines A498 (A), ACHN (B) and MZ1774(C). A pronounced decrease in cell numbers was found for all YAP-knockdown mass clones. * $p < 0.05$, ** $p < 0.01$, *** $p < 0.001$ Three randomly selected microscopic fields of representative experiments were selected and cells were counted. Results are shown as means ± SD.

YAP-knockdown potently and reproducibly abrogated anchorage-independent growth of ACHN cells in soft agar (reduction of colony counts by more than 90.3% ± 2.16%, n=6, $p < 0.0001$, Figure 4.20, B). Similar to what was observed in replating assays, the remaining colonies formed by ACHN-YAPshRNA mass clones were not only less numerous but also significantly smaller as compared to their mock-transduced counterparts in this 3D culture setting.

YAP-knockdown cells display decreased tumorigenicity in a tumor xenograft model

The above mentioned results of the *in vitro* assays suggest that dysfunctional Hippo-signaling and resulting aberrant YAP-activity contribute to tumor progression and metastasis in ccRCC. The *in vivo* relevance of these findings was evaluated using a subcutaneous xenograft model. Male athymic $CD1^{nu/nu}$ nude mice, six to eight weeks of age, were injected subcutaneously with 2.5×10^6 ACHN-YAPshRNA or ACHN-mock cells into both flanks. Tumor volumes were assessed weekly using digital calipers starting one week post injection. Xenograft growth of ACHN-YAPshRNA cells was significantly delayed as compared to ACHN-mock controls ($p = 0.0182$; Figure 4.21, A, left panel & B, see page 110), while at the same time the overall body mass of xenograft-bearing mice was not significantly altered between the two study arms (Figure 4.21 A, right panel).

At five weeks post injection, mice were sacrificed and tumors were harvested for histopathological and immunohistochemical evaluation, or snap-frozen for mRNA extraction and subsequent quantitative real-time RT-PCR analysis, respectively. Immunohistochemistry of formalin fixed and paraffin embedded xenograft tumor tissue confirmed retained YAP-knockdown in ACHN-YAPshRNA tumors (Figure 4.21, C).

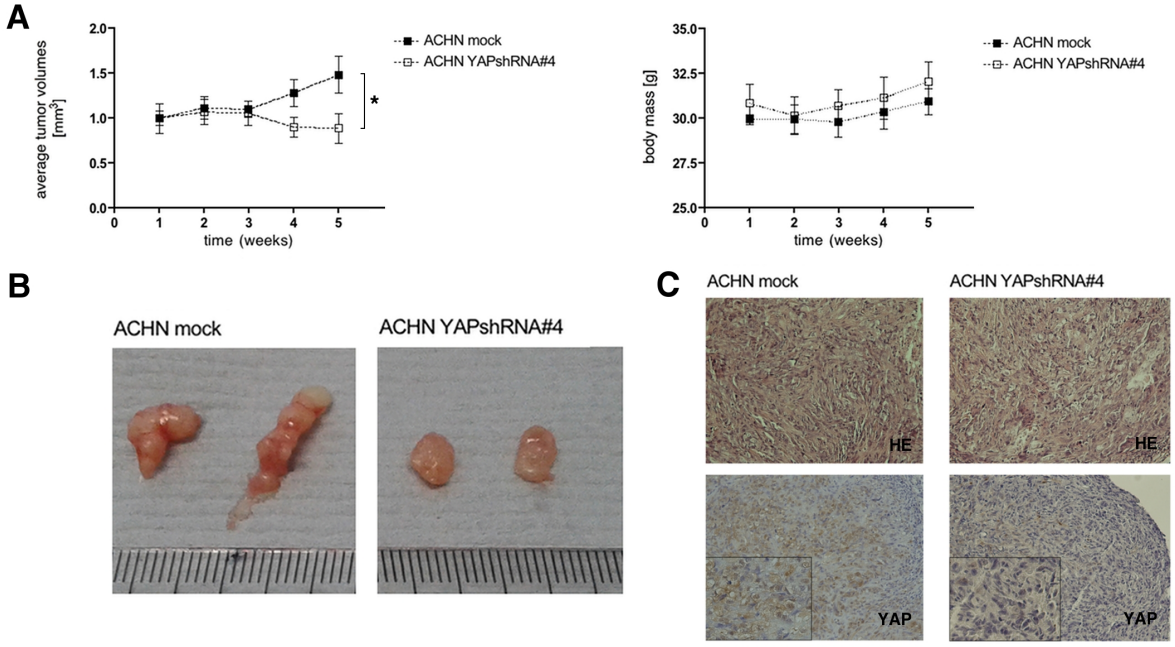

Figure 4.21.: YAP-knockdown inhibits tumor growth in a subcutaneous xenograft model. Subcutaneous injection of YAP-knockdown cells into the flanks of CD1$^{nu/nu}$ mice resulted in significantly smaller tumors compared to mock-transduced cells while not affecting the body mass of the mice (A, B). Immunohistochemistry of formalin fixed and paraffin embedded xenograft tissue confirmed significant downregulation of YAP in tumors derived from ACHN YAP-knockdown cells (C). Representative images are shown in × 200, with insets in × 400 magnification.

4.2.4. Summary and Conclusion

In summary, the experimental data presented here demonstrate that YAP exerts pro-proliferative functions and enhances colony formation in PDAC, biliary cancer as well as ccRCC. This is in line with previous findings by others (see [33] for PDAC and [105] for ccRCC) who reported that YAP enhances tumor formation of PDAC cell lines in nude mice (see [34], supplemental data).

The finding of a nearly universal phenotype with regard to proliferation and tumor formation is at the same time remarkable in light of results published by different groups, who found that YAP functions as a tumor suppressor in breast cancer [179] and reported that YAP restricts the expansion of intestinal stem cells by repressing uncontrolled signaling via the Wnt-pathway [9]. shRNA-mediated YAP-knockdown in breast cancer cell lines suppressed anoikis, increased migration, and promoted tumor growth in nude mice [179], while signaling through the Hippo/ YAP-axis seems to have a balancing effect on the intestinal stem/ progenitor cell compartment [8]. Uncontrolled YAP activation in intestinal stem cells leads to the expansion of multipotent, undifferentiated progenitor cells which differentiate upon cessation of YAP expression [22]. On the other hand, YAP also has an unexpected growth-suppressive function restricting Wnt-signals during intestinal regeneration, and complete loss of the protein is observed in a subset of highly aggressive and undifferentiated human colorectal carcinomas that are associated with poor survival and stage IV disease [9].

These findings point towards a crucial context- and tissue-dependency of YAP-signaling in the adult organism that ties in neatly with the putative manifold upstream signals feeding into the core signaling cassette and influencing the many direct interaction partners of YAP. It will therefore be very interesting to elucidate potential downstream interaction partners in order to gain clues for the identification of crucial players that might act as counterbalance to the pro-proliferative signals of YAP.

With regard to the histology results, that suggest a role of YAP in tumor invasion for all cancer entities analyzed, it is a little surprising to find that shRNA-mediated knockdown of the protein impairs *in vitro* migration of cancer cells only in ccRCC cell lines, while no phenotype could be observed in pancreatobiliary cancer cell lines. It will therefore be intriguing to analyze downstream targets and interesting to determine to what degree those genes are commonly regulated by YAP in different tumor entities.

4.3. Transcriptomic profiling of YAP-knockdowns – YAP controls a distinct set of target genes in different tumor entities

4.3.1. There is little overlap in YAP target gene signatures

The phenotypic characterization of YAP-knockdown cell lines *in vitro* and *in vivo* led to comparable results in PDAC, biliary cancer and ccRCC cell lines and revealed that YAP functions as a crucial mediator of proliferation and colony formation in all three entities analyzed. YAP was further identified as a critical promotor of cell migration and invasion exclusively in ccRCC. In order to gain insight into the mechanism by which YAP exerts its proproliferative and tumor promoting properties and to identify potential downstream target genes, transcriptomic profiling of YAP-knockdown mass clones of PK9, G415 and MZ1774 cells was performed using 100 ng of total RNA extracted from the respective cell lines as raw material (refer to 3.2.3 on page 67 for details on the experimental procedure).

The striking similarity regarding the phenotypic consequences of YAP knockdown in PDAC, biliary cancer and ccRCC cell lines suggests a considerable overlap in the target gene signature of the three tumor entities analyzed with the possible exception of ccRCC, where a distinct signature regarding genes regulating cell migration and tumor invasion might be expected. It is therefore very intriguing to observe that the portion of genes similarly regulated by YAP is very small in PK9, G415 and MZ1774 cells as shown in figure 4.22.

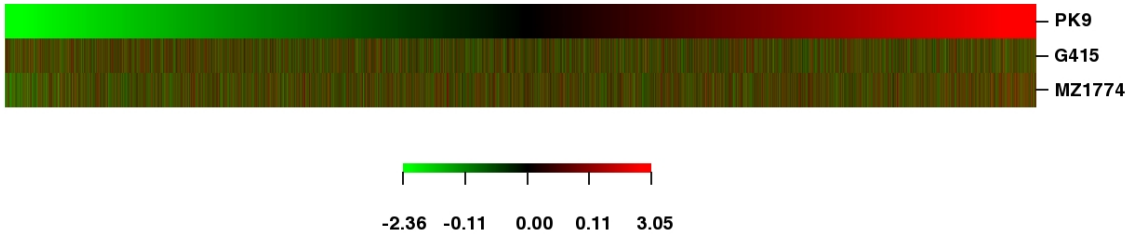

Figure 4.22.: Heatmap of all cell lines submitted to transcriptomic profiling. The signals given by the respective probes are aligned to match the pattern of differential expression observed in PK9 YAP-knockdown as compared to mock-transduced cells. No broad areas of common genetic regulation can be observed.

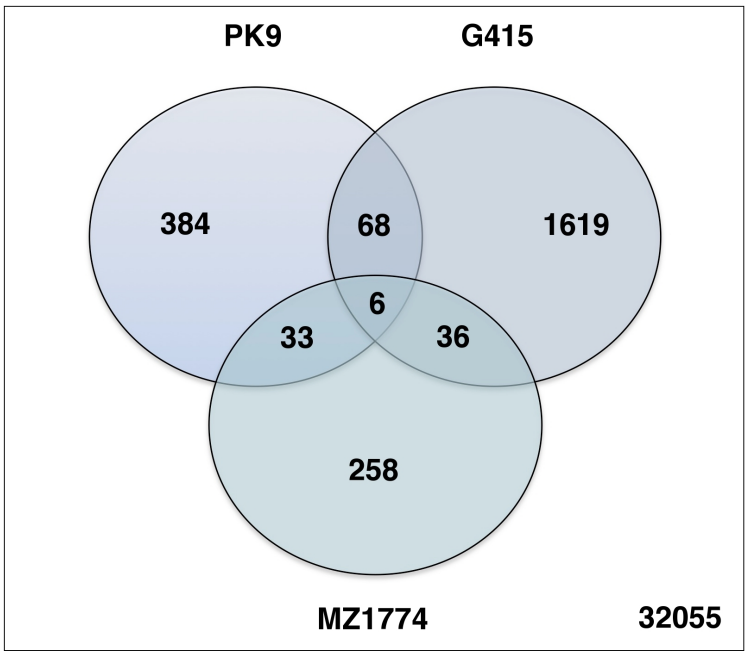

Figure 4.23.: Venn diagram of microarray results.

This impression is further corroborated when the focus is shifted to a more detailed, single-gene perspective: only a total of six genes were found to be similarly differentially expressed in all three cell lines analyzed (please see figure 4.4 on page 114 for a list of those six genes). The overlap between two cell lines at a time was only little higher, with 68 genes being similarly regulated by YAP in PK9 and G415 cells, 36 genes in G415 and MZ1774 cells and 33 genes in PK9 and MZ1774 cells with a grand total of 32055 genes analyzed (see Figure 4.23 on page 113).

Rationale for third generation pathway analysis

In a landmark review, Vogelstein and coauthors proposed a model which clarifies our understanding of oncogenic driver genes. A selective growth advantage is conferred to a neoplastic cell by either driver gene mutations (this specific variant is termed *Mut-Driver gene*) or by epigenetic changes leading to aberrant expression of the driver gene (*Epi-Driver gene*) [168]. All known driver genes seem to influence one of three key cellular functions in order to provide a selective growth advantage to the cell: cell fate, cell survival and genome maintenance. These functions are affected via roughly twelve core signaling pathways as graphically depicted in Figure 4.24. This model provides excellent guidance through the thicket of cancer genomes and the multitude of somatic mutations in any

Table 4.4.: Genes similarly regulated upon YAP-knockdown in all three cell lines

Gene ID	Symbol	Gene name	FC PK9	FC G415	FC MZ1774	BH adj. p Value
4312	MMP1	matrix metallopeptidase 1 (interstitial collagenase)	3,89	2,64	1,55	2,09E-08
3656	IRAK2	interleukin-1 receptor-associated kinase 2	1,83	1,57	1,24	3,45E-07
85463	ZC3H12C	zinc finger CCCH-type containing 12C	1,46	1,65	1,25	5,91E-07
10413	YAP1	Yes-associated protein 1	0,195	0,295	0,395	2,92E-16
2181	ACSL3	acyl-CoA synthetase long-chain family member 3	0,503	0,645	0,720	1,27E-05
1490	CTGF	connective tissue growth factor	0,503	0,616	0,805	4,44E-05

FC: fold change, *BH adj. p Value:* Benjamini-Hochberg adjusted p Value

given tumor, because it shifts perspective towards a conceptual, "30,000-feet view" [168]. In full appreciation of this perspective, one has to regard the core signaling pathways as headlines and concede that the precise mutations influencing a giving pathway are unlikely to affect the same genes in different tumors.

If applied to the Hippo-YAP axis in cancer, this concept leads to the following considerations:

- Overexpression of YAP does confer a selective growth advantage to cancer cells in several tumor types, including the three tumor entities examined in this study.
- Since somatic mutations within the *YAP* gene itself are scarce [64] the observed widespread aberrant overexpression of the transcriptional coactivator YAP can be explained either by mutation of an upstream member of the Hippo pathway and subsequent derepression of YAP (mut-driver gene hypothesis) or epigenetic changes leading to the observed overexpression (epi-driver gene hypothesis).
- Evidence for the mut-driver gene hypothesis is so far only available in the case of NF2 in ccRCC. NF2 constitutes the sole member of the upstream Hippo-signaling network that has been identified as a *bona fide* tumor suppressor gene and is listed in the Catalogue Of Somatic Mutations In Cancer (COSMIC) database [64]. Mutations

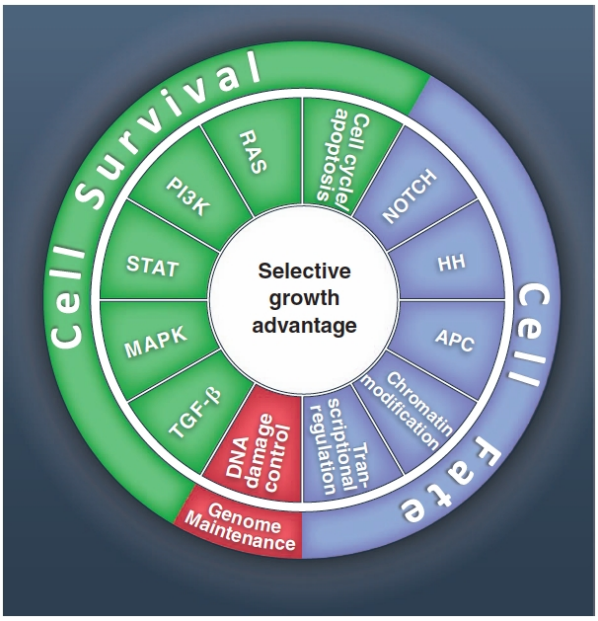

Figure 4.24.: Core signaling pathways affected by driver gene mutations in cancer. Vogelstein *et al.* demonstrated that all known driver genes can be classified into one or more of twelve core signaling pathways that confer a selective growth advantage to the affected cell. Figure from [168]. Reprinted with permission from AAAS.

of other pathway members have been described, but are low in frequency and don't qualify as driver gene mutations. This lends plausibility to the hypothesis, that in the majority of cases, *YAP* might function as an epi-driver gene.

- Aberrant YAP activation will result in transduction of growth-promoting signals downstream of growth promoting pathways, putatively involved in cell survival and cell fate. Transcriptomic profiling and pathway analysis of differentially expressed genes of YAP-deficient vs. YAP-intact mass clones should therefore provide clues towards the downstream mechanism of oncogenic signaling via YAP.

- Although individual differentially expressed genes may vary considerably, affected pathways might still overlap and reveal a common mechanism, when assuming the "30,000 feet"-perspective.

Pathway analysis is an analytical tool that helps to contextualize gene expression data collected by microarray experiments and shifts focus from the single-gene perspective towards a conceptual view. This approach was therefore also used for the data presented in this dissertation. Methodologically, a third generation-approach to pathway analysis

was chosen and Signaling Pathway Impact Analysis (SPIA) was performed as previously described [159]. Classical signaling pathway analyses identify affected pathways either by the number of differentially expressed genes (overrepresentation or enrichment analyses with arbitrarily determined cutoffs regarding false discovery rate (FDR) and fold-change (FC) thresholds; also termed first generation methods) or by application of the hypothesis that although large changes in individual genes can have significant effects on pathways, weaker but coordinated changes in sets of functionally related genes (i.e., pathways) can also have significant effects (functional class scoring or second generation methods) [79]. Third generation methods expand this view by including topological information and therefore taking into account the hierarchy of gene products inside a given pathway. SPIA combines evidence obtained from enrichment analyses with topological information arriving at information about the actual perturbation of a pathway under a given condition. A global pathway significance p-value (pG) is calculated by the combination of individually determined enrichment (pNDE) and perturbation (pPERT) p-values. pG is then corrected by two statistical methods: false discovery rate (pGFDR) and familywise error rate (pGFWER) [159]. For the purpose of this study, results were deemed significant if either pGFDR or pGFWER was ≤ 0.05.

Limitations The most obvious limitation of a pathway topology based approach is that it relies on the quality and accuracy of the pathway annotation and gene ontology databases. However, this problem is inherent to analytical approaches of all generations and constitutes an uncertainty that might be minimized but never completely abolished. For the purpose of the bioinformatical analysis at hand, the Kyoto Encyclopedia of Genes and Genomes (KEGG) PATHWAY database was used. A graphic overview of the observed pathway perturbation can be accessed by following the link in the last column of the respective results tables in the appendix (see tables B.1, B.2 and B.3 on pages 151 through 158).

Evaluation and presentation of results for the respective tumor entities In the subsequent section, prominent differentially expressed genes as well as the results of the pathway analyses are presented and discussed for each tumor entity separately, starting with PK9 YAP-knockdown cells. Comprehensive tables of differentially expressed genes (fold change-cutoff at 2, unless otherwise indicated) as well as the results of SPIA are printed in the appendix to this dissertation (see pages 140 through 158).

4.3.2. Transcriptional regulation by YAP in PDAC

Differentially expressed genes in YAP-knockdown cells

Tables A.1 and Table A.2 on page 140 ff. provide an overview of those genes found to be twofold up- or downregulated in PK9 YAP-knockdown cells. Among the most prominently differentially expressed genes were several genes that had previously been identified to play a role in carcinogenesis or were found to be overexpressed in PDAC (see Table 4.5 on 118). Some of these genes were picked to validate the microarray results by RT-qPCR. All genes reported to be downregulated by the expression array analysis were also highly significantly downregulated if analyzed by RT-qPCR (see figure 4.25). Some of the most interesting "hits" will be discussed in more detail in the following part.

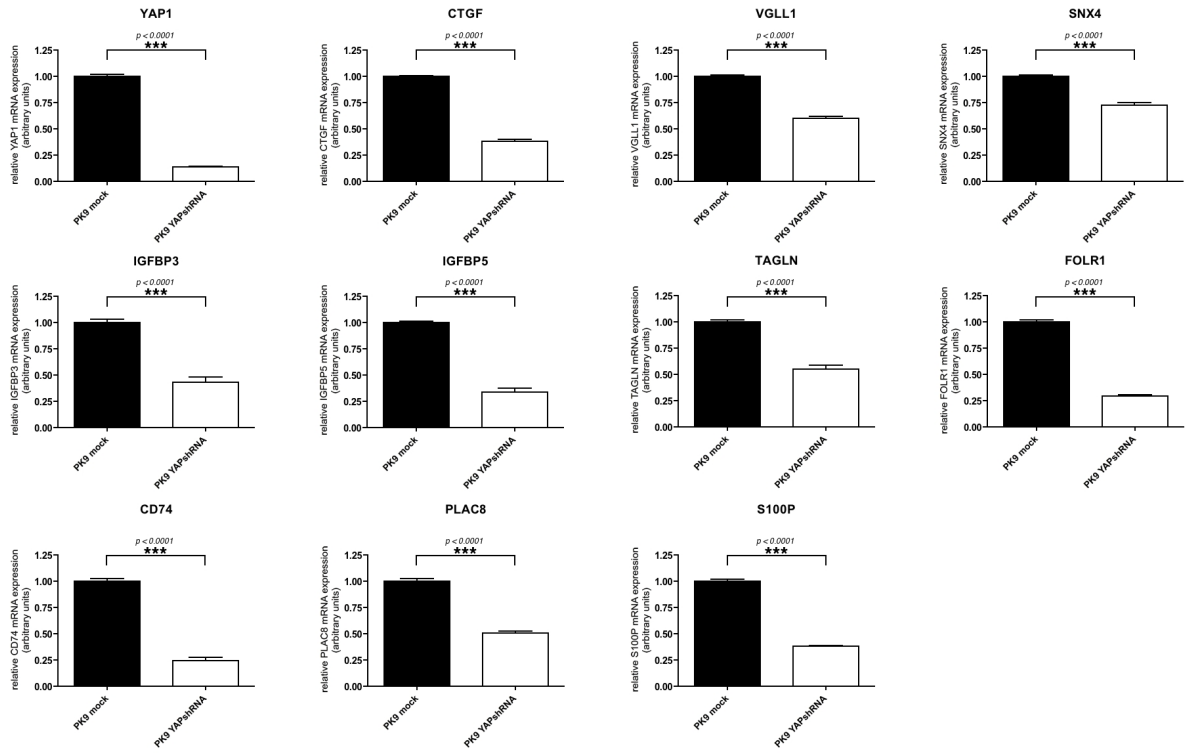

Figure 4.25.: Validation of putative YAP target genes by RT-qPCR. Eleven differentially expressed genes identified by microarray analysis were picked and differential expression was confirmed by RT-qPCR.

Table 4.5.: Differentially expressed genes previously described to be overexpressed in PDAC

Gene name	Symbol	FC	Annotation	Ref.
Yes associated protein	YAP	0,195	Confirms validity of assay	
Connective tissue growth factor	CTGF	0,451	*bona fide* target gene of YAP; important regulator of ECM construction and tumor-stroma cross-talk; promotes growth, migration and angiogenesis	[10, 116, 173]
Vestigial like 1 (drosophila)	VGLL1	0,290	Co-transcription factor and interaction partner of TEAD; competitor of YAP	[128, 129]
Sorting nexin 4	SNX4	0,498	implied in endosomal sorting; interacts with Hippo pathway member KIBRA	[150, 162]
Insulin-like growth factor binding protein 3	IGFBP3	0,368	expression lost in PanIN, IPMN, MCN and PDAC; expression correlates inversely with poor survival	[66]
Insulin-like growth factor binding protein 5	IGFBP5	0,361	mediator of cell growth in pancreatic cancer cell lines; overexpressed in chronic pancreatitis, IPMN and PDAC	[74]
Transgelin	TGLN	0,203	cross-links actin; target of TGF-β signaling; overexpressed in PDAC	[4, 185]
Folate receptor 1 (adult)	FOLR1	0,296	overexpressed in various cancer tissues; antibody Farletuzumab is currently in clinical evaluation	[124, 169]
Major histocompatibility complex, class II invariant chain	CD74	0,415	overexpressed in PanIN and PDAC; expression is associated with perineural invasion and poor prognosis	[85, 181]
Placenta specific 8	PLAC8	0,475	inhibits differentiation of AML-cells by PMA and ATRA; overexpression in PanIN, IPMN and PDAC	[19, 96]
S100 calcium binding protein P	S100P	0,426	overexpressed in PanIN, IPMN, MCN and PDAC	[19]

Connective tissue growth factor (CTGF)

CTGF (CCN2), a cysteine-rich, secreted matricellular protein and member of the CCN family of proteins was consistently downregulated upon YAP knockdown in PK9 (fold change YAPshRNA#5 0.33 ± 0.01, $p < 0.0001$) as well as Panc 10.05 cells (fold change YAPshRNA#5 0.46 ± 0.01, $p = 0.001$; see figure 4.26 A on page 122). CCN proteins are synthesized in response to mitogenic signals such as serum, growth factors or oncogenes. They bind to heparan-sulphate proteoglycans in the extracellular matrix (ECM) as well as on the cell surface. They are further binding partners of integrins and engage with cell surface receptors such as *low density lipoprotein receptor-related protein 1* (LRP1) and *neurotrophic tyrosine kinase, receptor, type1* (TrkA) [23]. CCN proteins observe a regulatory role within the complex network of the extracellular space and modulate the interaction of the plethora of cell types that reside in, communicate across, or produce matricellular components. Consequently, they have been described to influence a variety of cellular functions and biological properties, such as cell migration, proliferation and survival, as well as angiogenesis, fibrosis and wound healing. Furthermore, members of the CCN family reportedly influence other signaling pathways, among those TGF-β, *bone morphogenic protein* (BMP), and VEGF-regulated pathways. Recent work has led to the conclusion that CCN proteins form a functionally integral part of the ECM while their structural contribution to tissue architecture is limited [23].

CTGF in pancreatic development and disease CTGF is involved in pancreatic development (regulation of islet morphogenesis and function) and functions as one of the key cytokines in the pathogenesis of pancreatic fibrosis following pancreatitis. In this scenario, production of the CTGF-protein by both acinar cells and fibroblasts including activated pancreatic stellate cells at the site of injury, is induced following the over-expression of TGF-β [23]. Chronic pancreatitis is a well-known risk factor for the development of pancreatic cancer and it is therefore no surprise, that CTGF expression is evident in the mutated ductal cells of PanINs and PDAC [10, 23, 173]. There are indications that the extent of CTGF-overexpression is proportional to the intensity of the desmoplastic reaction and the cytokine is likewise expressed by stromal cells within the pancreatic tumor tissue [10, 23]. CTGF is therefore a candidate master-regulator of molecular cross-talk between tumor and stroma in pancreatic cancer and experimental therapies targeting CTGF have been successfully employed in a mouse model of pancreatic cancer [116].

CTGF as a direct target of YAP signaling in pancreatic cancer cells *CTGF* and another member of the CCN family of proteins *cysteine-rich, angiogenic inducer 61* (*CYR61*) are *bona fide* target genes of the transcriptional coactivator YAP and CTGF was markedly downregulated upon YAP-knockdown in PK9 as well as Panc10.05 cells (see figure 4.26 A on page 122). *CTGF* was among the first genes discovered to be regulated by the YAP/TEAD complex and serves as a positive control for YAP/TEAD-regulated gene expression in many studies [183]. Dysfunctional Hippo-signaling and subsequent YAP-overexpression in PDAC might be the missing link to explain the observed CTGF-hyperactivity in pancreatic cancer. Strong YAP immunoreactivity was observed in neoplastic as well as stromal cells in tissue samples of patients with PDAC (see 4.1 on page 82), conclusive with the model of CTGF as a dynamic auto- and paracrine regulator of tumor-stroma cross-talk. Targeting YAP in PDAC would therefore mean to target tumor and stromal cells alike, which presents a promising therapeutic concept for pancreatic cancer patients.

CD74

Major histocompatibility complex, class II invariant chain (CD74) is involved in the production, processing and transport of the MHC class II protein functioning as a cleft-like placeholder and blocking the antigen-binding site until the MHC class II-complex is fully assembled, stable and present on the cell surface [29]. Its expression by human pancreatic cancer cells has been studied and seems to be linked to particularly invasive cancers, resulting in a poor prognosis [85, 181]. Koide and colleagues found overexpression of the CD74 protein in the tumor tissue of 52/67 of PDAC patients (analysis by immunohistochemistry) [85]. Staining intensity was particularly high in patients with perineural invasion or liver metastasis and this was prognostically relevant. These results were confirmed by Zhang et al. in 2014 who found that high CD74 expression severely worsened the prognosis for PDAC patients who had their tumors resected [181].

CD74 was initially identified to be associated with perineural invasion by means of gene expression studies performed on neoplastic cells from a mouse model of perineural invasion in PDAC [85]. In the same gene expression analysis, elevated expression levels of *vestigial like 1* (VGLL1) were likewise associated with an invasive phenotype. Interestingly, VGLL1 was also prominently downregulated upon YAP-knockdown in PK9 as well as Panc 10.05 cells (see figure 4.26 A on page 122).

Vestigial like 1 (VGLL1)

Vestigial like 1 (VGLL1) was consistently downregulated upon YAP knockdown in PK9 (fold change YAPshRNA#5 0.17 ± 0.003, $p < 0.0001$) as well as Panc 10.05 cells (fold change YAPshRNA#5 0.15 ± 0.003, $p < 0.0001$; see figure 4.26 A on page 122).

VGLL1 codes for the protein VGLL1, a transcriptional co-activator evolutionary related to the drosophila protein vestigial (vg), a master regulator of wing development. VGLL1 and vg, however, only share a short, 25 amino acids-long motif ("tondu"-domain) while all other sequence stretches do not display any similarity [129]. Drosophila vg interacts with scalloped (sd), which constitutes the drosophila counterpart of mammalian TEAD [59, 149] and also mammalian VGLL proteins were recently identified as transcriptional coactivators of TEAD1-4 [129]. Despite a highly different primary sequence, the VGLL1-TEAD and the YAP-TEAD complex are structurally very similar and VGLL1 and YAP are competing for TEAD-binding [129]. Although this structural similarity is mirrored to some degree by a functional similarity - VGLL1-TEAD4 upregulates pro-proliferative genes in prostate cancer cell lines - both complexes recruit a distinct set of target genes [129]. While VGLL1-TEAD results in upregulation of genes associated with myogenesis and proliferation like *MYHC*, *VEGFA* and *IGFBP5*, YAP-TEAD recruits *CTGF*, *CYR61*, *IGFBP3* and *CMYC* in order to maintain organ size and a stem-like phenotype [128]. This is consistent with observations in the fruit fly, where vg can alter target selectivity of sd, putatively by recruitment of a distinct set of transcriptional regulatory factors [57]. As of now, information about the regulation of VGLL1 has been scarce except for the conjecture that phosphorylation by the Hippo signaling cascade is unlikely because VGLL1 lacks the lats-recognition motif [129]. The data presented here is the first report, that YAP-TEAD actively regulates the expression of its own competitor.

In order to further evaluate the possibility of YAP-VGLL1 competition in PDAC, expression analysis of *VGLL1* mRNA was performed using RT-qPCR in a panel of PDAC cell lines (see figure 4.26 B on page 122). Transcripts were present in 8/14 cell lines analyzed, although correlation with YAP protein expression was sketchy underscoring the need for further elucidation of the YAP-VGLL1 relationship in PDAC (e.g. L3.6pl; see figure 4.2 on page 84).

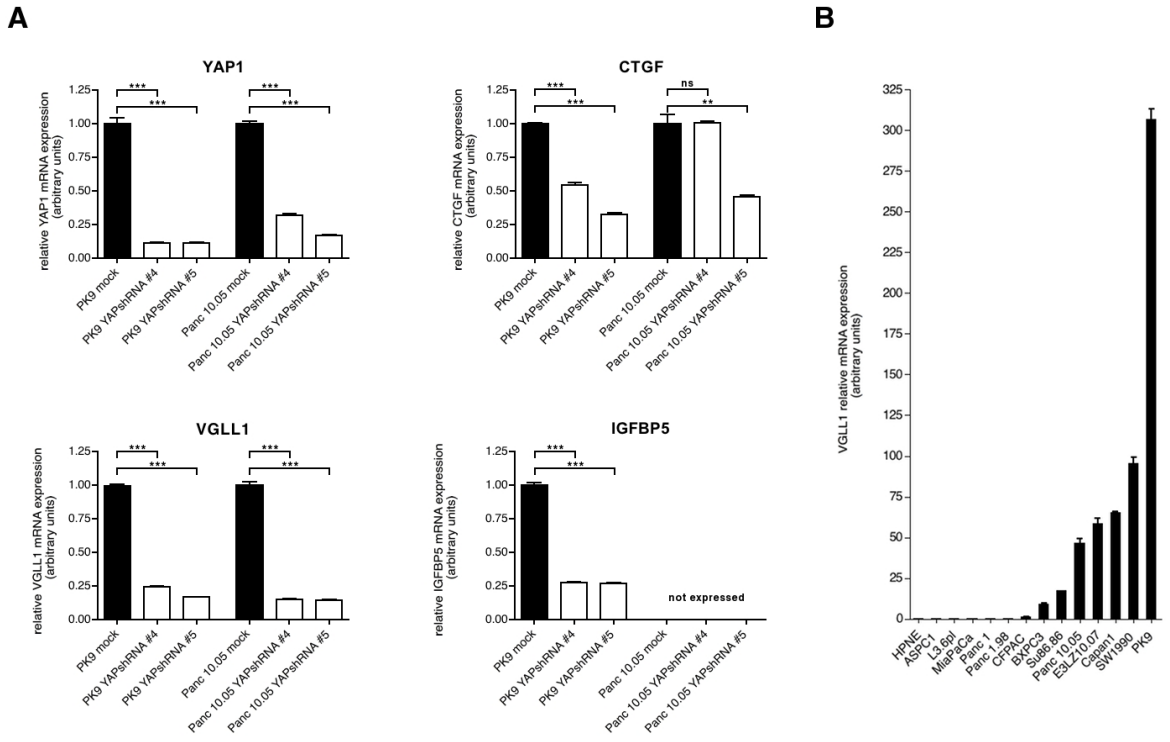

Figure 4.26.: Crossvalidation of putative YAP target genes in PK9 and Panc10.05 cells. Crossvalidation of putative YAP target genes *CTGF*, *VGLL1* and *IGFBP5* in PK9 and Panc 10.05 YAP-knockdown cells (A). mRNA expression of *VGLL1* transcripts in a panel of PDAC cell lines (B).

Insulin-like growth factor binding proteins (IGFBPs)

Two *insulin-like growth factor binding proteins* (IGFBPs) were downregulated upon YAP knockdown in PK9 cells. The proteins IGFBP3 (fold change 0.43 ± 0.05, $p < 0.0001$) and IGFBP5 (fold change 0.34 ± 0.03, $p < 0.0001$) are members of the IGF-signaling axis which is involved in the maintenance of tissue homeostasis by regulation of cellular proliferation, differentiation and migration [35]. Insulin-like growth factors (IGF-1 and IGF-2) are single chain polypeptides that are produced by almost any cell in the body and interact with the cell membrane-bound receptor IGF-1R which in turn activates intracellular signaling pathways like the Ras/MAPK/ERK as well as the PI3K/AKT/mTOR cascades. Activation of the IGF-axis therefore results in pro-proliferative and anti-apoptotic cellular cues and contributes to tumorigenesis [35, 113]. IGF-signaling further contributes to tumor-stroma crosstalk in pancreatic cancer with stromal cells producing IGF-1 that binds

to IGF-1R on cancer cells [66]. IGF-1 and IGF-2 circulate in 1000-fold higher concentrations than most other peptide hormones and their action is modified by binding proteins which function as major determinants of IGF bioavailability [113]. About 99% of IGF is bound to one of six different IGFBPs at any given moment. Among those, IGFBP1-5 share high sequence similarity as well as a high affinity for IGF-1, while IGFBP6 displays a higher affinity for IGF-2 [113].

IGFBP expression is regulated by a wide array of growth enhancing signals that are cell type-specific and include hormones (steroid hormones, growth hormone, follicle-stimulating hormone etc.), growth factors (IGFs, platelet-derived growth factor, epithelial growth factor, fibroblast growth factor etc.) and other mediators (vitamin D, retinoic acid, p53 etc.) [113]. In pancreatic cancer, at least part of the IGFBP3 and IGFBP5 expression appears to be triggered by YAP. Cross validation in Panc 10.05 YAP knockdown cell lines, however, could not wholeheartedly confirm this chain of command due to very low concentration of IGFBP3 and IGFBP5 mRNA and resulting high quantification cycles (see figure 4.26 A on page 122, data for IGFBP3 not shown).

Binding of IGFs to specific IGFBPs may result in distinct consequences: IGFBP3 decreases the bioavailability of IGF-1 and 2 whereas IGFBP5 leads to an increased biological activity, putatively by regulating their relative distance to the receptor IGF-1R [35]. Consistent with this observation, overexpression of IGFBP3 in pancreatic cancer has been reported to be inversely correlated with venous invasion while tumors positive for IGF1R and negative for IGFBP3 were associated with significantly shorter overall survival [66]. IGFBP5 on the other hand functions as a mediator of cell growth in PDAC cell lines, an action dependent on MAPK and PI3K signaling [74]. Their conflicting functions in cell growth and tissue homeostasis tie in with the observation that YAP induces transcription of its own competitor for its main interaction partner TEAD. Pobbati *et al.* reported IGFBP5 to be a target gene of the VGLL1-TEAD complex while the YAP/TAZ-TEAD complex induced IGFBP3 expression in PC-3 cells [129], which suggests that IGFPB5 might be an indirect target of YAP in PDAC. YAP and its putative counterpart VGLL1 might be required for maintenance of tissue homeostasis in PDAC.

Pathways affected by YAP-knockdown in PK9 cells

SPIA returned 26 pathways that were significantly affected by YAP-knockdown in PK9 cells (see figure 4.27 and table B.1 on page 151 ff.). At first glance there appears to be a lot of seemingly unspecific perturbation of immune-pathways. However this is not surprising

when considering the relatively high number of soluble cytokines and mediators that were differentially expressed upon YAP-knockdown in PK9 cells, such as IL-1 and IL-6, GM-CSF as well as MMP1, which were curiously upregulated (see table A.2 on page 142 ff.). This lends support to the hypothesis that YAP modifies the tumor microenvironment, shaping local humoral immunity into a tumor-permissive state to facilitate immune evasion by the neoplastic cells.

One of the most interesting charts is provided by entry number five "Pathways in Cancer" (KEGG ID 5200) which agglomerates the key pathways contributing to the hallmark features of cancerous transformation. This is a true example of the usefulness of pathway analyses of microarray data, as most of the genes that lead to significant pathway perturbation are individually not markedly affected. Coordinated, smaller changes lead to significant consequences in case of the Wnt signaling pathway, cell cycle regulation as well as the ErbB-signaling pathway.

Wnt-signaling Wnt signaling has previously been connected to the Hippo-YAP axis in epidermal stem cells as well as intestinal crypts [9, 137]. YAP has been shown to act downstream of α-catenin to control epidermal proliferation. Activation of YAP-induced transcription results in an expansion of the epidermal stem cell compartment that can eventually progress to squamous cell carcinoma-like tumors, while loss of YAP leads to failure of skin expansion and is embryonically lethal [137]. In the intestine on the other hand, YAP oversees a surprising growth-suppressive function by restricting Wnt-signals during intestinal regeneration. Not unlike its paralogue TAZ which functions as a negative regulator of Wnt/β-catenin signaling in mammalian kidney development [166], YAP restricts nuclear translocation of the transducer protein Dishevelled (dvl) and therefore prohibits elevated Wnt-signaling [9]. This once more underlines the tissue-context dependency of the Hippo-YAP axis which can lead to growth-promotion in one setting and growth-restriction in the next, even through interaction with the same signaling pathways.

In PK9 cells, YAP knockdown seems to modulate Wnt-signaling mainly by downregulation of the membrane-bound receptor Frizzled (Fz) and interference with the homeostasis of individual members of the Wnt-gene family as well as upregulation of the planar-cell polarity protein Prickle-like 1.

Cell cycle regulation YAP knockdown led to downregulation of Neuregulin 4 (NRG4) and subsequent upregulation of Cyclin-dependent kinase inhibitor 1A (p21; fold change 1,74, p = 1,00E-05), directing the cellular program towards growth arrest and upregulation

of apoptosis. This is in line with the observed inhibition of cell growth in different PDAC cell lines as described in the results section on functional *in vitro* data.

ErbB signaling Input into the ErbB signaling pathway was enhanced in PK9 YAP knockdown cells by means of upregulation of Transforming growth factor, α (TGF-α), Heparin-binding EGF-like growth factor (Hb-EGF) as well as Neuregulins 1 (NRG1). Protein kinase C (PKC), an activator of oncogenic transcription and target of experimental therapies in pancreatic cancer [38] was downregulated upon YAP knockdown in PK9 cells, consistent with the observed decreased tumorigenicity.

ECM receptor interaction Interestingly, especially in light of the presence of stromal cells that are highly positive for YAP in the tumor surrounding stroma in PDAC patients, YAP knockdown increased expression of Integrin α and activated the ECM receptor interaction pathway. This once more indicates a role for the Hippo-YAP axis in the organization of tumor-stroma crosstalk and metastasis and compliments the observation that nodal involvement was significantly higher in patients with high YAP-immunoreactivity (see section 4.1.1 on page 81).

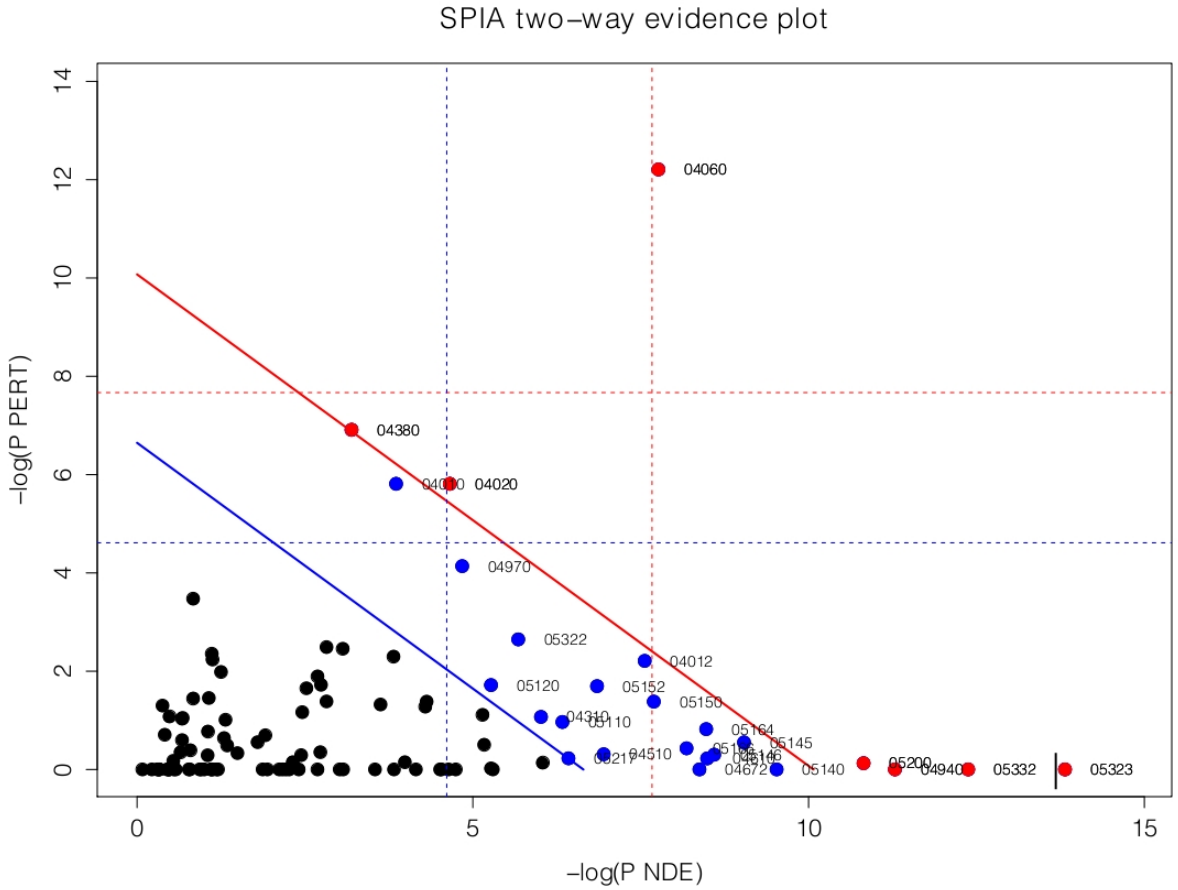

Figure 4.27.: SPIA two-way evidence plot of pathways affected by YAP-knockdown in PK9 cells. Each point represents a biological pathway affected by YAP-knockdown in PK9 cells. The coordinates of the point are a measure of two aspects of pathway perturbation that form the two components of the global pathway significance p-value (pG): the enrichment (pNDE) p-value is a measure for the number of affected genes, whereas the perturbation (pPERT) p-value takes into account the position of those genes within a given pathway. All pathways are represented by their KEGG-ID number. Please refer to table B.1 on page 151 ff. and follow the hyperlink in the last column for a graphic representation of the affected genes and their position within the pathway topology.

4.3.3. Transcriptomic landscape in G415 cells

Transcriptomic profiling of G415 YAP-knockdown cells by cDNA microarray analysis identified 36 genes that were upregulated more than twofold (Table A.4 on page 145 presents the top 49 upregulated genes), and another 42 genes that were downregulated by more than 50% as compared to mock-transfected G415 cells (Table A.3 on page 143).

Although at first glance the genes represented in the toplists seem interesting, pointing towards involvement of the Wnt-signaling pathway (DKK1) and modification of tumor-stroma interaction (ITGB2, FGFBP1, ECM2), the signaling pathway impact analysis only returned one pathway significantly affected by YAP-knockdown in G415 cells: "Cytokine-cytokine receptor interaction" (KEGG ID 4060, see figure 4.28). However, this pathway merely constitutes of an aggregation of receptor-ligand pairs that are not interconnected and therefore does not provide an interesting lead towards the biologic mechanism of YAP action in biliary cancer.

A potential way forward would be to repeat the gene expression analysis and include both a comparison of two mass clones generated by two different shRNA sequences targeting YAP as well as a second biliary cancer cell line.

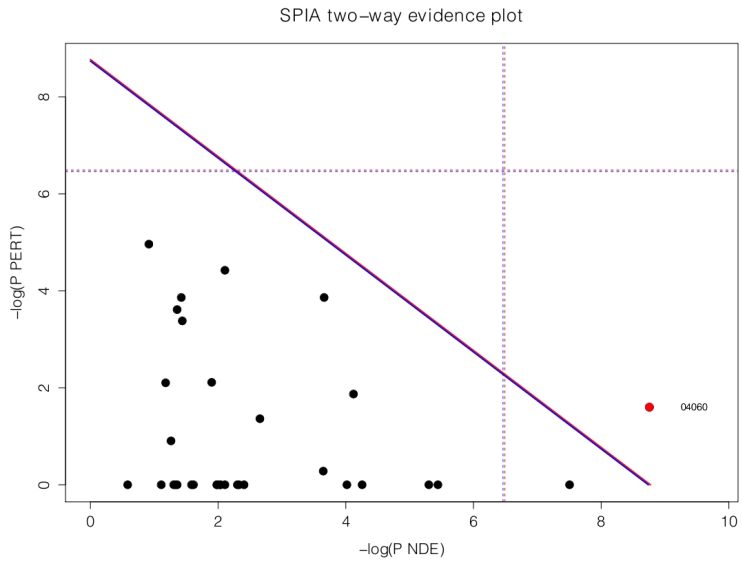

Figure 4.28.: SPIA two-way evidence plot of pathways affected by YAP-knockdown in G415 cells. Each point represents a biological pathway affected by YAP-knockdown in G415 cells. All pathways are represented by their KEGG-ID number. Please refer to table B.2 on page 156 ff. and follow the hyperlink in the last column for a graphic representation of the affected genes and their position within the pathway topology.

4.3.4. Transcriptomic profile of YAP in MZ1774 cells

Transcriptomic profiling of MZ1774 YAP-knockdown cells by cDNA microarray analysis returned 14 genes that were upregulated more than twofold (Table A.6 on page 149 presents the top 20 upregulated genes), and another 42 genes that were downregulated by more than 50% as compared to mock-transfected MZ1774 cells (Table A.5 on page 147). Of these, 8 targets were picked for validation by quantitative real-time PCR. All eight targets found to be downregulated by microarray analysis were confirmed to be downregulated using RT–qPCR. CDH6 is an example of a target found to be overexpressed in the microarray analysis was also found to be upregulated using RT–qPCR (Figure 4.29). Some of the most interesting genes, which were selected based on their pathophysiological relevance as deduced from previously published literature and their mechanistic implications will be discussed in more detail below.

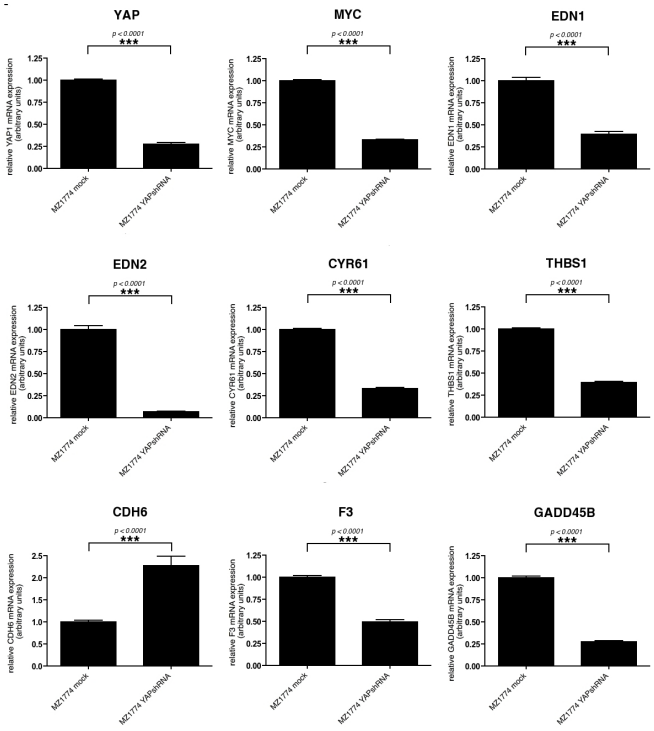

Figure 4.29.: Validation of putative YAP target genes by RT-qPCR. Nine differentially expressed genes identified by microarray analysis were picked and differential expression was confirmed by RT-qPCR.

Endothelin axis

Among the most prominently downregulated genes were two members of the endothelin family, Endothelin-1 and -2. Cross-validation of mRNA expression of these genes in MZ1774, A498 and ACHN YAP-knockdown cells confirmed significant Endothelin-1 downregulation in MZ1774 and A498 upon YAP-knockdown (fold changes for MZ1774 0.41 ± 0.009, $p < 0.0001$ and 0.41 ± 0.019, $p = 0.0001$ for A498, respectively; see Figure 4.30 on page 130). Endothelin-2 expression was significantly reduced in all three cell lines examined (fold changes 0.06 ± 0.003, $p < 0.0001$, for MZ1774, 0.62 ± 0.025, $p = 0.001$ for A498, and 0.17 ± 0.0067, $p < 0.0001$ for ACHN, respectively).

Immunohistochemistry and quantitative real-time RT-PCR confirmed consistent knockdown of YAP as well as downregulation of Endothelin-2, both at the mRNA- and protein-level in murine xenografts of human ccRCCs (Figure 4.31 on page 129).

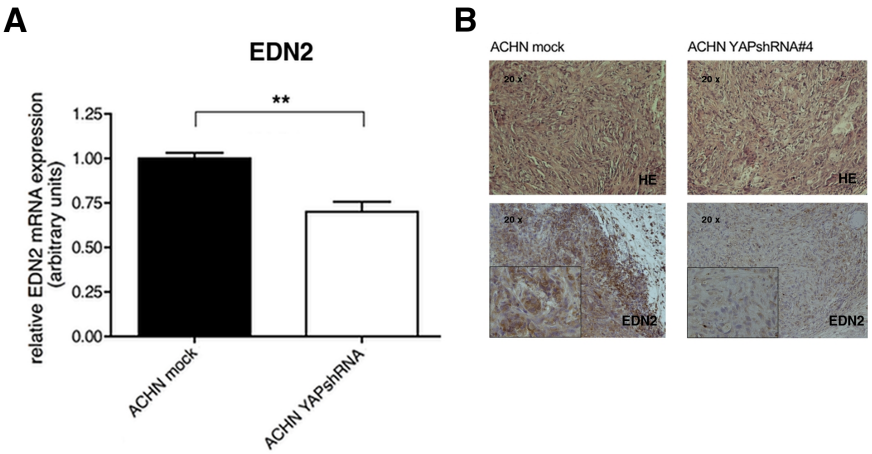

Figure 4.31.: The putative YAP target EDN2 is downregulated in ACHN YAP knockdown xenografts. RT-qPCR of freshly frozen xenograft tissue confirmed significant downregulation of EDN2 mRNA in tumors derived from ACHN YAP knockdown cells (A). Hematoxylin and eosin stainings and immunohistochemistry of EDN2 in ACHN mock and ACHN YAP knockdown xenograft tissues illustrate downregulation on the protein level (B). Representative images are shown in $\times 20$, with insets in $\times 40$ magnification.

Endothelins are important regulators of kidney function and endogenous endothelin is involved in the regulation of renal cell growth and proliferation, as well as fluid and electrolyte excretion. Production of endothelins in the kidney is increased in numerous renal diseases [84] and ccRCC tumors have been reported to express Endothelin-1 and

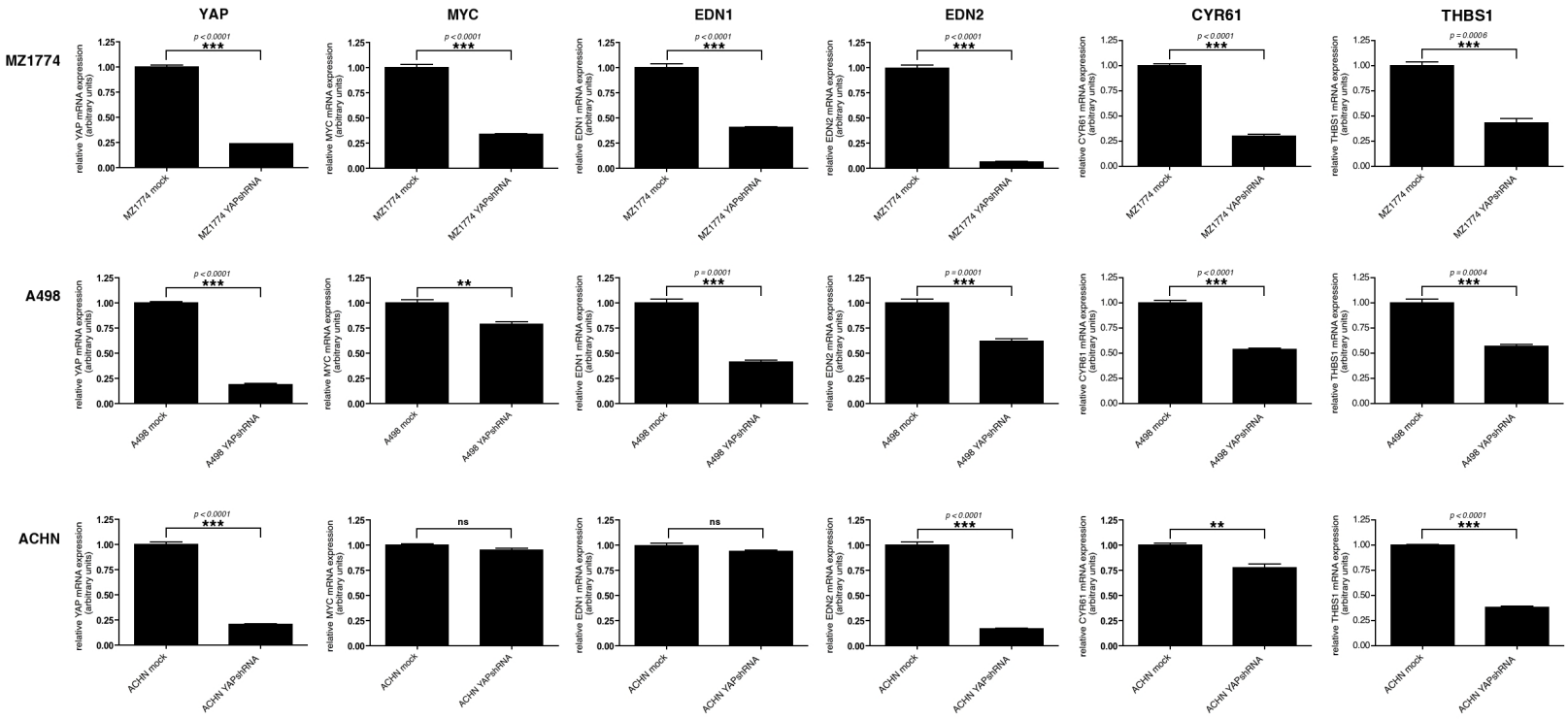

Figure 4.30.: Crossvalidation of putative YAP target genes in two other RCC cell lines. Cross-validation in two other YAPshRNA-transfected ccRCC cell lines revealed uniform EDN2, CYR61, and THBS1 downregulation as well as EDN1 and cMYC downregulation in two tested cell lines.

its receptor ETA with ccRCC cell lines secreting endothelin-1 [36, 127]. The selective endothelin-A-receptor antagonist Atrasentan has been used in combination with IFN-alpha in a phase I study in metastatic RCC, albeit with moderate clinical anti-tumor effects [52]. The impact of YAP-knockdown on Endothelin-2 expression was most pronounced and present in all three cell lines tested, whereas Endothelin-1 downregulation could be cross-validated in A498 but not in ACHN YAP-knockdown cells. As ACHN YAP-knockdown cells displayed the same phenotype in respect to reduced cancer cell proliferation and migration and did form smaller xenograft tumors *in vivo*, Endothelin-2 seems to be one of the main effectors responsible for these effects. In line with this hypothesis, we found that Endothelin-2 expression significantly correlates with YAP positivity in clinical tumor specimen of ccRCC patients as assessed by immunohistochemistry (see figure 4.32 on page 131 and table 4.6 on page 132). Chromatin immunoprecipitation (ChIP) confirmed the presence of the YAP-TEAD complex in the promotor regions of the EDN2 and EDN1 genes in MZ1774 cells and established those genes as direct transcriptional targets of YAP in ccRCC (see figure 4.33 on page 134).

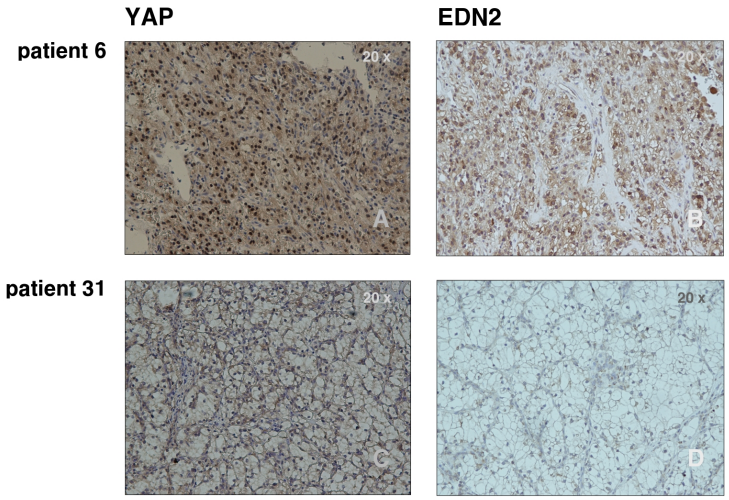

Figure 4.32.: EDN2 expression correlates with YAP positivity in RCC patient tissue. Immunohistochemistry of tumor tissues of 30 patients with ccRCC confirmed that EDN2 expression correlates with YAP positivity. Double positivity for YAP and EDN2 was frequently observed (A, B), whereas loss of YAP expression often results in minimal to absent EDN2 expression (C, D).

Table 4.6.: EDN2 expression correlates YAP positivity in ccRCC.

		YAP expression		
		positive	weak or negative	total
EDN2	positive	20	3	23
	weak or negative	2	5	7
	total	22	8	30
	Fisher's exact test P = 0,0067			

Endothelins in cancer Research on the endothelin axis in cancer has focused mainly on Endothelin-1 and results have largely been extrapolated to Endothelin-2. It has been assumed that Endothelin-2 would mimic the actions of its more abundant counterpart Endothelin-1, but recent findings *in vitro* and in knockout mice underscore that Endothelin-2 does not simply amplify or duplicate Endothelin-1 action and imply a distinct function of Endothelin-2 in physiological and pathophysiological processes [100]. Furthermore, Endothelin-2 and not the more abundant Endothelin-1, was first isolated from RCC cell lines [120]. A recent paper reported Endothelin-2 expression to be a common and early event in patients with localized ccRCC undergoing nephrectomy and proposed a potential role in ccRCC progression [15]. An association of higher tumor expression of Endothelin-2 with longer progression-free survival could not be confirmed after adjustment for known clinicopathological factors and it would be interesting to compare expression levels with tumors of patients with advanced, metastatic disease.

Grimshaw *et al.* reported an important influence of Endothelin-2 on the invasive potential of breast cancer cells and proposed a mechanism where Endothelin-2 secreting tumor cells provide chemotactic cues to tumor infiltrating macrophages, which in turn secrete MMP-2 and MMP-9 to facilitate tumor cell invasion and metastasis [51]. The observed effect was dependent on both endothelin receptor B and MAPK-signaling, and expression of Endothelin-2 and its receptor was stronger at the invasive margin of the tumor tissue. Of note, we observed inhibition of the MAPK-signaling pathway upon YAP-knockdown in MZ1774 cells. Overexpression of Endothelin-2 increases the invasive potential of breast cancer cell lines *in vitro* but is not sufficient to induce an invasive phenotype in benign cells, indicating the cooperation with other signaling networks [56]. Concordantly, Said *et al.* reported an instrumental role of Endothelin-1 signaling via endothelin receptor A

in the development of metastatic bladder cancer and delineated a proinvasive network governed by members of the endothelin-family. This involves direct actions like the activation of proinflammatory transcription factors such as AP-1 and NF-kappaB in human monocytes and cancer cells and the stimulation of the production of a range of proinvasive cytokines like interleukin-6, COX2, CCL2, MMP2 and MMP9 as well as indirect modulation of the tumor-microenvironment by influencing tumor-stroma-interactions as well as tumor-associated immune cells [135]. These endothelin functions were instrumental in the process of metastatic colonization, the first step of the establishment of a filial tumor at a distant site. Pharmacologic blockade of endothelin receptor signaling inhibited metastasis significantly in an experimental animal model, despite having only modest effects on primary tumor growth. We observed that these reported target genes of Endothelin-1 signaling, namely interleukin-6, COX2, VEGFA and CCL2 were also moderately, but significantly downregulated in MZ1774 YAP-knockdown cells as determined by microarray or RT-PCR analysis (fold changes were 0.74, $p < 0.0008$ for interleukin-6, 0.60, $p = 0.002$ for COX2, 0.67, $p = 0.0065$ for VEGFA and 0.82, $p = 0.032$ for CCL2, respectively).

c-Myc

Cross-validation of differential mRNA expression in MZ1774, A498 and ACHN YAP knockdown cells confirmed significant c-Myc downregulation in MZ1774 and A498 upon YAP-knockdown (fold change MZ1774 0.34 $\pm$ 0.006, $p < 0.0001$; fold change A498 0.79 $\pm$ 0.026, $p = 0.0085$; see figure 4.30 on page 130). Differential expression could not be confirmed in ACHN cells. However there was no information available regarding the mutational status of the c-Myc protein in this cell line and constitutive activation or amplification of the protein would provide one possible explanation. Upregulation of c-Myc expression has been reported to occur in a majority of ccRCC cases [42, 157], although amplification of the MYC gene is only found in a small subset of cases [89, 157] leading to the assumption that c-Myc is activated by other mechanisms in addition to amplification. We observed strong c-Myc downregulation upon YAP-knockdown in MZ1774 cells. c-Myc knockdown by siRNA in ccRCC cell lines leads to a phenotype that resembles that of YAP-knockdown with marked inhibition of proliferation and anchorage-independent growth [157]. c-Myc expression is stimulated by Endothelin-1 via MAPK signaling in neoplastic cells [80, 117] and our data show inhibition of the MAPK signaling pathway along with Endothelin-1 and concomitant c-Myc downregulation upon YAP-knockdown in MZ1774 and A498 cells whereas mRNA expression levels of these genes were not affected

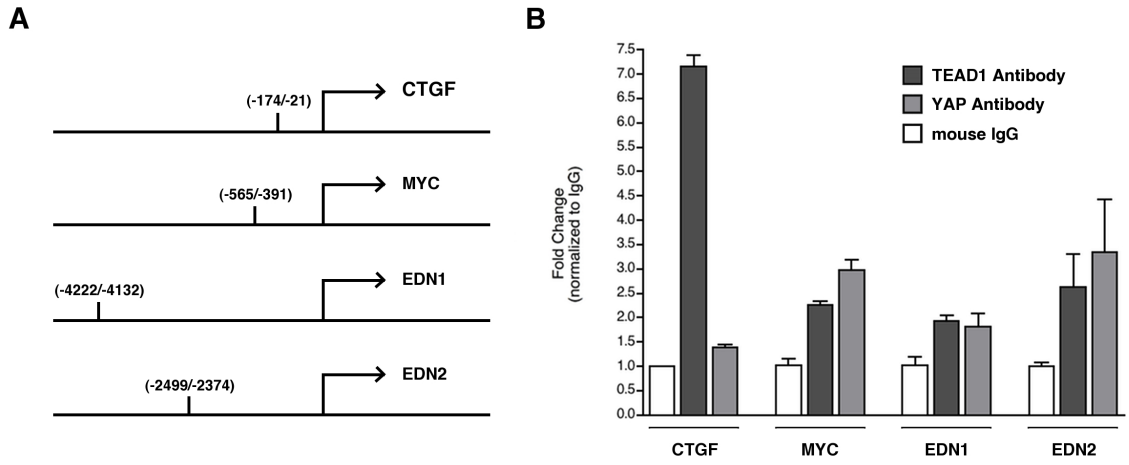

Figure 4.33.: The YAP-TEAD1 complex is present in the promotor regions of putative YAP target genes. Potential TEAD binding sites were picked by identification of consensus sequences in the promotor regions of putative YAP target genes in ccRCC and primers flanking these regions were designed. A well-characterized YAP/TEAD1-binding site in the promotor region of the bona fide YAP target gene *CTGF* was selected as a positive control. We found YAP and TEAD to be simultaneously present on the promotor regions of the *MYC*, *EDN1* as well as *EDN2* genes in MZ1774.

in ACHN cells, indicating that c-Myc might be an indirect target of YAP, downstream of endothelin-1 in ccRCC. However, the MYC-promoter region features GT-IIC consensus sequences as potential binding sites for the YAP/TEAD complex and the YAP/TEAD complex is indeed present on those binding sites in MZ1774 cells (see figure 4.33 on page 134), providing evidence that c-Myc functions as a direct transcriptional target of YAP in ccRCC.

CYR61 We observed consistent downregulation of the *bona-fide* YAP target gene CYR61 upon YAP-knockdown in all cell lines examined. CYR61 is a positive regulator of cell growth [126] and has been implicated as a proangiogenic factor in highly vascularized RCC, acting alongside VEGF and exerting additive, non-overlapping functions [25]. CYR61 upregulation correlated with loss of von Hippel-Lindau protein expression, although its expression was only partly dependent on HIF-2α function, suggesting additional mechanisms that contribute to CYR61 upregulation in RCC [25]. Furthermore, recent reports linked CYR61 with integrin-mediated cell migration and invasion in prostate cancer cell lines, hinting at a potential role in metastasis [138].

THBS1 Thrombospondin-1 is one of the most potent physiological antiangiogenic factors and its expression has been reported as an independent prognostic factor in ccRCC with retained expression being associated with increased survival [186]. It is therefore somewhat surprising to observe downregulation of THBS1-mRNA upon YAP-knockdown in all cell lines analyzed. YAP might interfere with the network of pro- and antiangiogenic factors, such as CYR61 and THBS1, in ccRCC, tipping the balance towards a homeostasis that favors the proliferation and survival of the tumor cells.

CDH6 Cadherin 6-mRNA expression was found to be upregulated in MZ1774 YAP-knockdown cells. Normal renal epithelium and RCC express multiple members of the cadherin family in a distinct pattern with E-cadherin being expressed in Bowman's capsule and all tubular segments except the proximal convoluted and straight tubules [145]. Consequently, E-cadherin expression frequency in RCC is lower than in other cancers and even low-grade tumors infrequently express E-cadherin [77]. Conversely, cadherin-6 is expressed in proximal renal tubules and renal cell carcinoma, especially when E-cadherin is absent, and seems partly to take over E-cadherin function [146]. Detectable cadherin-6-mRNA from circulating tumor cells in the peripheral blood of RCC patients has been proposed as a prognostic marker associated with increased risk of metastasis [97, 146] hinting not necessarily at an active role of the cadherin-6-protein in metastasis but rather highlighting the inadequate ability of cadherin-6 to replace E-cadherin in cell adhesion. Upregulation of the cell adhesion molecule cadherin-6 in response to YAP-knockdown is therefore not contradictory to a less invasive phenotype.

miR-21 In light of the most recent report published by the Cancer Genome Research Atlas Network [28], which found frequently altered promoter methylation of miR-21 with subsequent high miR-21 expression in high stage ccRCCs that inversely correlated with outcome, it is intriguing to note the significant downregulation of miR-21 upon YAP-knockdown. Recent work from Dey *et al.* showed that miR-21 targets PTEN protein expression and promotes ccRCC survival and invasion via Akt/TORC1 signaling [32].

Pathway analysis

The top three pathways found to be affected were the p53-, MAP kinase as well as cell cycle progression pathways, all of which have long been well-established as centrally involved in carcinogenesis and maintenance of a malignant phenotype across several tumor entities (see Figure 4.34 on page 136 and Table B.3 on 158). Consistent with the phenotypic

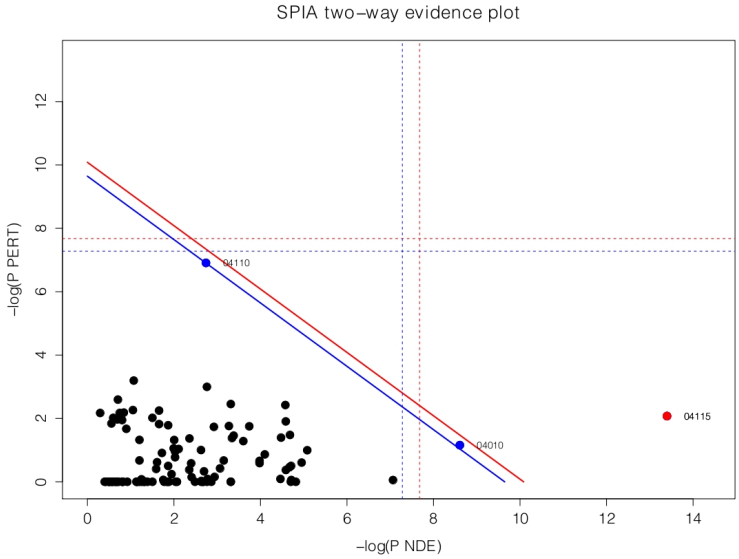

Figure 4.34.: SPIA two-way evidence plot of pathways affected by YAP-knockdown in MZ1774 cells. Each point represents a biological pathway affected by YAP-knockdown in MZ1774 cells. The coordinates of the point are a measure of two aspects of pathway perturbation that form the two components of the global pathway significance p-value (pG): the enrichment (pNDE) p-value is a measure for the number of affected genes, whereas the perturbation (pPERT) p-value takes into account the position of those genes within a given pathway . All pathways are represented by their KEGG-ID number. Please refer to table B.3 on page 158 ff. and follow the hyperlink in the last column for a graphic representation of the affected genes and their position within the pathway topology.

observations, the p53-signaling pathway was activated by YAP knockdown, while the MAP kinase pathway was inhibited. Curiously, the cell cycle machinery was activated, which might counterbalance the activation of the pro-apoptotic p53-pathway.

On the whole the presented data provides strong evidence that the transcriptional co-activator YAP plays an important role in regulating proliferation, invasiveness and metastatic potential of ccRCC and might serve as a target for therapeutic intervention in the future. Disrupted Hippo signaling and consecutive derepression and activation of YAP leads to increased production of the YAP target genes Endothelin-1, Endothelin-2 and c-Myc. Increased endothelin-signaling in turn results in increased production of pro-proliferative and proinvasive mediators by ccRCC cells and might thus enhance metastatic colonization. Figure 4.35 on page 137 provides a graphic overview of the putative mechanistic consequences of YAP-hyperactivity for ccRCC tumor progression. Future studies aimed at developing specific inhibitory drugs of the Hippo signaling pathway or its downstream effectors described here seem warranted in order to generate novel therapeutic regimens against ccRCC.

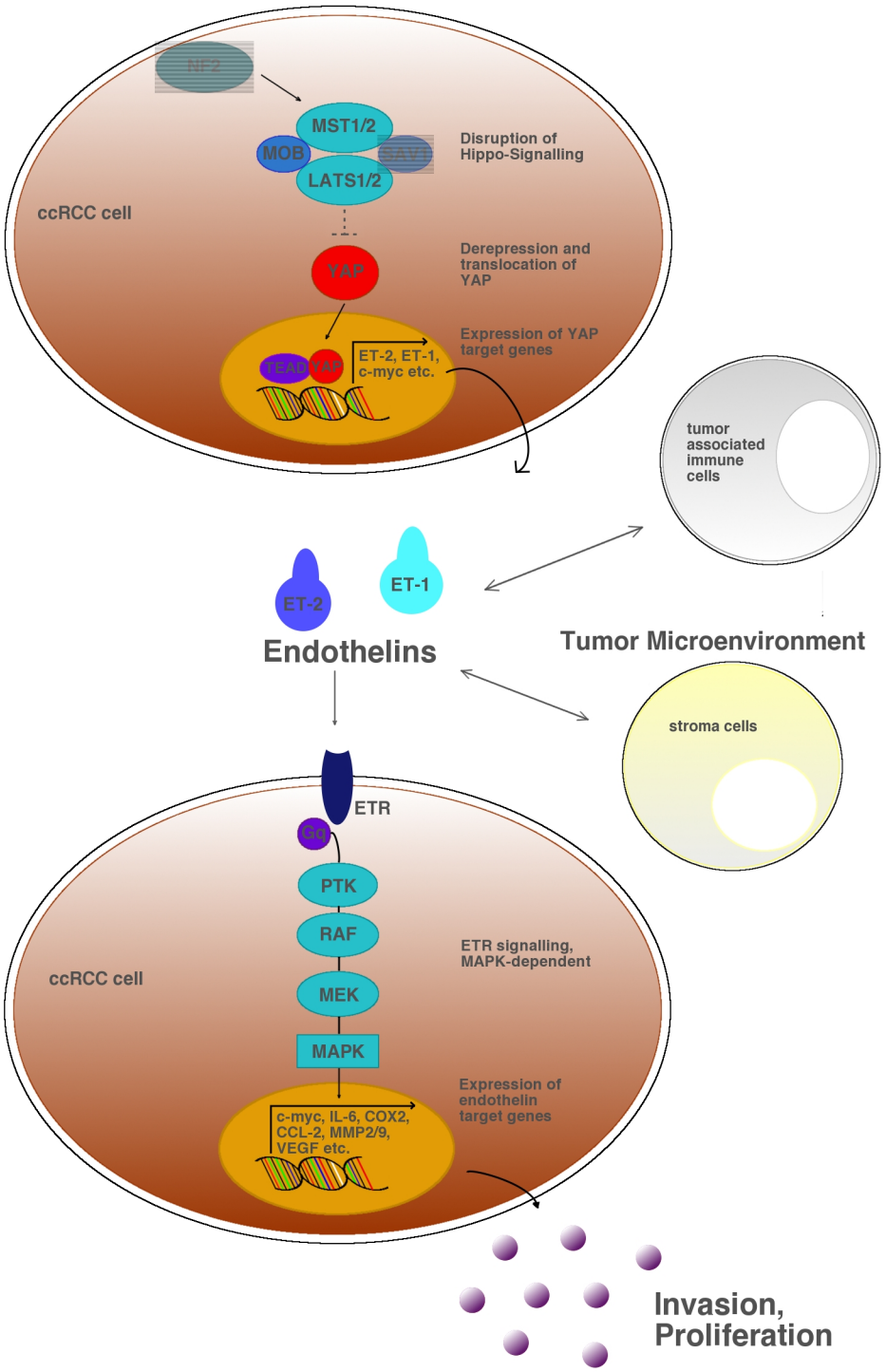

Figure 4.35.: Putative interaction of YAP with the endothelin axis in ccRCC.

5. Conclusion and perspective

5.1. The transcriptional output of the Hippo-YAP axis is functionally related but highly tissue context-dependent in PDAC, biliary cancer and RCC

Hippo pathway perturbation and consecutive YAP-hyperactivity frequently occur in neoplasia of many tissues, including PDAC, biliary cancers and ccRCC. This contributes to tumorigenicity and YAP knockdown in cancer cell lines impairs proliferation, as well as anchorage-dependent and independent colony formation in PDAC, biliary cancer and RCC cell lines, while an influence on *in vitro*-migration was only observed in RCC cell lines.

This phenotypic uniformity was however not mirrored by a direct, uniform downstream expression pathway in the different cancers studied in this work. This apparently high level of genetic complexity could only be partially resolved when shifting from a single-gene towards pathway-based analysis models. In fact, certain pathways were activated by YAP knockdown in one cell line while they were inhibited in another (e.g. MAPK in PK9 vs. MZ1774 cells).

This confirms the general observation of the enormously high tissue-context dependency of the transcriptional output of the Hippo-YAP-axis [64].

One common feature identified was the involvement of stromal compartments and the discovery of single, highly YAP-positive, fibroblast-like cells residing in the tumor-adjacent stroma which were present in all tumor entities analyzed. Mechanistically, transcriptomic profiling returned candidates for the regulation of tumor-stroma interaction in all cases, albeit different individual genes.

5.2. Future directions

The investigation of the role of the Hippo-YAP signaling axis in the formation of the neoplastic stroma as well as tissue homeostasis and tumor-stroma interaction is surely one of the most interesting avenue for future research. Especially in cancers that elicit an intense desmoplastic reaction such as PDAC as well as biliary cancers, a better understanding of the tumor microenvironment could lead to novel and innovative therapeutic concepts. Potential starting points could be co-expression studies with YAP and markers for activated fibroblasts in patient tissues (e.g. α-smooth muscle actin) and *in vitro* co-culture models [102].

Another interesting line of investigation is further the role of the YAP-paralogue TAZ as well as the determination of YAP-TEAD initiated transcription in relation to transcription initiated by YAP in association with other transcription factors like SMADs. This is potentially interesting in PDAC as SMAD4 and deregulated TGF-β signaling play a major role during pathogenesis.

Appendix A.

Raw data of DNA transcriptomic profiling

A.1. Differentially expressed genes in PK9 YAP-knockdown cells

Table A.1.: Downregulated genes in PK9 YAP-knockdown cells

Gene ID	Symbol	Gene name	Accession number	Fold change	p Value
10413	YAP1	Yes-associated protein 1	NM_001130145.2	0,20	2,23E-14
6876	TAGLN	transgelin	NM_001001522.1	0,20	4,43E-09
51442	VGLL1	vestigial like 1 (Drosophila)	NM_016267.3	0,29	2,92E-14
2348	FOLR1	folate receptor 1 (adult)	NM_000802.3	0,30	3,11E-08
3488	IGFBP5	insulin-like growth factor binding protein 5	NM_000599.3	0,34	3,62E-09
3488	IGFBP5	insulin-like growth factor binding protein 5	NM_000599.3	0,36	2,44E-10
2348	FOLR1	folate receptor 1 (adult)	NM_000802.3	0,37	5,69E-07
3486	IGFBP3	insulin-like growth factor binding protein 3	NM_001013398.1	0,37	4,59E-05
92747	BPIFB1	BPI fold containing family B, member 1	NM_033197.2	0,38	6,61E-10
3122	HLA-DRA	major histocompatibility complex, class II, DR alpha	NM_019111.4	0,39	2,05E-05
629	CFB	complement factor B	NM_001710.5	0,40	2,39E-05
1591	CYP24A1	cytochrome P450, family 24, subfamily A, polypeptide 1	NM_000782.4	0,40	1,26E-08

Table A.1.: Downregulated genes in PK9 YAP-knockdown cells (continued)

Gene ID	Symbol	Gene name	Accession number	Fold change	p Value
2628	GATM	glycine amidinotransferase (L-arginine:glycine amidinotransferase)	NM_001482.2	0,40	3,28E-07
6876	TAGLN	transgelin	NM_001001522.1	0,41	4,64E-07
56983	POGLUT1	protein O-glucosyltransferase 1	NM_152305.2	0,41	2,41E-09
523	ATP6V1A	ATPase, H^+ transporting, lysosomal 70kDa, V1 subunit A	NM_001690.3	0,41	4,08E-12
972	CD74	CD74 molecule, major histocompatibility complex, class II invariant chain	NM_001025159.2	0,42	2,87E-06
284018	C17orf58	chromosome 17 open reading frame 58	NM_181655.2	0,42	2,54E-11
972	CD74	CD74 molecule, major histocompatibility complex, class II invariant chain	NM_001025159.2	0,42	2,72E-05
3486	IGFBP3	insulin-like growth factor binding protein 3	NM_001013398.1	0,42	7,72E-05
6286	S100P	S100 calcium binding protein P	NM_005980.2	0,43	3,37E-05
3128	HLA-DRB6	major histocompatibility complex, class II, DR beta 6 (pseudogene)	NG_002432.1	0,43	6,41E-06
27063	ANKRD1	ankyrin repeat domain 1 (cardiac muscle)	NM_014391.2	0,43	1,17E-07
27032	ATP2C1	ATPase, Ca^{2+} transporting, type 2C, member 1	NM_001001485.2	0,44	1,08E-07
3122	HLA-DRA	major histocompatibility complex, class II, DR alpha	NM_019111.4	0,45	7,76E-08
1490	CTGF	connective tissue growth factor	NM_001901.2	0,45	2,05E-04
11167	FSTL1	follistatin-like 1	NM_007085.4	0,46	7,40E-08
284018	C17orf58	chromosome 17 open reading frame 58	NM_181655.2	0,47	5,77E-09
619279	ZNF704	zinc finger protein 704	NM_001033723.2	0,47	5,65E-08
NA	NA	NA	NA	0,47	7,25E-07
54575	UGT1A10	UDP glucuronosyltransferase 1 family, polypeptide A10	NM_019075.2	0,47	1,21E-04
284018	C17orf58	chromosome 17 open reading frame 58	NM_181655.2	0,47	5,10E-10
525	ATP6V1B1	ATPase, H^+ transporting, lysosomal 56/58kDa, V1 subunit B1	NM_001692.3	0,47	1,59E-07
51316	PLAC8	placenta-specific 8	NM_001130716.1	0,47	6,00E-06
1955	MEGF9	multiple EGF-like-domains 9	NM_001080497.2	0,48	6,17E-07

Table A.1.: Downregulated genes in PK9 YAP-knockdown cells (continued)

Gene ID	Symbol	Gene name	Accession number	Fold change	p Value
89846	FGD3	FYVE, RhoGEF and PH domain containing 3	NM_001083536.1	0,48	2,36E-06
8723	SNX4	sorting nexin 4	NM_003794.3	0,50	6,25E-11

Table A.2.: Upregulated genes in PK9 YAP-knockdown cells

Gene ID	Symbol	Gene name	Accession number	Fold change	p Value
4312	MMP1	matrix metallopeptidase 1 (interstitial collagenase)	NM_001145938.1	3,89	4,46E-08
10468	FST	follistatin	NM_006350.3	3,29	5,39E-08
5055	SERPINB2	serpin peptidase inhibitor, clade B (ovalbumin), member 2	NM_001143818.1	3,18	8,55E-07
6947	TCN1	transcobalamin I (vitamin B12 binding protein, R binder family)	NM_001062.3	3,12	1,44E-10
6364	CCL20	chemokine (C-C motif) ligand 20	NM_001130046.1	3,07	1,00E-06
5055	SERPINB2	serpin peptidase inhibitor, clade B (ovalbumin), member 2	NM_001143818.1	2,82	6,19E-06
7857	SCG2	secretogranin II	NM_003469.4	2,67	3,75E-08
3553	IL1B	interleukin 1, beta	NM_000576.2	2,60	2,88E-07
NA	NA	NA	NA	2,53	1,37E-08
1437	CSF2	colony stimulating factor 2 (granulocyte-macrophage)	NM_000758.3	2,52	2,31E-05
794	CALB2	calbindin 2	NM_001740.4	2,47	1,23E-09
3552	IL1A	interleukin 1, alpha	NM_000575.3	2,43	1,55E-08
7431	VIM	vimentin	NM_003380.3	2,33	1,25E-09
118429	ANTXR2	anthrax toxin receptor 2	NM_001145794.1	2,32	6,12E-08
794	CALB2	calbindin 2	NM_001740.4	2,30	1,09E-10
9638	FEZ1	fasciculation and elongation protein zeta 1 (zygin I)	NM_005103.4	2,24	3,17E-09
10013-2240	LOC100-132240	hypothetical LOC100132240	NC_000001.10	2,22	8,74E-08
5744	PTHLH	parathyroid hormone-like hormone	NM_198965.1	2,21	2,03E-04
6698	SPRR1A	small proline-rich protein 1A	NM_001199828.1	2,19	4,32E-08
389336	C5orf46	chromosome 5 open reading frame 46	NM_206966.2	2,19	3,02E-07
3956	LGALS1	lectin, galactoside-binding, soluble, 1	NM_002305.3	2,15	4,12E-07

Table A.2.: Upregulated genes in PK9 YAP-knockdown cells (continued)

Gene ID	Symbol	Gene name	Accession number	Fold change	p Value
207107	SFTA1P	surfactant associated 1, pseudogene	NR_027082.1	2,11	2,62E-11
7424	VEGFC	vascular endothelial growth factor C	NM_005429.2	2,09	5,32E-07
1839	HBEGF	heparin-binding EGF-like growth factor	NM_001945.2	2,07	5,91E-05
4319	MMP10	matrix metallopeptidase 10 (stromelysin 2)	NM_002425.2	2,07	6,85E-04
2533	FYB	FYN binding protein	NM_001243093.1	2,03	1,87E-10
6699	SPRR1B	small proline-rich protein 1B	NM_003125.2	2,03	7,97E-09
1848	DUSP6	dual specificity phosphatase 6	NM_001946.2	2,02	2,67E-05

A.2. Differentially expressed genes in G415 YAP-knockdown cells

Table A.3.: Downregulated genes in G415 YAP-knockdown cells

Gene ID	Symbol	Gene name	Accession number	Fold change	p Value
1455	CSNK1G2	casein kinase 1, gamma 2	NM_001319.6	0,25	1,82E-18
3689	ITGB2	integrin, beta 2 (complement component 3 receptor 3 and 4 subunit)	NM_000211.3	0,25	3,10E-14
55643	BTBD2	BTB (POZ) domain containing 2	NM_017797.3	0,26	7,66E-17
83729	INHBE	inhibin, beta E	NM_031479.3	0,29	3,49E-11
10413	YAP1	Yes-associated protein 1	NM_001130145.2	0,30	5,72E-13
11082	ESM1	endothelial cell-specific molecule 1	NM_007036.4	0,32	2,03E-10
2872	MKNK2	MAP kinase interacting serine/threonine kinase 2	NM_199054.2	0,33	6,93E-10
619383	SCARNA9	small Cajal body-specific RNA 9	NR_002569.2	0,33	9,08E-10
3689	ITGB2	integrin, beta 2 (complement component 3 receptor 3 and 4 subunit)	NM_000211.3	0,34	1,66E-13
11082	ESM1	endothelial cell-specific molecule 1	NM_007036.4	0,34	2,96E-13
9982	FGFBP1	fibroblast growth factor binding protein 1	NM_005130.4	0,35	8,93E-12
5673	PSG5	pregnancy specific beta-1-glycoprotein 5	NM_002781.3	0,35	1,89E-10

Table A.3.: Downregulated genes in G415 YAP-knockdown cells (continued)

Gene ID	Symbol	Gene name	Accession number	Fold change	p Value
11170	FAM107A	family with sequence similarity 107, member A	NM_001076778.2	0,35	2,53E-15
1958	EGR1	early growth response 1	NM_001964.2	0,37	2,90E-05
6876	TAGLN	transgelin	NM_001001522.1	0,37	6,27E-09
115948	CCDC151	coiled-coil domain containing 151	NM_145045.4	0,40	1,82E-09
3936	LCP1	lymphocyte cytosolic protein 1 (L-plastin)	NM_002298.4	0,41	4,33E-08
440	ASNS	asparagine synthetase (glutamine-hydrolyzing)	NM_001178075.1	0,41	6,72E-06
51754	TMEM8B	transmembrane protein 8B	NM_001042589.2	0,42	8,95E-10
79974	CPED1	cadherin-like and PC-esterase domain containing 1	NM_024913.4	0,42	9,91E-12
23108	RAP1GAP2	RAP1 GTPase activating protein 2	NM_015085.4	0,43	2,65E-09
5678	PSG5	pregnancy specific beta-1-glycoprotein 9	NM_002781.3	0,43	3,27E-08
8943	AP3D1	adaptor-related protein complex 3, delta 1 subunit	NM_001261826.1	0,43	8,62E-11
10761	PLAC1	placenta-specific 1	NM_021796.3	0,44	1,17E-10
6023	RMRP	RNA component of mitochondrial RNA processing endoribonuclease	NR_003051.3	0,45	4,27E-09
6876	TAGLN	transgelin	NM_001001522.1	0,45	2,87E-05
8076	MFAP5	microfibrillar associated protein 5	NM_003480.2	0,45	3,11E-11
11009	IL24	interleukin 24	NM_001185156.1	0,45	2,07E-09
3224	HOXC8	homeobox C8	NM_022658.3	0,45	3,19E-10
221416	C6orf223	chromosome 6 open reading frame 223	NM_001171992.1	0,46	7,91E-08
55902	ACSS2	acyl-CoA synthetase short-chain family member 2	NM_001076552.2	0,46	2,10E-07
375061	FAM89A	family with sequence similarity 89, member A	NM_198552.2	0,46	1,97E-09
54541	DDIT4	DNA-damage-inducible transcript 4	NM_019058.2	0,46	1,86E-04
284415	VSTM1	V-set and transmembrane domain containing 1	NM_001288791.1	0,47	1,31E-10
8943	AP3D1	adaptor-related protein complex 3, delta 1 subunit	NM_001261826.1	0,47	7,94E-09
59277	NTN4	netrin 4	NM_021229.3	0,47	1,40E-08
55902	ACSS2	acyl-CoA synthetase short-chain family member 2	NM_001076552.2	0,47	7,01E-07

Table A.3.: Downregulated genes in G415 YAP-knockdown cells (continued)

Gene ID	Symbol	Gene name	Accession number	Fold change	p Value
59277	NTN4	netrin 4	NM_021229.3	0,47	8,83E-09
11009	IL24	interleukin 24	NM_001185156.1	0,47	2,89E-06
1843	DUSP1	dual specificity phosphatase 1	NM_004417.3	0,48	1,08E-04
375061	FAM89A	family with sequence similarity 89, member A	NM_198552.2	0,48	1,85E-09
87769	GGACT	gamma-glutamylamine cyclotransferase	NM_001195087.1	0,49	1,26E-07
677800	SNORA12	small nucleolar RNA, H/ACA box 12	NR_002954.1	0,49	1,29E-08
2172	FABP6	fatty acid binding protein 6, ileal	NM_001040442.1	0,49	1,29E-06
6303	SAT1	spermidine/spermine N1-acetyltransferase 1	NM_002970.2	0,49	8,78E-10
440	ASNS	asparagine synthetase (glutamine-hydrolyzing)	NM_001178075.1	0,49	1,14E-05
27147	DENND2A	DENN/MADD domain containing 2A	NM_015689.3	0,50	9,31E-12
1842	ECM2	extracellular matrix protein 2, female organ and adipocyte specific	NM_001197295.1	0,50	6,88E-10
9699	RIMS2	regulating synaptic membrane exocytosis 2	NM_001100117.2	0,50	9,22E-10

Table A.4.: Upregulated genes in G415 YAP-knockdown cells

Gene ID	Symbol	Gene name	Accession number	Fold change	p Value
58538	MPP4	membrane protein, palmitoylated 4 (MAGUK p55 subfamily member 4)	NM_033066.2	8,27	2,50E-23
57214	CEMIP	cell migration inducing protein, hyaluronan binding	NM_018689.1	4,57	7,40E-16
22943	DKK1	dickkopf WNT signaling pathway inhibitor 1	NM_012242.2	3,88	5,20E-09
6288	SAA1	serum amyloid A1	NM_000331.4	3,67	9,54E-09
163071	ZNF114	zinc finger protein 114	NM_153608.1	3,16	1,21E-09
219736	STOX1	storkhead box 1	NM_152709.4	2,85	8,22E-10
4982	TNFRSF11B	tumor necrosis factor receptor superfamily, member 11b	NM_002546.3	2,66	5,49E-11
5055	SERPINB2	serpin peptidase inhibitor, clade B (ovalbumin), member 2	NM_001143818.1	2,65	1,68E-06

Table A.4.: Upregulated genes in G415 YAP-knockdown cells (continued)

Gene ID	Symbol	Gene name	Accession number	Fold change	p Value
4312	MMP1	matrix metallopeptidase 1 (interstitial collagenase)	NM_002421.3	2,64	1,09E-06
5055	SERPINB2	serpin peptidase inhibitor, clade B (ovalbumin), member 2	NM_001143818.1	2,63	1,40E-06
5801	PTPRR	protein tyrosine phosphatase, receptor type, R	NM_002849.3	2,62	3,84E-11
22943	DKK1	dickkopf WNT signaling pathway inhibitor 1	NM_012242.2	2,58	1,21E-07
7008	TEF	thyrotrophic embryonic factor	NM_003216.3	2,55	3,65E-08
3575	IL7R	interleukin 7 receptor	NM_002185	2,51	2,84E-10
4496	MT1H	metallothionein 1H	NM_005951.2	2,51	2,55E-08
10526	IPO8	importin 8	NM_006390.3	2,50	1,94E-13
8347	HIST1H2BC	histone cluster 1, H2bc	NM_003526.2	2,39	3,32E-08
8638	OASL	2'-5'-oligoadenylate synthetase-like	NM_003733.3	2,27	2,15E-07
440498	HSBP1L1	heat shock factor binding protein 1-like 1	XM_006722476.1	2,18	5,84E-09
10468	FST	follistatin	NM_013409.2	2,18	4,91E-06
389816	LRRCC26	leucine rich repeat containing 26	NM_001013653.2	2,17	4,88E-11
114907	FBXO32	F-box protein 32	NM_058229.3	2,17	1,81E-07
1583	CYP11A1	cytochrome P450, family 11, subfamily A, polypeptide 1	NM_000781.2	2,10	3,60E-06
6000	RGS7	regulator of G-protein signaling 7	NM_002924.5	2,10	8,72E-07
6275	S100A4	S100 calcium binding protein A4	NM_019554.2	2,10	9,27E-09
3321	IGSF3	immunoglobulin superfamily, member 3	NM_001542.3	2,09	3,55E-07
57535	KIAA1324	KIAA1324	NM_020775.4	2,05	5,41E-08
23643	LY96	lymphocyte antigen 96	NM_015364.4	2,05	1,42E-09
348093	RBPMS2	RNA binding protein with multiple splicing 2	NM_194272.1	2,05	8,54E-09
6296	ACSM3	acyl-CoA synthetase medium-chain family member 3	NM_005622.3	2,04	1,38E-07
3321	IGSF3	immunoglobulin superfamily, member 3	NM_001542.3	2,04	6,77E-10
4494	MT1F	metallothionein 1F	NM_005949.3	2,02	2,66E-09
2202	EFEMP1	EGF containing fibulin-like extracellular matrix protein 1	NM_001039348.2	2,01	7,86E-09

Table A.4.: Upregulated genes in G415 YAP-knockdown cells (continued)

Gene ID	Symbol	Gene name	Accession number	Fold change	p Value
4352	MPL	myeloproliferative leukemia virus oncogene	NM_005373.2	2,01	5,72E-08
4973	OLR1	oxidized low density lipoprotein (lectin-like) receptor 1	NM_002543.3	2,01	2,18E-08
389816	LRRC26	leucine rich repeat containing 26	NM_001013653.2	2,00	1,70E-12

A.3. Differentially expressed genes in MZ1774 YAP-knockdown cells

Table A.5.: Downregulated genes in MZ1774 YAP-knockdown cells

Gene ID	Symbol	Gene name	Accession number	Fold change	p Value
1907	EDN2	endothelin 2	NM_001956.3	0,24	1,16E-11
1906	EDN1	endothelin 1	NM_001955.4	0,31	8,57E-06
7057	THBS1	thrombospondin 1	NM_003246.2	0,33	2,34E-05
4616	GADD45B	growth arrest and DNA-damage-inducible, beta	NM_015675.3	0,34	7,53E-05
3491	CYR61	cysteine-rich, angiogenic inducer, 61	NM_001554.4	0,36	1,73E-04
10175	CNIH	cornichon homolog (Drosophila)	NM_005776.2	0,37	3,02E-06
1646	AKR1C2	aldo-keto reductase family 1, member C2 (dihydrodiol dehydrogenase 2, bile acid binding protein, 3-alpha hydroxysteroid dehydrogenase, type III)	NM_001354.5	0,37	4,71E-06
4609	MYC	v-myc myelocytomatosis viral oncogene homolog (avian)	NM_002467.4	0,37	1,05E-06
523	ATP6V1A	ATPase, H^+ transporting, lysosomal 70kDa, V1 subunit A	NM_001690.3	0,38	4,44E-12
4609	MYC	v-myc myelocytomatosis viral oncogene homolog (avian)	NM_002467.4	0,38	2,34E-06
6520	SLC3A2	solute carrier family 3 (activators of dibasic and neutral amino acid transport), member 2	NM_001012662.2	0,39	3,40E-06
284018	C17orf58	chromosome 17 open reading frame 58	NM_181655.2	0,39	7,44E-10

Table A.5.: Downregulated genes in MZ1774 YAP-knockdown cells (continued)

Gene ID	Symbol	Gene name	Accession number	Fold change	p Value
10413	YAP1	Yes-associated protein 1	NM_001130145.2	0,40	2,42E-08
81788	NUAK2	NUAK family, SNF1-like kinase, 2	NM_030952.1	0,40	4,10E-05
1316	KLF6	Kruppel-like factor 6	NM_001160124.1	0,40	4,23E-04
586	BCAT1	branched chain amino-acid transaminase 1, cytosolic	NM_001178091.1	0,41	7,35E-08
81788	NUAK2	NUAK family, SNF1-like kinase, 2	NM_030952.1	0,41	5,60E-06
6526	SLC5A3	solute carrier family 5 (sodium/myo-inositol cotransporter), member 3	NM_006933.4	0,41	1,85E-07
59345	GNB4	guanine nucleotide binding protein (G protein), beta polypeptide 4	NM_021629.3	0,42	2,34E-08
54206	ERRFI1	ERBB receptor feedback inhibitor 1	NM_018948.3	0,42	4,98E-09
27032	ATP2C1	ATPase, Ca^{2+} transporting, type 2C, member 1	NM_001199180.1	0,42	2,63E-07
84706	GPT2	glutamic pyruvate transaminase (alanine aminotransferase) 2	NM_001142466.1	0,44	4,04E-08
9518	GDF15	growth differentiation factor 15	NM_004864.2	0,44	8,31E-05
406991	MIR21	microRNA 21	NR_029493.1	0,44	4,12E-07
59272	ACE2	angiotensin I converting enzyme (peptidyl-dipeptidase A) 2	NM_021804.2	0,44	2,76E-07
8140	SLC7A5	solute carrier family 7 (amino acid transporter light chain, L system), member 5	NM_003486.5	0,44	9,39E-07
51125	GOLGA7	golgin A7	NM_001002296.1	0,44	1,41E-11
4703	NEB	nebulin	NM_001164507.1	0,44	2,93E-05
79660	PPP1R3B	protein phosphatase 1, regulatory (inhibitor) subunit 3B	NM_001201329.1	0,44	4,58E-06
10175	CNIH	cornichon homolog (Drosophila)	NM_005776.2	0,45	2,71E-05
57761	TRIB3	tribbles homolog 3 (Drosophila)	NM_021158.3	0,46	8,68E-06
388272	C16orf87	chromosome 16 open reading frame 87	NM_001001436.2	0,46	1,76E-06
6185	RPN2	ribophorin II	NM_002951.3	0,46	1,28E-07
27063	ANKRD1	ankyrin repeat domain 1 (cardiac muscle)	NM_014391.2	0,47	2,80E-06
29968	PSAT1	phosphoserine aminotransferase 1	NM_021154.3	0,47	1,45E-04
2152	F3	coagulation factor III (thromboplastin, tissue factor)	NM_001993.4	0,47	4,45E-06
81539	SLC38A1	solute carrier family 38, member 1	NM_001077484.1	0,48	1,17E-04

Table A.5.: Downregulated genes in MZ1774 YAP-knockdown cells (continued)

Gene ID	Symbol	Gene name	Accession number	Fold change	p Value
6397	SEC14L1	SEC14-like 1 (S. cerevisiae)	NM_001039573.2	0,48	3,67E-08
10397	NDRG1	N-myc downstream regulated 1	NM_001135242.1	0,48	5,34E-06
5638	PRRG1	proline rich Gla (G-carboxyglutamic acid) 1	NM_000950.2	0,48	5,42E-08
10797	MTHFD2	methylenetetrahydrofolate dehydrogenase ($NADP^+$ dependent) 2, methenyltetrahydrofolate cyclohydrolase	NM_006636.3	0,49	7,56E-08
2530	FUT8	fucosyltransferase 8 (alpha (1,6) fucosyltransferase)	NM_178155.2	0,49	3,76E-07
80115	BAIAP2L2	BAI1-associated protein 2-like 2	NM_025045.4	0,49	1,06E-05
5209	PFKFB3	6-phosphofructo-2-kinase/fructose-2,6-biphosphatase 3	NM_004566.3	0,49	3,49E-05
10175	CNIH	cornichon homolog (Drosophila)	NM_005776.2	0,50	2,86E-05

Table A.6.: Upregulated genes in MZ1774 YAP-knockdown cells

Gene ID	Symbol	Gene name	Accession number	Fold change	p Value
84952	CGNL1	cingulin-like 1	NM_001252335.1	2,97	2,23E-11
5265	SERPINA1	serpin peptidase inhibitor, clade A (alpha-1 antiproteinase, antitrypsin), member 1	NM_000295.4	2,49	6,10E-07
80117	ARL14	ADP-ribosylation factor-like 14	NM_025047.2	2,49	1,91E-07
10344	CCL26	chemokine (C-C motif) ligand 26	NM_006072.4	2,47	2,00E-05
1004	CDH6	cadherin 6, type 2, K-cadherin (fetal kidney)	NM_004932.3	2,27	7,61E-10
266977	GPR110	G protein-coupled receptor 110	NM_153840.2	2,22	5,90E-07
283460	HNF1A-AS1	HNF1A antisense RNA 1 (non-protein coding)	NR_024345.1	2,11	2,20E-04
55195	C14orf105	chromosome 14 open reading frame 105	NM_018168.2	2,07	4,97E-03
266977	GPR110	G protein-coupled receptor 110	NM_153840.2	2,06	1,09E-06
11074	TRIM31	tripartite motif containing 31	NM_007028.3	2,04	1,00E-05
55775	TDP1	tyrosyl-DNA phosphodiesterase 1	NM_001008744.1	2,03	7,20E-04

Table A.6.: Upregulated genes in MZ1774 YAP-knockdown cells (continued)

Gene ID	Symbol	Gene name	Accession number	Fold change	p Value
283209	PGM2L1	phosphoglucomutase 2-like 1	NM_173582.3	2,02	5,00E-05
5265	SERPINA1	serpin peptidase inhibitor, clade A (alpha-1 antiproteinase, antitrypsin), member 1	NM_000295.4	2,02	1,30E-04
11221	DUSP10	dual specificity phosphatase 10	NM_007207.4	2,01	1,00E-04
3767	KCNJ11	potassium inwardly-rectifying channel, subfamily J, member 16	NM_000525.3	1,97	1,00E-05
2353	FOS	FBJ murine osteosarcoma viral oncogene homolog B	NM_005252.3	1,97	5,91E-02
56829	ZC3HAV1	zinc finger CCCH-type, antiviral 1	NM_020119.3	1,97	1,50E-04
158295	MGC24103	hypothetical MGC24103	XR_108934.3	1,96	4,91E-03
7327	UBE2G2	ubiquitin-conjugating enzyme E2G 2	NM_003343.5	1,95	8,77E-03
56664	VTRNA1-1	vault RNA 1-1	NR_026703.1	1,94	1,20E-04

Appendix B.

Raw data of Signaling Pathway Impact Analysis

Table B.1.: Signaling Pathway Impact Analysis of PK9 YAP-knockdown cells

	KEGG pathway	ID	pNDE	pPERT	pG	pGFDR	pGFWER	Status	KEGG-link
1	Rheumatoid arthritis	5323	5,3E-10	1,0E+00	1,2E-08	1,3E-06	1,3E-06	Inhibited	http://www.genome.jp/dbget-bin/show_pathway?hsa05323+3552+3553+3569+1437+4312+4314+3108+3113+3122+155066+523+525+6364
2	Cytokine-cytokine receptor interaction	4060	4,3E-04	5,0E-06	4,5E-08	2,4E-06	4,8E-06	Activated	http://www.genome.jp/dbget-bin/show_pathway?hsa04060+3553+3552+268+3604+3460+7424+1437+3569+6367+6364+58191
3	Graft-versus-host disease	5332	4,2E-06	1,0E+00	5,7E-05	2,0E-03	6,1E-03	Inhibited	http://www.genome.jp/dbget-bin/show_pathway?hsa05332+3108+3113+3122+3569+3552+3553
4	Type I diabetes mellitus	4940	1,3E-05	1,0E+00	1,5E-04	4,2E-03	1,7E-02	Inhibited	http://www.genome.jp/dbget-bin/show_pathway?hsa04940+1363+3108+3113+3122+3552+3553
5	Pathways in cancer	5200	2,0E-05	8,8E-01	2,1E-04	4,6E-03	2,3E-02	Activated	http://www.genome.jp/dbget-bin/show_pathway?hsa05200+54361+7476+80326+3914+3918+3655+2535+7039+8313+5578+1488+6256+1026+330+7424+4312+3569
6	Calcium signaling pathway	4020	9,5E-03	3,0E-03	3,3E-04	5,9E-03	3,5E-02	Activated	http://www.genome.jp/dbget-bin/show_pathway?hsa04020+5578+147+1909+4923+488+154+493
7	Osteoclast differentiation	4380	4,1E-02	1,0E-03	4,6E-04	7,0E-03	4,9E-02	Activated	http://www.genome.jp/dbget-bin/show_pathway?hsa04380+3552+3553+3460+5971+4688
8	ErbB signaling pathway	4012	5,2E-04	1,1E-01	6,2E-04	7,6E-03	6,7E-02	Activated	http://www.genome.jp/dbget-bin/show_pathway?hsa04012+1026+5058+7039+5578+1839+3084+145957
9	MAPK signaling pathway	4010	2,1E-02	3,0E-03	6,8E-04	7,6E-03	7,3E-02	Activated	http://www.genome.jp/dbget-bin/show_pathway?hsa04010+1848+5495+5971+5578+10912+3552+3553+5058+2318
10	Toxoplasmosis	5145	1,2E-04	5,8E-01	7,3E-04	7,6E-03	7,9E-02	Inhibited	http://www.genome.jp/dbget-bin/show_pathway?hsa05145+330+3108+3113+3122+240+3655+3914+3918+3460

Table B.1.: Signaling Pathway Impact Analysis of PK9 YAP-knockdown cells (continued)

	KEGG pathway	ID	pNDE	pPERT	pG	pGFDR	pGFWER	Status	KEGG-link
11	Leishmaniasis	5140	7,3E-05	1,0E+00	7,7E-04	7,6E-03	8,3E-02	Activated	http://www.genome.jp/dbget-bin/show_pathway?hsa05140+3108+3113+3122+3552+3553+3460+4688
12	Influenza A	5164	2,1E-04	4,4E-01	9,5E-04	8,5E-03	1,0E-01	Inhibited	http://www.genome.jp/dbget-bin/show_pathway?hsa05164+5644+3553+3108+3113+3122+3552+3569+6041+5578+3460
13	Staphylococcus aureus infection	5150	4,6E-04	2,5E-01	1,2E-03	9,6E-03	1,3E-01	Inhibited	http://www.genome.jp/dbget-bin/show_pathway?hsa05150+629+715+3108+3113+3122
14	Salivary secretion	4970	7,9E-03	1,6E-02	1,3E-03	9,7E-03	1,4E-01	Activated	http://www.genome.jp/dbget-bin/show_pathway?hsa04970+154+147+493+5578+1469
15	Amoebiasis	5146	1,9E-04	7,4E-01	1,4E-03	9,8E-03	1,5E-01	Activated	http://www.genome.jp/dbget-bin/show_pathway?hsa05146+3553+3914+3918+3569+1437+5578+1992+5055
16	Complement and coagulation cascades	4610	2,1E-04	8,0E-01	1,6E-03	1,1E-02	1,7E-01	Inhibited	http://www.genome.jp/dbget-bin/show_pathway?hsa04610+5329+5328+5327+629+725+715
17	HTLV-I infection	5166	2,8E-04	6,5E-01	1,8E-03	1,1E-02	1,9E-01	Inhibited	http://www.genome.jp/dbget-bin/show_pathway?hsa05166+1026+8881+3569+1437+5971+330+54361+7476+80326+2535+3108+3113+3122
18	Tuberculosis	5152	1,1E-03	1,8E-01	1,9E-03	1,1E-02	2,0E-01	Activated	http://www.genome.jp/dbget-bin/show_pathway?hsa05152+3460+972+3108+3113+3122+3552+3553+3569+3656
19	Intestinal immune network for IgA production	4672	2,3E-04	1,0E+00	2,2E-03	1,2E-02	2,3E-01	Inhibited	http://www.genome.jp/dbget-bin/show_pathway?hsa04672+3569+3108+3113+3122+5284
20	Systemic lupus erythematosus	5322	3,4E-03	7,1E-02	2,3E-03	1,2E-02	2,5E-01	Inhibited	http://www.genome.jp/dbget-bin/show_pathway?hsa05322+715+3108+3113+3122+8344+8365
21	Asthma	5310	2,8E-03	NA	2,8E-03	1,5E-02	3,1E-01	Inhibited	http://www.genome.jp/dbget-bin/show_pathway?hsa05310+3108+3113+3122
22	Vibrio cholerae infection	5110	1,8E-03	3,8E-01	5,6E-03	2,7E-02	6,1E-01	Inhibited	http://www.genome.jp/dbget-bin/show_pathway?hsa05110+155066+523+525+9414+5578
23	Focal adhesion	4510	9,6E-04	7,4E-01	5,8E-03	2,7E-02	6,3E-01	Activated	http://www.genome.jp/dbget-bin/show_pathway?hsa04510+3655+2318+4659+5578+3914+3918+6696+330+7424+5058
24	Wnt signaling pathway	4310	2,4E-03	3,4E-01	6,8E-03	3,1E-02	7,3E-01	Activated	http://www.genome.jp/dbget-bin/show_pathway?hsa04310+5578+2535+144165+1488+8313+54361+7476+80326
25	Epithelial cell signaling in Helicobacter pylori infection	5120	5,1E-03	1,8E-01	7,4E-03	3,2E-02	8,0E-01	Activated	http://www.genome.jp/dbget-bin/show_pathway?hsa05120+155066+523+525+5058+1839
26	Basal cell carcinoma	5217	0,00	0,80	0,01	0,04	1	Activated	http://www.genome.jp/dbget-bin/show_pathway?hsa05217+54361+7476+80326+8313+2535
27	Pertussis	5133	0,01	0,33	0,01	0,06	1	Activated	http://www.genome.jp/dbget-bin/show_pathway?hsa05133+3552+3553+3569+715+725
28	Salmonella infection	5132	0,00	0,87	0,01	0,06	1	Inhibited	http://www.genome.jp/dbget-bin/show_pathway?hsa05132+2318+3553+3460+3552+3569+1437

Table B.1.: Signaling Pathway Impact Analysis of PK9 YAP-knockdown cells (continued)

	KEGG pathway	ID	pNDE	pPERT	pG	pGFDR	pGFWER	Status	KEGG-link
29	Neuroactive ligand-receptor interaction	4080	0,02	0,10	0,02	0,06	1	Activated	http://www.genome.jp/dbget-bin/show_pathway?hsa04080+5644+2568+7433+4923+1909+147+154
30	Small cell lung cancer	5222	0,01	0,25	0,02	0,08	1	Activated	http://www.genome.jp/dbget-bin/show_pathway?hsa05222+3655+6256+3914+3918+330
31	Notch signaling pathway	4330	0,01	0,61	0,02	0,08	1	Activated	http://www.genome.jp/dbget-bin/show_pathway?hsa04330+1488+8650+182+28514
32	Antigen processing and presentation	4612	0,01	0,28	0,03	0,08	1	Inhibited	http://www.genome.jp/dbget-bin/show_pathway?hsa04612+972+3108+3113+3122
33	Apoptosis	4210	0,05	0,09	0,03	0,09	1	Activated	http://www.genome.jp/dbget-bin/show_pathway?hsa04210+330+3656+3552+3553
34	Pathogenic Escherichia coli infection	5130	0,06	0,08	0,03	0,10	1	Activated	http://www.genome.jp/dbget-bin/show_pathway?hsa05130+79861+5578+9181
35	Herpes simplex infection	5168	0,01	1	0,03	0,10	1	Inhibited	http://www.genome.jp/dbget-bin/show_pathway?hsa05168+3553+3569+6041+3460+972+3108+3113+3122
36	ECM-receptor interaction	4512	0,01	0,98	0,03	0,10	1	Inhibited	http://www.genome.jp/dbget-bin/show_pathway?hsa04512+3914+3918+6696+3655+6385
37	p53 signaling pathway	4115	0,03	0,27	0,04	0,12	1	Activated	http://www.genome.jp/dbget-bin/show_pathway?hsa04115+3486+10912+55240+1026
38	Allograft rejection	5330	0,01	1	0,05	0,14	1	Inhibited	http://www.genome.jp/dbget-bin/show_pathway?hsa05330+3108+3113+3122
39	Autoimmune thyroid disease	5320	0,01	1	0,05	0,15	1	Inhibited	http://www.genome.jp/dbget-bin/show_pathway?hsa05320+3108+3113+3122
40	NOD-like receptor signaling pathway	4621	0,07	0,15	0,06	0,16	1	Activated	http://www.genome.jp/dbget-bin/show_pathway?hsa04621+330+3553+3569
41	Prion diseases	5020	0,01	1	0,06	0,16	1	Inhibited	http://www.genome.jp/dbget-bin/show_pathway?hsa05020+3552+3553+3569
42	Pancreatic secretion	4972	0,01	1	0,06	0,16	1	Inhibited	http://www.genome.jp/dbget-bin/show_pathway?hsa04972+493+5578+9635+5644+488
43	Chagas disease (American trypanosomiasis)	5142	0,06	0,18	0,06	0,16	1	Activated	http://www.genome.jp/dbget-bin/show_pathway?hsa05142+3553+3460+5521+3569
44	GnRH signaling pathway	4912	0,44	0,03	0,07	0,18	1	Activated	http://www.genome.jp/dbget-bin/show_pathway?hsa04912+5578+1839
45	Legionellosis	5134	0,06	0,25	0,08	0,19	1	Activated	http://www.genome.jp/dbget-bin/show_pathway?hsa05134+3553+1917+3569
46	PPAR signaling pathway	3320	0,08	0,19	0,08	0,19	1	Inhibited	http://www.genome.jp/dbget-bin/show_pathway?hsa03320+6256+2181+4312
47	African trypanosomiasis	5143	0,02	1	0,08	0,19	1	Inhibited	http://www.genome.jp/dbget-bin/show_pathway?hsa05143+3553+3569+5578
48	Melanogenesis	4916	0,02	0,87	0,08	0,19	1	Activated	http://www.genome.jp/dbget-bin/show_pathway?hsa04916+2535+5578+54361+7476+80326
49	Malaria	5144	0,02	1	0,11	0,23	1	Inhibited	http://www.genome.jp/dbget-bin/show_pathway?hsa05144+6385+3569+3553

Table B.1.: Signaling Pathway Impact Analysis of PK9 YAP-knockdown cells (continued)

	KEGG pathway	ID	pNDE	pPERT	pG	pGFDR	pGFWER	Status	KEGG-link
50	Vascular smooth muscle contraction	4270	0,09	0,31	0,12	0,27	1	Activated	http://www.genome.jp/dbget-bin/show_pathway?hsa04270+4659+5578+147+1909
51	Bladder cancer	5219	0,03	1	0,13	0,28	1	Inhibited	http://www.genome.jp/dbget-bin/show_pathway?hsa05219+4312+7424+1026
52	Tight junction	4530	0,33	0,10	0,14	0,29	1	Activated	http://www.genome.jp/dbget-bin/show_pathway?hsa04530+5578+5521+9414
53	Pancreatic cancer	5212	0,33	0,11	0,15	0,31	1	Activated	http://www.genome.jp/dbget-bin/show_pathway?hsa05212+7039+7424
54	Chemokine signaling pathway	4062	0,29	0,14	0,17	0,34	1	Activated	http://www.genome.jp/dbget-bin/show_pathway?hsa04062+58191+6364+6367+5058
55	Non-small cell lung cancer	5223	0,07	0,71	0,19	0,37	1	Inhibited	http://www.genome.jp/dbget-bin/show_pathway?hsa05223+5578+7039+6256
56	Cytosolic DNA-sensing pathway	4623	0,05	1	0,19	0,37	1	Inhibited	http://www.genome.jp/dbget-bin/show_pathway?hsa04623+3553+3569+10622
57	Hedgehog signaling pathway	4340	0,05	1	0,20	0,37	1	Inhibited	http://www.genome.jp/dbget-bin/show_pathway?hsa04340+54361+7476+80326
58	Glioma	5214	0,09	0,75	0,24	0,45	1	Inhibited	http://www.genome.jp/dbget-bin/show_pathway?hsa05214+7039+5578+1026
59	Viral myocarditis	5416	0,07	1	0,25	0,46	1	Inhibited	http://www.genome.jp/dbget-bin/show_pathway?hsa05416+3108+3113+3122
60	Hepatitis C	5160	0,15	0,50	0,27	0,48	1	Activated	http://www.genome.jp/dbget-bin/show_pathway?hsa05160+5521+6041+1026+6256
61	Chronic myeloid leukemia	5220	0,34	0,23	0,28	0,50	1	Inhibited	http://www.genome.jp/dbget-bin/show_pathway?hsa05220+1488+1026
62	Natural killer cell mediated cytotoxicity	4650	0,10	0,87	0,30	0,51	1	Activated	http://www.genome.jp/dbget-bin/show_pathway?hsa04650+3460+1437+5578+5058
63	Arrhythmogenic right ventricular cardiomyopathy (ARVC)	5412	0,09	1	0,31	0,53	1	Inhibited	http://www.genome.jp/dbget-bin/show_pathway?hsa05412+488+1832+3655
64	Toll-like receptor signaling pathway	4620	0,17	0,58	0,32	0,54	1	Inhibited	http://www.genome.jp/dbget-bin/show_pathway?hsa04620+6696+3553+3569
65	Gastric acid secretion	4971	0,27	0,36	0,32	0,54	1	Inhibited	http://www.genome.jp/dbget-bin/show_pathway?hsa04971+5578+3776
66	Prostate cancer	5215	0,44	0,24	0,34	0,55	1	Activated	http://www.genome.jp/dbget-bin/show_pathway?hsa05215+1026+7039
67	Renal cell carcinoma	5211	0,10	1	0,34	0,55	1	Inhibited	http://www.genome.jp/dbget-bin/show_pathway?hsa05211+7424+7039+5058
68	Measles	5162	0,11	1	0,35	0,56	1	Inhibited	http://www.genome.jp/dbget-bin/show_pathway?hsa05162+3460+3552+3553+3569
69	GABAergic synapse	4727	0,12	1	0,36	0,57	1	Inhibited	http://www.genome.jp/dbget-bin/show_pathway?hsa04727+2568+18+5578
70	SNARE interactions in vesicular transport	4130	0,12	1	0,38	0,58	1	Inhibited	http://www.genome.jp/dbget-bin/show_pathway?hsa04130+55014+10228

Table B.1.: Signaling Pathway Impact Analysis of PK9 YAP-knockdown cells (continued)

	KEGG pathway	ID	pNDE	pPERT	pG	pGFDR	pGFWER	Status	KEGG-link
71	Mineral absorption	4978	0,14	1	0,42	0,64	1	Inhibited	http://www.genome.jp/dbget-bin/show_pathway?hsa04978+30061+261729
72	Long-term potentiation	4720	0,27	0,53	0,43	0,64	1	Activated	http://www.genome.jp/dbget-bin/show_pathway?hsa04720+5578+4659
73	Jak-STAT signaling pathway	4630	0,15	1	0,44	0,65	1	Inhibited	http://www.genome.jp/dbget-bin/show_pathway?hsa04630+10252+3460+3569+1437
74	RIG-I-like receptor signaling pathway	4622	0,26	0,62	0,46	0,65	1	Activated	http://www.genome.jp/dbget-bin/show_pathway?hsa04622+54941+80143
75	Regulation of actin cytoskeleton	4810	0,22	0,72	0,46	0,65	1	Activated	http://www.genome.jp/dbget-bin/show_pathway?hsa04810+5305+4659+5058+89846+3655
76	Cell cycle	4110	0,35	0,46	0,46	0,65	1	Activated	http://www.genome.jp/dbget-bin/show_pathway?hsa04110+8881+1026+10912
77	Endocrine and other factor-regulated calcium reabsorption	4961	0,51	0,35	0,49	0,68	1	Inhibited	http://www.genome.jp/dbget-bin/show_pathway?hsa04961+5578
78	Glutamatergic synapse	4724	0,51	0,36	0,49	0,68	1	Inhibited	http://www.genome.jp/dbget-bin/show_pathway?hsa04724+5578+9455
79	VEGF signaling pathway	4370	0,69	0,27	0,50	0,69	1	Inhibited	http://www.genome.jp/dbget-bin/show_pathway?hsa04370+5578
80	Neurotrophin signaling pathway	4722	0,62	0,34	0,54	0,73	1	Activated	http://www.genome.jp/dbget-bin/show_pathway?hsa04722+10019+3656
81	TGF-beta signaling pathway	4350	0,35	0,75	0,61	0,82	1	Activated	http://www.genome.jp/dbget-bin/show_pathway?hsa04350+10468+268
82	Leukocyte transendothelial migration	4670	0,51	0,55	0,64	0,84	1	Activated	http://www.genome.jp/dbget-bin/show_pathway?hsa04670+5578+4688
83	Adipocytokine signaling pathway	4920	0,30	1	0,66	0,85	1	Inhibited	http://www.genome.jp/dbget-bin/show_pathway?hsa04920+2181+6256
84	Axon guidance	4360	0,31	1	0,67	0,85	1	Inhibited	http://www.genome.jp/dbget-bin/show_pathway?hsa04360+59277+5058+9037
85	Fc gamma R-mediated phagocytosis	4666	0,45	0,68	0,67	0,85	1	Inhibited	http://www.genome.jp/dbget-bin/show_pathway?hsa04666+5058+5578
86	Lysosome	4142	0,32	1	0,69	0,85	1	Inhibited	http://www.genome.jp/dbget-bin/show_pathway?hsa04142+1075+9374+7805
87	Melanoma	5218	0,66	0,50	0,69	0,85	1	Inhibited	http://www.genome.jp/dbget-bin/show_pathway?hsa05218+1026
88	RNA degradation	3018	0,33	1	0,70	0,85	1	Inhibited	http://www.genome.jp/dbget-bin/show_pathway?hsa03018+5073+10950
89	Fc epsilon RI signaling pathway	4664	0,33	1	0,70	0,85	1	Inhibited	http://www.genome.jp/dbget-bin/show_pathway?hsa04664+1437+5578
90	Dilated cardiomyopathy	5414	0,37	1	0,74	0,88	1	Inhibited	http://www.genome.jp/dbget-bin/show_pathway?hsa05414+488+3655
91	Oocyte meiosis	4114	0,52	0,71	0,74	0,88	1	Inhibited	http://www.genome.jp/dbget-bin/show_pathway?hsa04114+8881+9985
92	Gap junction	4540	0,39	1	0,75	0,88	1	Inhibited	http://www.genome.jp/dbget-bin/show_pathway?hsa04540+5578+79861

Table B.1.: Signaling Pathway Impact Analysis of PK9 YAP-knockdown cells (continued)

	KEGG pathway	ID	pNDE	pPERT	pG	pGFDR	pGFWER	Status	KEGG-link
93	Thyroid cancer	5216	0,39	1	0,76	0,88	1	Inhibited	http://www.genome.jp/dbget-bin/show_pathway?hsa05216+6256
94	T cell receptor signaling pathway	4660	0,46	1	0,82	0,93	1	Inhibited	http://www.genome.jp/dbget-bin/show_pathway?hsa04660+1437+5058
95	Aldosterone-regulated sodium reabsorption	4960	0,46	1	0,82	0,93	1	Inhibited	http://www.genome.jp/dbget-bin/show_pathway?hsa04960+5578
96	Dopaminergic synapse	4728	0,58	0,84	0,84	0,95	1	Inhibited	http://www.genome.jp/dbget-bin/show_pathway?hsa04728+5578+5521
97	mTOR signaling pathway	4150	0,56	1	0,89	0,98	1	Inhibited	http://www.genome.jp/dbget-bin/show_pathway?hsa04150+7424
98	Endometrial cancer	5213	0,58	1	0,90	0,98	1	Inhibited	http://www.genome.jp/dbget-bin/show_pathway?hsa05213+8313
99	Long-term depression	4730	0,62	1	0,92	0,98	1	Inhibited	http://www.genome.jp/dbget-bin/show_pathway?hsa04730+5578
100	Insulin signaling pathway	4910	0,63	1	0,92	0,98	1	Inhibited	http://www.genome.jp/dbget-bin/show_pathway?hsa04910+5834+10211
101	Bile secretion	4976	0,63	1	0,92	0,98	1	Inhibited	http://www.genome.jp/dbget-bin/show_pathway?hsa04976+6256
102	Colorectal cancer	5210	0,64	1	0,93	0,98	1	Inhibited	http://www.genome.jp/dbget-bin/show_pathway?hsa05210+8313
103	RNA transport	3013	0,72	1	0,96	0,98	1	Inhibited	http://www.genome.jp/dbget-bin/show_pathway?hsa03013+1917+10799
104	B cell receptor signaling pathway	4662	0,72	1	0,96	0,98	1	Inhibited	http://www.genome.jp/dbget-bin/show_pathway?hsa04662+8519
105	Alzheimer's disease	5010	0,73	1	0,96	0,98	1	Inhibited	http://www.genome.jp/dbget-bin/show_pathway?hsa05010+488+3553
106	Progesterone-mediated oocyte maturation	4914	0,74	1	0,96	0,98	1	Inhibited	http://www.genome.jp/dbget-bin/show_pathway?hsa04914+8881
107	Cholinergic synapse	4725	0,80	1	0,98	0,99	1	Inhibited	http://www.genome.jp/dbget-bin/show_pathway?hsa04725+5578
108	Olfactory transduction	4740	0,93	1	1,00	1,00	1	Inhibited	http://www.genome.jp/dbget-bin/show_pathway?hsa04740+9635

Table B.2.: Signaling Pathway Impact Analysis of G415 YAP-knockdown cells

	KEGG pathway	ID	pNDE	pPERT	pG	pGFDR	pGFWER	Status	KEGG-link
1	Cytokine-cytokine receptor interaction	4060	0,0002	0,20	0,0004	0,0119	0,01	Inhibited	http://www.genome.jp/dbget-bin/show_pathway?hsa04060+83729+11009+4352+3575+4982
2	Amoebiasis	5146	0,0258	0,02	0,0046	0,0515	0,15	Inhibited	http://www.genome.jp/dbget-bin/show_pathway?hsa05146+3689+5055
3	PPAR signaling pathway	3320	0,0006	1	0,0047	0,0515	0,15	Inhibited	http://www.genome.jp/dbget-bin/show_pathway?hsa03320+2172+4973+4312
4	Hedgehog signaling pathway	4340	0,1218	0,01	0,0110	0,0908	0,36	Activated	http://www.genome.jp/dbget-bin/show_pathway?hsa04340+1455
5	TGF-beta signaling pathway	4350	0,0163	0,15	0,0175	0,1062	0,58	Activated	http://www.genome.jp/dbget-bin/show_pathway?hsa04350+83729+10468

Table B.2.: Signaling Pathway Impact Analysis of G415 YAP-knockdown cells (continued)

	KEGG pathway	ID	pNDE	pPERT	pG	pGFDR	pGFWER	Status	KEGG-link
6	Regulation of actin cytoskeleton	4810	0,4013	0,01	0,0193	0,1062	0,64	Inhibited	http://www.genome.jp/dbget-bin/show_pathway?hsa04810+3689
7	Jak-STAT signaling pathway	4630	0,0043	1	0,0279	0,1168	0,92	Inhibited	http://www.genome.jp/dbget-bin/show_pathway?hsa04630+3575+4352+11009
8	Mineral absorption	4978	0,0050	1	0,0315	0,1168	1	Inhibited	http://www.genome.jp/dbget-bin/show_pathway?hsa04978+4494+4496
9	Natural killer cell mediated cytotoxicity	4650	0,2415	0,02	0,0319	0,1168	1	Inhibited	http://www.genome.jp/dbget-bin/show_pathway?hsa04650+3689
10	Osteoclast differentiation	4380	0,2578	0,03	0,0415	0,1371	1	Inhibited	http://www.genome.jp/dbget-bin/show_pathway?hsa04380+4982
11	Leukocyte transendothelial migration	4670	0,2374	0,03	0,0470	0,1409	1	Inhibited	http://www.genome.jp/dbget-bin/show_pathway?hsa04670+3689
12	Pertussis	5133	0,0142	1	0,0746	0,2000	1	Inhibited	http://www.genome.jp/dbget-bin/show_pathway?hsa05133+3689+23643
13	Rheumatoid arthritis	5323	0,0180	1	0,0904	0,2000	1	Inhibited	http://www.genome.jp/dbget-bin/show_pathway?hsa05323+4312+3689
14	Prion diseases	5020	0,0705	0,26	0,0905	0,2000	1	Inhibited	http://www.genome.jp/dbget-bin/show_pathway?hsa05020+1958
15	Leishmaniasis	5140	0,1499	0,12	0,0909	0,2000	1	Inhibited	http://www.genome.jp/dbget-bin/show_pathway?hsa05140+3689
16	MAPK signaling pathway	4010	0,0261	0,76	0,0972	0,2004	1	Inhibited	http://www.genome.jp/dbget-bin/show_pathway?hsa04010+1843+5801+2872
17	Wnt signaling pathway	4310	0,3084	0,12	0,1610	0,3126	1	Inhibited	http://www.genome.jp/dbget-bin/show_pathway?hsa04310+22943
18	Malaria	5144	0,0904	1	0,3076	0,5229	1	Inhibited	http://www.genome.jp/dbget-bin/show_pathway?hsa05144+3689
19	Staphylococcus aureus infection	5150	0,0977	1	0,3250	0,5229	1	Inhibited	http://www.genome.jp/dbget-bin/show_pathway?hsa05150+3689
20	Bladder cancer	5219	0,1002	1	0,3307	0,5229	1	Inhibited	http://www.genome.jp/dbget-bin/show_pathway?hsa05219+4312
21	Insulin signaling pathway	4910	0,2835	0,41	0,3634	0,5229	1	Inhibited	http://www.genome.jp/dbget-bin/show_pathway?hsa04910+2872
22	mTOR signaling pathway	4150	0,1218	1	0,3783	0,5229	1	Inhibited	http://www.genome.jp/dbget-bin/show_pathway?hsa04150+54541
23	Pathogenic Escherichia coli infection	5130	0,1313	1	0,3979	0,5229	1	Inhibited	http://www.genome.jp/dbget-bin/show_pathway?hsa05130+23643
24	Legionellosis	5134	0,1313	1	0,3979	0,5229	1	Inhibited	http://www.genome.jp/dbget-bin/show_pathway?hsa05134+3689
25	HTLV-I infection	5166	0,1373	1	0,4099	0,5229	1	Inhibited	http://www.genome.jp/dbget-bin/show_pathway?hsa05166+3689+1958
26	Viral myocarditis	5416	0,1383	1	0,4120	0,5229	1	Inhibited	http://www.genome.jp/dbget-bin/show_pathway?hsa05416+3689
27	Toll-like receptor signaling pathway	4620	0,1992	1	0,5206	0,6257	1	Inhibited	http://www.genome.jp/dbget-bin/show_pathway?hsa04620+23643
28	Systemic lupus erythematosus	5322	0,2057	1	0,5309	0,6257	1	Inhibited	http://www.genome.jp/dbget-bin/show_pathway?hsa05322+8347
29	Toxoplasmosis	5145	0,2578	1	0,6072	0,6662	1	Inhibited	http://www.genome.jp/dbget-bin/show_pathway?hsa05145+23643
30	Axon guidance	4360	0,2638	1	0,6153	0,6662	1	Inhibited	http://www.genome.jp/dbget-bin/show_pathway?hsa04360+59277
31	Lysosome	4142	0,2718	1	0,6258	0,6662	1	Inhibited	http://www.genome.jp/dbget-bin/show_pathway?hsa04142+8943
32	Tuberculosis	5152	0,3306	1	0,6965	0,7183	1	Inhibited	http://www.genome.jp/dbget-bin/show_pathway?hsa05152+3689

Table B.2.: Signaling Pathway Impact Analysis of G415 YAP-knockdown cells (continued)

	KEGG pathway	ID	pNDE	pPERT	pG	pGFDR	pGFWER	Status	KEGG-link
33	Pathways in cancer	5200	0,5590	1	0,8841	0,8841	1	Inhibited	http://www.genome.jp/dbget-bin/show_pathway?hsa05200+4312

Table B.3.: Signaling Pathway Impact Analysis of MZ1774 YAP-knockdown cells

	KEGG pathway	ID	pNDE	pPERT	pG	pGFDR	pGFWER	Status	KEGG-link
1	p53 signaling pathway	4115	1,5E-06	0,13	3,2E-06	0,00	0,000	Activated	http://www.genome.jp/dbget-bin/show_pathway?hsa04115+3486+1647+4616+7057+8795+54205+1021+27244
2	MAPK signaling pathway	4010	1,8E-04	0,32	6,2E-04	0,02	0,067	Inhibited	http://www.genome.jp/dbget-bin/show_pathway?hsa04010+11221+2247+627+9261+1649+51776+1647+4616+3554+4609+2872
3	Cell cycle	4110	6,5E-02	0,00	6,9E-04	0,02	0,074	Activated	http://www.genome.jp/dbget-bin/show_pathway?hsa04110+1647+4616+1021+4609
4	Insulin signaling pathway	4910	8,6E-04	0,95	6,6E-03	0,16	0,713	Activated	http://www.genome.jp/dbget-bin/show_pathway?hsa04910+2872+5501+5507+79660+5295+5590+8660
5	Tuberculosis	5152	1,0E-02	0,09	7,3E-03	0,16	0,793	Activated	http://www.genome.jp/dbget-bin/show_pathway?hsa05152+1051+1054+7096+54205+3592+3456
6	HTLV-I infection	5166	1,0E-02	0,15	1,1E-02	0,21	1	Activated	http://www.genome.jp/dbget-bin/show_pathway?hsa05166+6513+821+4609+115+3554+5295+64784+94241
7	Regulation of actin cytoskeleton	4810	9,3E-03	0,23	1,5E-02	0,21	1	Activated	http://www.genome.jp/dbget-bin/show_pathway?hsa04810+26999+85477+7414+4659+5501+5295+2247
8	Cholinergic synapse	4725	6,2E-03	0,37	1,6E-02	0,21	1	Inhibited	http://www.genome.jp/dbget-bin/show_pathway?hsa04725+115+3710+59345+9586+5295
9	Type II diabetes mellitus	4930	1,1E-02	0,25	1,9E-02	0,21	1	Inhibited	http://www.genome.jp/dbget-bin/show_pathway?hsa04930+5295+8660+5590
10	Colorectal cancer	5210	3,6E-02	0,09	2,1E-02	0,21	1	Inhibited	http://www.genome.jp/dbget-bin/show_pathway?hsa05210+5295+4609+54205
11	Neurotrophin signaling pathway	4722	6,3E-02	0,05	2,1E-02	0,21	1	Inhibited	http://www.genome.jp/dbget-bin/show_pathway?hsa04722+627+5295+8660+9261
12	Vascular smooth muscle contraction	4270	7,1E-03	0,55	2,5E-02	0,22	1	Activated	http://www.genome.jp/dbget-bin/show_pathway?hsa04270+4659+5501+3710+136+115
13	Complement and coagulation cascades	4610	2,4E-02	0,17	2,7E-02	0,22	1	Inhibited	http://www.genome.jp/dbget-bin/show_pathway?hsa04610+2152+5265+5328
14	Cytokine-cytokine receptor interaction	4060	9,0E-03	0,61	3,4E-02	0,23	1	Activated	http://www.genome.jp/dbget-bin/show_pathway?hsa04060+3554+3456+3592+10344+27242+51330+8795
15	Influenza A	5164	9,4E-03	0,63	3,6E-02	0,23	1	Inhibited	http://www.genome.jp/dbget-bin/show_pathway?hsa05164+5295+3456+3592+8795+54205+10625
16	Long-term potentiation	4720	3,8E-02	0,17	3,9E-02	0,23	1	Activated	http://www.genome.jp/dbget-bin/show_pathway?hsa04720+4659+5501+3710

Table B.3.: Signaling Pathway Impact Analysis of MZ1774 YAP-knockdown cells (continued)

	KEGG pathway	ID	pNDE	pPERT	pG	pGFDR	pGFWER	Status	KEGG-link
17	Apoptosis	4210	1,7E-02	0,42	4,2E-02	0,23	1	Inhibited	http://www.genome.jp/dbget-bin/show_pathway?hsa04210+54205+5295+3554+8795
18	Measles	5162	1,0E-02	0,69	4,2E-02	0,23	1	Inhibited	http://www.genome.jp/dbget-bin/show_pathway?hsa05162+3456+5295+3592+8795+1021
19	Amoebiasis	5146	2,7E-02	0,28	4,4E-02	0,23	1	Activated	http://www.genome.jp/dbget-bin/show_pathway?hsa05146+3554+3592+5295+7414
20	Pathways in cancer	5200	3,4E-02	0,23	4,6E-02	0,23	1	Inhibited	http://www.genome.jp/dbget-bin/show_pathway?hsa05200+5295+4609+7428+54205+1488+1021+6513+2247
21	Adipocytokine signaling pathway	4920	8,1E-03	1	4,7E-02	0,23	1	Inhibited	http://www.genome.jp/dbget-bin/show_pathway?hsa04920+2182+51703+6513+8660
22	Renal cell carcinoma	5211	9,0E-03	0,95	4,9E-02	0,23	1	Activated	http://www.genome.jp/dbget-bin/show_pathway?hsa05211+6513+7428+201163+5295
23	Glutamatergic synapse	4724	3,6E-02	0,25	5,1E-02	0,23	1	Activated	http://www.genome.jp/dbget-bin/show_pathway?hsa04724+115+81539+3710+59345
24	Malaria	5144	9,1E-03	1	5,2E-02	0,23	1	Inhibited	http://www.genome.jp/dbget-bin/show_pathway?hsa05144+6383+3592+7057
25	GABAergic synapse	4727	5,4E-02	0,18	5,4E-02	0,23	1	Activated	http://www.genome.jp/dbget-bin/show_pathway?hsa04727+115+59345+81539
26	Small cell lung cancer	5222	1,9E-02	0,52	5,5E-02	0,23	1	Inhibited	http://www.genome.jp/dbget-bin/show_pathway?hsa05222+4609+5295+54205+1021
27	Toll-like receptor signaling pathway	4620	1,9E-02	0,55	5,8E-02	0,23	1	Inhibited	http://www.genome.jp/dbget-bin/show_pathway?hsa04620+3456+7096+5295+3592
28	Chronic myeloid leukemia	5220	1,2E-02	0,91	5,9E-02	0,23	1	Inhibited	http://www.genome.jp/dbget-bin/show_pathway?hsa05220+1488+4609+1021+5295
29	Huntington's disease	5016	3,4E-01	0,04	7,4E-02	0,28	1	Inhibited	http://www.genome.jp/dbget-bin/show_pathway?hsa05016+627+54205+9586
30	ECM-receptor interaction	4512	1,9E-01	0,11	9,9E-02	0,36	1	Inhibited	http://www.genome.jp/dbget-bin/show_pathway?hsa04512+7057+6383
31	Melanoma	5218	4,3E-02	0,51	1,1E-01	0,37	1	Inhibited	http://www.genome.jp/dbget-bin/show_pathway?hsa05218+2247+1021+5295
32	Notch signaling pathway	4330	9,5E-02	0,26	1,1E-01	0,39	1	Activated	http://www.genome.jp/dbget-bin/show_pathway?hsa04330+1488+8650
33	Toxoplasmosis	5145	1,6E-01	0,17	1,2E-01	0,39	1	Inhibited	http://www.genome.jp/dbget-bin/show_pathway?hsa05145+3592+54205+5295
34	Aldosterone-regulated sodium reabsorption	4960	7,3E-02	0,37	1,2E-01	0,39	1	Inhibited	http://www.genome.jp/dbget-bin/show_pathway?hsa04960+8660+5295
35	TGF-beta signaling pathway	4350	2,2E-01	0,13	1,3E-01	0,40	1	Inhibited	http://www.genome.jp/dbget-bin/show_pathway?hsa04350+7057+4609
36	Chemokine signaling pathway	4062	4,7E-02	0,66	1,4E-01	0,40	1	Inhibited	http://www.genome.jp/dbget-bin/show_pathway?hsa04062+10344+5295+59345+115+5590
37	Bacterial invasion of epithelial cells	5100	1,9E-01	0,16	1,4E-01	0,40	1	Inhibited	http://www.genome.jp/dbget-bin/show_pathway?hsa05100+5295+7414

Table B.3.: Signaling Pathway Impact Analysis of MZ1774 YAP-knockdown cells (continued)

	KEGG pathway	ID	pNDE	pPERT	pG	pGFDR	pGFWER	Status	KEGG-link
38	Legionellosis	5134	1,3E-01	0,27	1,6E-01	0,41	1	Inhibited	http://www.genome.jp/dbget-bin/show_pathway?hsa05134+54205+3592
39	Leukocyte transendothelial migration	4670	3,5E-01	0,10	1,6E-01	0,41	1	Inhibited	http://www.genome.jp/dbget-bin/show_pathway?hsa04670+5295+7414
40	PPAR signaling pathway	3320	3,6E-02	1	1,6E-01	0,41	1	Inhibited	http://www.genome.jp/dbget-bin/show_pathway?hsa03320+2182+51703+51129
41	Gastric acid secretion	4971	3,6E-02	1	1,6E-01	0,41	1	Inhibited	http://www.genome.jp/dbget-bin/show_pathway?hsa04971+115+3710+3773
42	Viral myocarditis	5416	5,0E-01	0,08	1,6E-01	0,41	1	Inhibited	http://www.genome.jp/dbget-bin/show_pathway?hsa05416+54205
43	Herpes simplex infection	5168	1,2E-01	0,36	1,8E-01	0,45	1	Activated	http://www.genome.jp/dbget-bin/show_pathway?hsa05168+3592+5501+3456+54205
44	Dopaminergic synapse	4728	5,3E-02	0,86	1,9E-01	0,45	1	Activated	http://www.genome.jp/dbget-bin/show_pathway?hsa04728+3710+59345+9586+5501
45	Protein processing in endoplasmic reticulum	4141	1,4E-01	0,35	1,9E-01	0,45	1	Activated	http://www.genome.jp/dbget-bin/show_pathway?hsa04141+1649+821+6185+55432
46	Focal adhesion	4510	6,8E-02	0,72	2,0E-01	0,45	1	Activated	http://www.genome.jp/dbget-bin/show_pathway?hsa04510+4659+5501+7414+5295+7057
47	Hepatitis C	5160	4,3E-01	0,11	2,0E-01	0,45	1	Inhibited	http://www.genome.jp/dbget-bin/show_pathway?hsa05160+3456+5295
48	Vasopressin-regulated water reabsorption	4962	9,1E-02	0,56	2,0E-01	0,45	1	Inhibited	http://www.genome.jp/dbget-bin/show_pathway?hsa04962+115+9586
49	Oocyte meiosis	4114	1,3E-01	0,39	2,0E-01	0,45	1	Inhibited	http://www.genome.jp/dbget-bin/show_pathway?hsa04114+3710+115+5501
50	Pathogenic Escherichia coli infection	5130	4,8E-01	0,11	2,1E-01	0,45	1	Activated	http://www.genome.jp/dbget-bin/show_pathway?hsa05130+113457
51	Taste transduction	4742	6,2E-02	0,91	2,2E-01	0,45	1	Activated	http://www.genome.jp/dbget-bin/show_pathway?hsa04742+5136+3710
52	Lysosome	4142	5,7E-02	1	2,2E-01	0,45	1	Inhibited	http://www.genome.jp/dbget-bin/show_pathway?hsa04142+3423+427+1497+3482
53	Natural killer cell mediated cytotoxicity	4650	1,3E-01	0,46	2,3E-01	0,45	1	Inhibited	http://www.genome.jp/dbget-bin/show_pathway?hsa04650+3456+8795+5295
54	Jak-STAT signaling pathway	4630	6,3E-02	1	2,4E-01	0,45	1	Inhibited	http://www.genome.jp/dbget-bin/show_pathway?hsa04630+4609+5295+3592+3456
55	Amyotrophic lateral sclerosis (ALS)	5014	4,5E-01	0,14	2,4E-01	0,45	1	Inhibited	http://www.genome.jp/dbget-bin/show_pathway?hsa05014+54205
56	Chagas disease (American trypanosomiasis)	5142	9,5E-02	0,69	2,4E-01	0,45	1	Inhibited	http://www.genome.jp/dbget-bin/show_pathway?hsa05142+3592+3456+5295
57	SNARE interactions in vesicular transport	4130	6,9E-02	1	2,5E-01	0,45	1	Inhibited	http://www.genome.jp/dbget-bin/show_pathway?hsa04130+55014+8676
58	Carbohydrate digestion and absorption	4973	6,9E-02	1	2,5E-01	0,45	1	Inhibited	http://www.genome.jp/dbget-bin/show_pathway?hsa04973+280+5295

Table B.3.: Signaling Pathway Impact Analysis of MZ1774 YAP-knockdown cells (continued)

	KEGG pathway	ID	pNDE	pPERT	pG	pGFDR	pGFWER	Status	KEGG-link
59	Wnt signaling pathway	4310	5,0E-01	0,14	2,6E-01	0,45	1	Activated	http://www.genome.jp/dbget-bin/show_pathway?hsa04310+4609+1488
60	Gap junction	4540	7,2E-02	0,98	2,6E-01	0,45	1	Activated	http://www.genome.jp/dbget-bin/show_pathway?hsa04540+115+113457+3710
61	Pancreatic secretion	4972	7,2E-02	1	2,6E-01	0,45	1	Inhibited	http://www.genome.jp/dbget-bin/show_pathway?hsa04972+3710+280+115
62	Tight junction	4530	1,8E-01	0,40	2,6E-01	0,45	1	Activated	http://www.genome.jp/dbget-bin/show_pathway?hsa04530+2035+5590+51776
63	Alzheimer's disease	5010	5,5E-01	0,13	2,6E-01	0,45	1	Inhibited	http://www.genome.jp/dbget-bin/show_pathway?hsa05010+54205+3710
64	Axon guidance	4360	4,1E-01	0,19	2,7E-01	0,46	1	Inhibited	http://www.genome.jp/dbget-bin/show_pathway?hsa04360+285220+9901
65	Calcium signaling pathway	4020	9,0E-02	0,87	2,8E-01	0,46	1	Inhibited	http://www.genome.jp/dbget-bin/show_pathway?hsa04020+5136+3710+115+136
66	Melanogenesis	4916	3,0E-01	0,27	2,8E-01	0,46	1	Inhibited	http://www.genome.jp/dbget-bin/show_pathway?hsa04916+115+1906
67	Bladder cancer	5219	8,4E-02	1	2,9E-01	0,47	1	Inhibited	http://www.genome.jp/dbget-bin/show_pathway?hsa05219+7057+4609
68	Parkinson's disease	5012	7,5E-01	0,11	2,9E-01	0,47	1	Inhibited	http://www.genome.jp/dbget-bin/show_pathway?hsa05012+54205
69	Fc epsilon RI signaling pathway	4664	5,8E-01	0,16	3,1E-01	0,49	1	Inhibited	http://www.genome.jp/dbget-bin/show_pathway?hsa04664+5295
70	Osteoclast differentiation	4380	1,6E-01	0,61	3,2E-01	0,49	1	Activated	http://www.genome.jp/dbget-bin/show_pathway?hsa04380+3456+5295+3554
71	VEGF signaling pathway	4370	2,0E-01	0,54	3,5E-01	0,53	1	Inhibited	http://www.genome.jp/dbget-bin/show_pathway?hsa04370+9261+5295
72	Non-small cell lung cancer	5223	1,4E-01	0,79	3,6E-01	0,54	1	Inhibited	http://www.genome.jp/dbget-bin/show_pathway?hsa05223+5295+1021
73	Endometrial cancer	5213	1,3E-01	1	3,9E-01	0,57	1	Inhibited	http://www.genome.jp/dbget-bin/show_pathway?hsa05213+4609+5295
74	Vibrio cholerae infection	5110	1,3E-01	1	4,0E-01	0,58	1	Inhibited	http://www.genome.jp/dbget-bin/show_pathway?hsa05110+523+115
75	Pancreatic cancer	5212	2,0E-01	0,67	4,1E-01	0,59	1	Inhibited	http://www.genome.jp/dbget-bin/show_pathway?hsa05212+5295+1021
76	Acute myeloid leukemia	5221	1,5E-01	1	4,4E-01	0,62	1	Inhibited	http://www.genome.jp/dbget-bin/show_pathway?hsa05221+4609+5295
77	Fc gamma R-mediated phagocytosis	4666	3,0E-01	0,51	4,4E-01	0,62	1	Inhibited	http://www.genome.jp/dbget-bin/show_pathway?hsa04666+5295+85477
78	Bile secretion	4976	1,6E-01	1	4,5E-01	0,62	1	Inhibited	http://www.genome.jp/dbget-bin/show_pathway?hsa04976+115+6513
79	RIG-I-like receptor signaling pathway	4622	1,6E-01	1	4,5E-01	0,62	1	Inhibited	http://www.genome.jp/dbget-bin/show_pathway?hsa04622+3456+3592
80	Glioma	5214	1,7E-01	0,94	4,6E-01	0,62	1	Inhibited	http://www.genome.jp/dbget-bin/show_pathway?hsa05214+5295+1021

Table B.3.: Signaling Pathway Impact Analysis of MZ1774 YAP-knockdown cells (continued)

	KEGG pathway	ID	pNDE	pPERT	pG	pGFDR	pGFWER	Status	KEGG-link
81	Maturity onset diabetes of the young	4950	1,7E-01	1	4,7E-01	0,63	1	Inhibited	http://www.genome.jp/dbget-bin/show_pathway?hsa04950+6928
82	Salivary secretion	4970	2,2E-01	1	5,6E-01	0,73	1	Inhibited	http://www.genome.jp/dbget-bin/show_pathway?hsa04970+115+3710
83	Progesterone-mediated oocyte maturation	4914	2,5E-01	1	6,0E-01	0,78	1	Inhibited	http://www.genome.jp/dbget-bin/show_pathway?hsa04914+115+5295
84	ErbB signaling pathway	4012	2,7E-01	0,99	6,2E-01	0,78	1	Activated	http://www.genome.jp/dbget-bin/show_pathway?hsa04012+5295+4609
85	Prostate cancer	5215	2,9E-01	0,93	6,2E-01	0,78	1	Inhibited	http://www.genome.jp/dbget-bin/show_pathway?hsa05215+9586+5295
86	Allograft rejection	5330	2,7E-01	1	6,2E-01	0,78	1	Inhibited	http://www.genome.jp/dbget-bin/show_pathway?hsa05330+3592
87	RNA transport	3013	2,7E-01	1	6,3E-01	0,78	1	Inhibited	http://www.genome.jp/dbget-bin/show_pathway?hsa03013+11260+10605+26999
88	GnRH signaling pathway	4912	2,9E-01	1	6,5E-01	0,79	1	Inhibited	http://www.genome.jp/dbget-bin/show_pathway?hsa04912+115+3710
89	Thyroid cancer	5216	3,0E-01	1	6,6E-01	0,81	1	Inhibited	http://www.genome.jp/dbget-bin/show_pathway?hsa05216+4609
90	Type I diabetes mellitus	4940	3,2E-01	1	6,8E-01	0,81	1	Inhibited	http://www.genome.jp/dbget-bin/show_pathway?hsa04940+3592
91	African trypanosomiasis	5143	3,2E-01	1	6,8E-01	0,81	1	Inhibited	http://www.genome.jp/dbget-bin/show_pathway?hsa05143+3592
92	Neuroactive ligand-receptor interaction	4080	3,2E-01	1	6,9E-01	0,81	1	Inhibited	http://www.genome.jp/dbget-bin/show_pathway?hsa04080+2743+1903+136
93	Endocrine and other factor-regulated calcium reabsorption	4961	4,0E-01	1	7,7E-01	0,89	1	Inhibited	http://www.genome.jp/dbget-bin/show_pathway?hsa04961+115
94	Fanconi anemia pathway	3460	4,4E-01	1	8,0E-01	0,91	1	Inhibited	http://www.genome.jp/dbget-bin/show_pathway?hsa03460+2067
95	Cytosolic DNA-sensing pathway	4623	4,4E-01	1	8,0E-01	0,91	1	Inhibited	http://www.genome.jp/dbget-bin/show_pathway?hsa04623+3456
96	mTOR signaling pathway	4150	4,5E-01	1	8,1E-01	0,91	1	Inhibited	http://www.genome.jp/dbget-bin/show_pathway?hsa04150+5295
97	Antigen processing and presentation	4612	4,9E-01	1	8,4E-01	0,93	1	Inhibited	http://www.genome.jp/dbget-bin/show_pathway?hsa04612+821
98	Long-term depression	4730	5,0E-01	1	8,5E-01	0,93	1	Inhibited	http://www.genome.jp/dbget-bin/show_pathway?hsa04730+3710
99	Shigellosis	5131	5,2E-01	1	8,6E-01	0,93	1	Inhibited	http://www.genome.jp/dbget-bin/show_pathway?hsa05131+7414
100	Leishmaniasis	5140	5,3E-01	1	8,6E-01	0,93	1	Inhibited	http://www.genome.jp/dbget-bin/show_pathway?hsa05140+3592
101	Epithelial cell signaling in Helicobacter pylori infection	5120	5,5E-01	1	8,8E-01	0,93	1	Inhibited	http://www.genome.jp/dbget-bin/show_pathway?hsa05120+523
102	Pertussis	5133	5,7E-01	1	8,9E-01	0,93	1	Inhibited	http://www.genome.jp/dbget-bin/show_pathway?hsa05133+3592
103	RNA degradation	3018	5,8E-01	1	8,9E-01	0,93	1	Inhibited	http://www.genome.jp/dbget-bin/show_pathway?hsa03018+167227
104	B cell receptor signaling pathway	4662	6,0E-01	1	9,1E-01	0,93	1	Inhibited	http://www.genome.jp/dbget-bin/show_pathway?hsa04662+5295
105	Dilated cardiomyopathy	5414	6,1E-01	1	9,1E-01	0,93	1	Inhibited	http://www.genome.jp/dbget-bin/show_pathway?hsa05414+115

Table B.3.: Signaling Pathway Impact Analysis of MZ1774 YAP-knockdown cells (continued)

	KEGG pathway	ID	pNDE	pPERT	pG	pGFDR	pGFWER	Status	KEGG-link
106	Rheumatoid arthritis	5323	6,1E-01	1	9,1E-01	0,93	1	Inhibited	http://www.genome.jp/dbget-bin/show_pathway?hsa05323+523
107	Systemic lupus erythematosus	5322	6,5E-01	1	9,3E-01	0,94	1	Inhibited	http://www.genome.jp/dbget-bin/show_pathway?hsa05322+3014
108	T cell receptor signaling pathway	4660	6,7E-01	1	9,4E-01	0,94	1	Inhibited	http://www.genome.jp/dbget-bin/show_pathway?hsa04660+5295

Mein Dank gilt an dieser Stelle

- Herrn PD Dr. med. Georg Feldmann für die interessante Themenstellung und die kontinuierliche Unterstützung und Betreuung. Herzlich gedankt sei ihm auch für die Gelegenheiten, diese Arbeit immer wieder auf Konferenzen, auch in internationalem Rahmen, zu präsentieren und zu diskutieren.

- Herrn Prof. Dr. med. Peter Brossart für die Vermittlung an die AG Feldmann, seine Betreuung und fortwährende Unterstützung dieses Dissertationsprojekts.

- Herrn Prof. Gerd Bendas für die Übernahme der Betreuung dieses Projekts auf der Seite der naturwissenschaftlichen Fakultät und sein fortwährendes, wertvolles Feedback während der experimentellen Phase und der Erstellung der Dissertationsschrift.

- allen Kooperationspartnern, ohne die Teilprojekte dieser Arbeit nicht möglich gewesen wären. Besonders danken möchte ich Herrn Prof. Hui Zhou für unermüdliche Unterstützung in allen Fragen der Pankreashistologie sowie PD Dr. Lukas Heukamp und Prof. Reinhard Büttner für die großzügige Bereitstellung ihrer Zeit und Expertise und die Gelegenheit zur Nutzung der Ressourcen der Institute für Pathologie der Unikliniken Bonn und Köln. Herrn PD Dr. Moritz Kebschull danke ich herzlich für die bioinformatische Auswertung der Expressionsarray-Rohdaten.

- allen Kollegen der AG Feldmann für die angenehme und von alltäglicher Hilfsbereitschaft und Freundschaftlichkeit geprägte Arbeitsatmosphäre. Besonders danke ich Frau Dr. Savita Bisht für anregende Diskussionen und ermutigende Unterstützung.

- allen Kollegen der Medizinischen Klinik III, ob zu Anfang in der Wilhelmstraße 35 oder zuletzt in den neuen Labors im Biomedizinischen Zentrum, für eine fruchtbare Arbeitsatmosphäre und das alltägliche, freundschaftliche Miteinander über Arbeitsgruppen- und Institutsgrenzen hinweg.

- allen Kollegen aus der Apotheke im Alten Rathaus in Köln-Deutz und der Klini-Pharm GmbH in Frankfurt am Main für die Unterstützung während des letzten Jahres, als es galt den Spagat zwischen zwei Aufgaben zu meistern.

- meiner Familie und allen Freunden in Bonn und anderswo für ihre unermüdliche persönliche Unterstützung und Motivation. Besonders danken möchte ich Frau Dr. Julia Sagave für das Korrekturlesen der Arbeit und Herrn Dr. Philipp Kühl für seine wertvolle Hilfe in allen LaTeX-Fragen.

Bibliography

[1] C. Alarcón, A.-I. Zaromytidou, Q. Xi, S. Gao, J. Yu, S. Fujisawa, A. Barlas, A. N. Miller, K. Manova-Todorova, M. J. Macias, G. Sapkota, D. Pan, and J. Massagué. Nuclear cdks drive smad transcriptional activation and turnover in bmp and tgf-beta pathways. *Cell*, 139(4):757–769, Nov 2009. doi: 10.1016/j.cell.2009.09.035. URL http://dx.doi.org/10.1016/j.cell.2009.09.035.

[2] Y. Allory, S. Culine, and A. de la Taille. Kidney cancer pathology in the new context of targeted therapy. *Pathobiology*, 78(2):90–8, 2011. doi: 10.1159/000315543. URL http://www.karger.com/Article/FullText/315543.

[3] American Cancer Society (ACS). Cancer facts & figures 2013. Technical report, American Cancer Society, Atlanta, 2013.

[4] M. V. Apte, J. S. Wilson, A. Lugea, and S. J. Pandol. A starring role for stellate cells in the pancreatic cancer microenvironment. *Gastroenterology*, 144(6):1210–1219, Jun 2013. doi: 10.1053/j.gastro.2012.11.037. URL http://dx.doi.org/10.1053/j.gastro.2012.11.037.

[5] T. Asano, Y. Yao, J. Zhu, D. Li, J. L. Abbruzzese, and S. A. G. Reddy. The pi 3-kinase/akt signaling pathway is activated due to aberrant pten expression and targets transcription factors nf-kappab and c-myc in pancreatic cancer cells. *Oncogene*, 23(53):8571–8580, Nov 2004. doi: 10.1038/sj.onc.1207902. URL http://dx.doi.org/10.1038/sj.onc.1207902.

[6] Y. Bao, K. Nakagawa, Z. Yang, M. Ikeda, K. Withanage, M. Ishigami-Yuasa, Y. Okuno, S. Hata, H. Nishina, and Y. Hata. A cell-based assay to screen stimulators of the hippo pathway reveals the inhibitory effect of dobutamine on the yap-dependent gene transcription. *J Biochem*, 150(2):199–208, Aug 2011. doi: 10.1093/jb/mvr063. URL http://dx.doi.org/10.1093/jb/mvr063.

[7] J. A. Barltrop, T. C. Owen, A. H. Cory, and J. G. Cory. "5-(3-carboxymethoxyphenyl)-2-(4,5-dimethylthiazolyl)-3-(4-sulfophenyl)tetrazolium, inner salt (mts) and related analogs of 3-(4,5-dimethylthiazolyl)-2,5-diphenyltetrazolium bromide (mtt) reducing to purple water-soluble formazans as cell-viability indicators ". *Bioorganic & Medicinal Chemistry Letters*, 1(11):611 – 614, 1991.

[8] E. R. Barry and F. D. Camargo. The hippo superhighway: signaling crossroads converging on the hippo/yap pathway in stem cells and development. *Curr Opin Cell Biol*, 25(2):247–253, Apr 2013. doi: 10.1016/j.ceb.2012.12.006. URL http://dx.doi.org/10.1016/j.ceb.2012.12.006.

[9] E. R. Barry, T. Morikawa, B. L. Butler, K. Shrestha, R. de la Rosa, K. S. Yan, C. S. Fuchs, S. T. Magness, R. Smits, S. Ogino, C. J. Kuo, and F. D. Camargo. Restriction of intestinal stem cell expansion and the regenerative response by yap. *Nature*, 493(7430):106–110, Jan 2013. doi: 10.1038/nature11693. URL http://dx.doi.org/10.1038/nature11693.

[10] K. L. Bennewith, X. Huang, C. M. Ham, E. E. Graves, J. T. Erler, N. Kambham, J. Feazell, G. P. Yang, A. Koong, and A. J. Giaccia. The role of tumor cell-derived connective tissue growth factor (ctgf/ccn2) in pancreatic tumor growth. *Cancer Res*, 69(3):775–784, Feb 2009. doi: 10.1158/0008-5472.CAN-08-0987. URL http://dx.doi.org/10.1158/0008-5472.CAN-08-0987.

[11] A. V. Biankin, N. Waddell, K. S. Kassahn, M.-C. Gingras, L. B. Muthuswamy, A. L. Johns, D. K. Miller, P. J. Wilson, A.-M. Patch, J. Wu, D. K. Chang, M. J. Cowley, B. B. Gardiner, S. Song, I. Harliwong, S. Idrisoglu, C. Nourse, E. Nourbakhsh, S. Manning, S. Wani, M. Gongora, M. Pajic, C. J. Scarlett, A. J. Gill, A. V. Pinho, I. Rooman, M. Anderson, O. Holmes, C. Leonard, D. Taylor, S. Wood, Q. Xu, K. Nones, J. L. Fink, A. Christ, T. Bruxner, N. Cloonan, G. Kolle, F. Newell, M. Pinese, R. S. Mead, J. L. Humphris, W. Kaplan, M. D. Jones, E. K. Colvin, A. M. Nagrial, E. S. Humphrey, A. Chou, V. T. Chin, L. A. Chantrill, A. Mawson, J. S. Samra, J. G. Kench, J. A. Lovell, R. J. Daly, N. D. Merrett, C. Toon, K. Epari, N. Q. Nguyen, A. Barbour, N. Zeps, A. P. C. G. I. , N. Kakkar, F. Zhao, Y. Q. Wu, M. Wang, D. M. Muzny, W. E. Fisher, F. C. Brunicardi, S. E. Hodges, J. G. Reid, J. Drummond, K. Chang, Y. Han, L. R. Lewis, H. Dinh, C. J. Buhay, T. Beck, L. Timms, M. Sam, K. Begley, A. Brown, D. Pai, A. Panchal, N. Buchner, R. De

Borja, R. E. Denroche, C. K. Yung, S. Serra, N. Onetto, D. Mukhopadhyay, M.-S. Tsao, P. A. Shaw, G. M. Petersen, S. Gallinger, R. H. Hruban, A. Maitra, C. A. Iacobuzio-Donahue, R. D. Schulick, C. L. Wolfgang, R. A. Morgan, R. T. Lawlor, P. Capelli, V. Corbo, M. Scardoni, G. Tortora, M. A. Tempero, K. M. Mann, N. A. Jenkins, P. A. Perez-Mancera, D. J. Adams, D. A. Largaespada, L. F. A. Wessels, A. G. Rust, L. D. Stein, D. A. Tuveson, N. G. Copeland, E. A. Musgrove, A. Scarpa, J. R. Eshleman, T. J. Hudson, R. L. Sutherland, D. A. Wheeler, J. V. Pearson, J. D. McPherson, R. A. Gibbs, and S. M. Grimmond. Pancreatic cancer genomes reveal aberrations in axon guidance pathway genes. *Nature*, 491(7424):399–405, Nov 2012. doi: 10.1038/nature11547. URL http://dx.doi.org/10.1038/nature11547.

[12] S. S. Blair. Genetic mosaic techniques for studying drosophila development. *Development*, 130(21):5065–5072, Nov 2003. doi: 10.1242/dev.00774. URL http://dx.doi.org/10.1242/dev.00774.

[13] B. Blechacz and G. J. Gores. Cholangiocarcinoma: advances in pathogenesis, diagnosis, and treatment. *Hepatology*, 48(1):308–321, Jul 2008. doi: 10.1002/hep.22310. URL http://dx.doi.org/10.1002/hep.22310.

[14] W. Bossuyt, C.-L. Chen, Q. Chen, M. Sudol, H. McNeill, D. Pan, A. Kopp, and G. Halder. An evolutionary shift in the regulation of the hippo pathway between mice and flies. *Oncogene*, 33(10):1218–1228, Mar 2014. doi: 10.1038/onc.2013.82. URL http://dx.doi.org/10.1038/onc.2013.82.

[15] B. M. Bot, J. E. Eckel-Passow, S. N. LeGrand, T. Hilton, J. C. Cheville, T. Igel, and A. S. Parker. Expression of endothelin 2 and localized clear cell renal cell carcinoma. *Hum Pathol*, 43(6):843–9, 2012. doi: 10.1016/j.humpath.2011.07.011. URL http://www.sciencedirect.com/science/article/pii/S004681.

[16] S. Boyden. The chemotactic effect of mixtures of antibody and antigen on polymorphonuclear leucocytes. *J Exp Med*, 115:453–466, Mar 1962. URL http://jem.rupress.org/content/115/3/453.long.

[17] A. Brazma, P. Hingamp, J. Quackenbush, G. Sherlock, P. Spellman, C. Stoeckert, J. Aach, W. Ansorge, C. A. Ball, H. C. Causton, T. Gaasterland, P. Glenisson, F. C. Holstege, I. F. Kim, V. Markowitz, J. C. Matese, H. Parkinson, A. Robinson, U. Sarkans, S. Schulze-Kremer, J. Stewart, R. Taylor, J. Vilo, and M. Vingron. Minimum information about a microarray experiment (miame)-toward standards

for microarray data. *Nat Genet*, 29(4):365–371, Dec 2001. doi: 10.1038/ng1201-365. URL http://dx.doi.org/10.1038/ng1201-365.

[18] C. J. Bruns, M. T. Harbison, H. Kuniyasu, I. Eue, and I. J. Fidler. In vivo selection and characterization of metastatic variants from human pancreatic adenocarcinoma by using orthotopic implantation in nude mice. *Neoplasia*, 1(1):50–62, 1999. URL http://www.neoplasia.com/oldAbstract.php?msid=5.

[19] M. Buchholz, M. Braun, A. Heidenblut, H. A. Kestler, G. Klöppel, W. Schmiegel, S. A. Hahn, J. Lüttges, and T. M. Gress. Transcriptome analysis of microdissected pancreatic intraepithelial neoplastic lesions. *Oncogene*, 24(44):6626–6636, Oct 2005. doi: 10.1038/sj.onc.1208804. URL http://dx.doi.org/10.1038/sj.onc.1208804.

[20] P. Cairns. Renal cell carcinoma. *Cancer Biomark*, 9(1-6):461–473, 2010. doi: 10.3233/CBM-2011-0176. URL http://dx.doi.org/10.3233/CBM-2011-0176.

[21] F. Calvo, N. Ege, A. Grande-Garcia, S. Hooper, R. P. Jenkins, S. I. Chaudhry, K. Harrington, P. Williamson, E. Moeendarbary, G. Charras, and E. Sahai. Mechanotransduction and yap-dependent matrix remodelling is required for the generation and maintenance of cancer-associated fibroblasts. *Nat Cell Biol*, 15(6):637–646, Jun 2013. doi: 10.1038/ncb2756. URL http://dx.doi.org/10.1038/ncb2756.

[22] F. D. Camargo, S. Gokhale, J. B. Johnnidis, D. Fu, G. W. Bell, R. Jaenisch, and T. R. Brummelkamp. Yap1 increases organ size and expands undifferentiated progenitor cells. *Curr Biol*, 17(23):2054–2060, Dec 2007. doi: 10.1016/j.cub.2007.10.039. URL http://dx.doi.org/10.1016/j.cub.2007.10.039.

[23] A. Charrier and D. R. Brigstock. Regulation of pancreatic function by connective tissue growth factor (ctgf, ccn2). *Cytokine Growth Factor Rev*, 24(1):59–68, Feb 2013. doi: 10.1016/j.cytogfr.2012.07.001. URL http://dx.doi.org/10.1016/j.cytogfr.2012.07.001.

[24] D. Chen, Y. Sun, Y. Wei, P. Zhang, A. H. Rezaeian, J. Teruya-Feldstein, S. Gupta, H. Liang, H.-K. Lin, M.-C. Hung, and L. Ma. Lifr is a breast cancer metastasis suppressor upstream of the hippo-yap pathway and a prognostic marker. *Nat Med*, 18(10):1511–1517, Oct 2012. doi: 10.1038/nm.2940. URL http://dx.doi.org/10.1038/nm.2940.

[25] M. R. Chintalapudi, M. Markiewicz, N. Kose, V. Dammai, K. J. Champion, R. S. Hoda, M. Trojanowska, and T. Hsu. Cyr61/ccn1 and ctgf/ccn2 mediate the proangiogenic activity of vhl-mutant renal carcinoma cells. *Carcinogenesis*, 29(4):696–703, 2008. doi: 10.1093/carcin/bgn019. URL http://carcin.oxfordjournals.org/content/29/4/696.long.

[26] M. Cordenonsi, F. Zanconato, L. Azzolin, M. Forcato, A. Rosato, C. Frasson, M. Inui, M. Montagner, A. R. Parenti, A. Poletti, M. G. Daidone, S. Dupont, G. Basso, S. Bicciato, and S. Piccolo. The hippo transducer taz confers cancer stem cell-related traits on breast cancer cells. *Cell*, 147(4):759–72, 2011. doi: 10.1016/j.cell.2011.09.048. URL http://www.sciencedirect.com/science/article/pii/S0092867411012189.

[27] A. Cory, T. Owen, J. Barltrop, and J. G. Cory. Use of an aqueous soluble tetrazolium/formazan assay for cell growth assays in culture. *Cancer Commun*, 3(7):207 – 2012, 1991. URL http://www.ncbi.nlm.nih.gov/pubmed?Db=pubmed&Cmd=Retrieve&list_uids=1867954&dopt=abstractplus.

[28] C. J. Creighton, M. Morgan, P. H. Gunaratne, D. A. Wheeler, R. A. Gibbs, A. Gordon Robertson, A. Chu, R. Beroukhim, K. Cibulskis, S. Signoretti, F. Vandin Hsin-Ta Wu, B. J. Raphael, R. G. Verhaak, P. Tamboli, W. Torres-Garcia, R. Akbani, J. N. Weinstein, V. Reuter, J. J. Hsieh, A. Rose Brannon, A. Ari Hakimi, A. Jacobsen, G. Ciriello, B. Reva, C. J. Ricketts, W. Marston Linehan, J. M. Stuart, W. Kimryn Rathmell, H. Shen, P. W. Laird, D. Muzny, C. Davis, L. Xi, K. Chang, N. Kakkar, L. R. Trevino, S. Benton, J. G. Reid, D. Morton, H. Doddapaneni, Y. Han, L. Lewis, H. Dinh, C. Kovar, Y. Zhu, J. Santibanez, M. Wang, W. Hale, D. Kalra, G. Getz, M. S. Lawrence, C. Sougnez, S. L. Carter, A. Sivachenko, L. Lichtenstein, C. Stewart, D. Voet, S. Fisher, S. B. Gabriel, E. Lander, S. E. Schumacher, B. Tabak, G. Saksena, R. C. Onofrio, A. D. Cherniack, J. Gentry, K. Ardlie, M. Meyerson, H. J. Chun, A. J. Mungall, P. Sipahimalani, D. Stoll, A. Ally, M. Balasundaram, Y. S. Butterfield, R. Carlsen, C. Carter, E. Chuah, R. J. Coope, N. Dhalla, S. Gorski, R. Guin, C. Hirst, M. Hirst, R. A. Holt, C. Lebovitz, D. Lee, H. I. Li, M. Mayo, R. A. Moore, E. Pleasance, P. Plettner, J. E. Schein, A. Shafiei, J. R. Slobodan, A. Tam, N. Thiessen, R. J. Varhol, N. Wye, Y. Zhao, et al. Comprehensive molecular characterization of clear cell renal cell carcinoma. *Nature*, 2013.

[29] P. Cresswell. Assembly, transport, and function of mhc class ii molecules. *Annu Rev Immunol*, 12:259–293, 1994. doi: 10.1146/annurev.iy.12.040194.001355. URL http://dx.doi.org/10.1146/annurev.iy.12.040194.001355.

[30] Y. Cui, J. A. Brosnan, A. L. Blackford, S. Sur, R. H. Hruban, K. W. Kinzler, B. Vogelstein, A. Maitra, J. Diaz, L. A., C. A. Iacobuzio-Donahue, and J. R. Eshleman. Genetically defined subsets of human pancreatic cancer show unique in vitro chemosensitivity. *Clin Cancer Res*, 18(23):6519–30, 2012. doi: 10.1158/1078-0432.CCR-12-0827. URL http://clincancerres.aacrjournals.org/content/18/23/6519.long.

[31] G. L. Dalgliesh, K. Furge, C. Greenman, L. Chen, G. Bignell, A. Butler, H. Davies, S. Edkins, C. Hardy, C. Latimer, J. Teague, J. Andrews, S. Barthorpe, D. Beare, G. Buck, P. J. Campbell, S. Forbes, M. Jia, D. Jones, H. Knott, C. Y. Kok, K. W. Lau, C. Leroy, M. L. Lin, D. J. McBride, M. Maddison, S. Maguire, K. McLay, A. Menzies, T. Mironenko, L. Mulderrig, L. Mudie, S. O'Meara, E. Pleasance, A. Rajasingham, R. Shepherd, R. Smith, L. Stebbings, P. Stephens, G. Tang, P. S. Tarpey, K. Turrell, K. J. Dykema, S. K. Khoo, D. Petillo, B. Wondergem, J. Anema, R. J. Kahnoski, B. T. Teh, M. R. Stratton, and P. A. Futreal. Systematic sequencing of renal carcinoma reveals inactivation of histone modifying genes. *Nature*, 463(7279):360–3, 2010. doi: 10.1038/nature08672. URL http://www.nature.com/nature/journal/v463/n7279/full/n.

[32] N. Dey, F. Das, N. Ghosh-Choudhury, C. C. Mandal, D. J. Parekh, K. Block, B. S. Kasinath, H. E. Abboud, and G. G. Choudhury. microrna-21 governs torc1 activation in renal cancer cell proliferation and invasion. *PLoS One*, 7(6):e37366, 2012. doi: 10.1371/journal.pone.0037366. URL http://www.plosone.org/article/info%3Adoi%2F10.1371%2Fjournal.pone.0037366.

[33] C. H. Diep, K. M. Zucker, G. Hostetter, A. Watanabe, C. Hu, R. M. Munoz, D. D. Von Hoff, and H. Han. Down-regulation of yes associated protein 1 expression reduces cell proliferation and clonogenicity of pancreatic cancer cells. *PLoS One*, 7(3):e32783, 2012. doi: 10.1371/journal.pone.0032783. URL http://dx.doi.org/10.1371/journal.pone.0032783.

[34] J. Dong, G. Feldmann, J. Huang, S. Wu, N. Zhang, S. A. Comerford, M. F. Gayyed, R. A. Anders, A. Maitra, and D. Pan. Elucidation of a universal

size-control mechanism in drosophila and mammals. *Cell*, 130(6):1120–33, 2007. doi: 10.1016/j.cell.2007.07.019. URL http://www.ncbi.nlm.nih.gov/pubmed?Db=pubmed&Cmd=Retrieve&list_uids=17889654&dopt=abstractplus.

[35] X. Dong, M. Javle, K. R. Hess, R. Shroff, J. L. Abbruzzese, and D. Li. Insulin-like growth factor axis gene polymorphisms and clinical outcomes in pancreatic cancer. *Gastroenterology*, 139(2):464–73, 473.e1–3, Aug 2010. doi: 10.1053/j.gastro.2010.04.042. URL http://dx.doi.org/10.1053/j.gastro.2010.04.042.

[36] M. L. Douglas, M. M. Richardson, and D. L. Nicol. Endothelin axis expression is markedly different in the two main subtypes of renal cell carcinoma. *Cancer*, 100 (10):2118–24, 2004. doi: 10.1002/cncr.20222. URL http://onlinelibrary.wiley.com/doi/10.1002/cncr.20222/abstract.

[37] S. Dupont, L. Morsut, M. Aragona, E. Enzo, S. Giulitti, M. Cordenonsi, F. Zanconato, J. Le Digabel, M. Forcato, S. Bicciato, N. Elvassore, and S. Piccolo. Role of yap/taz in mechanotransduction. *Nature*, 474(7350):179–183, Jun 2011. doi: 10.1038/nature10137. URL http://dx.doi.org/10.1038/nature10137.

[38] B. F. El-Rayes, S. Ali, P. A. Philip, and F. H. Sarkar. Protein kinase c: a target for therapy in pancreatic cancer. *Pancreas*, 36(4):346–352, May 2008. doi: 10.1097/MPA.0b013e31815ceaf7. URL http://dx.doi.org/10.1097/MPA.0b013e31815ceaf7.

[39] E. E. Embuscado, D. Laheru, F. Ricci, K. J. Yun, S. de Boom Witzel, A. Seigel, K. Flickinger, M. Hidalgo, G. S. Bova, and C. A. Iacobuzio-Donahue. Immortalizing the complexity of cancer metastasis: genetic features of lethal metastatic pancreatic cancer obtained from rapid autopsy. *Cancer Biol Ther*, 4(5):548–54, 2005. doi: 10.4161/cbt.4.5.1663. URL http://www.tandfonline.com/doi/abs/10.4161/cbt.4.5.1663.

[40] M. Enjoji, M. Nakashima, M. Honda, H. Sakai, and H. Nawata. Hepatocytic phenotypes induced in sarcomatous cholangiocarcinoma cells treated with 5-azacytidine. *Hepatology*, 26(2):288–294, Aug 1997. doi: 10.1002/hep.510260206. URL http://dx.doi.org/10.1002/hep.510260206.

[41] M. Enjoji, H. Sakai, H. Nawata, K. Kajiyama, and M. Tsuneyoshi. Sarcomatous and adenocarcinoma cell lines from the same nodule of cholangiocarcinoma. *In Vitro*

Cell Dev Biol Anim, 33(9):681–683, Oct 1997. doi: 10.1007/s11626-997-0125-z. URL http://dx.doi.org/10.1007/s11626-997-0125-z.

[42] Y. Fan, Z. Liu, X. Fang, Z. Ge, N. Ge, Y. Jia, P. Sun, F. Lou, M. Bjorkholm, A. Gruber, P. Ekman, and D. Xu. Differential expression of full-length telomerase reverse transcriptase mrna and telomerase activity between normal and malignant renal tissues. *Clin Cancer Res*, 11(12):4331–7, 2005. doi: 10.1158/1078-0432.CCR-05-0099. URL http://clincancerres.aacrjournals.org/content/11/12/4331.long.

[43] G. Feldmann, V. Fendrich, K. McGovern, D. Bedja, S. Bisht, H. Alvarez, J. B. Koorstra, N. Habbe, C. Karikari, M. Mullendore, K. L. Gabrielson, R. Sharma, W. Matsui, and A. Maitra. An orally bioavailable small-molecule inhibitor of hedgehog signaling inhibits tumor initiation and metastasis in pancreatic cancer. *Mol Cancer Ther*, 7(9):2725–35, 2008. doi: 10.1158/1535-7163.MCT-08-0573. URL http://mct.aacrjournals.org/content/7/9/2725.long.

[44] G. Feldmann, S. Rauenzahn, and A. Maitra. In vitro models of pancreatic cancer for translational oncology research. *Expert Opin Drug Discov*, 4(4):429–443, Apr 2009. doi: 10.1517/17460440902821657. URL http://dx.doi.org/10.1517/17460440902821657.

[45] A. Fire, S. Xu, M. K. Montgomery, S. A. Kostas, S. E. Driver, and C. C. Mello. Potent and specific genetic interference by double-stranded rna in caenorhabditis elegans. *Nature*, 391(6669):806–811, Feb 1998. doi: 10.1038/35888. URL http://dx.doi.org/10.1038/35888.

[46] S. P. Flanagan. 'nude', a new hairless gene with pleiotropic effects in the mouse. *Genet Res*, 8(3):295–309, Dec 1966.

[47] R. C. Gentleman, V. J. Carey, D. M. Bates, B. Bolstad, M. Dettling, S. Dudoit, B. Ellis, L. Gautier, Y. Ge, J. Gentry, K. Hornik, T. Hothorn, W. Huber, S. Iacus, R. Irizarry, F. Leisch, C. Li, M. Maechler, A. J. Rossini, G. Sawitzki, C. Smith, G. Smyth, L. Tierney, J. Y. H. Yang, and J. Zhang. Bioconductor: open software development for computational biology and bioinformatics. *Genome Biol*, 5(10):R80, 2004. doi: 10.1186/gb-2004-5-10-r80. URL http://dx.doi.org/10.1186/gb-2004-5-10-r80.

[48] D. S. Gilmour and J. T. Lis. Detecting protein-dna interactions in vivo: distribution of rna polymerase on specific bacterial genes. *Proc Natl Acad Sci U S A*, 81(14): 4275–4279, Jul 1984. URL http://www.pnas.org/content/81/14/4275.long.

[49] A. H. Girgis, V. V. Iakovlev, B. Beheshti, J. Bayani, J. A. Squire, A. Bui, M. Mankaruos, Y. Youssef, B. Khalil, H. Khella, M. Pasic, and G. M. Yousef. Multi-level whole-genome analysis reveals candidate biomarkers in clear cell renal cell carcinoma. *Cancer Res*, 72(20):5273–84, 2012. doi: 10.1158/0008-5472.CAN-12-0656. URL http://cancerres.aacrjournals.org/content/72/20/5273.long.

[50] F. L. Graham, J. Smiley, W. C. Russell, and R. Nairn. Characteristics of a human cell line transformed by dna from human adenovirus type 5. *J Gen Virol*, 36(1): 59–74, Jul 1977.

[51] M. J. Grimshaw, T. Hagemann, A. Ayhan, C. E. Gillett, C. Binder, and F. R. Balkwill. A role for endothelin-2 and its receptors in breast tumor cell invasion. *Cancer Res*, 64(7):2461–8, 2004. URL http://cancerres.aacrjournals.org/content/64/7/2461.long.

[52] G. Groenewegen, M. Walraven, J. Vermaat, B. de Gast, E. Witteveen, R. Giles, J. Haanen, and E. Voest. Targeting the endothelin axis with atrasentan, in combination with ifn-alpha, in metastatic renal cell carcinoma. *Br J Cancer*, 106(2): 284–9, 2012. doi: 10.1038/bjc.2011.515. URL http://www.nature.com/bjc/journal/v106/n2/full/bjc2011515a.html.

[53] C. Haan and I. Behrmann. A cost effective non-commercial ecl-solution for western blot detections yielding strong signals and low background. *J Immunol Methods*, 318(1-2):11–19, Jan 2007. doi: 10.1016/j.jim.2006.07.027. URL http://dx.doi.org/10.1016/j.jim.2006.07.027.

[54] S. Habbig, M. P. Bartram, R. U. Muller, R. Schwarz, N. Andriopoulos, S. Chen, J. G. Sagmuller, M. Hoehne, V. Burst, M. C. Liebau, H. C. Reinhardt, T. Benzing, and B. Schermer. Nphp4, a cilia-associated protein, negatively regulates the hippo pathway. *J Cell Biol*, 193(4):633–42, 2011. doi: 10.1083/jcb.201009069. URL http://jcb.rupress.org/content/193/4/633.long.

[55] S. Habbig, M. P. Bartram, J. G. Sagmuller, A. Griessmann, M. Franke, R. U. Muller, R. Schwarz, M. Hoehne, C. Bergmann, C. Tessmer, H. C. Reinhardt,

V. Burst, T. Benzing, and B. Schermer. The ciliopathy disease protein nphp9 promotes nuclear delivery and activation of the oncogenic transcriptional regulator taz. *Hum Mol Genet*, 21(26):5528–38, 2012. doi: 10.1093/hmg/dds408. URL http://hmg.oxfordjournals.org/content/21/26/5528.long.

[56] T. Hagemann, C. Binder, L. Binder, T. Pukrop, L. Trumper, and M. J. Grimshaw. Expression of endothelins and their receptors promotes an invasive phenotype of breast tumor cells but is insufficient to induce invasion in benign cells. *DNA Cell Biol*, 24(11):766–76, 2005. doi: 10.1089/dna.2005.24.766. URL http://online.liebertpub.com/doi/abs/10.1089/dna.2005.24.766.

[57] G. Halder and S. B. Carroll. Binding of the vestigial co-factor switches the dna-target selectivity of the scalloped selector protein. *Development*, 128(17):3295–3305, Sep 2001. URL http://dev.biologists.org/content/128/17/3295.long.

[58] G. Halder and R. L. Johnson. Hippo signaling: growth control and beyond. *Development*, 138(1):9–22, Jan 2011. doi: 10.1242/dev.045500. URL http://dx.doi.org/10.1242/dev.045500.

[59] G. Halder, P. Polaczyk, M. E. Kraus, A. Hudson, J. Kim, A. Laughon, and S. Carroll. The vestigial and scalloped proteins act together to directly regulate wing-specific gene expression in drosophila. *Genes Dev*, 12(24):3900–3909, Dec 1998. URL http://genesdev.cshlp.org/content/12/24/3900.long.

[60] C. A. Hall, R. Wang, J. Miao, E. Oliva, X. Shen, T. Wheeler, S. G. Hilsenbeck, S. Orsulic, and S. Goode. Hippo pathway effector yap is an ovarian cancer oncogene. *Cancer Res*, 70(21):8517–8525, Nov 2010. doi: 10.1158/0008-5472.CAN-10-1242. URL http://dx.doi.org/10.1158/0008-5472.CAN-10-1242.

[61] G. Hamilton, K. S. Yee, S. Scrace, and E. O'Neill. Atm regulates a rassf1a-dependent dna damage response. *Curr Biol*, 19(23):2020–2025, Dec 2009. doi: 10.1016/j.cub.2009.10.040. URL http://dx.doi.org/10.1016/j.cub.2009.10.040.

[62] D. Hanahan and R. A. Weinberg. The hallmarks of cancer. *Cell*, 100(1):57–70, 2000. doi: 10.1016/j.cell.2011.02.013. URL http://www.sciencedirect.com/science/article/pii/S0092867411001279.

[63] K. F. Harvey, C. M. Pfleger, and I. K. Hariharan. The drosophila mst ortholog, hippo, restricts growth and cell proliferation and promotes apoptosis. *Cell*, 114

(4):457–467, Aug 2003. URL http://www.sciencedirect.com/science/article/pii/S0092867403005579.

[64] K. F. Harvey, X. Zhang, and D. M. Thomas. The hippo pathway and human cancer. *Nat Rev Cancer*, 13(4):246–57, Apr 2013. doi: 10.1038/nrc3458. URL http://www.nature.com/nrc/journal/v13/n4/full/nrc3458.html.

[65] A. F. Hezel, V. Deshpande, and A. X. Zhu. Genetics of biliary tract cancers and emerging targeted therapies. *J Clin Oncol*, 28(21):3531–3540, Jul 2010. doi: 10.1200/JCO.2009.27.4787. URL http://dx.doi.org/10.1200/JCO.2009.27.4787.

[66] T. Hirakawa, M. Yashiro, A. Murata, K. Hirata, K. Kimura, R. Amano, N. Yamada, B. Nakata, and K. Hirakawa. Igf-1 receptor and igf binding protein-3 might predict prognosis of patients with resectable pancreatic cancer. *BMC Cancer*, 13:392, 2013. doi: 10.1186/1471-2407-13-392. URL http://dx.doi.org/10.1186/1471-2407-13-392.

[67] A. Holczbauer, V. M. Factor, J. B. Andersen, J. U. Marquardt, D. E. Kleiner, C. Raggi, M. Kitade, D. Seo, H. Akita, M. E. Durkin, and S. S. Thorgeirsson. Modeling pathogenesis of primary liver cancer in lineage-specific mouse cell types. *Gastroenterology*, 145(1):221–231, Jul 2013. doi: 10.1053/j.gastro.2013.03.013. URL http://dx.doi.org/10.1053/j.gastro.2013.03.013.

[68] R. W. Holley. Control of growth of mammalian cells in cell culture. *Nature*, 258 (5535):487–490, Dec 1975.

[69] J.-H. Hong and M. B. Yaffe. Taz: a beta-catenin-like molecule that regulates mesenchymal stem cell differentiation. *Cell Cycle*, 5(2):176–179, Jan 2006. URL http://www.landesbioscience.com/journals/cc/article/2362/.

[70] J. Huang, S. Wu, J. Barrera, K. Matthews, and D. Pan. The hippo signaling pathway coordinately regulates cell proliferation and apoptosis by inactivating yorkie, the drosophila homolog of yap. *Cell*, 122(3):421–434, Aug 2005. doi: 10.1016/j.cell.2005.06.007. URL http://dx.doi.org/10.1016/j.cell.2005.06.007.

[71] P. O. Humbert, N. A. Grzeschik, A. M. Brumby, R. Galea, I. Elsum, and H. E. Richardson. Control of tumourigenesis by the scribble/dlg/lgl polarity module. *Oncogene*, 27(55):6888–6907, Nov 2008. doi: 10.1038/onc.2008.341. URL http://dx.doi.org/10.1038/onc.2008.341.

[72] K. D. Irvine. Integration of intercellular signaling through the hippo pathway. *Semin Cell Dev Biol*, 23(7):812–817, Sep 2012. doi: 10.1016/j.semcdb.2012.04.006. URL http://dx.doi.org/10.1016/j.semcdb.2012.04.006.

[73] M. Jaiswal, N. F. LaRusso, L. J. Burgart, and G. J. Gores. Inflammatory cytokines induce dna damage and inhibit dna repair in cholangiocarcinoma cells by a nitric oxide-dependent mechanism. *Cancer Res*, 60(1):184–190, Jan 2000.

[74] S. K. Johnson and R. S. Haun. Insulin-like growth factor binding protein-5 influences pancreatic cancer cell growth. *World J Gastroenterol*, 15(27):3355–3366, Jul 2009. URL http://www.wjgnet.com/1007-9327/full/v15/i27/3355.htm.

[75] S. Jones, X. Zhang, D. W. Parsons, J. C.-H. Lin, R. J. Leary, P. Angenendt, P. Mankoo, H. Carter, H. Kamiyama, A. Jimeno, S.-M. Hong, B. Fu, M.-T. Lin, E. S. Calhoun, M. Kamiyama, K. Walter, T. Nikolskaya, Y. Nikolsky, J. Hartigan, D. R. Smith, M. Hidalgo, S. D. Leach, A. P. Klein, E. M. Jaffee, M. Goggins, A. Maitra, C. Iacobuzio-Donahue, J. R. Eshleman, S. E. Kern, R. H. Hruban, R. Karchin, N. Papadopoulos, G. Parmigiani, B. Vogelstein, V. E. Velculescu, and K. W. Kinzler. Core signaling pathways in human pancreatic cancers revealed by global genomic analyses. *Science*, 321(5897):1801–1806, Sep 2008. doi: 10.1126/science.1164368. URL http://dx.doi.org/10.1126/science.1164368.

[76] M. Kango-Singh, R. Nolo, C. Tao, P. Verstreken, P. R. Hiesinger, H. J. Bellen, and G. Halder. Shar-pei mediates cell proliferation arrest during imaginal disc growth in drosophila. *Development*, 129(24):5719–5730, Dec 2002. URL http://dev.biologists.org/content/129/24/5719.long.

[77] A. Katagiri, R. Watanabe, and Y. Tomita. E-cadherin expression in renal cell cancer and its significance in metastasis and survival. *Br J Cancer*, 71(2): 376–9, 1995. URL http://www.ncbi.nlm.nih.gov/pubmed?Db=pubmed&Cmd=Retrieve&list_uids=7841055&dopt=abstractplus.

[78] S. A. Khan, B. R. Davidson, R. D. Goldin, N. Heaton, J. Karani, S. P. Pereira, W. M. C. Rosenberg, P. Tait, S. D. Taylor-Robinson, A. V. Thillainayagam, H. C. Thomas, H. Wasan, and B. S. o. G. . Guidelines for the diagnosis and treatment of cholangiocarcinoma: an update. *Gut*, 61(12):1657–1669, Dec 2012. doi: 10.1136/gutjnl-2011-301748. URL http://gut.bmj.com/content/61/12/1657.long.

[79] P. Khatri, M. Sirota, and A. J. Butte. Ten years of pathway analysis: current approaches and outstanding challenges. *PLoS Comput Biol*, 8(2):e1002375, 2012. doi: 10.1371/journal.pcbi.1002375. URL http://dx.doi.org/10.1371/journal.pcbi.1002375.

[80] A. K. Khimji and D. C. Rockey. Endothelin–biology and disease. *Cell Signal*, 22(11): 1615–25, 2010. doi: 10.1016/j.cellsig.2010.05.002. URL http://www.sciencedirect.com/science/article/pii/S0898656810001208.

[81] A. Khokhlatchev, S. Rabizadeh, R. Xavier, M. Nedwidek, T. Chen, X.-f. Zhang, B. Seed, and J. Avruch. Identification of a novel ras-regulated proapoptotic pathway. *Curr Biol*, 12(4):253–265, Feb 2002. URL http://www.ncbi.nlm.nih.gov/pubmed?Db=pubmed&Cmd=Retrieve&list_uids=11864565&dopt=abstractplus.

[82] G. Kloeppel, V. Adsay, B. Konukiewitz, J. Kleeff, A. M. Schlitter, and I. Esposito. Precancerous lesions of the biliary tree. *Best Pract Res Clin Gastroenterol*, 27(2): 285–297, Apr 2013. doi: 10.1016/j.bpg.2013.04.002. URL http://dx.doi.org/10.1016/j.bpg.2013.04.002.

[83] M. Kobari, H. Hisano, S. Matsuno, T. Sato, M. Kan, and T. Tachibana. Establishment of six human pancreatic cancer cell lines and their sensitivities to anti-tumor drugs. *Tohoku J Exp Med*, 150(3):231–48, 1986. URL https://www.jstage.jst.go.jp/article/tjem1920/150/3/150_3_231/_article.

[84] D. E. Kohan, J. G. Cleland, L. J. Rubin, D. Theodorescu, and M. Barton. Clinical trials with endothelin receptor antagonists: what went wrong and where can we improve? *Life Sci*, 91(13-14):528–39, 2012. doi: 10.1016/j.lfs.2012.07.034. URL http://www.sciencedirect.com/science/article/pii/S0024320512004122.

[85] N. Koide, T. Yamada, R. Shibata, T. Mori, M. Fukuma, K. Yamazaki, K. Aiura, M. Shimazu, S. Hirohashi, Y. Nimura, and M. Sakamoto. Establishment of perineural invasion models and analysis of gene expression revealed an invariant chain (cd74) as a possible molecule involved in perineural invasion in pancreatic cancer. *Clin Cancer Res*, 12(8):2419–2426, Apr 2006. doi: 10.1158/1078-0432.CCR-05-1852. URL http://dx.doi.org/10.1158/1078-0432.CCR-05-1852.

[86] J. Kononen, L. Bubendorf, A. Kallionimeni, M. Bärlund, P. Schraml, S. Leighton, J. Torhorst, M. J. Mihatsch, G. Sauter, and O.-P. Kallionimeni. Tissue microarrays

for high-throughput molecular profiling of tumor specimens. *Nature medicine*, 4(7): 844–847, 1998. URL http://www.nature.com/nm/journal/v4/n7/abs/nm0798-844.html.

[87] T. Koressaar and M. Remm. Enhancements and modifications of primer design program primer3. *Bioinformatics*, 23(10):1289–1291, May 2007. doi: 10.1093/bioinformatics/btm091. URL http://dx.doi.org/10.1093/bioinformatics/btm091.

[88] S. Koyama, T. Yoshioka, A. Mizushima, I. Kawakita, S. Yamagata, H. Fukutomi, T. Sakita, I. Kondo, and M. Kikuchi. Establishment of a cell line (g-415) from a human gallbladder carcinoma. *Gann*, 71(4):574–575, Aug 1980. URL http://www.ncbi.nlm.nih.gov/pubmed?Db=pubmed&Cmd=Retrieve&list_uids=7429092&dopt=abstractplus.

[89] L. Kozma, I. Kiss, A. Nagy, S. Szakall, and I. Ember. Investigation of c-myc and k-ras amplification in renal clear cell adenocarcinoma. *Cancer Lett*, 111(1-2):127–31, 1997. URL http://www.sciencedirect.com/science/article/pii/S0304383596045272.

[90] N. Kramer, A. Walzl, C. Unger, M. Rosner, G. Krupitza, M. Hengstschläger, and H. Dolznig. In vitro cell migration and invasion assays. *Mutat Res*, 752(1):10–24, 2013. doi: 10.1016/j.mrrev.2012.08.001. URL http://dx.doi.org/10.1016/j.mrrev.2012.08.001.

[91] J.-L. Ku, K.-A. Yoon, I.-J. Kim, W.-H. Kim, J.-Y. Jang, K.-S. Suh, S.-W. Kim, Y.-H. Park, J.-H. Hwang, Y.-B. Yoon, and J.-G. Park. Establishment and characterisation of six human biliary tract cancer cell lines. *Br J Cancer*, 87(2):187–193, Jul 2002. doi: 10.1038/sj.bjc.6600440. URL http://dx.doi.org/10.1038/sj.bjc.6600440.

[92] V. Kumar, A. K. Abbas, N. Fausto, and R. N. Mitchell. *Robbins basic pathology*. Elsevier Health Sciences, 2007.

[93] J. M. Lamar, P. Stern, H. Liu, J. W. Schindler, Z. G. Jiang, and R. O. Hynes. The hippo pathway target, yap, promotes metastasis through its tead-interaction domain. *Proc Natl Acad Sci U S A*, 109(37):E2441–50, 2012. doi: 10.1073/pnas.1212021109. URL http://www.pnas.org/content/109/37/E2441.long.

[94] K. M. Lee, H. Yasuda, M. A. Hollingsworth, and M. M. Ouellette. Notch 2-positive progenitors with the intrinsic ability to give rise to pancreatic ductal cells. *Lab*

Invest, 85(8):1003–12, 2005. doi: 10.1038/labinvest.3700298. URL http://www.nature.com/labinvest/journal/v85/n8/full/3700298a.html.

[95] K.-P. Lee, J.-H. Lee, T.-S. Kim, T.-H. Kim, H.-D. Park, J.-S. Byun, M.-C. Kim, W.-I. Jeong, D. F. Calvisi, J.-M. Kim, and D.-S. Lim. The hippo-salvador pathway restrains hepatic oval cell proliferation, liver size, and liver tumorigenesis. *Proc Natl Acad Sci U S A*, 107(18):8248–8253, May 2010. doi: 10.1073/pnas.0912203107. URL http://dx.doi.org/10.1073/pnas.0912203107.

[96] C. Li, H. Ma, Y. Wang, Z. Cao, R. Graves-Deal, A. E. Powell, A. Starchenko, G. D. Ayers, M. K. Washington, V. Kamath, K. Desai, M. J. Gerdes, L. Solnica-Krezel, and R. J. Coffey. Excess plac8 promotes an unconventional erk2-dependent emt in colon cancer. *J Clin Invest*, 124(5):2172–2187, May 2014. doi: 10.1172/JCI71103. URL http://dx.doi.org/10.1172/JCI71103.

[97] G. Li, K. Passebosc-Faure, A. Gentil-Perret, C. Lambert, C. Genin, and J. Tostain. Cadherin-6 gene expression in conventional renal cell carcinoma: a useful marker to detect circulating tumor cells. *Anticancer Res*, 25(1A):377–81, 2005. URL http://ar.iiarjournals.org/content/25/1A/377.long.

[98] H. Li, H. Shimura, Y. Aoki, K. Date, K. Matsumoto, T. Nakamura, and M. Tanaka. Hepatocyte growth factor stimulates the invasion of gallbladder carcinoma cell lines in vitro. *Clin Exp Metastasis*, 16(1):74–82, Jan 1998. URL http://www.ncbi.nlm.nih.gov/pubmed?Db=pubmed&Cmd=.

[99] I. Lian, J. Kim, H. Okazawa, J. Zhao, B. Zhao, J. Yu, A. Chinnaiyan, M. A. Israel, L. S. B. Goldstein, R. Abujarour, S. Ding, and K.-L. Guan. The role of yap transcription coactivator in regulating stem cell self-renewal and differentiation. *Genes Dev*, 24(11):1106–1118, Jun 2010. doi: 10.1101/gad.1903310. URL http://dx.doi.org/10.1101/gad.1903310.

[100] L. Ling, J. J. Maguire, and A. P. Davenport. Endothelin-2, the forgotten isoform: emerging role in the cardiovascular system, ovarian development, immunology and cancer. *Br J Pharmacol*, 168(2):283–95, 2013. doi: 10.1111/j.1476-5381.2011.01786.x. URL http://onlinelibrary.wiley.com/doi/10.1111/j.1476-5381.2011.01786.x/abstract.

[101] K. J. Livak and T. D. Schmittgen. Analysis of relative gene expression data using real-time quantitative pcr and the 2(-delta delta c(t)) method. *Methods*, 25(4): 402–8, 2001.

[102] D. Mahadevan and D. D. Von Hoff. Tumor-stroma interactions in pancreatic ductal adenocarcinoma. *Mol Cancer Ther*, 6(4):1186–1197, Apr 2007. doi: 10.1158/1535-7163.MCT-06-0686. URL http://dx.doi.org/10.1158/1535-7163.MCT-06-0686.

[103] A. Maitra, N. V. Adsay, P. Argani, C. Iacobuzio-Donahue, A. De Marzo, J. L. Cameron, C. J. Yeo, and R. H. Hruban. Multicomponent analysis of the pancreatic adenocarcinoma progression model using a pancreatic intraepithelial neoplasia tissue microarray. *Mod Pathol*, 16(9):902–912, Sep 2003. doi: 10.1097/01.MP.0000086072.56290.FB. URL http://dx.doi.org/10.1097/01.MP.0000086072.56290.FB.

[104] A. Maitra, S. E. Kern, and R. H. Hruban. Molecular pathogenesis of pancreatic cancer. *Best Pract Res Clin Gastroenterol*, 20(2):211–226, Apr 2006. doi: 10.1016/j.bpg.2005.10.002. URL http://dx.doi.org/10.1016/j.bpg.2005.10.002.

[105] K. Matsuura, C. Nakada, M. Mashio, T. Narimatsu, T. Yoshimoto, M. Tanigawa, Y. Tsukamoto, N. Hijiya, I. Takeuchi, T. Nomura, F. Sato, H. Mimata, M. Seto, and M. Moriyama. Downregulation of sav1 plays a role in pathogenesis of high-grade clear cell renal cell carcinoma. *BMC Cancer*, 11:523, 2011. doi: 10.1186/1471-2407-11-523. URL http://www.biomedcentral.com/1471-2407/11/523.

[106] A. I. McClatchey, I. Saotome, K. Mercer, D. Crowley, J. F. Gusella, R. T. Bronson, and T. Jacks. Mice heterozygous for a mutation at the nf2 tumor suppressor locus develop a range of highly metastatic tumors. *Genes Dev*, 12(8):1121–1133, Apr 1998. URL http://genesdev.cshlp.org/content/12/8/1121.long.

[107] J. Meza-Junco, A. J. Montano-Loza, M. Ma, W. Wong, M. B. Sawyer, and V. G. Bain. Cholangiocarcinoma: has there been any progress? *Can J Gastroenterol*, 24(1):52–57, Jan 2010. URL http://www.ncbi.nlm.nih.gov/pubmed?Db=pubmed&Cmd=Retrieve&list_uids=20186357&dopt=abstractplus.

[108] Millipore Corporation. *Magna ChIP A/ EZ-Magna ChIP A Instruction Manual*. Millipore Corporation, 2007.

[109] M. Miyagiwa, T. Ichida, T. Tokiwa, J. Sato, and H. Sasaki. A new human cholangiocellular carcinoma cell line (hucc-t1) producing carbohydrate antigen 19/9 in serum-free medium. *In Vitro Cell Dev Biol*, 25(6):503–510, Jun 1989. URL http://www.ncbi.nlm.nih.gov/pubmed?Db=pubmed&Cmd=Retrieve&list_uids=2544546&dopt=abstractplus.

[110] R. T. Morgan, L. K. Woods, G. E. Moore, L. A. Quinn, L. McGavran, and S. G. Gordon. Human cell line (colo 357) of metastatic pancreatic adenocarcinoma. *Int J Cancer*, 25(5):591–598, May 1980.

[111] M. Mori, R. Triboulet, M. Mohseni, K. Schlegelmilch, K. Shrestha, F. D. Camargo, and R. I. Gregory. Hippo signaling regulates microprocessor and links cell-density-dependent mirna biogenesis to cancer. *Cell*, 156(5):893–906, Feb 2014. doi: 10.1016/j.cell.2013.12.043. URL http://dx.doi.org/10.1016/j.cell.2013.12.043.

[112] Z. S. Morris and A. I. McClatchey. Aberrant epithelial morphology and persistent epidermal growth factor receptor signaling in a mouse model of renal carcinoma. *Proc Natl Acad Sci U S A*, 106(24):9767–72, 2009. doi: 10.1073/pnas.0902031106. URL http://www.pnas.org/content/106/24/9767.long.

[113] S. J. Moschos and C. S. Mantzoros. The role of the igf system in cancer: from basic to clinical studies and clinical applications. *Oncology*, 63(4):317–332, 2002. doi: 66230. URL http://dx.doi.org/66230.

[114] C. A. Moskaluk, R. H. Hruban, and S. E. Kern. p16 and k-ras gene mutations in the intraductal precursors of human pancreatic adenocarcinoma. *Cancer Res*, 57 (11):2140–2143, Jun 1997. URL http://cancerres.aacrjournals.org/content/57/11/2140.long.

[115] L. Naldini, U. Blömer, F. H. Gage, D. Trono, and I. M. Verma. Efficient transfer, integration, and sustained long-term expression of the transgene in adult rat brains injected with a lentiviral vector. *Proc Natl Acad Sci U S A*, 93(21):11382–11388, Oct 1996. doi: 10.1126/science.272.5259.263. URL http://www.sciencemag.org/content/272/5259/263.long.

[116] A. Neesse, K. K. Frese, T. E. Bapiro, T. Nakagawa, M. D. Sternlicht, T. W. Seeley, C. Pilarsky, D. I. Jodrell, S. M. Spong, and D. A. Tuveson. Ctgf antagonism with mab fg-3019 enhances chemotherapy response without increasing drug delivery in

murine ductal pancreas cancer. *Proc Natl Acad Sci U S A*, 110(30):12325–12330, Jul 2013. doi: 10.1073/pnas.1300415110. URL http://dx.doi.org/10.1073/pnas.1300415110.

[117] J. Nelson, A. Bagnato, B. Battistini, and P. Nisen. The endothelin axis: emerging role in cancer. *Nat Rev Cancer*, 3(2):110–6, 2003. doi: 10.1038/nrc990. URL http://www.nature.com/nrc/journal/v3/n2/full/nrc990.html.

[118] H. B. Nguyen, J. T. Babcock, C. D. Wells, and L. A. Quilliam. Lkb1 tumor suppressor regulates amp kinase/mtor-independent cell growth and proliferation via the phosphorylation of yap. *Oncogene*, 32(35):4100–4109, Aug 2013. doi: 10.1038/onc.2012.431. URL http://dx.doi.org/10.1038/onc.2012.431.

[119] M. R. O'Dell, J. L. Huang, C. L. Whitney-Miller, V. Deshpande, P. Rothberg, V. Grose, R. M. Rossi, A. X. Zhu, H. Land, N. Bardeesy, and A. F. Hezel. Kras(g12d) and p53 mutation cause primary intrahepatic cholangiocarcinoma. *Cancer Res*, 72 (6):1557–1567, Mar 2012. doi: 10.1158/0008-5472.CAN-11-3596. URL http://dx.doi.org/10.1158/0008-5472.CAN-11-3596.

[120] S. Ohkubo, K. Ogi, M. Hosoya, H. Matsumoto, N. Suzuki, C. Kimura, H. Ondo, and M. Fujino. Specific expression of human endothelin-2 (et-2) gene in a renal adenocarcinoma cell line. molecular cloning of cdna encoding the precursor of et-2 and its characterization. *FEBS Lett*, 274(1-2): 136–40, 1990. URL http://www.ncbi.nlm.nih.gov/pubmed?Db=pubmed&Cmd=Retrieve&list_uids=1701397&dopt=abstractplus.

[121] V. Orlando, H. Strutt, and R. Paro. Analysis of chromatin structure by in vivo formaldehyde cross-linking. *Methods*, 11(2):205–214, Feb 1997. doi: 10.1006/meth.1996.0407. URL http://dx.doi.org/10.1006/meth.1996.0407.

[122] M. Overholtzer, J. Zhang, G. A. Smolen, B. Muir, W. Li, D. C. Sgroi, C. X. Deng, J. S. Brugge, and D. A. Haber. Transforming properties of yap, a candidate oncogene on the chromosome 11q22 amplicon. *Proc Natl Acad Sci U S A*, 103(33):12405–10, 2006. doi: 10.1073/pnas.0605579103. URL http://www.pnas.org/content/103/33/12405.long.

[123] B. S. Parekh and T. Maniatis. Virus infection leads to localized hyperacetylation of histones h3 and h4 at the ifn-beta promoter. *Mol Cell*, 3(1):125–129, Jan 1999. URL http://www.sciencedirect.com/science/article/pii/S1097276500801811.

[124] N. Parker, M. J. Turk, E. Westrick, J. D. Lewis, P. S. Low, and C. P. Leamon. Folate receptor expression in carcinomas and normal tissues determined by a quantitative radioligand binding assay. *Anal Biochem*, 338(2):284–293, Mar 2005. doi: 10.1016/j.ab.2004.12.026. URL http://dx.doi.org/10.1016/j.ab.2004.12.026.

[125] S. Pena-Llopis, A. Christie, X.-J. Xie, and J. Brugarolas. Cooperation and antagonism among cancer genes: the renal cancer paradigm. *Cancer Res*, 73(14):4173–4179, Jul 2013. doi: 10.1158/0008-5472.CAN-13-0360. URL http://dx.doi.org/10.1158/0008-5472.CAN-13-0360.

[126] B. Perbal. Nov (nephroblastoma overexpressed) and the ccn family of genes: structural and functional issues. *Mol Pathol*, 54(2):57–79, 2001. URL http://mp.bmj.com/content/54/2/57.long.

[127] B. R. Pflug, H. Zheng, M. S. Udan, J. M. D'Antonio, F. F. Marshall, J. D. Brooks, and J. B. Nelson. Endothelin-1 promotes cell survival in renal cell carcinoma through the et(a) receptor. *Cancer Lett*, 246(1-2):139–48, 2007. doi: 10.1016/j.canlet.2006.02.007. URL http://www.sciencedirect.com/science/article/pii/S0304383506001133.

[128] A. V. Pobbati and W. Hong. Emerging roles of tead transcription factors and its coactivators in cancers. *Cancer Biol Ther*, 14(5):390–398, May 2013. doi: 10.4161/cbt.23788. URL http://dx.doi.org/10.4161/cbt.23788.

[129] A. V. Pobbati, S. W. Chan, I. Lee, H. Song, and W. Hong. Structural and functional similarity between the vgll1-tead and the yap-tead complexes. *Structure*, 20(7):1135–1140, Jul 2012. doi: 10.1016/j.str.2012.04.004. URL http://dx.doi.org/10.1016/j.str.2012.04.004.

[130] K. L. Pogue-Geile, R. Chen, M. P. Bronner, T. Crnogorac-Jurcevic, K. W. Moyes, S. Dowen, C. A. Otey, D. A. Crispin, R. D. George, D. C. Whitcomb, and T. A. Brentnall. Palladin mutation causes familial pancreatic cancer and suggests a new cancer mechanism. *PLoS Med*, 3(12):e516, Dec 2006. doi: 10.1371/journal.pmed.0030516. URL http://dx.doi.org/10.1371/journal.pmed.0030516.

[131] B. I. Rini, S. C. Campbell, and B. Escudier. Renal cell carcinoma. *Lancet*, 373(9669):1119–32, 2009. doi: 10.1016/S0140-6736(09)60229-4. URL http://www.sciencedirect.com/science/article/pii/S0140673609602294.

[132] S. Rizvi and G. J. Gores. Pathogenesis, diagnosis, and management of cholangiocarcinoma. *Gastroenterology*, 145(6):1215–1229, Dec 2013. doi: 10.1053/j.gastro.2013.10.013. URL http://dx.doi.org/10.1053/j.gastro.2013.10.013.

[133] B. A. Ruggeri, L. Huang, M. Wood, J. Q. Cheng, and J. R. Testa. Amplification and overexpression of the akt2 oncogene in a subset of human pancreatic ductal adenocarcinomas. *Mol Carcinog*, 21(2):81–86, Feb 1998. doi: 10.1002/(SICI)1098-2744(199802)21:2<81::AID-MC1>3.0.CO;2-R. URL http://onlinelibrary.wiley.com/doi/10.1002/(SICI)1098-2744(199802)21:2%3C81::AID-MC1%3E3.0.CO;2-R/abstract;jsessionid=6F98819B58B976920AD4202971087D0A.f03t01.

[134] S. J. Rulyak and T. A. Brentnall. Inherited pancreatic cancer: improvements in our understanding of genetics and screening. *Int J Biochem Cell Biol*, 36(8):1386–1392, Aug 2004. doi: 10.1016/j.biocel.2004.02.010. URL http://dx.doi.org/10.1016/j.biocel.2004.02.010.

[135] N. Said, S. Smith, M. Sanchez-Carbayo, and D. Theodorescu. Tumor endothelin-1 enhances metastatic colonization of the lung in mouse xenograft models of bladder cancer. *J Clin Invest*, 121(1):132–47, 2011. doi: 10.1172/JCI42912. URL http://www.jci.org/articles/view/42912.

[136] S. Saijyo, T. Kudo, M. Suzuki, Y. Katayose, M. Shinoda, T. Muto, K. Fukuhara, T. Suzuki, and S. Matsuno. Establishment of a new extrahepatic bile duct carcinoma cell line, tfk-1. *Tohoku J Exp Med*, 177(1):61–71, Sep 1995. URL https://www.jstage.jst.go.jp/article/tjem1920/177/1/177_1_61/_article.

[137] K. Schlegelmilch, M. Mohseni, O. Kirak, J. Pruszak, J. R. Rodriguez, D. Zhou, B. T. Kreger, V. Vasioukhin, J. Avruch, T. R. Brummelkamp, and F. D. Camargo. Yap1 acts downstream of -catenin to control epidermal proliferation. *Cell*, 144(5):782–795, Mar 2011. doi: 10.1016/j.cell.2011.02.031. URL http://dx.doi.org/10.1016/j.cell.2011.02.031.

[138] P. Schmitz, U. Gerber, E. Jungel, N. Schutze, R. Blaheta, and G. Bendas. Cyr61/ccn1 affects the integrin-mediated migration of prostate cancer cells (pc-3) in vitro. *Int J Clin Pharmacol Ther*, 51(1):47–50, 2013. doi: 10.5414/CPP51047. URL http://www.dustri.com/nc/article-response-page.html?artI.

[139] M. C. Schroeder and G. Halder. Regulation of the hippo pathway by cell architecture and mechanical signals. *Semin Cell Dev Biol*, 23(7):803–811, Sep 2012. doi: 10.1016/j.semcdb.2012.06.001. URL http://dx.doi.org/10.1016/j.semcdb.2012.06.001.

[140] M. Schutte, R. H. Hruban, J. Geradts, R. Maynard, W. Hilgers, S. K. Rabindran, C. A. Moskaluk, S. A. Hahn, I. Schwarte-Waldhoff, W. Schmiegel, S. B. Baylin, S. E. Kern, and J. G. Herman. Abrogation of the rb/p16 tumor-suppressive pathway in virtually all pancreatic carcinomas. *Cancer Res*, 57(15):3126–3130, Aug 1997. URL http://cancerres.aacrjournals.org/content/57/15/3126.long.

[141] U. Schütte, S. Bisht, P. Brossart, and G. Feldmann. Recent developments of transgenic and xenograft mouse models of pancreatic cancer for translational research. *Expert Opinion on Drug Discovery*, 6(1):33–48, 2011. URL http://informahealthcare.com/doi/abs/10.1517/17460441.2011.534453.

[142] M. A. Schwartz. Integrins, oncogenes, and anchorage independence. *J Cell Biol*, 139(3):575–578, Nov 1997. URL http://jcb.rupress.org/content/139/3/575.long.

[143] B. Seliger, A. Hohne, A. Knuth, H. Bernhard, B. Ehring, R. Tampe, and C. Huber. Reduced membrane major histocompatibility complex class i density and stability in a subset of human renal cell carcinomas with low tap and lmp expression. *Clin Cancer Res*, 2(8):1427–33, 1996. URL http://clincancerres.aacrjournals.org/content/2/8/1427.long.

[144] D. D. Shao, W. Xue, E. B. Krall, A. Bhutkar, F. Piccioni, X. Wang, A. C. Schinzel, S. Sood, J. Rosenbluh, J. W. Kim, Y. Zwang, T. M. Roberts, D. E. Root, T. Jacks, and W. C. Hahn. Kras and yap1 converge to regulate emt and tumor survival. *Cell*, 158(1):171–184, Jul 2014. doi: 10.1016/j.cell.2014.06.004. URL http://dx.doi.org/10.1016/j.cell.2014.06.004.

[145] T. Shimazui, L. A. Giroldi, P. P. Bringuier, E. Oosterwijk, and J. A. Schalken. Complex cadherin expression in renal cell carcinoma. *Cancer Res*, 56(14):3234–7, 1996. URL http://cancerres.aacrjournals.org/content/56/14/3234.lon.

[146] T. Shimazui, K. Yoshikawa, H. Uemura, Y. Hirao, S. Saga, and H. Akaza. The level of cadherin-6 mrna in peripheral blood is associated with the site of metastasis and with the subsequent occurrence of metastases in renal cell carcinoma. *Cancer*, 101

(5):963–8, 2004. doi: 10.1002/cncr.20479. URL http://onlinelibrary.wiley.com/doi/10.1002/cncr.20479/ab.

[147] H. Shimura, K. Date, K. Matsumoto, T. Nakamura, and M. Tanaka. Induction of invasive growth in a gallbladder cancer cell line by hepatocyte growth factor in vitro. *Jpn J Cancer Res*, 86(7):662–669, Jul 1995.

[148] E. Sievers, P. Dreimuller, A. Haferkamp, I. G. Schmidt-Wolf, M. W. Buchler, J. Schmidt, and A. Marten. Characterization of primary renal carcinoma cultures. *Urol Int*, 79(3):235–43, 2007. doi: 10.1159/000107956. URL http://www.karger.com/Article/FullText/107956.

[149] A. J. Simmonds, X. Liu, K. H. Soanes, H. M. Krause, K. D. Irvine, and J. B. Bell. Molecular interactions between vestigial and scalloped promote wing formation in drosophila. *Genes Dev*, 12(24):3815–3820, Dec 1998. URL http://genesdev.cshlp.org/content/12/24/3815.long.

[150] S. S. Skånland, S. Wälchli, A. Brech, and K. Sandvig. Snx4 in complex with clathrin and dynein: implications for endosome movement. *PLoS One*, 4(6):e5935, 2009. doi: 10.1371/journal.pone.0005935. URL http://dx.doi.org/10.1371/journal.pone.0005935.

[151] G. K. Smyth. Linear models and empirical bayes methods for assessing differential expression in microarray experiments. *Stat Appl Genet Mol Biol*, 3:Article3, 2004. doi: 10.2202/1544-6115.1027. URL http://dx.doi.org/10.2202/1544-6115.1027.

[152] A. Spandidos, X. Wang, H. Wang, S. Dragnev, T. Thurber, and B. Seed. A comprehensive collection of experimentally validated primers for polymerase chain reaction quantitation of murine transcript abundance. *BMC Genomics*, 9:633, 2008. doi: 10.1186/1471-2164-9-633. URL http://dx.doi.org/10.1186/1471-2164-9-633.

[153] A. Spandidos, X. Wang, H. Wang, and B. Seed. Primerbank: a resource of human and mouse pcr primer pairs for gene expression detection and quantification. *Nucleic Acids Res*, 38(Database issue):D792–D799, Jan 2010. doi: 10.1093/nar/gkp1005. URL http://dx.doi.org/10.1093/nar/gkp1005.

[154] A. A. Steinhardt, M. F. Gayyed, A. P. Klein, J. Dong, A. Maitra, D. Pan, E. A. Montgomery, and R. A. Anders. Expression of yes-associated protein in common

solid tumors. *Hum Pathol*, 39(11):1582–9, 2008. doi: 10.1016/j.humpath.2008.04.012.

[155] S. A. Stewart, D. M. Dykxhoorn, D. Palliser, H. Mizuno, E. Y. Yu, D. S. An, D. M. Sabatini, I. S. Y. Chen, W. C. Hahn, P. A. Sharp, R. A. Weinberg, and C. D. Novina. Lentivirus-delivered stable gene silencing by rnai in primary cells. *RNA*, 9 (4):493–501, Apr 2003. URL http://rnajournal.cshlp.org/content/9/4/493.long.

[156] S. Strano, O. Monti, N. Pediconi, A. Baccarini, G. Fontemaggi, E. Lapi, F. Mantovani, A. Damalas, G. Citro, A. Sacchi, G. Del Sal, M. Levrero, and G. Blandino. The transcriptional coactivator yes-associated protein drives p73 gene-target specificity in response to dna damage. *Mol Cell*, 18(4):447–459, May 2005. doi: 10.1016/j.molcel.2005.04.008. URL http://dx.doi.org/10.1016/j.molcel.2005.04.008.

[157] S. W. Tang, W. H. Chang, Y. C. Su, Y. C. Chen, Y. H. Lai, P. T. Wu, C. I. Hsu, W. C. Lin, M. K. Lai, and J. Y. Lin. Myc pathway is activated in clear cell renal cell carcinoma and essential for proliferation of clear cell renal cell carcinoma cells. *Cancer Lett*, 273(1):35–43, 2009. doi: 10.1016/j.canlet.2008.07.038. URL http://www.cancerletters.info/article/S0304-3835(08)0058.

[158] N. Tapon, K. F. Harvey, D. W. Bell, D. C. R. Wahrer, T. A. Schiripo, D. A. Haber, and I. K. Hariharan. salvador promotes both cell cycle exit and apoptosis in drosophila and is mutated in human cancer cell lines. *Cell*, 110(4):467–478, Aug 2002. URL http://www.sciencedirect.com/science/article/pii/S0092867402008243.

[159] A. L. Tarca, S. Draghici, P. Khatri, S. S. Hassan, P. Mittal, J. S. Kim, C. J. Kim, J. P. Kusanovic, and R. Romero. A novel signaling pathway impact analysis. *Bioinformatics*, 25(1):75–82, 2009. doi: 10.1093/bioinformatics/btn577. URL http://bioinformatics.oxfordjournals.org/content/25/1/7.

[160] L. K. Taylor, H. C. Wang, and R. L. Erikson. Newly identified stress-responsive protein kinases, krs-1 and krs-2. *Proc Natl Acad Sci U S A*, 93(19):10099–10104, Sep 1996.

[161] The RNAi Consortium (TRC). *The RNAi Consortium (TRC) Lentiviral shRNA Technical Manual*. Fisher Thermo Scientific Corporation, 2013.

[162] C. J. Traer, A. C. Rutherford, K. J. Palmer, T. Wassmer, J. Oakley, N. Attar, J. G. Carlton, J. Kremerskothen, D. J. Stephens, and P. J. Cullen. Snx4 coordinates endosomal sorting of tfnr with dynein-mediated transport into the endocytic recycling compartment. *Nat Cell Biol*, 9(12):1370–1380, Dec 2007. doi: 10.1038/ncb1656. URL http://dx.doi.org/10.1038/ncb1656.

[163] B. Trojaneck, S. Niemitz, B. Micka, P. Lefterova, R. Blasczyk, C. Scheffold, D. Huhn, and I. G. Schmidt-Wolf. Establishment and characterization of colon carcinoma and renal cell carcinoma primary cultures. *Cancer Biother Radiopharm*, 15(2):169–74, 2000.

[164] A. Untergasser, I. Cutcutache, T. Koressaar, J. Ye, B. C. Faircloth, M. Remm, and S. G. Rozen. Primer3–new capabilities and interfaces. *Nucleic Acids Res*, 40(15): e115, Aug 2012. doi: 10.1093/nar/gks596. URL http://dx.doi.org/10.1093/nar/gks596.

[165] F. J. van Kuppeveld, J. T. van der Logt, A. F. Angulo, M. J. van Zoest, W. G. Quint, H. G. Niesters, J. M. Galama, and W. J. Melchers. Genus- and species-specific identification of mycoplasmas by 16s rrna amplification. *Appl Environ Microbiol*, 58(8):2606–15, 1992. URL http://aem.asm.org/content/59/2/655.long.

[166] X. Varelas, B. W. Miller, R. Sopko, S. Song, A. Gregorieff, F. A. Fellouse, R. Sakuma, T. Pawson, W. Hunziker, H. McNeill, J. L. Wrana, and L. Attisano. The hippo pathway regulates wnt/beta-catenin signaling. *Dev Cell*, 18(4):579–591, Apr 2010. doi: 10.1016/j.devcel.2010.03.007. URL http://dx.doi.org/10.1016/j.devcel.2010.03.007.

[167] B. Vogelstein and K. W. Kinzler. Cancer genes and the pathways they control. *Nat Med*, 10(8):789–799, Aug 2004. doi: 10.1038/nm1087. URL http://dx.doi.org/10.1038/nm1087.

[168] B. Vogelstein, N. Papadopoulos, V. E. Velculescu, S. Zhou, J. Diaz, L. A., and K. W. Kinzler. Cancer genome landscapes. *Science*, 339(6127):1546–58, 2013. doi: 10.1126/science.1235122. URL http://www.sciencemag.org/content/339/6127/1546.long.

[169] C. L. Walters, R. C. Arend, D. K. Armstrong, R. W. Naumann, and R. D. Alvarez. Folate and folate receptor alpha antagonists mechanism of action in ovarian cancer.

Gynecol Oncol, 131(2):493–498, Nov 2013. doi: 10.1016/j.ygyno.2013.07.080. URL http://dx.doi.org/10.1016/j.ygyno.2013.07.080.

[170] X. Wang and B. Seed. A pcr primer bank for quantitative gene expression analysis. *Nucleic Acids Res*, 31(24):e154, Dec 2003. doi: 10.1093/nar/gng154. URL http://nar.oxfordjournals.org/content/31/24/e154.long.

[171] X. Wang, A. Spandidos, H. Wang, and B. Seed. Primerbank: a pcr primer database for quantitative gene expression analysis, 2012 update. *Nucleic Acids Res*, 40(Database issue):D1144–D1149, Jan 2012. doi: 10.1093/nar/gkr1013. URL http://dx.doi.org/10.1093/nar/gkr1013.

[172] Y. Wang, Q. Dong, Q. Zhang, Z. Li, E. Wang, and X. Qiu. Overexpression of yes-associated protein contributes to progression and poor prognosis of non-small-cell lung cancer. *Cancer Sci*, 101(5):1279–1285, May 2010. doi: 10.1111/j.1349-7006.2010.01511.x. URL http://dx.doi.org/10.1111/j.1349-7006.2010.01511.x.

[173] C. Wenger, V. Ellenrieder, B. Alber, U. Lacher, A. Menke, H. Hameister, M. Wilda, T. Iwamura, H. G. Beger, G. Adler, and T. M. Gress. Expression and differential regulation of connective tissue growth factor in pancreatic cancer cells. *Oncogene*, 18(4):1073–1080, Jan 1999. doi: 10.1038/sj.onc.1202395. URL http://dx.doi.org/10.1038/sj.onc.1202395.

[174] R. E. Wilentz, J. Geradts, R. Maynard, G. J. Offerhaus, M. Kang, M. Goggins, C. J. Yeo, S. E. Kern, and R. H. Hruban. Inactivation of the p16 (ink4a) tumor-suppressor gene in pancreatic duct lesions: loss of intranuclear expression. *Cancer Res*, 58(20):4740–4744, Oct 1998. URL http://cancerres.aacrjournals.org/content/58/20/4740.long.

[175] M. Z. Xu, T. J. Yao, N. P. Lee, I. O. Ng, Y. T. Chan, L. Zender, S. W. Lowe, R. T. Poon, and J. M. Luk. Yes-associated protein is an independent prognostic marker in hepatocellular carcinoma. *Cancer*, 115(19):4576–85, 2009. doi: 10.1002/cncr.24495. URL http://www3.interscience.wiley.com/journal/122465278/abstract?CRETRY=1&SRETRY=0.

[176] T. Yoshimoto, K. Matsuura, S. Karnan, H. Tagawa, C. Nakada, M. Tanigawa, Y. Tsukamoto, T. Uchida, K. Kashima, S. Akizuki, I. Takeuchi, F. Sato, H. Mimata,

M. Seto, and M. Moriyama. High-resolution analysis of dna copy number alterations and gene expression in renal clear cell carcinoma. *J Pathol*, 213(4):392–401, 2007. doi: 10.1002/path.2239. URL http://onlinelibrary.wiley.com/doi/10.1002/path.2239/abstract;jsessionid=C10BE651B5744536F4CF45874E7CF801.d03t01.

[177] F.-X. Yu and K.-L. Guan. Transcription and processing: multilayer controls of rna biogenesis by the hippo pathway. *EMBO J*, 33(9):942–944, May 2014. doi: 10.1002/embj.201488329. URL http://dx.doi.org/10.1002/embj.201488329.

[178] F.-X. Yu, B. Zhao, N. Panupinthu, J. L. Jewell, I. Lian, L. H. Wang, J. Zhao, H. Yuan, K. Tumaneng, H. Li, X.-D. Fu, G. B. Mills, and K.-L. Guan. Regulation of the hippo-yap pathway by g-protein-coupled receptor signaling. *Cell*, 150(4):780–791, Aug 2012. doi: 10.1016/j.cell.2012.06.037. URL http://dx.doi.org/10.1016/j.cell.2012.06.037.

[179] M. Yuan, V. Tomlinson, R. Lara, D. Holliday, C. Chelala, T. Harada, R. Gangeswaran, C. Manson-Bishop, P. Smith, S. A. Danovi, O. Pardo, T. Crook, C. A. Mein, N. R. Lemoine, L. J. Jones, and S. Basu. Yes-associated protein (yap) functions as a tumor suppressor in breast. *Cell Death Differ*, 15(11):1752–1759, Nov 2008. doi: 10.1038/cdd.2008.108. URL http://dx.doi.org/10.1038/cdd.2008.108.

[180] L. Zender, M. S. Spector, W. Xue, P. Flemming, C. Cordon-Cardo, J. Silke, S.-T. Fan, J. M. Luk, M. Wigler, G. J. Hannon, D. Mu, R. Lucito, S. Powers, and S. W. Lowe. Identification and validation of oncogenes in liver cancer using an integrative oncogenomic approach. *Cell*, 125(7):1253–1267, Jun 2006. doi: 10.1016/j.cell.2006.05.030. URL http://dx.doi.org/10.1016/j.cell.2006.05.030.

[181] J.-F. Zhang, R. Hua, D.-J. Liu, W. Liu, Y.-M. Huo, and Y.-W. Sun. Effect of cd74 on the prognosis of patients with resectable pancreatic cancer. *Hepatobiliary Pancreat Dis Int*, 13(1):81–86, Feb 2014. URL http://www.hbpdint.com/EN/Y2014/V13/I1/81.

[182] B. Zhao, X. Wei, W. Li, R. S. Udan, Q. Yang, J. Kim, J. Xie, T. Ikenoue, J. Yu, L. Li, P. Zheng, K. Ye, A. Chinnaiyan, G. Halder, Z.-C. Lai, and K.-L. Guan. Inactivation of yap oncoprotein by the hippo pathway is involved in cell contact inhibition and tissue growth control. *Genes Dev*, 21(21):2747–2761, Nov 2007. doi: 10.1101/gad.1602907. URL http://dx.doi.org/10.1101/gad.1602907.

[183] B. Zhao, X. Ye, J. Yu, L. Li, W. Li, S. Li, J. Yu, J. D. Lin, C.-Y. Wang, A. M. Chinnaiyan, Z.-C. Lai, and K.-L. Guan. Tead mediates yap-dependent gene induction and growth control. *Genes Dev*, 22(14):1962–1971, Jul 2008. doi: 10.1101/gad.1664408. URL http://dx.doi.org/10.1101/gad.1664408.

[184] B. Zhao, L. Li, L. Wang, C. Y. Wang, J. Yu, and K. L. Guan. Cell detachment activates the hippo pathway via cytoskeleton reorganization to induce anoikis. *Genes Dev*, 26(1):54–68, 2012. doi: 10.1101/gad.173435.111. URL http://genesdev.cshlp.org/content/26/1/54.long.

[185] L. Zhou, R. Zhang, L. Zhang, Y. Sun, W. Yao, A. Zhao, J. Li, and Y. Yuan. Upregulation of transgelin is an independent factor predictive of poor prognosis in patients with advanced pancreatic cancer. *Cancer Sci*, 104(4):423–430, Apr 2013. doi: 10.1111/cas.12107. URL http://dx.doi.org/10.1111/cas.12107.

[186] D. P. Zubac, L. Bostad, B. Kihl, T. Seidal, T. Wentzel-Larsen, and S. A. Haukaas. The expression of thrombospondin-1 and p53 in clear cell renal cell carcinoma: its relationship to angiogenesis, cell proliferation and cancer specific survival. *J Urol*, 182(5):2144–9, 2009. doi: 10.1016/j.juro.2009.07.015. URL http://www.sciencedirect.com/science/article/pii/S002253470901739X.